

INVESTIGATIONS ON THE MESOZOIC GEOLOGIC AND TECTONIC HISTORY
OF THE JACKSON MOUNTAINS, NORTHWEST NEVADA

by

Thomas Anthony Colby

A dissertation
submitted in partial fulfillment
of the requirements for the degree of
Doctor of Philosophy in Geosciences
Boise State University

May 2017

© 2017

Thomas Anthony Colby

ALL RIGHTS RESERVED

BOISE STATE UNIVERSITY GRADUATE COLLEGE

DEFENSE COMMITTEE AND FINAL READING APPROVALS

of the dissertation submitted by

Thomas Anthony Colby

Dissertation Title: Investigations on the Mesozoic Geologic and Tectonic History of
the Jackson Mountains, Northwest Nevada

Date of Final Oral Examination: 17 March 2017

The following individuals read and discussed the dissertation submitted by student Thomas Anthony Colby, and they evaluated his presentation and response to questions during the final oral examination. They found that the student passed the final oral examination.

Clyde J. Northrup, Ph.D.	Chair, Supervisory Committee
Mark Schmitz, Ph.D.	Member, Supervisory Committee
Walter Snyder, Ph.D.	Member, Supervisory Committee
Todd LaMaskin, Ph.D.	External Examiner

The final reading approval of the dissertation was granted by Clyde J. Northrup, Ph.D., Chair of the Supervisory Committee. The dissertation was approved by the Graduate College.

ACKNOWLEDGEMENTS

To my advisors, Dr. CJ Northrup, Dr. Mark Schmitz, and Dr. Walt Snyder, I have the utmost thanks and appreciation for all your help and encouragement through the years. I thank you for allowing me to come to Boise State University and pursue my dreams. To CJ, thank you for the support and fantastic geology and tectonics conversations. You were always excited to hear what I was thinking about and help with future direction and staying on target. Additionally, thank you for the opportunity to help with field camp in Sardinia. Those were truly amazing experiences that I will never forget. To Mark, thank you for allowing me to work in the Isotope Geology Laboratory and for always being willing to chat and work through data and interpretations. Your help and guidance helped immensely in getting me through this dissertation and I treasure what you've taught me. To Walt, thank you for the great discussions and insight into Great Basin geology. I also thank you for the geologic tour of northern Nevada when I arrived at Boise State. That trip helped enormously when trying to wrap my head around the geology of Nevada and some of the unresolved questions and problems. To Dr. Todd LaMaskin, thank you for the detailed and thoughtful edits and comments of this dissertation and for serving as my External Examiner. Your comments helped immeasurably in improving this dissertation and provided considerations for future research. To Dr. Jim Crowley, thank you for the analytical help and guidance and conversations about zircon. I also thank you for the talks about the snow conditions and upcoming storms that helped me through the long hours of lab work. To Debbie Pierce,

thank you for the help and assistance in sample preparation and mineral separation. To Dr. Marion Lytle, thank you for the help in setting up and running experiments with the ICPMS. To Dr. Karen Viskupic, thank you for giving me the chance to broaden my graduate studies and take part in programs outside of teaching in the department. My time with RTOP and GK-12 made me think about my teaching style and activities and will truly help me become a better teacher moving forward. To my fellow graduate students, thank you for the conversations and support throughout the PhD process. Specifically, thank you Vince Isakson for all the great conversations, friendship, and help working in the IGL. To the other faculty at Boise State, I thank you for the great classes and expertise that has truly broadened my Earth Sciences background. To the Department of Geosciences administrative staff, specifically Liz Johansen and Tami Olsen, thank you for the help working through the paperwork and bureaucratic hoops of the University system. I thank the Burnham Research Grant for providing me with financial support to get my gas guzzling 1990 GMC truck down to Nevada and the food to sustain the long days of hiking and sampling in the Jackson Mountains.

To the Department of Geological Sciences at San Diego State University, I thank you immensely for my time spent there. Specifically, Dr. Gary Girty and Dr. Vic Camp, I wouldn't be where I am today or the geologist I am today without your help and inspiration. Thank you for believing in me and pushing me to become better. Thank you to the other faculty at San Diego State that helped along the way and taught amazing and inspiring courses that fostered my love for the Earth Sciences.

To my wonderful family, thank you for your endless support, encouragement, and love in seeing me through my college career. To my parents, Ed and Diane Colby, your

infinite love and encouragement helped me get to where I am today. You helped foster a strong love of the outdoors that ultimately led me to the Earth Sciences. To my brother Michael (spouse Jessica) and sister Brenda (spouse Mike), thank you for being the best siblings I could have imagined. To my grandparents, thank you for the continual support and excitement to hear what I've been up to. To all my other aunts, uncles, and cousins in California, Idaho, and South Dakota, thank you for always being there and embodying what family is truly about.

Finally, to my amazing wife Tara. I would not be where I am today nor the man I am today without your continual love, support, and encouragement. I thank you from the bottom of my heart for coming along on this adventure and being the best friend and companion that I could ask for. From listening to me drone on about rocks to bringing me dinner in the lab to sticking with me during the writing process, I cannot thank you enough. I love you forever and always. To my furry children, Mono, Matilda, Meow, and Furr, thank you for keeping me sane(ish) during this process and always being up for whatever crazy adventure dad comes up with.

Thank you.

ABSTRACT

New geologic mapping, high-precision U-Pb zircon geochronology, and isotope geochemistry provide insight into the early Mesozoic paleogeography and magmatic, stratigraphic, and structural evolution of the Jackson Mountains in the Black Rock Desert region of northwest Nevada. The magmatic history of the Jackson Mountains records Late Triassic to Early Jurassic (~215-195 Ma) marine deposition of the Boulder Creek Beds adjacent to the arc followed by the Early Jurassic (~193-189 Ma) eruption and emplacement of the Happy Creek Igneous Complex and associated plutons of the Early Mesozoic Intrusive Suite. Pb, Sr, and Nd isotopic data from Early Jurassic intrusive rocks of the Jackson Mountains plot along a binary mixing relationship of DMM and EMII end-member mantle components and suggest some contribution of enriched continental material in the production of melts. Detrital zircon from the Boulder Creek Beds show primarily unimodal Late Triassic-Early Jurassic age distributions implying marine deposition adjacent to an active Triassic and Jurassic volcanic arc with minimal input from other sources. Together with regional geologic and tectonic relationships, these data are consistent with Triassic-Early Jurassic paleogeographic reconstructions of the Jackson Mountains as a fringing-arc separated from the continent by a deep-marine basin.

Though of shorter duration, the timing of magmatism in the Jackson Mountains overlaps with the timing of magmatism in the Olds Ferry terrane of the Blue Mountains Province. Pb, Sr, and Nd isotopic data from intrusive rocks of the Jackson Mountains consistently plot within the field of intrusive rocks from the Olds Ferry terrane.

Comparison of detrital zircon ages in the Boulder Creek Beds and Blue Mountains Province is consistent with this relationship and paleogeographic setting. Combined with similarities in lithology and paleogeography, these new data provide compelling evidence for the correlation of Triassic-Jurassic arc-affinity rocks of the Jackson Mountains and the Olds Ferry terrane as fragments of the same arc separated and displaced by ~400 km of Cretaceous dextral translation. Furthermore, considering recent correlations of the Olds Ferry and Quesnellia terranes, these data indicate that the Jackson Mountains, Olds Ferry, and Quesnellia terranes may represent fragments of an early Mesozoic fringing-arc system.

Two main phases of Mesozoic NW-SE shortening are documented in the Jackson Mountains. Between the middle Early Jurassic and early Late Jurassic (post ~189 Ma and pre ~162 Ma) NW-SE shortening resulted in the production of thrust faults, folding, and cleavage development. Given the geographic proximity to the Luning-Fencemaker fold-and-thrust belt (LFTB), strong similarities in timing, structural style, and shortening direction suggests that Jurassic shortening in the Jackson Mountains was associated with the development of the LFTB and closure of the early Mesozoic marine basin that culminated in the eastward thrusting of the arc terrane over the basinal terrane. Isotopic data for intrusions from the Early Mesozoic Intrusive Suite provide further insight into this structural event. While initial $^{87}\text{Sr}/^{86}\text{Sr}$ and ϵNd exhibit no significant variation with emplacement age, initial Pb ratios are consistently elevated in Late Jurassic plutons. These changes are likely the result of crustal shortening and eastward movement of the upper crust during the development of the LFTB whereby younger intrusions are sourced

from and travel through a more eastern crustal column that may include small fragments of enriched continental material.

In Early Cretaceous time (~118 Ma), NW-SE shortening resulted in movement along the NW-directed Deer Creek thrust and syncontractional deposition of the King Lear Formation. The timing and kinematics of this structural event relate to several significant, temporally overlapping changes in the forearc, arc, and retroarc regions that correspond with a significant change in plate motions. As such, Early Cretaceous shortening in the Jackson Mountains may be in response to a change in the Pacific-Farallon-North American velocity structure and reflect internal shortening of the hinterland. In this model, the Deer Creek thrust represents an out-of-sequence back thrust that overall aided in shortening the orogenic wedge.

TABLE OF CONTENTS

ACKNOWLEDGEMENTS	iv
ABSTRACT.....	vii
LIST OF TABLES	xv
LIST OF FIGURES	xvii
CHAPTER ONE: GENERAL INTRODUCTION	1
General Geology of the Jackson Mountains	3
Scope of Dissertation	6
References	9
CHAPTER TWO: EARLY CRETACEOUS (~118 MA) SYNDEPOSITIONAL SHORTENING IN THE CENTRAL CORDILLERAN HINTERLAND, JACKSON MOUNTAINS, NORTHWEST NEVADA, USA	15
Abstract	15
Introduction and Background	16
General Geology of the Jackson Mountains	18
Happy Creek Igneous Complex and Early Mesozoic Intrusive Suite.....	18
King Lear Formation.....	19
Structural Geology of the Jackson Mountains	20
Observations	22
Deer Creek Thrust.....	22
Subsidiary Fault Surfaces	23

Folding Within the King Lear Formation	23
U-Pb Zircon Geochronology.....	24
King Lear Tuff	24
King Lear Sandstones	26
Early Mesozoic Intrusive Suite.....	27
Discussion	27
Structural and Stratigraphic Model	29
Regional Implications	31
Early Cretaceous Continental-Arc System	31
Sevier Orogenic Belt and Adjacent Hinterland	33
Summary and Conclusions	34
Acknowledgements.....	35
References.....	54
 CHAPTER THREE: U-PB ZIRCON GEOCHRONOLOGY PROVIDES INSIGHT INTO THE MESOZOIC TECTONIC EVOLUTION, PALEOGEOGRAPHY, AND STRUCTURAL ARCHITECTURE OF THE JACKSON MOUNTAINS, NORTHWEST NEVADA, USA.....	59
Abstract	59
Introduction.....	60
Background.....	63
Regional Geology	63
Geology of the Jackson Mountains.....	66
Sample Collection and Analytical Procedures.....	74
Boulder Creek Beds Detrital Zircon	74
Happy Creek Igneous Complex	75

Early Mesozoic Intrusive Suite.....	75
Results.....	75
Detrital Zircon Analysis.....	75
Magmatic Zircon Analysis.....	77
Discussion	78
Boulder Creek Beds Provenance and Paleogeography	78
Comparison to Olds Ferry terrane.....	80
Correlation With Strata in the Pine Forest Range?.....	82
Boulder Creek Beds Maximum Depositional Age	83
Jurassic Structural Evolution	86
Latest Triassic to Early Jurassic Shortening	90
Summary and Conclusions	91
Acknowledgements.....	92
References.....	117
 CHAPTER FOUR: PB, SR, AND ND ISOTOPIC DATA AND U-PB ZIRCON GEOCHRONOLOGY OF JURASSIC INTRUSIVE ROCKS IN THE JACKSON MOUNTAINS, NORTHWEST NEVADA: IMPLICATIONS FOR MESOZOIC PALEOGEOGRAPHY, TERRANE CORRELATION, AND LUNING-FENCEMAKER FOLD-AND-THRUST BELT DEFORMATION	126
Abstract	126
Introduction.....	127
Background.....	130
Regional Geology	130
Geology of the Jackson Mountains.....	132
Sample Collection and Analytical Procedures.....	136

U-Pb Zircon Geochronology.....	137
Isotope Geochemistry	138
Results.....	139
U-Pb Zircon Geochronology.....	139
Isotope Geochemistry	141
Discussion	142
Timing of Mesozoic Magmatism in the Jackson Mountains	142
Assessment of Magma Source Reservoirs and Paleogeography	144
Isotopic Signature of Early and Late Jurassic Plutons.....	148
Correlation to the Olds Ferry Arc Terrane.....	152
Summary and Conclusions	156
Acknowledgments.....	157
References.....	179
CHAPTER FIVE: CONCLUDING COMMENTS	192
APPENDIX A.....	196
U-Pb Isotopic Data for Magmatic and Detrital Zircon Analyzed By LA-ICPMS and CA-IDTIMS From Chapter 2.....	196
APPENDIX B	221
U-Pb Isotopic Data for Magmatic and Detrital Zircon Analyzed By LA-ICPMS and CA-IDTIMS From Chapter 3.....	221
APPENDIX C	249
U-Pb Isotopic Data for Magmatic and Detrital Zircon Analyzed By LA-ICPMS and CA-IDTIMS From Chapter 4.....	249
APPENDIX D	256
Pb, Sr, and Nd Isotopic Data for Intrusive Rocks of the Jackson Mountains.....	256

APPENDIX E	260
Compilation of Pb, Sr, and Nd Isotopic Data for Jurassic Plutons from the Western United States.....	260

LIST OF TABLES

Table 2.1.	Summary of Samples and Corresponding $^{206}\text{Pb}/^{238}\text{U}$ ages	36
Table 3.1.	Summary of Dominant Lithology and Published Age Constraints for Subunits of the Boulder Creek Beds. Modified from tables in Quinn (1996).	93
Table 3.2.	Summary of Samples and Corresponding $^{206}\text{Pb}/^{238}\text{U}$ ages	95
Table 4.1.	Summary of Lithologies and Previously Reported Ages for Plutons from the Early Mesozoic Intrusive Suite.	158
Table 4.2.	Summary of Samples and Corresponding $^{206}\text{Pb}/^{238}\text{U}$ ages	159
Table 4.3.	Summary of the Age and Pb, Sr, and Nd Isotopic Composition for Plutons of the Early Mesozoic Intrusive Suite.....	160
Table 4.4.	Geochemical and Isotopic Parameters for Mantle and Binary Mixing Components.	161
Table A.1.	U-Pb Isotopic Data for Magmatic Zircon from the Jackson Mountains for Chapter 2	197
Table A.2.	U-Pb Isotopic Data for Detrital Zircon from the Jackson Mountains for Chapter 2	198
Table A.3.	Magmatic Zircon LA-ICPMS U-Pb Geochronology for Chapter 2	199
Table A.4.	Detrital Zircon LA-ICPMS U-Pb Geochronology for Chapter 2	203
Table B.1.	U-Pb Isotopic Data for Magmatic Zircon from the Jackson Mountains for Chapter 3	222
Table B.2.	U-Pb Isotopic Data for Detrital Zircon from the Jackson Mountains for Chapter 3	223
Table B.3.	Magmatic Zircon LA-ICPMS U-Pb Geochronology for Chapter 3	225
Table B.4.	Detrital Zircon LA-ICPMS U-Pb Geochronology for Chapter 3	230

Table C.1.	U-Pb Isotopic Data for Magmatic Zircon from the Jackson Mountains for Chapter 4	250
Table C.2.	Magmatic Zircon LA-ICPMS U-Pb Geochronology for Chapter 4	252
Table D.1.	Pb Isotopic Data for Intrusive Rocks of the Jackson Mountains	257
Table D.2.	Rb-Sr Isotopic Data for Intrusive Rocks of the Jackson Mountains.....	258
Table D.3.	Sm-Nd Isotopic Data for Intrusive Rocks of the Jackson Mountains....	259
Table E.1.	Compilation of Pb, Sr, and Nd Isotopic Data for Jurassic Plutons (165-150 Ma) Located Between 38°-42°N and 113°-121°W	261

LIST OF FIGURES

Figure 2.1.	Generalized Geotectonic Map of the Western United States. Simplified to show the major elements of the Cordilleran arc and retroarc regions. Not palinsastically restored. Modified from DeCelles & Coogan (2006), Dumitru et al. (2010), Ernst, (2011), LaMaskin et al. (2011), Long et al. (2014). Abbreviations are as follows: FAC = Franciscan accretionary complex, SNB = Sierra Nevada batholith, LFTB = Luning-Fencemaker fold-thrust belt, CNTB = Central Nevada thrust belt, SFTB = Sevier fold-thrust belt (expanded), IB = Idaho batholith.....	37
Figure 2.2.	Simplified Geologic Maps Modified from (A) Willden (1958) and (B) Quinn et al. (1997) of the Central Portion of the Jackson Mountains. Both maps have been scaled the same to highlight the different interpretations surrounding the upper contact between the King Lear Formation and pre-Cretaceous rocks (mostly Happy Creek Igneous Complex). Note the thrust fault (i.e. the Deer Creek thrust) in (A) and the normal fault (i.e. the DeLong Peak fault) in (B).....	38
Figure 2.3.	Geologic Map of the Central Jackson Mountains. Revised and simplified from Russell (1984) and Quinn et al. (1997). PPP = Parrot Peak pluton, DPP = Delong Peak pluton, TCS = Trout Creek stock.....	39
	40	
Figure 2.4.	Generalized Stratigraphic Column for the Early Cretaceous King Lear Formation. Modified from Martin et al. (2010), Quinn (1996), and Quinn et al. (1997). Thicknesses are not to scale.	40
Figure 2.5.	Summary of the Interpreted Mesozoic Structural History of the Jackson Mountains from Russell (1981; 1984), Maher (1989), Quinn (1996), and Quinn et al. (1997).	41
Figure 2.6.	Field Photographs (A, B, and D) and Google Earth Images (C) of the Happy Creek Igneous Complex (HCu) and King Lear Formation (Kkl) Contact Geometry. A.) View looking to the SW in the vicinity Deer Creek Peak. PSP = Prospect Springs pluton. B.) Same location as A but looking to the SE. C.) Google Earth image in the vicinity of Parrot Peak. View looking to the S. Tf = Tertiary felsite. D.) View looking to the N in the central Jackson Mountains.....	42

- Figure 2.7. 3 Point Problem of the Happy Creek Igneous Complex (HCu) and King Lear Formation (Kkl) Contact Geometry in the Vicinity of Deer Creek Peak. A.) Oblique Google Earth view to the N-NE. This is in the same area as the photos from Figure 6a and 6b. B.) Calculation of strike and dip in map view. Calculated structure contours are in red..... 43
- Figure 2.8. Field Photographs and Stereonet of Subsidiary Fault Surfaces Within the King Lear Formation. Hammer (~33 cm) and Mono the black dog for scale. A.) Close-up view looking to the SE. B.) Slickensided block that has fallen from wall directly above. C.) Thrust sense offset along subsidiary fault surface. View looking to the S. D.) Stereonet analysis of orientation of fault surfaces and slickenlines compared to the orientation of the Deer Creek thrust..... 44
- Figure 2.9. Annotated Field Photograph and Stereonets of Folds. View looking to the S-SE in photograph. Stereonet analysis show a pair of open, moderately-inclined, moderately-plunging folds trending ~NE-SW with axial surfaces dipping ~60 SE. Note the decrease in the degree of folding as you move up-section..... 45
- Figure 2.10. Results of U-Pb Zircon Geochronology Using Both LA-ICPMS (A) and CA-IDTIMS (B, C) of Magmatic Zircon From the King Lear Tuff (KLT-1). For CA-IDTIMS results, zircon analyses included in the weighted mean $^{206}\text{Pb}/^{238}\text{U}$ crystallization age are represented by solid bold ellipses (B). Gray outlined ellipses were not used in any age calculation (B). Ranked age charts (C) located to the right of the concordia diagram show the distribution of $^{206}\text{Pb}/^{238}\text{U}$ ages. Bar heights depict their associated 2σ uncertainties. The gray band set behind the group represents the weighted mean of those analyses where the height illustrates the related uncertainty. Line-type designations on bar charts mimic those described for the concordia diagrams. MSWD—mean squared weighted deviation. 46
- Figure 2.11. Relative Probability Plots, Histograms, and Ranked Age Plot for Detrital Zircons for Sandstones of the King Lear Formation in the Jackson Mountains, NV. Top 2 curves represent dates obtained using LA-ICPMS. The bottom ranked age plot is for CA-IDTIMS dates from the youngest zircon distribution found in KLS-1. Note the significant difference in zircon provenance between the base (KLS-2) and the top (KLS-1) of the King Lear Formation. Curves represent the summation of individual detrital zircon ages and associated 2σ Gaussian errors; associated y-axes represent relative probability. Histograms are based on individual detrital zircon grain ages and do not incorporate errors; associated y-axes represent number of grains in a given age bin. 47
- Figure 2.12. Results of U-Pb Zircon Geochronology Using Both LA-ICPMS (A) and CA-IDTIMS (B, C) of Magmatic Zircon From the Parrot Peak Pluton

(PPP-1). For CA-IDTIMS results, zircon analyses included in the weighted mean $^{206}\text{Pb}/^{238}\text{U}$ crystallization age are represented by solid bold ellipses (B). Ranked age charts (C) located to the right of the concordia diagram show the distribution of $^{206}\text{Pb}/^{238}\text{U}$ ages. Bar heights depict their associated 2σ uncertainties. The gray band set behind the group represents the weighted mean of those analyses where the height illustrates the related uncertainty. Line-type designations on bar charts mimic those described for the concordia diagrams. MSWD—mean squared weighted deviation.....	48
Figure 2.13. Results of U-Pb Zircon Geochronology Using Both LA-ICPMS (A) and CA-IDTIMS (B, C) of Magmatic Zircon From the Prospect Springs Pluton (PSP-1). For CA-IDTIMS results, zircon analyses included in the weighted mean $^{206}\text{Pb}/^{238}\text{U}$ crystallization age are represented by solid bold ellipses (B). Ranked age charts (C) located to the right of the concordia diagram show the distribution of $^{206}\text{Pb}/^{238}\text{U}$ ages. Bar heights depict their associated 2σ uncertainties. The gray band set behind the group represents the weighted mean of those analyses where the height illustrates the related uncertainty. Line-type designations on bar charts mimic those described for the concordia diagrams. MSWD—mean squared weighted deviation.....	49
Figure 2.14. Stratigraphic and Structural Model for the Deposition of the King Lear Formation Associated with Early Cretaceous Movement Along the Deer Creek Thrust. Arrows indicate sediment source regions and pathways. For all diagrams: HCu = Happy Creek undivided, PPP = Parrot Peak Pluton, DPP = DeLong Peak Pluton, PSP = Prospect Springs Pluton, CCC = Clover Creek Complex. Members of the King Lear Formation include: JCm = Jackson Creek Member, QCm = Quartzite-Chert Member, and CCm = Clover Creek Member.....	51
Figure 2.15. Summary of the Timing of Major Events in the Cordilleran Arc and Retroarc System. Modified from DeCelles & Coogan (2006), Dumitru et al. (2010), and Long et al. (2014). Emphasis is placed on Early Cretaceous events to compare with documented shortening in the Jackson Mountains (this study). Grey vertical bar shows how shortening in the Jackson Mountains compares temporally with events in other portions of the system. Data sources include: Franciscan belt = Dumitru et al. (2010), Great Valley = Constenius et al. (2000), Intrusions = Barton et al. (1998), Newark Canyon Fm = Druschke et al. (2010), Eureka culmination = Long et al. (2014), Sevier belt = DeCelles & Coogan (2006), Pacific plate = Sager (2007).....	53
Figure 3.1. Simplified Geotectonic Assemblages of the Western United States. Modified from LaMaskin et al. (2011). ST/QN = Stikinia/Quesnellia terranes, WLA = Wallowa terrane, OF = Olds Ferry terrane, KM =	

Klamath Mountains, BR = Black Rock, NS = Northern Sierra, LFTB = Luning-Fencemaker fold-and-thrust belt.	97
Figure 3.2. Simplified Map of the Great Basin and Western United States. Drafted to highlight the location of the Mesozoic Marine Province and Luning- Fencemaker fold-and-thrust belt in relation to Paleozoic and Mesozoic arc rocks. Modified after Wyld (2002).	98
Figure 3.3. Geologic Map of the Central Jackson Mountains. Results from new geologic mapping and compilation from Russell (1981; 1984), Maher (1989), Quinn (1996), and Quinn et al. (1997).	100
Figure 3.4. Simplified Stratigraphic Columns for Apparent Triassic Strata of the Pine Forest Range and Jackson Mountains. Refer to text and Table 3.1 for descriptions of subunits of the Boulder Creek Beds. Modified from Quinn (1996). Correlations of strata are from Quinn (1996). Red zircons mark the location of detrital zircon samples in this study.....	101
Figure 3.5. Summary of Interpreted Mesozoic Structural History of the Jackson Mountains.	102
Figure 3.6. Relative Probability Plots, Histograms, and Ranked Age Plots for Detrital Zircons for Sandstones of BCB-1 and BCB-2. (A) and (C) represent dates obtained using LA-ICPMS. Curves represent the summation of individual detrital zircon ages and associated 2σ Gaussian errors; associated y-axes represent relative probability. Histograms are based on individual detrital zircon grain ages and do not incorporate errors; associated y-axes represent number of grains in a given age bin. (B) and (D) are CA- IDTIMS dates from the tail of the youngest detrital zircon subpopulation from LA-ICPMS. Ranked age charts show the distribution of $^{206}\text{Pb}/^{238}\text{U}$ ages from those grains. Bar heights depict their associated 2σ uncertainties. Grey horizontal bar and black line represent calculated maximum depositional age from black analyses. Grey analyses were not used in calculation of maximum depositional age.....	103
Figure 3.7. Relative Probability Plots, Histograms, and Ranked Age Plots for Detrital Zircons for Sandstones of BCB-3 and BCB-5. (A) and (C) represent dates obtained using LA-ICPMS. Curves represent the summation of individual detrital zircon ages and associated 2σ Gaussian errors; associated y-axes represent relative probability. Histograms are based on individual detrital zircon grain ages and do not incorporate errors; associated y-axes represent number of grains in a given age bin. (B) and (D) are CA- IDTIMS dates from the tail of the youngest detrital zircon subpopulation from LA-ICPMS. Ranked age charts show the distribution of $^{206}\text{Pb}/^{238}\text{U}$ ages from those grains. Bar heights depict their associated 2σ uncertainties. Grey horizontal bar and black line represent calculated	

maximum depositional age from black analyses. Grey analyses were not used in calculation of maximum depositional age.....	105
Figure 3.8. Results of U-Pb Zircon Geochronology Using Both LA-ICPMS (A) and CA-IDTIMS (B, C) of Magmatic Zircon From the Happy Creek Igneous Complex (HC-JM-1). For CA-IDTIMS results, zircon analyses included in the weighted mean $^{206}\text{Pb}/^{238}\text{U}$ crystallization age are represented by solid bold ellipses (B). Gray outlined ellipses were not used in any age calculation (B). Ranked age charts (C) located to the right of the concordia diagram show the distribution of $^{206}\text{Pb}/^{238}\text{U}$ ages. Bar heights depict their associated 2σ uncertainties. The gray band set behind the group represents the weighted mean of those analyses where the height illustrates the related uncertainty. Line-type designations on bar charts mimic those described for the concordia diagrams. MSWD—mean squared weighted deviation.....	107
Figure 3.9. Results of U-Pb Zircon Geochronology Using Both LA-ICPMS (A) and CA-IDTIMS (B, C) of Magmatic Zircon From the Harrison Grove Pluton (HGP-1). For CA-IDTIMS results, zircon analyses included in the weighted mean $^{206}\text{Pb}/^{238}\text{U}$ crystallization age are represented by solid bold ellipses (B). Ranked age charts (C) located to the right of the concordia diagram show the distribution of $^{206}\text{Pb}/^{238}\text{U}$ ages. Bar heights depict their associated 2σ uncertainties. The gray band set behind the group represents the weighted mean of those analyses where the height illustrates the related uncertainty. Line-type designations on bar charts mimic those described for the concordia diagrams. MSWD—mean squared weighted deviation.....	108
Figure 3.10. Results of U-Pb Zircon Geochronology Using Both LA-ICPMS (A) and CA-IDTIMS (B, C) of Magmatic Zircon From the Willow Creek Pluton (WCP-1). For CA-IDTIMS results, zircon analyses included in the weighted mean $^{206}\text{Pb}/^{238}\text{U}$ crystallization age are represented by solid bold ellipses (B). Ranked age charts (C) located to the right of the concordia diagram show the distribution of $^{206}\text{Pb}/^{238}\text{U}$ ages. Bar heights depict their associated 2σ uncertainties. The gray band set behind the group represents the weighted mean of those analyses where the height illustrates the related uncertainty. Line-type designations on bar charts mimic those described for the concordia diagrams. MSWD—mean squared weighted deviation.....	109
Figure 3.11. Compilation and Comparison of Triassic-Jurassic Arc-Related Strata of the Western United States. All plots have equal areas under the curve for comparison.....	110
Figure 3.12. Late Triassic Reconstruction of the Western Margin of North America. Possible paleogeography following the restoration of ~400 km of dextral	

strike-slip motion in Cretaceous time. Modified from LaMaskin et al. (2011) and Manuszak et al. (2000). WA = Wallowa terrane, BT = Baker terrane, WB = Weatherby Formation, OF/BRT = Olds Ferry/Black Rock terrane, BCB = Boulder Creek Beds, KM = Klamath Mountains, SN = Sierra Nevada, CA = Cordilleran arc, PN = Pine Nut assemblage, LU = Luning assemblage, LL = Lovelock assemblage..... 111

- Figure 3.13. Relative Probability Plot and Histogram for Detrital Zircons From the Bishop Canyon Formation. Data from Darby et al. (2000). Curves represent the summation of individual detrital zircon ages and associated 2σ Gaussian errors; associated y-axes represent relative probability. Histograms are based on individual detrital zircon grain ages and do not incorporate errors; associated y-axes represent number of grains in a given age bin..... 112
- Figure 3.14. Field Photographs of the Contact Between the Happy Creek Igneous Complex and Massive Limestone From BCB-1. Note the highly sheared and brecciated zone behind the hammer handle. 113
- Figure 3.15. Geologic Cross Sections A-A' and B-B' of the Central Jackson Mountains. Refer to Figure 3.3 for location of cross sections. HGP=Harrison Grove pluton, DPP=Delong Peak pluton, WCP=Willow Creek pluton..... 114
- Figure 3.16. Summary of the Mesozoic Structural History of the Jackson Mountains. A) Thrust imbrication and duplexing between the middle Early Jurassic and early Late Jurassic. B) Large-scale folding of the thrust belt prior to intrusion of the Willow Creek pluton (WCP). C) Late Jurassic (162 Ma) intrusion of the WCP records the minimum age of Jurassic shortening in the Jackson Mountains. D) Erosion and denudation expose the paleosurface for deposition of the King Lear Formation. E) Early Cretaceous (~118 Ma) movement along the Deer Creek thrust and syncontractional deposition of the King Lear Formation. Abbreviations are as follows: Pzu=Paleozoic section undivided, BCB=Boulder Creek Beds, HGP=Harrison Grove pluton, HCu=Happy Creek Igneous Complex undivided, WCP=Willow Creek pluton..... 115
- Figure 4.1. Simplified Geotectonic Assemblages of the Western United States. Modified from LaMaskin et al. (2011). ST/QN = Stikinia/Quesnellia terranes, WLA = Wallowa terrane, OF = Olds Ferry arc, KM = Klamath Mountains, NS = Northern Sierra, LFTB = Luning-Fencemaker fold-and-thrust belt. 164
- Figure 4.2. Simplified Map of the Great Basin and Western United States. Drafted to highlight the location of the Mesozoic Marine Province and Luning-Fencemaker fold-and-thrust belt in relation to Paleozoic and Mesozoic arc

rocks. Modified after Wyld (2002). Initial $^{87}\text{Sr}/^{86}\text{Sr}$ 0.706 line from Elison et al. (1990) 165

Figure 4.3. Geologic Map of the Central Jackson Mountains. Results from new geologic mapping and compilation from Willden (1958; 1963); Russell (1981; 1984), Maher (1989), Quinn (1996), and Quinn et al. (1997)..... 166

Figure 4.4. Results of U-Pb Zircon Geochronology Using Both LA-ICPMS (A) and CA-IDTIMS (B, C) of Magmatic Zircon from the Deer Creek Peak Pluton (DCPP). For CA-IDTIMS results, zircon analyses included in the weighted mean $^{206}\text{Pb}/^{238}\text{U}$ crystallization age are represented by solid bold ellipses (B). Gray outlined ellipses were not used in any age calculation (B). Ranked age charts located to the right of the concordia diagram show the distribution of $^{206}\text{Pb}/^{238}\text{U}$ ages (C). Bar heights depict their associated 2σ uncertainties. The gray band set behind the group represents the weighted mean of those analyses where the height illustrates the related uncertainty. Line-type designations on bar charts mimic those described for the concordia diagrams. MSWD mean squared weighted deviation. 167

Figure 4.5. Results of U-Pb Zircon Geochronology Using Both LA-ICPMS (A) and CA-IDTIMS (B, C) of Magmatic Zircon from the Mary Sloan Dikes (MSD). For CA-IDTIMS results, zircon analyses included in the weighted mean $^{206}\text{Pb}/^{238}\text{U}$ crystallization age are represented by solid bold ellipses (B). Gray outlined ellipses were not used in any age calculation (B). Ranked age charts located to the right of the concordia diagram show the distribution of $^{206}\text{Pb}/^{238}\text{U}$ ages (C). Bar heights depict their associated 2σ uncertainties. The gray band set behind the group represents the weighted mean of those analyses where the height illustrates the related uncertainty. Line-type designations on bar charts mimic those described for the concordia diagrams. MSWD mean squared weighted deviation. 168

Figure 4.6. Results of U-Pb Zircon Geochronology Using CA-IDTIMS of Magmatic Zircon from the Trout Creek Stock (TCS). Zircon analyses included in the weighted mean $^{206}\text{Pb}/^{238}\text{U}$ crystallization age are represented by solid bold ellipses (A). Gray outlined ellipses were not used in any age calculation (A). Ranked age charts located to the right of the concordia diagram show the distribution of $^{206}\text{Pb}/^{238}\text{U}$ ages (B). Bar heights depict their associated 2σ uncertainties. The gray band set behind the group represents the weighted mean of those analyses where the height illustrates the related uncertainty. Line-type designations on bar charts mimic those described for the concordia diagrams. MSWD mean squared weighted deviation. 169

Figure 4.7. Results of U-Pb Zircon Geochronology Using CA-IDTIMS of Magmatic Zircon from the Delong Peak Pluton (DPP). Zircon analyses included in the weighted mean $^{206}\text{Pb}/^{238}\text{U}$ crystallization age are represented by solid bold ellipses (A). Ranked age charts located to the right of the concordia

diagram show the distribution of $^{206}\text{Pb}/^{238}\text{U}$ ages (B). Bar heights depict their associated 2σ uncertainties. The gray band set behind the group represents the weighted mean of those analyses where the height illustrates the related uncertainty. Line-type designations on bar charts mimic those described for the concordia diagrams. MSWD mean squared weighted deviation.....	170
Figure 4.8. Simplified Summary of the Early Mesozoic Magmatic History of the Jackson Mountains.....	171
Figure 4.9. Sr, Nd, and Pb Isotopic Data for Intrusive Rocks of the Jackson Mountains. Panels B-F follow the same naming and coloring as Panel A. Solid circles are Late Jurassic intrusive rocks of the Jackson Mountains. Light colored squares are Early Jurassic intrusive rocks of the Jackson Mountains. Binary mixing line between DMM and CC is dashed line. Binary mixing line between DMM and EMII is lighter weight solid line. Binary mixing line between WA and CC is heavier weight, more bold solid line. Percentages represent the % contribution of the more enriched end-member (i.e. EMII or CC). Light grey field is for intrusive rocks of the Olds Ferry (OF) arc from Kurz et al., 2016. End member abbreviations as follows: DMM = depleted MORB mantle, EMI = enriched mantle I, EMII = enriched mantle II, HIMU = high- μ mantle, WA = Wallowa mafic, CC = continental crust.	172
Figure 4.10. Sr, Nd, and Common Pb Isotope Diagrams for Intrusive Rocks of the Jackson Mountains Compared to Intrusive Rocks of Eastern California, Northern Nevada, and Western Utah. Panels A through E are isotope ratio vs isotope ratio plots. Panels F though J are isotope ratio plots against longitude. Panels K through O are isotope ratio plots against emplacement age. BSE=Bulk Silicate Earth, NHRL=Northern Hemisphere Reference Line, CHUR=Chondritic Uniform Reservoir, SK=Stacey and Kramers (1975) Pb evolution line curve. Data sources for western US intrusive rocks include Zartman, 1974; Stacey and Zartman, 1978; Farmer and DePaolo, 1983; Lee, 1984; Kistler and Lee, 1989; Wright and Wooden, 1991; Wooden et al., 1998; Wooden et al., 1999; King et al., 2004.....	174
Figure 4.11. Sample Locations for Sr, Pb, and Nd Data Plotted in Figure 4.10.	176
Figure 4.12. Simplified Triassic to Jurassic Tectonic Evolution of the Jackson Mountains and Adjacent Luning-Fencemaker Fold-and-Thrust Belt (LFTB). Late Triassic to Early Jurassic fringing-arc magmatism is followed by NW-SE shortening associated with the LFTB. Shortening results in eastward movement of the Jackson Mountains and thrusting over the basinal terrane and a more enriched crustal column that may include thinned fragments of continental crust and previously accreted terranes.	177

Figure 4.13. Comparison of the Triassic and Jurassic Magmatic and Tectonic History of the Jackson Mountains and Olds Ferry Terrane. See text for further descriptions and references to Olds Ferry terrane history. 178

CHAPTER 1: GENERAL INTRODUCTION

The North American Cordillera is one of the most extensive and longest-lived orogenic belts on Earth (e.g. Burchfiel, Cowan, and Davis, 1992; DeCelles, 2004; Dickinson, 2004). Running from the Gulf of California in the south to the Gulf of Alaska in the north, the Cordillera covers a length of ~5000 km and represents a portion of the much larger Circum-Pacific orogenic belt (Dickinson, 2004). Decades of research into the geologic and tectonic history of the Cordillera has vastly improved our understanding of the development and evolution of orogenic belts and provided numerous models related to the break-up and subsequent growth and assembly of continents. The terrane concept is one such model that was presented to explain the complicated “collage” of Cordilleran geology (e.g. Coney, Jones, and Monger, 1980). This model, when combined with plate tectonic theory, provided Cordilleran geologists with a revolutionary new framework to view the tectonic evolution of the Cordillera and a broader context to focus later studies on. Fundamentally, the Cordillera could be viewed as an assembly of diverse tectonic elements that individually could be associated with distinct tectonic and paleogeographic settings (e.g. Coney et al., 1980; Jones et al., 1983). This understanding provided an exciting approach to explain the distinct geologic and tectonic histories of adjacent areas as the result of terrane amalgamation and accretion at the margin coupled with lateral-translations along the margin. Through these studies, our understanding of individual terranes, in addition to their relationships to one another, is continuing to evolve and improve (e.g. Monger and Price, 2002; Colpron, Nelson, and Murphy, 2007).

Throughout the North American Cordillera, assemblages of plutonic, volcanic, and volcanogenic sedimentary rocks have been interpreted to represent portions of volcanic arc terranes and their associated arc-related basins (e.g. Burchfiel et al., 1992; Miller et al., 1992; Saleeby & Busby-Spera, 1992; DeCelles, 2004; Dickinson, 2004; Dickinson, 2006; Colpron et al., 2007; Lund et al., 2015). Some of these terranes may represent intraoceanic arcs that evolved at some unknown distance from the continent while others may have formed continental or continental-fringing arcs (e.g. Goldstrand, 1994; Vallier, 1995; Dickinson, 2004; Stevens, Stone, and Miller, 2005; Wyld, Umhoefer, and Wright, 2006; Tumpane, 2010; Kurz, 2010; LaMaskin et al., 2011; Tosdal & Wooden, 2015; Kurz et al., 2016). While it is generally accepted that these terranes record Paleozoic to Mesozoic magmatism and accretion that led to the overall westward growth of the North American continent, controversy remains regarding the age, origin, timing of accretion, and relationship to one another (e.g. Harper and Wright, 1984; Wright and Fahan, 1988; Oldow et al., 1989; McLelland, Gehrels, and Saleeby, 1992; Hacker et al., 1995; Moores, Wakabayashi, and Unruh, 2002; Dorsey and LaMaskin, 2007; Dickinson, 2004; Dickinson, 2008; Ernst, Snow, and Scherer, 2008; Schwartz et al., 2010; LaMaskin et al., 2015).

The Jackson Mountains, located in the Black Rock Desert region of northwest Nevada, contain an exposure of Paleozoic and Mesozoic arc-related rocks (the Black Rock terrane) that represent an important locality in our understanding of Cordilleran terranes. Geographically, due to Cenozoic cover, the Black Rock Desert region represents the first exposure of Paleozoic and Mesozoic basement rocks to the south and east of other well-documented arc and arc-related terranes (i.e. the Blue Mountains Province,

Klamath Mountains, and Sierra Nevada Mountains, respectively). Additionally, the Jackson Mountains are located inboard of major Cretaceous strike-slip faults and as such are essentially in place with respect to the North American continent. Therefore, the Jackson Mountains may provide a tie point between the continent and outboard terranes when assessing the role and magnitude of strike-slip displacement along the margin. Therefore, a comprehensive understanding of the geology and tectonics of the Jackson Mountains is vital in evaluations of terrane relationships and assessing the role of horizontal translations within the Cordillera. While previous studies have documented the general geology of the Jackson's (e.g. Willden, 1958; Willden, 1963; Russell, 1981; Russell, 1984; Maher, 1989; Quinn, 1996; Quinn, Wright, and Wyld, 1997; Martin et al., 2010), significant uncertainty remains regarding the timing and duration of magmatism, the setting of magmatism, the structural architecture, and the relationship to other arc terranes of the Cordillera. Therefore, this dissertation research focuses on developing a more complete and accurate picture of the structural and stratigraphic architecture along with the timing, duration, and setting of magmatism in the Jackson Mountains. From this enhanced understanding, I provide a clearer picture of the Triassic-Jurassic paleogeography of the Jackson Mountains and the relationship to other arc terranes of the North American Cordillera.

General Geology of the Jackson Mountains

Four main stratigraphic assemblages dominate the pre-Cenozoic geology of the Jackson Mountains (e.g. Willden, 1958; Willden, 1963; Russell, 1981; Russell, 1984; Maher, 1989; Quinn, 1996; Quinn et al., 1997). Found solely on the western side of the range, the oldest rocks include a Devonian to Early Permian sequence of

metasedimentary and metavolcanic rocks known as the Hobo Canyon and McGill Canyon blocks. These Paleozoic rocks are interpreted as either the depositional basement for Mesozoic rocks (e.g. Quinn, 1996) or represent a separate tectonostratigraphic assemblage distinct from younger rocks (e.g. Russell, 1981; Silberling et al., 1987; Jones, 1990). Flanking the eastern and western sides of the range is a Late Triassic to Early Jurassic sequence of volcanogenic marine rocks named the Boulder Creek Beds. Primarily within the center of the range is an Early Jurassic mafic to intermediate assemblage of volcanic, intrusive, and sedimentary rocks known as the Happy Creek Igneous Complex and Early Mesozoic Intrusive Suite. Finally, the youngest pre-Cenozoic rocks are an Early Cretaceous sequence of primarily clastic sedimentary rocks known as the King Lear Formation.

The Boulder Creek Beds, Happy Creek Igneous Complex, and Early Jurassic plutons from the Early Mesozoic Intrusive Suite reflect a period of Late Triassic to Early Jurassic arc magmatism (e.g. Russell, 1981; 1984; Maher, 1989; Quinn, 1996; Quinn et al., 1997). In this model, deposition of the Boulder Creek Beds preceded the eruption and emplacement of the mafic to intermediate Happy Creek Igneous Complex which was then followed by intrusion of the more silicic, later-stage Jurassic plutons (Quinn, 1996; Quinn et al., 1997). Early work by Russell (1981; 1984) named this same sequence the “Jackson Mountains Unit” and interpreted it to reflect Triassic deposition on a starved lower-slope basinal margin (i.e. Boulder Creek Beds) that transitioned into the eruption of a Late Triassic to Middle Jurassic intraoceanic magmatic arc (i.e. Happy Creek Igneous Complex).

Structurally, the Jackson Mountains have experienced at least one, and perhaps multiple episodes of Mesozoic shortening resulting in the production of folds, thrusts, and associated cleavage. In light of this complicated history, previous work in the Jackson Mountains has resulted in several interpretations regarding the structural history (Willden, 1963; Russell, 1981; 1984; Maher, 1989; Quinn, 1996; Quinn et al., 1997). Early detailed work by Russell (1981; 1984) concluded that several episodes of Mesozoic shortening affected the rocks of the Jackson Mountains between the Middle Jurassic and mid-Cretaceous. The earliest phase (D_1) resulted in the production of “cryptic”, large-scale (0.5-1 km wavelength) NW or SE trending open folds (Russell, 1981). This period of NE-SW shortening was constrained to between the Middle Jurassic and Early Cretaceous (Russell, 1981). Following D_1 , and by far the best documented, a period of NW-SE shortening (D_2) resulted in the production of thrust faults, NE trending folds, and a steeply dipping, NE striking axial planar cleavage (Russell, 1981). Following these events, an Early to mid-Cretaceous phase of thrusting (D_3) affected those earlier D_1 and D_2 structures (Russell, 1981; 1984). Maher (1989) concluded that a period of Middle Jurassic sinistral wrench faulting (D_1) was followed by late Middle to Late Jurassic E-vergent folding and thrusting (D_2). This was then followed by a period of late-Early Cretaceous W and E-vergent thrusting (D_3) (Maher, 1989).

More recent work by Quinn (1996) and Quinn et al. (1997) concluded that all shortening deformation in the Jackson Mountains was pre-Cretaceous. Like Russell (1981), these authors recognized an early period (D_1) of NE-SW shortening that resulted in NW-trending folds and a poorly developed axial planar cleavage. Overprinting and cutting this earlier fabric is the widespread and strongly developed NE-trending folds and

cleavage (D_2) recognized by previous workers (Quinn, 1996). Based on the conclusion that the D_2 fabric is exclusively developed in pre-King Lear rocks, this later phase of NW-SE shortening was constrained to post-late Early Jurassic and pre-Early Cretaceous (Quinn, 1996; Quinn et al., 1997).

Scope of Dissertation

The following three chapters were written to address specific problems associated with the geologic and tectonic history of the Jackson Mountains. While written as standalone manuscripts, the chapters complement each other and together provide the most complete picture of the Mesozoic structure, stratigraphy, and magmatism of the Jackson Mountains. Here, I provide a brief summary of the specific problem each chapter addresses, the methods and/or techniques used to address that problem, and the general results.

Chapter Two, EARLY CRETACEOUS (~118 MA) SYNDEPOSITIONAL SHORTENING IN THE CENTRAL CORDILLERAN HINTERLAND, JACKSON MOUNTAINS, NORTHWEST NEVADA, USA, has been written for submission to the American Geophysical Union journal of *Tectonics*. In this Chapter, I use a combination of new geologic mapping and U-Pb zircon geochronology to argue for at least one phase of Early Cretaceous NW-SE shortening documented in the Jackson Mountains. Using these new constraints on the timing and style of deformation, I then explore the regional implications and potential driving mechanisms of shortening within this portion of the Cordillera. From this evaluation, I propose that shortening in the hinterland is tied to a significant change in plate motions. In this model, Early Cretaceous shortening in the Jackson Mountains reflects out-of-sequence thrusting associated with internal shortening

of the hinterland in response to a change in the Pacific-Farallon-North American velocity structure.

Chapter Three, U-PB ZIRCON GEOCHRONOLOGY PROVIDES INSIGHT INTO THE MESOZOIC TECTONIC EVOLUTION AND PALEOGEOGRAPHY OF THE JACKSON MOUNTAINS, NORTHWEST NEVADA, USA, has been written for submission to one of the *Geological Society of America* publications. In this Chapter, I focus on the age, provenance, and paleogeography of the Boulder Creek Beds using a combination of detrital and magmatic U-Pb zircon geochronology. These results show the Boulder Creek Beds to be younger than previously thought and represent a Late Triassic (Norian) to Early Jurassic (Sinemurian) succession of volcanogenic marine rocks deposited adjacent to an active volcanic arc. These data support paleogeographic reconstructions that place a deep marine basin between a fringing arc (i.e. Jackson Mountains) and the continent. Comparison to the Blue Mountains Province provides strong support for the correlation of the Black Rock and Olds Ferry terranes representing fragments of the same fringing-arc that was later separated and displaced by ~400 km of dextral translation. When combined with U-Pb geochronologic constraints on intrusive rocks of the Jackson Mountains, these data provide strong support for a significant phase of NW-SE shortening between the middle Early Jurassic (post ~189 Ma) and earliest Late Jurassic (pre ~162 Ma). Based on the timing, kinematic compatibility, and geographic proximity, this contractional event is likely associated with the development of the Luning-Fencemaker fold-and-thrust belt involving the closure of the early Mesozoic marine basin and thrusting of the fringing-arc over the basinal terrane.

Chapter Four, PB, SR, AND ND ISOTOPIC DATA AND U-PB ZIRCON GEOCHRONOLOGY OF JURASSIC INTRUSIVE ROCKS IN THE JACKSON MOUNTAINS, NORTHWEST NEVADA: IMPLICATIONS FOR MESOZOIC PALEOGEOGRAPHY, TERRANE CORRELATION, AND LUNING-FENCEMAKER DEFORMATION, has been written for submission to one of the *Geological Society of America* publications. In this Chapter, I focus on the age and isotope geochemistry of the Early Mesozoic Intrusive Suite that when combined with detrital zircon data presented in Chapter 3, provide new constraints on the timing, duration, and setting of Mesozoic magmatism. These data provide a picture of Late Triassic (~215 Ma) to Early Jurassic (~195 Ma) marine sedimentation (i.e. the Boulder Creek Beds) followed by the Early Jurassic (~193-189 Ma) eruption and emplacement of the Happy Creek Igneous Complex and associated plutons of the Early Mesozoic Intrusive Suite. New Pb, Sr, and Nd isotopic data are consistent with a fringing-arc setting. Together, these data strongly support reconstructions that place the Jackson Mountains, Olds Ferry, and Quesnellia terranes as geographically separate fragments of an early Mesozoic fringing-arc system that collapsed against the margin sometime in the Early Jurassic to earliest Late Jurassic. Furthermore, differences in the isotopic composition of Early and Late Jurassic intrusive rocks in the Jackson Mountains are consistent with crustal shortening and eastward movement of the upper crust during the development of the Luning-Fencemaker fold-and-thrust belt.

References

- Burchfiel, B.C., Cowan, D.S., and Davis, G.A., 1992, Tectonic overview of the Cordilleran orogen in the western United States, *in* Burchfiel, B.C., et al., eds., The Cordilleran orogen: Conterminous U.S.: Boulder, Colorado, Geological Society of America, Geology of North America, v. G-3, p. 407–480.
- Colpron, M., Nelson, J.L., Murphy, D.C., 2007, Northern Cordilleran terranes and their interactions through time: GSA Today, v. 17, no. 4/5.
- Coney, P.L., Jones, D.L., and Monger, J.W.H., 1980, Cordilleran suspect terranes: Nature, v. 288, p. 329-333.
- DeCelles, P.G., 2004, Late Jurassic to Eocene evolution of the Cordilleran thrust belt and foreland basin system, western U.S.A.: American Journal of Science, v. 304, p. 105-168.
- Dickinson, W.R., 2004, Evolution of the North American Cordillera: Annual Review of Earth and Planetary Sciences, v. 32, p. 13-45.
- Dickinson, W.R., 2006, Geotectonic evolution of the Great Basin: Geosphere, v. 2, n. 7, p. 353-368.
- Dickinson, W.R., 2008, Accretionary Mesozoic-Cenozoic expansion of the Cordilleran continental margin in California and adjacent Oregon: Geosphere, v. 4, p. 329–353.
- Dorsey, R.J., and LaMaskin, T.A., 2007, Stratigraphic record of Triassic-Jurassic collisional tectonics in the Blue Mountains Province, northeastern Oregon: American Journal of Science, v. 307, p. 1167–1193.
- Ernst, W. G., Snow, C. A., and Scherer, H. H., 2008, Mesozoic transpression, transtension, subduction, and metallogenesis in northern and central California: Terra Nova, v. 20, p. 394–413.
- Goldstrand, P.M., 1994, The Mesozoic geologic evolution of the northern Wallowa Terrane, Northeastern Oregon and Western Idaho, *in* T.L. Vallier and H.C.

- Brooks, eds., Geology of the Blue Mountains Region of Oregon, Idaho, and Washington: U.S. Geological Survey Professional Paper 1439, p. 29-53.
- Hacker, B. R., Donato, M., Barnes, C., McWilliams, M. O., and Ernst, W. G., 1995, Timescales of orogeny: Jurassic construction of the Klamath Mountains: Tectonics, v. 14, p. 677–703.
- Harper, G. D., and Wright, J. E., 1984, Middle to Late Jurassic tectonic evolution of the Klamath Mountains, California-Oregon: Tectonics, v. 3, p. 759–772.
- Jones, D.L., Howell, D.G., Coney, P.J., and Monger, J.W.H., 1983, Recognition character, and analysis of tectonostratigraphic terranes in western North America, *in* M. Hashimoto, M. and Uyeda, S., eds., Advances in Earth and Planetary Sciences: Terra Scientific Publication Company, Tokyo, p. 21-35.
- Jones, A.E., 1990, Geology and tectonic significance of terranes near Quinn River Crossing, Nevada, *in* Harwood, D.S. and Miller, M.M., eds., Late Paleozoic and early Mesozoic paleogeographic relations: Klamath Mountains, Sierra Nevada, and related terranes: Geological Society of America Special Paper 255, p. 239-254.
- Kurz, G.A., 2010, Geochemical, isotopic, and U-Pb geochronologic investigations of intrusive basement rocks from the Wallowa and Olds Ferry arc terranes, Blue Mountains province, Oregon-Idaho [PhD thesis]: Boise State University, Boise, Idaho.
- Kurz, G.A., Schmitz, M.D., Northrup, C.J., and Vallier, T.L., 2016, Isotopic compositions of intrusive rocks from the Wallowa and Olds Ferry arc terranes of northeastern Oregon and western Idaho: Implications for Cordilleran evolution, lithospheric structure, and Miocene magmatism: *Lithosphere* L550.1.
- LaMaskin, T.A., Vervoort, J.D., Dorsey, R.J., Wright, J.E., 2011, Early Mesozoic paleogeography and tectonic evolution of the western United States: insights from detrital zircon U-Pb geochronology of the Blue Mountains province, northeastern Oregon, U.S.A.: *Geological Society of America Bulletin*, v. 123, p. 1939–1965.

- LaMaskin, T.A., Dorsey, R.J., Vervoort, J.D., Schmitz, M.D., Tumpane, K.P., and Moore, N.O., 2015, Westward growth of Laurentia by Pre-Late Jurassic terrane accretion, Eastern Oregon and Western Idaho, United States: *The Journal of Geology*, v. 123, p. 000-000.
- Lund, K., Box, S.E., Holm-Denoma, C.S., San Juan, C.A., Blakely, R.J., Saltus, R.W., Anderson, E.D., DeWitt, E.H., 2015, Basement domain map of the conterminous United States and Alaska: U.S. Geological Survey Data Series 898, 48 p.
- Maher, K.A., 1989, Geology of the Jackson Mountains, northwest Nevada [Ph.D. thesis]: Pasadena, California Institute of Technology, 491 p.
- Martin, A.J., Wyld, S.J., Wright, J.E., and Bradford, J.H., 2010, The Lower Cretaceous King Lear Formation, northwest Nevada: Implications for Mesozoic orogenesis in the western U.S. Cordillera: *Geological Society of America Bulletin*, v. 122, p. 537–562.
- McClelland, W. C., Gehrels, G. E., and Saleeby, J. B., 1992, Upper Jurassic–lower Cretaceous basinal strata along the Cordilleran margin: implications for the accretionary history of the Alexander-Wrangellia-Peninsular terrane: *Tectonics*, v. 11, p. 832–835.
- Miller, E.L., Miller, M.M., Stevens, C.H., Wright, J.E., and Madrid, R., 1992, Late Paleozoic paleogeographic and tectonic evolution of the western U.S. Cordillera, in Burchfiel, B.C., Lipman, P.W., and Zoback, M.L., eds., *The Cordilleran Orogen: Conterminous U.S.*: Boulder, Colorado, Geological Society of America: The Geology of North America, v. G-3.
- Monger, J., and Price, R., 2002, The Canadian Cordillera: Geology and tectonic evolution: *Canadian Society of Exploration Geophysicists Recorder*, p. 17-36.
- Moores, E. M., Wakabayashi, J., and Unruh, J. R., 2002, Crustal-scale cross-section of the U.S. Cordillera, California and beyond, its tectonic significance, and speculations on the Andean orogeny: *International Geology Review*, v. 44, p. 479–500.

- Oldow, J. S., Bally, A. W., Avé Lallement, H. G., and Leeman, W. P., 1989, Phanerozoic evolution of the North American Cordillera: United States and Canada (Geology of North America, vol. A): Boulder, Colorado, Geological Society of America, p. 139–232.
- Quinn, M.J., 1996, Pre-Tertiary stratigraphy, magmatism, and structural history of the central Jackson Mountains, Humboldt County, Nevada [Ph.D. thesis]: Houston, Texas, Rice University, 243 p.
- Quinn, M.J., Wright, J.E., and Wyld, S.J., 1997, Happy Creek Igneous Complex and tectonic evolution of the early Mesozoic arc in the Jackson Mountains, northwest Nevada: Geological Society of America Bulletin, v. 109, p. 461-482.
- Russell, B.J., 1981, Pre-Tertiary paleogeography and tectonic history of the Jackson Mountains, northwestern Nevada [Ph.D. dissert.]: Evanston, Illinois, Northwestern University, 205 p.
- Russell, B.J., 1984, Mesozoic geology of the Jackson Mountains, northwestern Nevada: Geological Society of America Bulletin, v. 95, p. 313–323.
- Saleeby, J.B., and Busby-Spera, C., 1992, Early Mesozoic tectonic evolution of the western U.S. Cordillera, *in* Burchfiel, B.C., Lipman, P.W., and Zoback, M.L., eds., The Cordilleran Orogen: Conterminous U.S.: The Geology of North America: Boulder, Colorado, Geological Society of America, v. G-3, p. 107-168.
- Schwartz, J. J., Snock, A. W., Frost, C. D., Barnes, C. G., Gromet, L. P., and Johnson, K., 2010, Analysis of the Walla-Walla-Baker terrane boundary: implications for tectonic accretion in the Blue Mountains province, northeastern Oregon: Geological Society of America Bulletin, v. 122, p. 517–536.
- Silberling, N.J., Jones, D.L., Blake, M.C., Jr., and Howell, D.G., 1987, Lithotectonic terrane map of the western conterminous United States, *in* Lithotectonic terrane maps of the North American Cordillera: U.S. Geological Survey Map MF-1874-C, scale 1:2,500,000.
- Stevens, C.H., Stone, P., and Miller, J.S., 2005, A new reconstruction of the Paleozoic continental margin of southwestern North America: Implications for the nature

- and timing of continental truncation and the possible role of the Mojave-Sonora megashear, *in* Anderson, T.H., Nourse, J.A., McKee, J.W., and Steiner, M.B., eds., The Mojave-Sonora Megashear Hypothesis: Development, Assessment, and Alternatives: Geological Society of America Special Paper 393, p. 597–618.
- Tosdal, R.M., and Wooden, J.L., 2015, Construction of the Jurassic magmatic arc, southeast California and southwest Arizona, *in* Anderson, T.H., Didenko, A.N., Johnson, C.L., Khanchuk, A.I., and MacDonald, J.H., Jr., eds., Late Jurassic Margin of Laurasia—A record of faulting accommodating plate rotation: Geological Society of America Special Paper 513.
- Tumpane, K.P., 2010, Age and isotopic investigations of the Olds Ferry terrane and its relation to other terranes of the Blue Mountains province, eastern Oregon and west-central Idaho [M.S. thesis]: Boise, Idaho, Boise State University, 220 p.
- Vallier, T.L., 1995, Petrology of pre-Tertiary igneous rocks in the Blue Mountains region of Oregon, Idaho, and Washington: Implications for the geologic evolution of a complex island arc, *in* Vallier, T.L., and Brooks, H.C., eds., Geology of the Blue Mountains region of Oregon, Idaho, and Washington; petrology and tectonic evolution of pre-Tertiary rocks of the Blue Mountains region: U.S. Geological Survey Professional Paper 1438, p. 125-209.
- Willden, R., 1958, Cretaceous and Tertiary orogeny in Jackson Mountains, Humboldt County, Nevada: American Association of Petroleum Geologists Bulletin, v. 42, p. 2378–2398.
- Willden, R., 1963, General Geology of the Jackson Mountains, Humboldt County, Nevada: U.S. Geological Survey Bulletin 1141-D, 65 p.
- Wright, J. E., and Faham, M. R., 1988, An expanded view of Jurassic orogenesis in the western United States Cordillera: Middle Jurassic (pre-Nevadan) regional metamorphism and thrust faulting within an active arc environment, Klamath Mountains, California: Geological Society of America Bulletin, v. 100, p. 859–876.

Wyld, S.J., Umhoefer, P.J., and Wright, J.E., 2006, Reconstructing northern Cordilleran terranes along known Cretaceous and Cenozoic strike-slip faults: Implications for the Baja British Columbia hypothesis and other models, *in* Haggart, J.W., Enkin, R.J., and Monger, J.W.H., eds., Paleogeography of the North American Cordillera: Evidence For and Against Large-Scale Displacements: Geological Association of Canada Special Paper 46, p. 277–298.

CHAPTER TWO: EARLY CRETACEOUS (~118 MA) SYNDEPOSITIONAL
SHORTENING IN THE CENTRAL CORDILLERAN HINTERLAND, JACKSON
MOUNTAINS, NORTHWEST NEVADA, USA

Abstract

New geologic mapping and structural observations combined with high-precision U-Pb zircon geochronology provide strong evidence for Early Cretaceous (~118 Ma), ~NW-directed shortening in the Jackson Mountains of northwest Nevada. Detailed mapping consistently reveals a shallow SE-dipping contact that places the older Happy Creek Igneous Complex over the King Lear Formation. Three-point analysis of this contact reveals a surface with an orientation of ~N22E, 19SE. Within the King Lear Formation, pervasive thrust-sense slickenside surfaces on minor shear fractures are documented near this contact. NW-vergent growth folds within the King Lear Formation confirm syndepositional shortening of the basin. Overall, these observations suggest a shallow SE-dipping thrust fault that placed the Happy Creek Igneous Complex over the King Lear Formation (ca. 118 Ma), as dated by U-Pb zircon geochronology of a felsic tuff in the upper Clover Creek member. Given the gentle folding of this tuff overlying more tightly folded strata, we interpret shortening to have initiated prior to ~118 Ma but may not have continued for considerably longer. New detrital zircon data document the changing provenance that we interpret to be associated with continued slip and topographic isolation of the King Lear basin. Based on regional geologic and tectonic

relationships, shortening in the hinterland is tied to a significant change in plate motions. We interpret Early Cretaceous NW-SE directed shortening in the Jackson Mountains to reflect out-of-sequence thrusting associated with internal shortening of the hinterland in response to a change in the Pacific-Farallon-North American velocity structure.

Introduction and Background

The Cretaceous geology and tectonics of the United States Cordillera was largely influenced by the east-directed subduction of the Farallon plate beneath North America [e.g. Burchfiel & Davis, 1972; Oldow et al., 1989; Burchfiel, Cowan, & Davis, 1992; Cowan & Bruhn, 1992; DeCelles, 2004; Dickinson, 2004; Snee, 2005]. The general results of this convergence were accretion at the margin (i.e. Franciscan belt), the deposition of sedimentary strata in the forearc (i.e. Great Valley Sequence), voluminous arc magmatism (i.e. the Sierra Nevada and Idaho batholiths), retroarc shortening, and foreland sedimentation related to the Sevier orogeny (Fig. 2.1) [e.g. Burchfiel et al., 1992; Dickinson, 2004; Martin et al., 2010]. While the Cretaceous Period is well represented in other portions of the arc-system (e.g. forearc, arc, foreland), very little is known about the backarc/hinterland region due primarily to the small amount of preserved supracrustal strata [e.g. Martin et al., 2010; Long et al., 2014]. Therefore, the Early Cretaceous King Lear Formation, found primarily in the Jackson Mountains, provides a rare and valuable glimpse into the Cretaceous tectonic evolution of this underrepresented and understudied region (Fig. 2.1).

During reconnaissance mapping, Willden [1958; 1963] noticed that the Happy Creek Igneous Complex had overrode the Early Cretaceous King Lear Formation along the E-dipping Deer Creek thrust, named for its excellent exposure to the SE of Deer

Creek Peak (Fig. 2.2a). Based on the identification of Early Cretaceous freshwater gastropods, Willden [1958; 1963] argued for post-Early Cretaceous shortening affecting the region. This interpretation was supported by the work of Russell [1981; 1984] and Maher [1989]. More recently however, Quinn [1996], Quinn, Wright, & Wyld [1997], and Martin et al. [2010] have argued for an opposing view in which the King Lear Formation has never experienced contractional deformation. Furthermore, these authors interpret the E-dipping Deer Creek thrust to instead be a steeply W-dipping normal fault named the Delong Peak fault (Fig. 2.2b). Martin et al. [2010] provided a seismic section from the central Jackson Mountains that claimed to image a steeply W-dipping reflector that they interpret as the Delong Peak fault of Quinn [1996] and Quinn et al. [1997]. While a faint W-dipping reflector is plausible, the seismic section did not extend to the east of the surface expression of the fault to account for a possible E-dipping reflector (Fig. 2.2b).

In this manuscript we first briefly summarize the regional and local geologic setting of the Jackson Mountains. Following this, we discuss the on-going debate regarding evidence for or against the existence of Cretaceous contractional deformation in the Jackson Mountains. We then provide the results of new geologic mapping and U-Pb zircon geochronology to provide strong evidence for at least one phase of Early Cretaceous shortening in the Jackson Mountains. Finally, we explore the potential implications and causes of Early Cretaceous shortening in this portion of the North American Cordillera (Fig. 2.1).

General Geology of the Jackson Mountains

The Jackson Mountains are a ~50 km long N-NE oriented mountain range in the Black Rock Desert region of northwestern Nevada (Fig. 2.1). Overall, the geology of the Jackson Mountains is dominated by four main rock groups: 1) a Paleozoic section of metasedimentary and metavolcanic rocks, 2) a Late Triassic to Early Jurassic succession of pelagic, carbonate, and volcanogenic rocks (the Boulder Creek Beds), 3) Jurassic mafic to intermediate volcanic and intrusive rocks (the Happy Creek Igneous Complex and Early Mesozoic Intrusive Suite), and 4) the Early Cretaceous sedimentary rocks of the King Lear Formation (Fig. 2.3) [Willden, 1958; Willden, 1963; Russell, 1981; Russell, 1984; Maher, 1989; Quinn, 1996; Quinn et al., 1997]. For the purpose of this paper, we will briefly discuss the geology of the Happy Creek Igneous Complex and the King Lear Formation, however more detailed descriptions can be found in the aforementioned references.

Happy Creek Igneous Complex and Early Mesozoic Intrusive Suite

An examination of previous studies reveals several interpretations regarding which rocks and rock types are actually included in the Happy Creek Igneous Complex [Willden, 1958; Willden, 1963; Russell, 1981; Russell, 1984; Maher, 1989; Quinn, 1996; Quinn et al., 1997]. We refer the reader to Quinn et al. [1997] for an exhaustive examination of this problem. Here, we describe the Happy Creek Igneous Complex to include an assemblage of Early Jurassic mafic to intermediate volcanic, volcaniclastic, and intrusive rocks that generally lie within the center of the Jackson Mountains. Rock types in this unit include a package of subgreenschist-facies, fine-grained volcanic and intrusive rocks ranging in composition from basaltic andesite to andesite, in addition to

packages of volcaniclastic strata that include conglomerate, breccia, sandstone, and mudstone [Russell, 1981; 1984; Quinn, 1996; Quinn et al., 1997]. Coupled with several gabbroic to granodioritic intrusive bodies of the Early Mesozoic Intrusive Suite, these rocks are interpreted to reflect Mesozoic arc volcanism in either a continental [Quinn, 1996; Quinn et al., 1997] or intraoceanic arc setting [Russell, 1981; 1984].

King Lear Formation

Willden [1958] provided the first descriptions of the Early Cretaceous King Lear Formation as a package of nonmetamorphosed, locally derived clastic rocks that include pebble to boulder conglomerate with interbedded siltstone and greywacke along with lenses of limestone. Age constraints were based on the recognition of mid-Early Cretaceous freshwater gastropods [Willden 1958; 1963]. More recent work by Martin et al. [2010] subdivided this unit into the basal Jackson Creek member, the middle Quartzite-Chert member, and the upper Clover Creek member (Fig. 2.4). The Jackson Creek member consists of locally derived strata ranging from boulder conglomerate to fine sandstone with occasional interbedded freshwater limestone (Fig. 2.4) [Willden, 1958; Martin et al., 2010]. Clasts within the Jackson Creek member are dominated by lithologies derived from the Happy Creek Igneous Complex and plutons of the Early Mesozoic Intrusive Suite [Martin et al., 2010]. The Quartzite-Chert member consists of boulder to granule conglomerate, sandstone, and siltstone with roughly ~80% of clasts originating from external sources [Martin et al., 2010]. Finally, the Clover Creek member consists primarily of interbedded sandstone, siltstone, and breccia with rare occurrences of conglomerate and limestone (Fig. 2.4) [Martin et al., 2010]. Clasts within the Clover Creek member are dominated by dacitic volcanic lithics and plagioclase crystal clasts

sourced from the nearby syndepositional Clover Creek volcanic center [Martin et al., 2010]. Also found within the Clover Creek member is a felsic volcanic tuff (KLT) that was sampled in this study for U-Pb zircon geochronology as discussed later (Fig. 2.4).

Based on the descriptions summarized above, Martin et al. [2010] interprets the Early Cretaceous depositional environment for the King Lear Formation as follows. First, deposition of the Jackson Creek member in a proximal alluvial fan environment with intermittent freshwater lakes, with debris being shed from the uplifted Happy Creek Igneous Complex and Early Mesozoic Intrusive Suite [Willden, 1958; Martin et al., 2010]. This was then followed by deposition of the Quartzite-Chert member in a braided fluvial system bringing detritus from external sources [Martin et al., 2010]. Finally, the Clover Creek member represents a return to proximal alluvial fan deposition with debris being shed from the active Clover Creek volcanic center [Martin et al., 2010].

Structural Geology of the Jackson Mountains

Structurally, the Jackson Mountains have experienced at least one, and perhaps multiple episodes of Mesozoic shortening that have resulted in the production of folds, thrusts, and associated cleavage. In light of this complicated history, previous work done in the Jackson Mountains has resulted in several interpretations regarding the structural history (Fig. 2.5) [Russell, 1981; 1984; Maher, 1989; Quinn, 1996; Quinn et al., 1997]. Russell [1981; 1984] concluded that several episodes of contractional deformation affected the Jackson Mountains between Middle Jurassic and mid-Cretaceous time. Between Middle Jurassic and Early Cretaceous time, SW-NE directed shortening produced broad, open folding (Fig. 2.5) [Russell, 1984]. Then, in Early Cretaceous time, SE-NW directed shortening resulted in the production of cleavage, thrusts, and folds (Fig.

2.5) [Russell, 1984]. Furthermore, Russell [1981; 1984] concluded that during this Early Cretaceous phase of shortening, local intermontane basins were formed in which the fluvial sediments of the King Lear Formation were deposited and deformed. Following these episodes, a late-Early to mid-Cretaceous phase of thrusting affected those earlier structures formed in the Early Cretaceous phase (Fig. 2.5) [Russell, 1981; 1984]. Maher [1989] concluded that a period of Middle Jurassic sinistral wrench faulting was followed by a period of late Middle to Late Jurassic E-vergent folding and thrusting (Fig. 2.5). This was then followed by a period of late-Early Cretaceous W and E-vergent thrusting (Fig. 2.5) (Maher, 1989). Generally speaking, this interpretation is compatible with that of Russell [1981; 1984]. Quinn [1996] and Quinn et al. [1997] however presented an alternative interpretation that concluded all contractional deformation in the Jackson Mountains was pre-Cretaceous time (Fig. 2.5). Furthermore, Quinn [1996] and Quinn et al. [1997] removed many of the thrust faults mapped by previous workers leaving only a single belt of Late Triassic to Early Jurassic thrusts on the west side of the range. The argument for this reinterpretation was that the Happy Creek Igneous Complex was primarily an intrusive unit. Along these lines, older over younger geologic relationships in the Jackson Mountains were explained by younger intrusive rocks intruding into and crosscutting older units without the need to invoke thrust faults [Quinn, 1996; Quinn et al., 1997].

Another conclusion of Quinn [1996] and Quinn et al. [1997] was that the King Lear Formation had never experienced shortening deformation and therefore contraction in the Jackson Mountains did not continue into the Early Cretaceous. These authors argued that previous workers misinterpreted the existence of Cretaceous shortening by

wrongly including deformed supracrustal rocks of the Happy Creek Igneous Complex as part of the King Lear Formation.

Observations

Deer Creek Thrust

As discussed above, Willden [1958] first recognized during early mapping that the metamorphosed volcanic and volcaniclastic rocks of the Happy Creek Igneous Complex had overrode the unmetamorphosed clastic rocks of the King Lear Formation along a feature he termed the Deer Creek thrust (Fig. 2.2a). However, later authors argued against this interpretation and envision the Deer Creek thrust to instead be a steeply west-dipping normal fault that has down dropped the King Lear Formation relative to the Happy Creek Igneous Complex (Fig. 2.2b) [Quinn, 1996; Quinn et al., 1997; Martin et al., 2010].

Figure 2.3 shows the results of new geologic mapping and detailed Happy Creek-King Lear contact investigations in the central Jackson Mountains. Although the nature of the contact is commonly obscured, an investigation of the relationship between the contact and how it interacts with topography reveals information on its orientation. In the vicinity of Deer Creek Peak, where Willden (1958; 1963) first named this fault, the Happy Creek Igneous Complex clearly overlies the King Lear Formation (Figs. 2.3, 2.6a, and 2.6b). Furthermore, a graphical three point analysis of the contact in this location estimates a surface dipping $\sim 19^\circ$ to the SE (Fig. 2.7). To the SW, near Parrot Peak, contact/topography relationships again point to the Happy Creek Igneous Complex overlying the King Lear Formation along a gently SE dipping contact (Figs. 2.3 & 2.6c). Even further to the SW, in the Delong Peak area, contact/topography relationships again

imply that the Happy Creek Igneous Complex directly overlies the King Lear Formation (Figs. 2.3 & 2.6d). In all instances, a surface dipping steeply to the west is not compatible with the observed contact/topography relationships. Moreover, the geologic relationships described above require an older (Happy Creek Igneous Complex) over younger (King Lear Formation) relationship.

Subsidiary Fault Surfaces

During geologic mapping, the authors noted the presence of numerous dip-slip slickensided fault surfaces in the King Lear Formation (Fig. 2.8). In outcrop, these surfaces can be followed for up to ~10 m with an anastomosing geometry that at times represents the contact between conglomerate and siltstone while at other times are wholly within conglomerate. In a stereonet analysis, the average orientation of these fault surfaces is N44E, 35SE with down-dip slicks raking ~84° from the SW (35° at S41E) in the fault surface (Fig. 2.8). Unfortunately, due to erosion and preservation the authors were unable to determine the sense of slip (i.e. normal vs. thrust) using the slickensided surfaces. However, in the Deer Creek Peak region, a small offset (~30 cm) was identified showing thrust sense of motion on one of these fault surfaces (Fig. 2.8). Further to the south, near Delong Peak, the authors also identified a small thrust fault and drag fold within the King Lear Formation.

Folding Within the King Lear Formation

In the central Jackson Mountains, the King Lear Formation is folded into an anticline-syncline pair of open, moderately-inclined, moderately-plunging folds trending ~NE-SW with axial surfaces dipping ~60 SE. These relationships are shown on the map in Figure 2.3 and in the photo and stereonet analyses in Figure 2.9.

U-Pb Zircon Geochronology

To investigate the age and sedimentary provenance of the King Lear Formation with the goal of helping to constrain the timing and style of Cretaceous deformation, we collected samples of a felsic tuff (KLT) and two sandstones (KLS-1 and KLS-2) from the King Lear Formation for high-precision U-Pb zircon geochronology. Additionally, we collected and processed two intrusive rocks from the Early Mesozoic Intrusive Suite (i.e. Parrot Peak pluton (PPP) and Prospect Springs pluton (PSP)) to further investigate local provenance. Sample locations can be found in Table 2.1 and Figure 2.3. Processing and analysis of the samples using both laser ablation-inductively coupled plasma mass spectrometry (LA-ICPMS) and chemical abrasion-isotope dilution thermal ionization mass spectrometry (CA-IDTIMS) took place at Boise State University following the methods described in Davydov et al. (2010) and Rivera et al. (2016). In the following section, we present our new results and age determinations for the felsic tuff, detrital zircon samples, and plutons.

King Lear Tuff

Geologic mapping by Quinn [1996] and Quinn et al. [1997] first identified this felsic tuff horizon in the central Jackson Mountains (Fig. 2.3). Based on its position ~200-300 m above the base of the King Lear Formation, these authors placed the unit within the lower section of the Formation. However, later, more-detailed mapping and subdivision of the King Lear Formation by Martin et al. [2010] instead placed this tuff in the upper section of the Formation within the Clover Creek Member (Fig. 2.4).

Quinn [1996] and Quinn et al. [1997] not only identified the King Lear tuff but also provided the first attempt at constraining its age using U-Pb zircon geochronology.

By fitting a discordia trajectory through recent Pb loss on a Terra-Wasserburg diagram of four multi-grain zircon size fractions, these authors concluded an age of 125 ± 1 Ma [Quinn et al., 1997]. However, these ages were obtained from ~3 to 12 mg bulk samples of zircon, which unfortunately likely reflect a mixture of ages that potentially include inherited cores as well as grains that may have experienced significant Pb-loss. Furthermore, these authors reported the $^{207}\text{Pb}/^{206}\text{Pb}$ ages whereas the $^{206}\text{Pb}/^{238}\text{U}$ ages would be more appropriate for Mesozoic rocks [Gehrels, 2012].

We applied a more accurate and precise method of single-grain U-Pb zircon analysis using both LA-ICPMS and CA-IDTIMS in tandem on the same crystals. Our analysis of the King Lear tuff provides a date of 119.1 ± 0.8 Ma from 47 analyses using LA-ICPMS (Fig. 2.10). From these grains, seven were selected for further processing using the more precise and accurate CA-IDTIMS [e.g. Krogh, 1973; Mattinson, 2005]. In selecting these grains, we targeted dates from the younger tail of LA-ICPMS data and used cathodoluminescence (CL) images to identify grains with relatively simple growth histories while avoiding grains with obvious cores and complicated growth zones. Four grains yielded concordant and equivalent isotope ratios with a weighted mean $^{206}\text{Pb}/^{238}\text{U}$ date of 118.57 ± 0.04 Ma (2σ , MSWD = 0.5, prob. fit = 0.6790) while three grains yielded slightly older dates suggesting minor inheritance (Fig. 2.10; Table 2.1). Therefore, we interpret the weighted mean date as the eruption and deposition age of the King Lear tuff in the Aptian Stage. Our new analysis of the King Lear tuff yields an age ~7 Ma younger than previously reported by Quinn et al. [1997].

King Lear Sandstones

Our sampling of sandstones from the King Lear Formation was aimed at documenting any significant changes in detrital zircon provenance to assist in our understanding of King Lear basin evolution. As such, we sampled a medium-grained sandstone from near the base of the Formation from within the Jackson Creek member exposed near Deer Creek Peak (KLS-2) and a medium- to coarse-grained sandstone from near the top of the Formation from the Clover Creek member exposed in the central Jackson Mountains (KLS-1) (Fig. 2.3 and 2.4).

Sample KLS-2 from near the base of the King Lear Formation contains a multimodal U-Pb age probability density function with dominate modes centered at ~157 Ma (Late Jurassic), ~186 Ma (Early Jurassic), ~272 Ma (Middle Permian), and ~321 Ma (Early Pennsylvanian) with minor modes at ~356 Ma (Early Mississippian) and ~420 Ma (Silurian) (Fig. 2.11), and 15 grains ranging in age from 539–1690 Ma

Sample KLS-1 from near the top of the King Lear Formation contains a roughly bimodal probability distribution with dominate modes centered at ~116 Ma (Early Cretaceous) and ~160 Ma (Late Jurassic) (Fig. 2.11) with 14 grains ranging in age from 192–2652 Ma. Four grains were then selected from the ~116 Ma peak for CA-IDTIMS to investigate provenance and maximum depositional age. These grains yielded ages of 119.02 ± 0.09 Ma, 118.93 ± 0.09 Ma, 118.89 ± 0.06 Ma, and 118.81 ± 0.09 Ma (Fig. 2.11).

Early Mesozoic Intrusive Suite

Parrot Peak Pluton

Our analysis of the Parrot Peak pluton yields a date of 188.0 ± 1.1 Ma from 65 analyses using LA-ICPMS (Fig. 2.12). From these grains, five were selected for further processing using CA-IDTIMS following the methods described above for the King Lear tuff [e.g. Krogh, 1973; Mattinson, 2005]. All five grains yielded concordant and equivalent isotope ratios with a weighted mean $^{206}\text{Pb}/^{238}\text{U}$ date of 190.28 ± 0.07 Ma (2σ , MSWD = 1.14, prob. fit = 0.3347) (Fig. 2.12; Table 2.1). We interpret this Early Jurassic CA-IDIMS weighted mean date as the emplacement age of the Parrot Peak pluton.

Prospect Springs Pluton

Our analysis of the Prospect Springs pluton yields a date of 158.6 ± 3.1 Ma from 10 analyses using LA-ICPMS (Fig. 2.13). From these grains, five were selected for further processing using CA-IDTIMS [e.g. Krogh, 1973; Mattinson, 2005]. These five grains yielded concordant and equivalent isotope ratios with a weighted mean $^{206}\text{Pb}/^{238}\text{U}$ date of 160.72 ± 0.06 Ma (2σ , MSWD = 1.36, prob. fit = 0.2454) (Fig. 2.13; Table 2.1), therefore, we interpret this Late Jurassic weighted mean date as the emplacement age of the Prospect Springs pluton.

Discussion

As mentioned previously, the recognition of Early Cretaceous compressional deformation in the Jackson Mountains hinges upon an understanding of the contact geometry between the Happy Creek Igneous Complex and King Lear Formation. In this regard, a roughly east-dipping contact would place the Early Jurassic Happy Creek Igneous Complex above the Early Cretaceous King Lear Formation, a relationship that

demands a thrust fault [e.g. Willden 1958; 1963]. On the other hand, a west dipping contact would suggest a steeply dipping normal fault [Quinn, 1996; Quinn et al., 1997; Martin et al., 2010]. As we present here, this interpretation of a west-dipping normal fault is not consistent with and furthermore is in direct conflict with geologic relationships found in the study area. A detailed investigation of this contact geometry demands that the Happy Creek Igneous Complex overlies the King Lear Formation along an east dipping contact (Fig. 2.6). Graphical three point analysis of this contact confirms that it dips $\sim 19^\circ$ to the SE (Fig. 2.7). Additionally, Russell (1984) used the orientation of Paleogene and Neogene volcanics to estimate that Cenozoic tilting in the central Jackson Mountains is not “significant” and is less than the 15° E tilt found to the north of the study area. Therefore, later Cenozoic tilting associated with Basin and Range extension has not significantly changed the geometry of the contact in question. These observations, combined with the identification of numerous thrust sense subsidiary faults (Fig. 2.8) in the King Lear Formation supports the conclusion that the Happy Creek Igneous Complex has indeed overrode the King Lear Formation along the shallowly E-dipping, top to the NW, Deer Creek thrust as first suggested by Willden [1958; 1963]. Additionally, the orientation and sense of slip along these subsidiary fault surfaces is consistent with the expected orientation of P-shears in the Riedel Shear Model [e.g. Riedel, 1929; Logan et al., 1979; Katz, Weinberger, & Aydin, 2004].

New geologic mapping in the central Jackson Mountains identifies a pair of NE-trending folds within the King Lear Formation where the intensity of folding decreases up section (Fig. 2.9). This relationship implies active folding during deposition of the King Lear Formation whereby the older, lowermost strata are more tightly folded than the

younger, uppermost strata. Furthermore, the NW-vergence implied by the orientation of these folds is compatible with the top to the NW movement on the Deer Creek thrust and subsidiary faults (Figs. 2.8 and 2.9). As such, we argue that these structures formed together during a period of Early Cretaceous NW-directed shortening.

To provide constraints on the timing of this episode of shortening in the Jackson Mountains, we refer to our new high-precision U-Pb zircon age of 118.57 ± 0.04 Ma for the King Lear tuff from the upper section of the King Lear Formation (Fig. 2.10). The location of the King Lear tuff near the top of the King Lear Formation is an important marker that provides insight into the youngest portions of the unit. Furthermore, as discussed above, we interpret shortening in the Jackson Mountains to be contemporaneous with deposition of the King Lear Formation. Therefore, the age of the King Lear tuff not only constrains the age of the youngest portions of the King Lear Formation but also provides an age of active shortening in the Jackson Mountains. While we are unable to tightly constrain the exact start, end, and total duration of this structural event, we are able to conclude that shortening was active sometime in the Early Cretaceous prior to and after ~ 118 Ma as discussed below.

Structural and Stratigraphic Model

The following model constructs an explanation for the structural and stratigraphic evolution of the King Lear basin and Deer Creek thrust that adheres to our new geologic mapping, structural observations, U-Pb zircon geochronology, and existing stratigraphic observations. While variations to this model may work with our data, the following is our preferred interpretation of the Early Cretaceous structural and stratigraphic history of the King Lear basin.

In Early Cretaceous time and prior to ~118 Ma, movement along the Deer Creek thrust initiated, possibly as a blind thrust, that resulted in the development of local topography and accommodation space for early sediments of the King Lear Formation (Fig. 2.14a). At this time, the Jackson Creek member of the King Lear Formation was being deposited and receiving detritus from both uplifted local and regional sources (Fig. 2.14a). Martin et al. [2010] described the Jackson Creek member as consisting of predominantly locally derived clasts of Happy Creek Igneous Complex and plutons from the Early Mesozoic Intrusive Suite deposited in alluvial fan type settings. Our new detrital zircon data support this interpretation; sandstone KLS-2 contains abundant detrital zircons at ~157 Ma likely sourced from the Prospect Springs pluton and ~186–195 Ma likely sourced from the Parrot Peak pluton. Also during this early phase, the King Lear Formation was being actively folded during deposition (i.e. NW-vergent growth folds). Still prior to 118 Ma, deformation and movement along the Deer Creek thrust continued to fold the King Lear Formation. During this time, regional uplift and/or continued subsidence in the King Lear basin was conducive to allowing more external sources of sediment into the basin (i.e. Quartzite-Chert member in a braided fluvial setting) (Fig 2.14b).

By ~118 Ma, the King Lear basin sees a significant change in sediment source and detrital zircon provenance. Martin et al. [2010] described the Clover Creek member as dominated by volcanic lithics shed from the adjacent syndepositional Clover Creek volcanic complex. Our new detrital zircon data for KLS-1 supports this observation with significant peaks at ~116 Ma and ~160 Ma (Fig. 2.11). Further CA-IDTMS work on the youngest grains from the ~116 Ma peak yields ages between 119.02 and 118.81 Ma that

we interpret to have been sourced from the same volcanic center as the King Lear tuff, likely the Clover Creek volcanic complex (Figs. 2.11 and 2.14c). A likely source for the ~160 Ma grains is the Prospect Springs pluton and associated plutons of the Early Mesozoic Intrusive Suite (Fig. 2.14c). We interpret this change in sedimentary and zircon provenance to strictly local sources to reflect continued movement along the Deer Creek thrust and topographic isolation of the King Lear basin (Fig. 2.14c). While speculative, movement along the Deer Creek thrust may not have continued much past ~118 Ma due to the gentle folding of the King Lear tuff and overlying section.

Regional Implications

To place this event into a larger context and investigate some possible driving mechanisms, we will first look into some significant, temporally overlapping changes and events occurring to the west (i.e. continental-arc system) and the east (i.e. Sevier orogenic belt and adjacent hinterland). After exploring these adjacent systems, we will attempt to place shortening in the Jackson Mountains into this regional framework and investigate some potential driving mechanisms to initiate shortening in this portion of the Cordillera.

Early Cretaceous Continental-Arc System

When considering some potential drivers for ~118 Ma shortening in the Jackson Mountains, an appropriate starting point is the tectonics of the adjacent plate boundary. Early Cretaceous paleogeographic reconstructions of the Central Cordillera place the main axis of a continental-arc system to the west of the Jackson Mountains. From west to east, the Franciscan belt, the Great Valley Sequence, and the Sierra Nevada batholith (Fig. 2.1) represent a coeval accretionary prism, forearc basin, and magmatic arc

associated with subduction of the Farallon plate beneath western North America [e.g. Ernst, 1970; Burchfiel et al., 1992; Dickinson, 2004].

Utilizing U-Pb detrital zircon and $^{40}\text{Ar}/^{39}\text{Ar}$ dating of metamorphic white micas, Dumitru et al. [2010] argued that the Franciscan belt experienced a significant shift from predominantly non-accretionary to accretionary behavior at ~ 123 Ma (Fig. 2.15). While exploring some possible mechanisms for this shift in behavior, these authors noted a series of adjacent coeval events at ~ 123 Ma in the Great Valley Sequence and Sierran arc. Within the northern Coast Ranges, Dumitru et al. [2010] referenced an important petrofacies change in Great Valley strata near the Barremian-Aptian stage boundary (~ 125 Ma) that probably reflects changing tectonics in the Klamath and Sierran source areas (Fig. 2.15) [e.g. Ingersoll, 1983]. Corresponding temporally with this petrofacies change, a major structural-stratigraphic discontinuity is found in most of the northern Great Valley whereby strata found below this discontinuity exhibit faulting, broad warping, and/or moderate erosion (Fig. 2.15) [Dumitru et al., 2010; Constenius et al., 2000]. To the east, in the Sierran magmatic arc, a major increase in intrusion rates began at ~ 122 Ma following the “magmatic lull” (Fig. 2.15) [Barton et al., 1988; Armstrong & Ward, 1993; Dumitru et al., 2010]. Furthermore, Ducea [2001] noted an episode of lower crustal ductile deformation in the southern Sierran arc from ~ 125 – 103 Ma (Fig. 2.15) [Dumitru et al., 2010]. Taken together, Dumitru et al. [2010] suggested the roughly coeval changes in the Franciscan belt, Great Valley Sequence, and Sierran arc may have been associated with a ~ 123 Ma change in Pacific plate motion from a predominantly southerly direction to more northerly (Fig. 2.15) [Sager, 2007]. As discussed before, we unfortunately cannot tightly constrain the timing of the initiation of shortening in the

Jackson Mountains but can conclude that shortening was active prior to and after ~118 Ma (Fig. 2.14). Therefore, these significant Early Cretaceous [~123–122 Ma] changes in the arc system, possibly related to a change in the Pacific-Farallon-North American plate motions, correspond temporally with shortening in the Jackson Mountains to the east.

Sevier Orogenic Belt and Adjacent Hinterland

Early Cretaceous supracrustal strata deposited within the backarc/hinterland region of Nevada is limited to the Newark Canyon Formation exposed near Eureka, NV and the King Lear Formation (this study). With such a limited dataset to investigate, we find it necessary here to briefly review the geologic, structural, and tectonic history of the Newark Canyon Formation to provide insight into the tectonics of the hinterland region.

The Newark Canyon Formation, much like the King Lear Formation, is predominantly composed of alternating beds of conglomerate, sandstone, siltstone, and limestone deposited in a fluviolacustrine environment [Nolan, 1962]. Age constraints, based on biostratigraphy, assign an Aptian-Albian age to the Formation (Fig. 2.15) [MacNeil, 1939; Smith & Ketner, 1976; Fouch, Hanley, & Forester, 1979; Swain, 1999]. More recent U-Pb zircon work by Druschke et al. [2011] constrained the depositional age further by the identification of a 116.1 ± 1.6 Ma waterlain tuff and a sandstone with a ~121 Ma youngest detrital zircon mode. In terms of tectonic setting, the Newark Canyon Formation has been interpreted as a series of piggyback basins associated with the “Eureka” or “Central Nevada” thrust belt [e.g. Vandervoort, 1987; Taylor et al., 1993]. More recent work by Long et al. [2014] presents a strong case that the Newark Canyon Formation was deposited and simultaneously folded in a piggyback basin on the eastern limb of the east-vergent Eureka culmination. Furthermore, deposition and deformation of

the Newark Canyon Formation overlaps temporally with movement in the Sevier fold-and-thrust belt along the Canyon Range thrust (Fig. 2.15) [e.g. DeCelles & Coogan, 2006; Long et al., 2014]. Therefore, the growth of the Eureka culmination represents out-of-sequence thrusting and may have been in response to internal shortening of the Sevier orogenic wedge to promote eastward movement along the Canyon Range thrust [Long et al., 2014].

As outlined above, the petrology, age, depositional setting, and syndepositional contraction observed in the Newark Canyon Formation correlates with the history of the King Lear Formation we have described previously. Taken together, we propose that the temporally overlapping nature and kinematic compatibility of these events strongly suggests a fundamental relationship whereby shortening in the hinterland (i.e. Eureka culmination and Jackson Mountains) is tied to a significant change in plate motions. Therefore, we interpret Early Cretaceous NW-SE directed shortening in the Jackson Mountains to reflect out-of-sequence thrusting associated with internal shortening of the hinterland in response to a change in the Pacific-Farallon-North American velocity structure. In modern geometry, the Deer Creek thrust would therefore represent a back-thrust that overall assisted in shortening the orogenic wedge.

Summary and Conclusions

New geologic mapping and structural observations coupled with new high-precision U-Pb zircon geochronology provide strong evidence for Early Cretaceous (~118 Ma), ~NW-directed shortening in the Jackson Mountains of northwest Nevada. New mapping of the Happy Creek Igneous Complex-King Lear Formation contact geometry in the northern and central part of the Jackson Mountains consistently indicates

a shallow easterly-dipping contact that places the older Happy Creek Igneous Complex over the King Lear Formation. Three-point analysis of this contact reveals a surface with an orientation of ~ N22E, 19SE, with pervasive thrust-sense slickenside surfaces on minor shear fractures near the contact. NW-vergent growth folds within the King Lear Formation confirm syndepositional shortening of the basin. Overall, these new observations suggest a shallowly east-dipping thrust fault that placed the Happy Creek Igneous Complex over the King Lear Formation ca. 118 Ma, as dated by U-Pb zircon geochronology of a felsic tuff in the upper Clover Creek member. Given the gentle folding of this tuff overlying more tightly folded strata, we interpret shortening to have initiated prior to ~118 Ma but may have not continued for considerably longer. New detrital zircon data document the changing provenance that we interpret to be associated with continued slip and topographic isolation of the King Lear basin, in its evolution as a piggy-back basin developed through out-of-sequence thrusting in the Sevier orogenic wedge.

Acknowledgements

Work related to this study was partially funded by Willis and Rose Burnham Graduate Student Research Grant of the Department of Geosciences, Boise State University.

Table 2.1. Summary of Samples and Corresponding $^{206}\text{Pb}/^{238}\text{U}$ ages

Sample Name	Geologic Map Unit	UTM Coordinates	$^{206}\text{Pb}/^{238}\text{U}$ Age (Ma)	MSWD	Prob. Of Fit	n
KLT-1	King Lear Formation	11T 379770 E 4573034 N	118.57 ± 0.04	0.5	0.679	4
KLS-1	King Lear Formation	11T 379924 E 4573077N				
KLS-2	King Lear Formation	11T 379777 E 4582644 N				
PPP-1	Parrot Peak Pluton	11T 373370 E 4580118 N	190.28 ± 0.07	1.14	0.3347	5
PSP-1	Prospect Springs Pluton	11T 380114 E 4582923 N	160.72 ± 0.06	1.36	0.2454	5

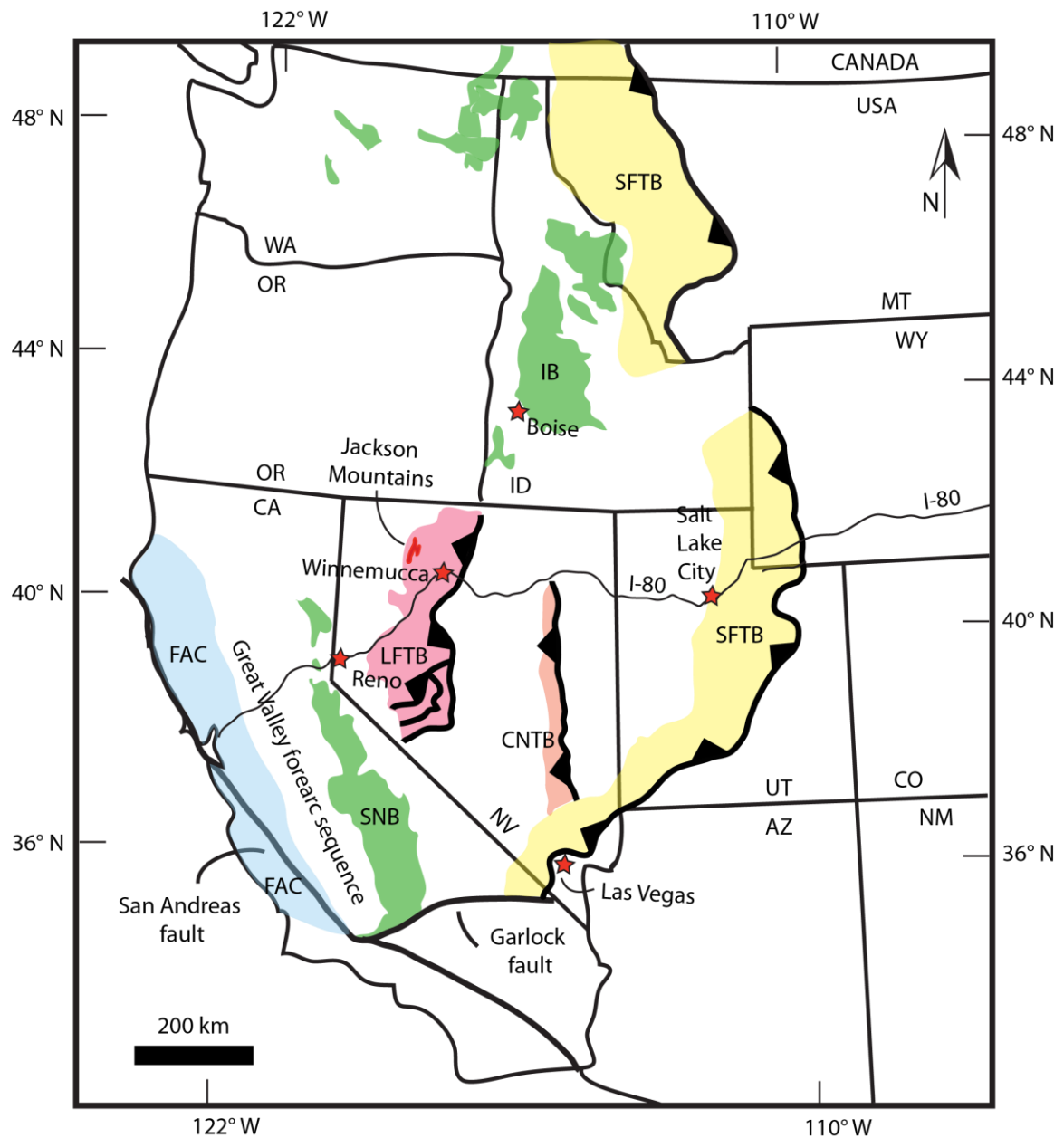


Figure 2.1. Generalized Geotectonic Map of the Western United States. Simplified to show the major elements of the Cordilleran arc and retroarc regions. Not palinspastically restored. Modified from DeCelles & Coogan (2006), Dumitru et al. (2010), Ernst, (2011), LaMaskin et al. (2011), Long et al. (2014). Abbreviations are as follows: FAC = Franciscan accretionary complex, SNB = Sierra Nevada batholith, LFTB = Luning-Fencemaker fold-thrust belt, CNTB = Central Nevada thrust belt, SFTB = Sevier fold-thrust belt (expanded), IB = Idaho batholith.

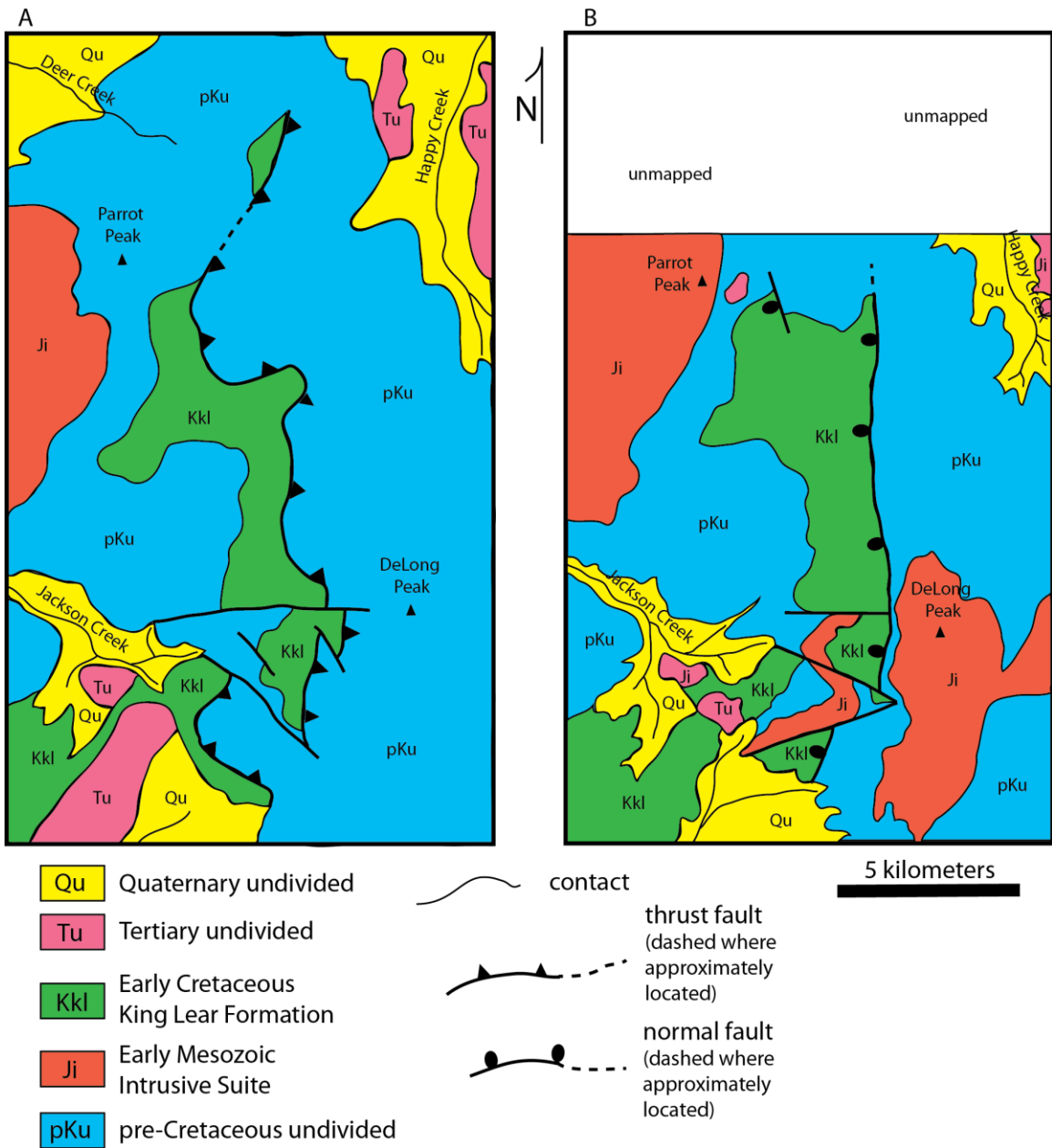


Figure 2.2. Simplified Geologic Maps Modified from (A) Willden (1958) and (B) Quinn et al. (1997) of the Central Portion of the Jackson Mountains. Both maps have been scaled the same to highlight the different interpretations surrounding the upper contact between the King Lear Formation and pre-Cretaceous rocks (mostly Happy Creek Igneous Complex). Note the thrust fault (i.e. the Deer Creek thrust) in (A) and the normal fault (i.e. the DeLong Peak fault) in (B).

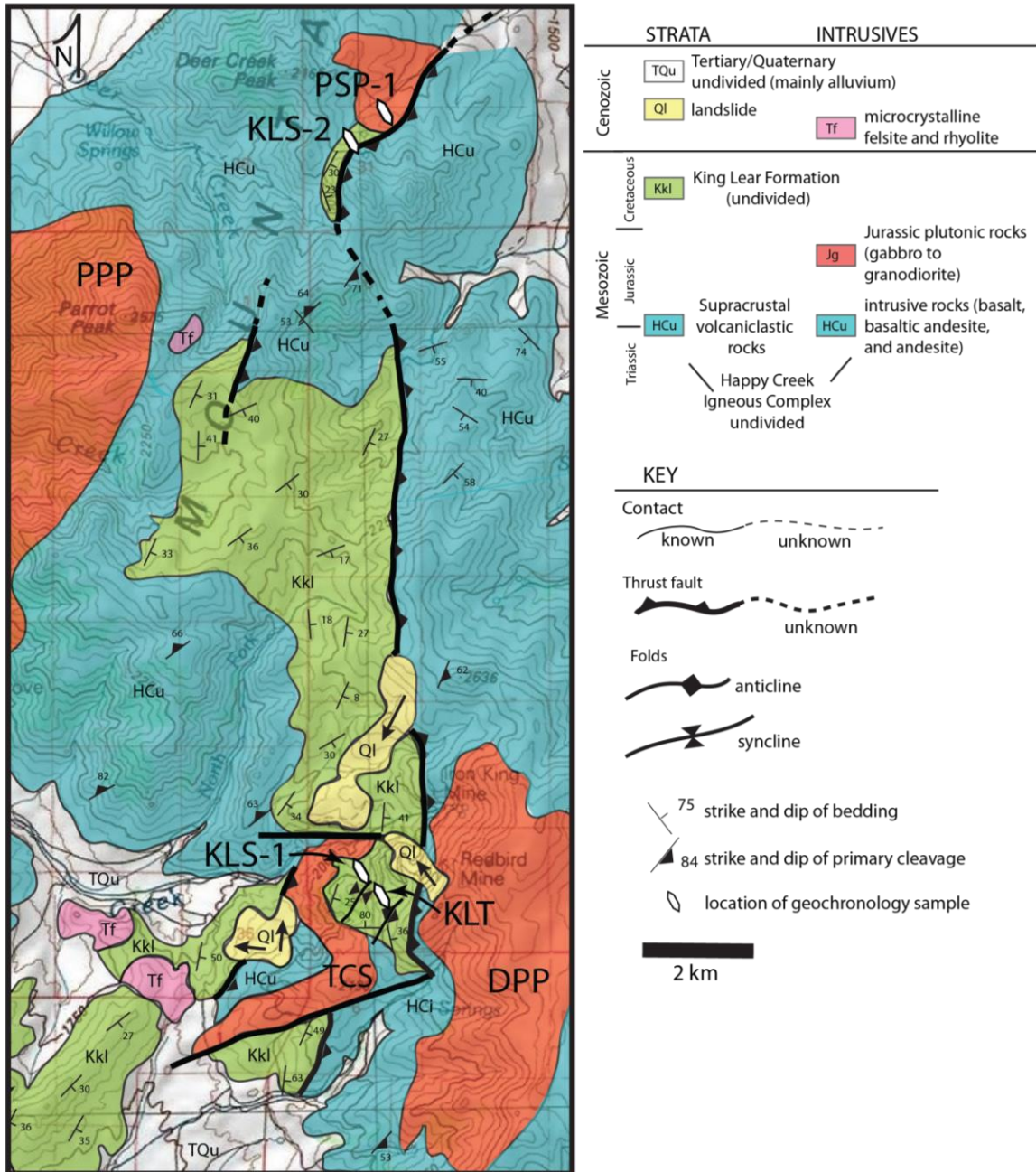


Figure 2.3. Geologic Map of the Central Jackson Mountains. Revised and simplified from Russell (1984) and Quinn et al. (1997). PPP = Parrot Peak pluton, DPP = Delong Peak pluton, TCS = Trout Creek stock.

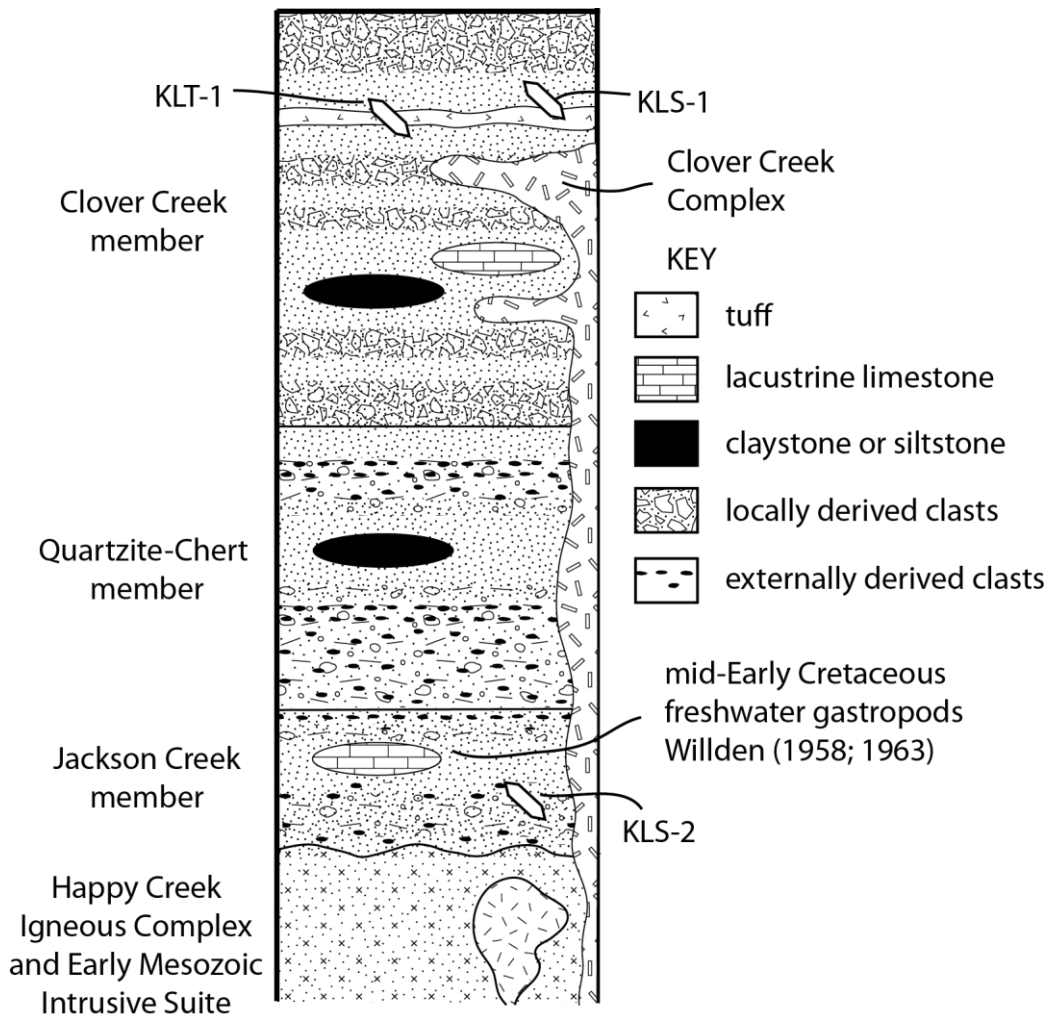


Figure 2.4. Generalized Stratigraphic Column for the Early Cretaceous King Lear Formation. Modified from Martin et al. (2010), Quinn (1996), and Quinn et al. (1997). Thicknesses are not to scale.

		Russell (1981; 1984)	Maher (1989)	Quinn (1996); Quinn et al. (1997)
CRETACEOUS	LATE			
		?		
JURASSIC	EARLY	Thrusting		
		SE-NW shortening (cleavage, thrusts, folds)	W & E-vergent thrusts	(no Cretaceous shortening)
	LATE	SW-NE shortening (broad to open folding)	E-vergent folds & thrusts Sinistral wrench faulting	SE-NW shortening (NE-trending folds, cleavage)
TRIASSIC	MIDDLE			SW-NE shortening (NW-trending folds, cleavage)
	EARLY			
	LATE			

Figure 2.5. Summary of the Interpreted Mesozoic Structural History of the Jackson Mountains from Russell (1981; 1984), Maher (1989), Quinn (1996), and Quinn et al. (1997).

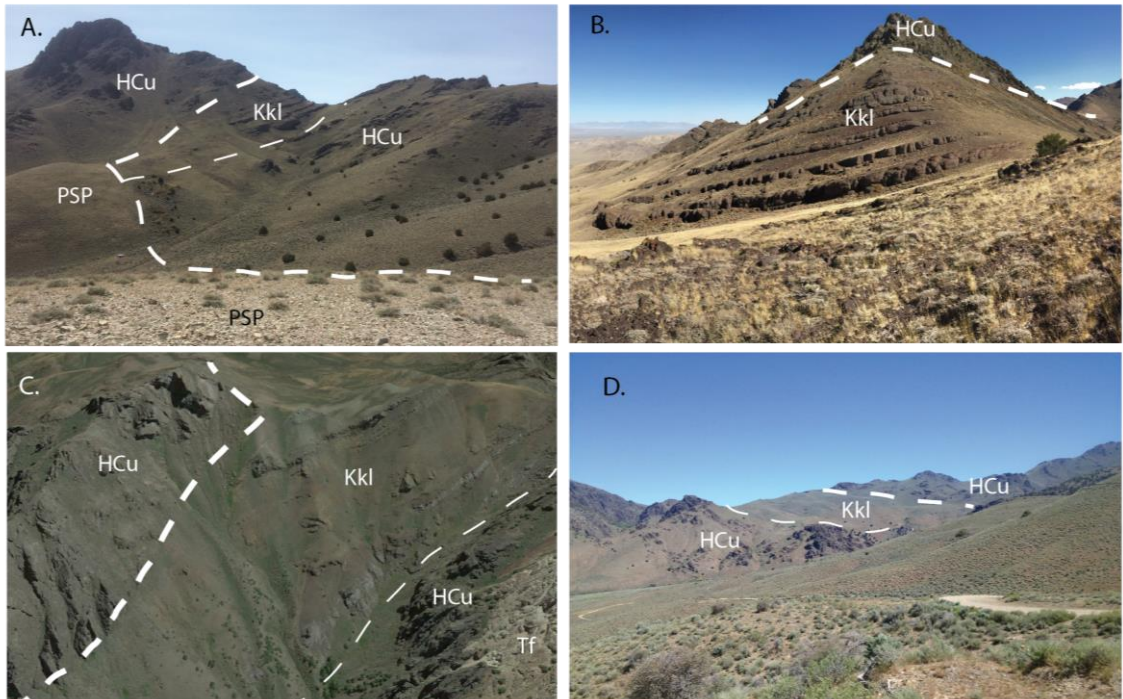


Figure 2.6. Field Photographs (A, B, and D) and Google Earth Images (C) of the Happy Creek Igneous Complex (HCu) and King Lear Formation (Kkl) Contact Geometry. A.) View looking to the SW in the vicinity Deer Creek Peak. PSP = Prospect Springs pluton. B.) Same location as A but looking to the SE. C.) Google Earth image in the vicinity of Parrot Peak. View looking to the S. Tf = Tertiary felsite. D.) View looking to the N in the central Jackson Mountains.

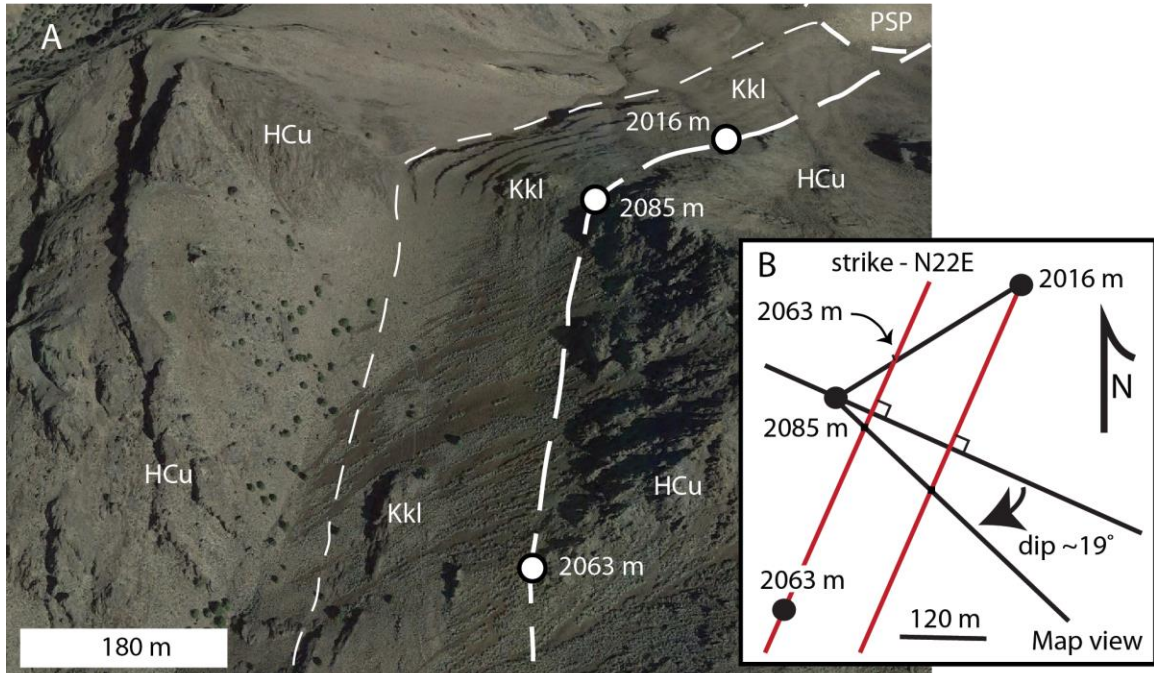


Figure 2.7. 3 Point Problem of the Happy Creek Igneous Complex (HCu) and King Lear Formation (Kkl) Contact Geometry in the Vicinity of Deer Creek Peak. A.) Oblique Google Earth view to the N-NE. This is in the same area as the photos from Figure 6a and 6b. B.) Calculation of strike and dip in map view. Calculated structure contours are in red.

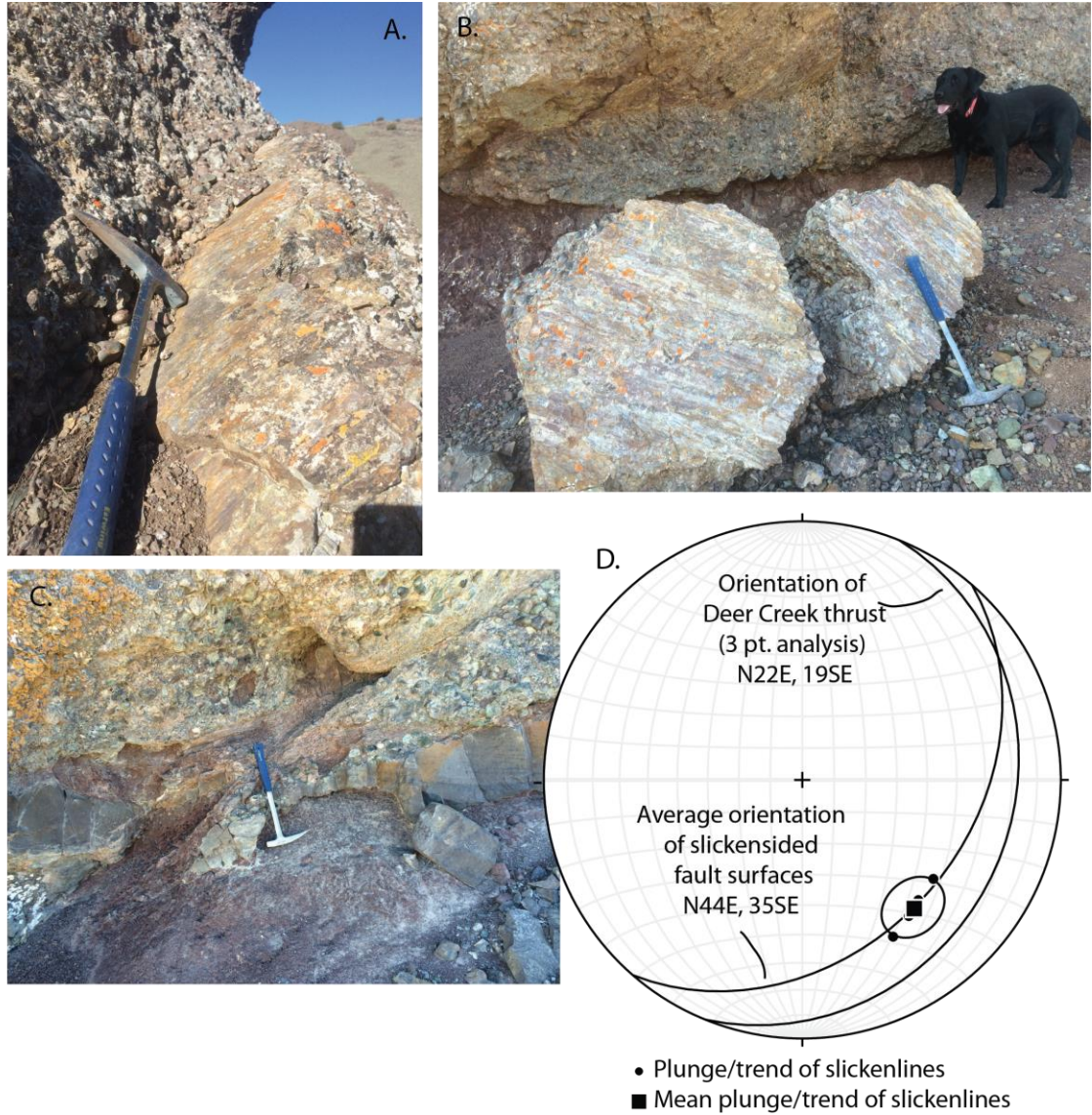


Figure 2.8. Field Photographs and Stereonet of Subsidiary Fault Surfaces Within the King Lear Formation. Hammer (~33 cm) and Mono the black dog for scale. A.) Close-up view looking to the SE. B.) Slickensided block that has fallen from wall directly above. C.) Thrust sense offset along subsidiary fault surface. View looking to the S. D.) Stereonet analysis of orientation of fault surfaces and slickenlines compared to the orientation of the Deer Creek thrust.

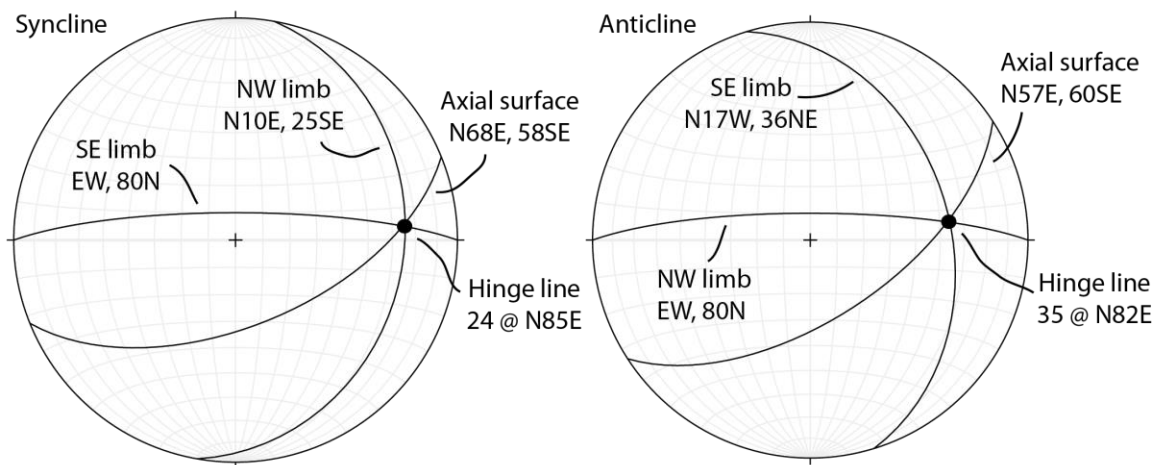


Figure 2.9. Annotated Field Photograph and Stereonets of Folds. View looking to the S-SE in photograph. Stereonet analysis show a pair of open, moderately-inclined, moderately-plunging folds trending ~NE-SW with axial surfaces dipping ~60 SE. Note the decrease in the degree of folding as you move up-section.

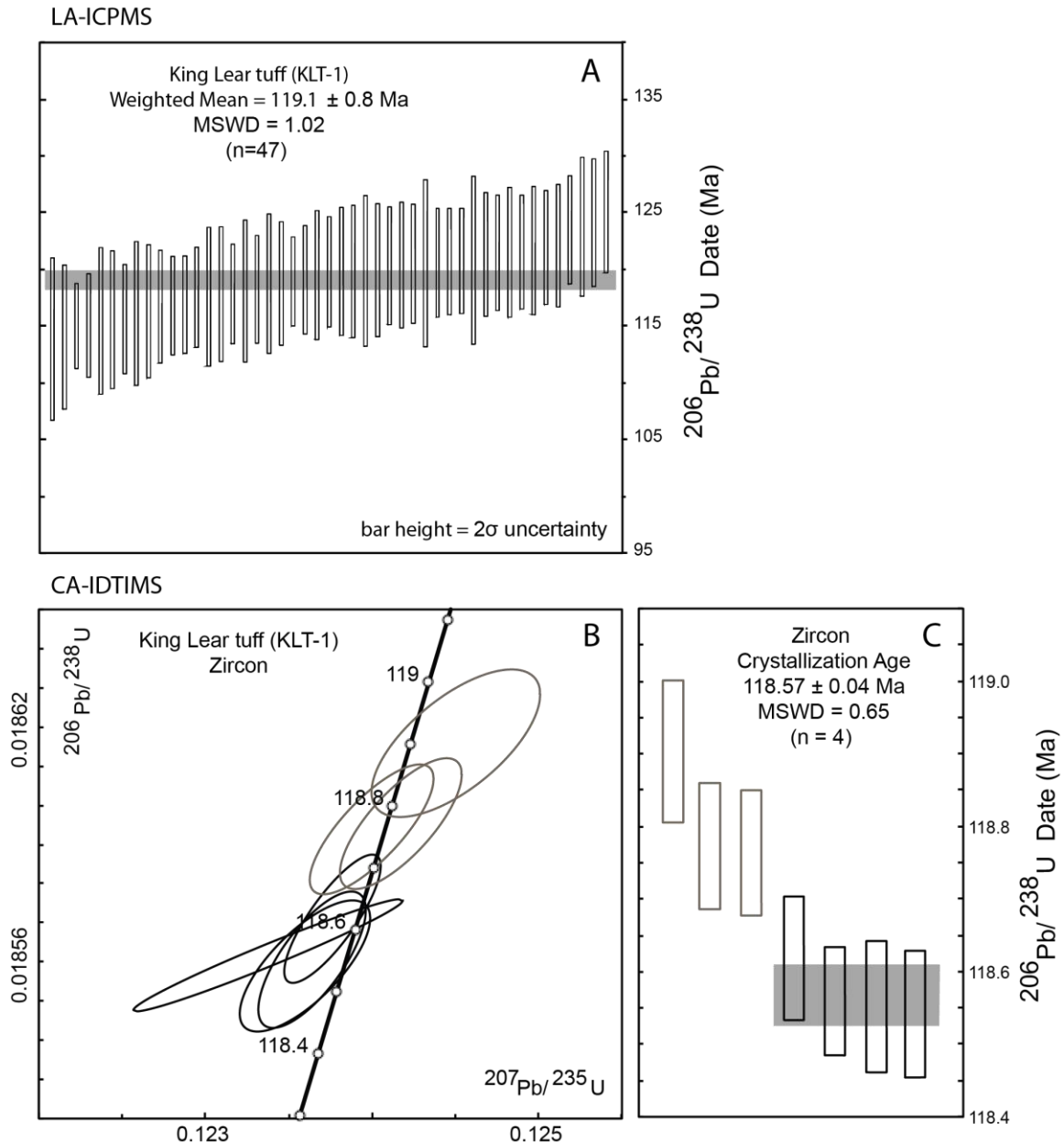


Figure 2.10. Results of U-Pb Zircon Geochronology Using Both LA-ICPMS (A) and CA-IDTIMS (B, C) of Magmatic Zircon From the King Lear Tuff (KLT-1). For CA-IDTIMS results, zircon analyses included in the weighted mean $^{206}\text{Pb}/^{238}\text{U}$ crystallization age are represented by solid bold ellipses (B). Gray outlined ellipses were not used in any age calculation (B). Ranked age charts (C) located to the right of the concordia diagram show the distribution of $^{206}\text{Pb}/^{238}\text{U}$ ages. Bar heights depict their associated 2σ uncertainties. The gray band set behind the group represents the weighted mean of those analyses where the height illustrates the related uncertainty. Line-type designations on bar charts mimic those described for the concordia diagrams. MSWD—mean squared weighted deviation.

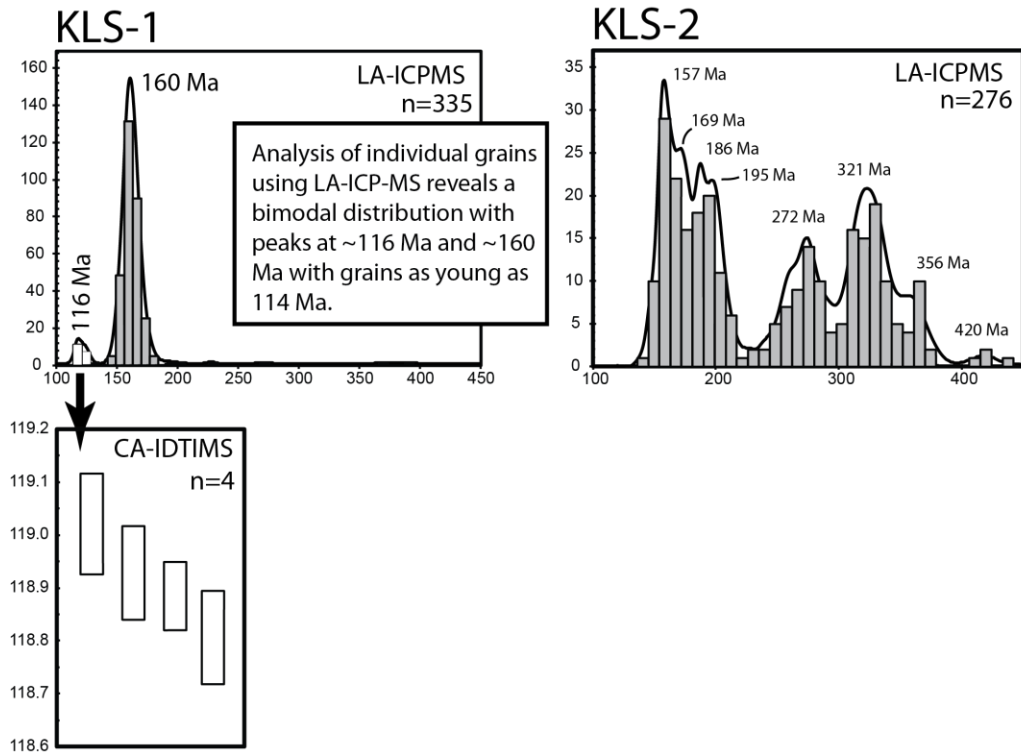


Figure 2.11. Relative Probability Plots, Histograms, and Ranked Age Plot for Detrital Zircons for Sandstones of the King Lear Formation in the Jackson Mountains, NV. Top 2 curves represent dates obtained using LA-ICPMS. The bottom ranked age plot is for CA-IDTIMS dates from the youngest zircon distribution found in KLS-1. Note the significant difference in zircon provenance between the base (KLS-2) and the top (KLS-1) of the King Lear Formation. Curves represent the summation of individual detrital zircon ages and associated 2σ Gaussian errors; associated y-axes represent relative probability. Histograms are based on individual detrital zircon grain ages and do not incorporate errors; associated y-axes represent number of grains in a given age bin.

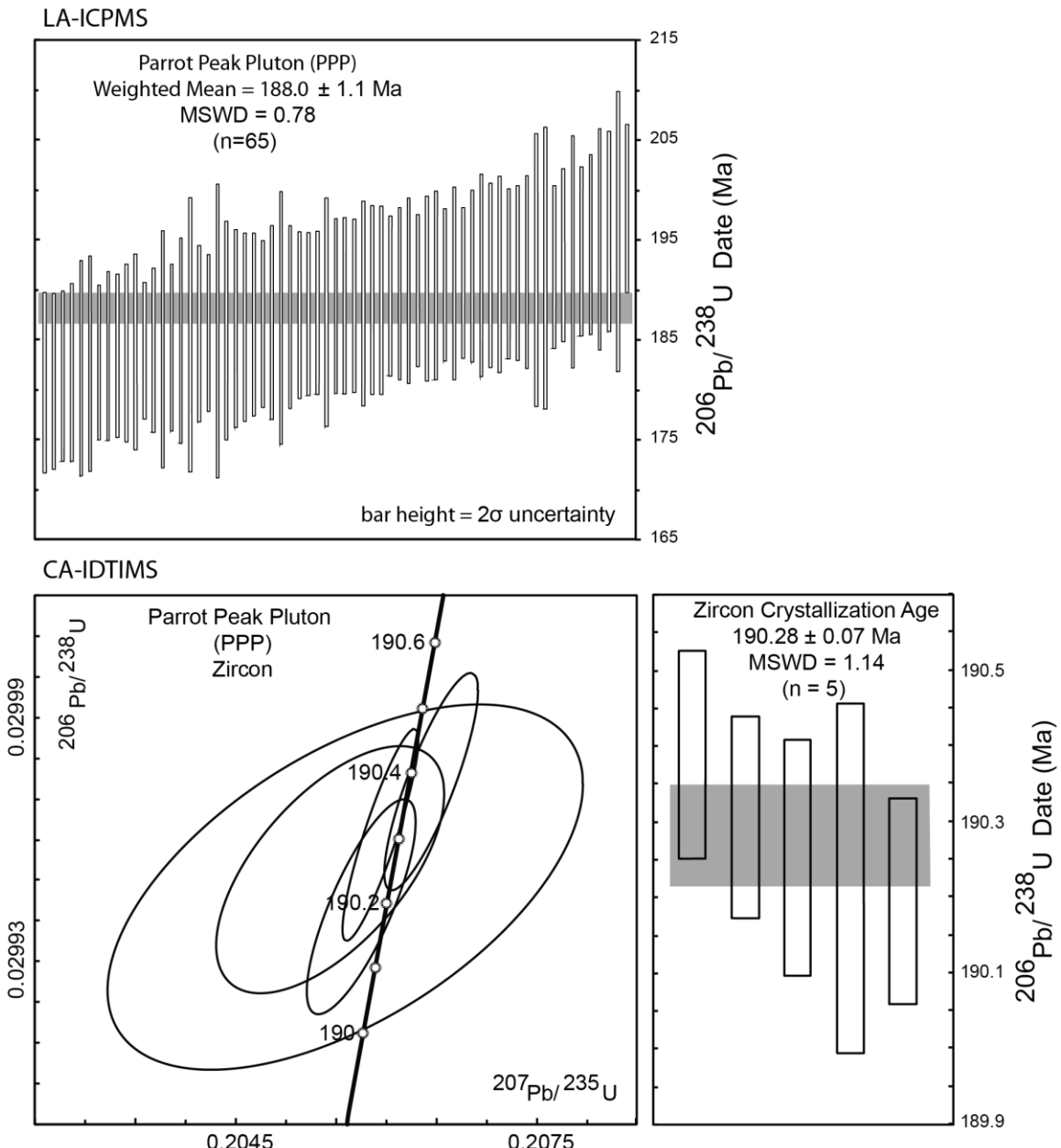


Figure 2.12. Results of U-Pb Zircon Geochronology Using Both LA-ICPMS (A) and CA-IDTIMS (B, C) of Magmatic Zircon From the Parrot Peak Pluton (PPP-1). For CA-IDTIMS results, zircon analyses included in the weighted mean $^{206}\text{Pb}/^{238}\text{U}$ crystallization age are represented by solid bold ellipses (B). Ranked age charts (C) located to the right of the concordia diagram show the distribution of $^{206}\text{Pb}/^{238}\text{U}$ ages. Bar heights depict their associated 2σ uncertainties. The gray band set behind the group represents the weighted mean of those analyses where the height illustrates the related uncertainty. Line-type designations on bar charts mimic those described for the concordia diagrams. MSWD—mean squared weighted deviation.

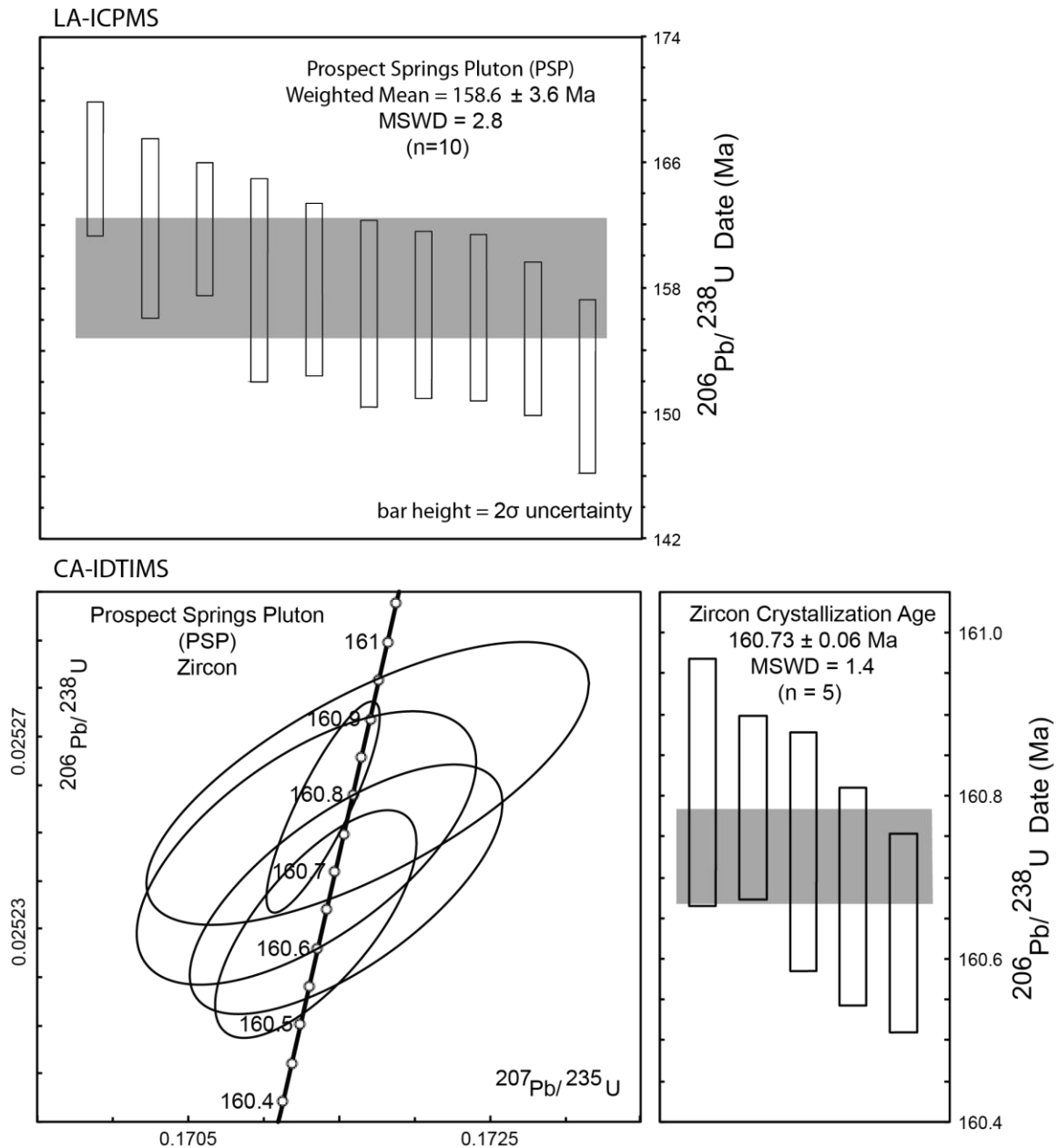


Figure 2.13. Results of U-Pb Zircon Geochronology Using Both LA-ICPMS (A) and CA-IDTIMS (B, C) of Magmatic Zircon From the Prospect Springs Pluton (PSP-1). For CA-IDTIMS results, zircon analyses included in the weighted mean $^{206}\text{Pb}/^{238}\text{U}$ crystallization age are represented by solid bold ellipses (B). Ranked age charts (C) located to the right of the concordia diagram show the distribution of $^{206}\text{Pb}/^{238}\text{U}$ ages. Bar heights depict their associated 2σ uncertainties. The gray band set behind the group represents the weighted mean of those analyses where the height illustrates the related uncertainty. Line-type designations on bar charts mimic those described for the concordia diagrams. MSWD—mean squared weighted deviation.

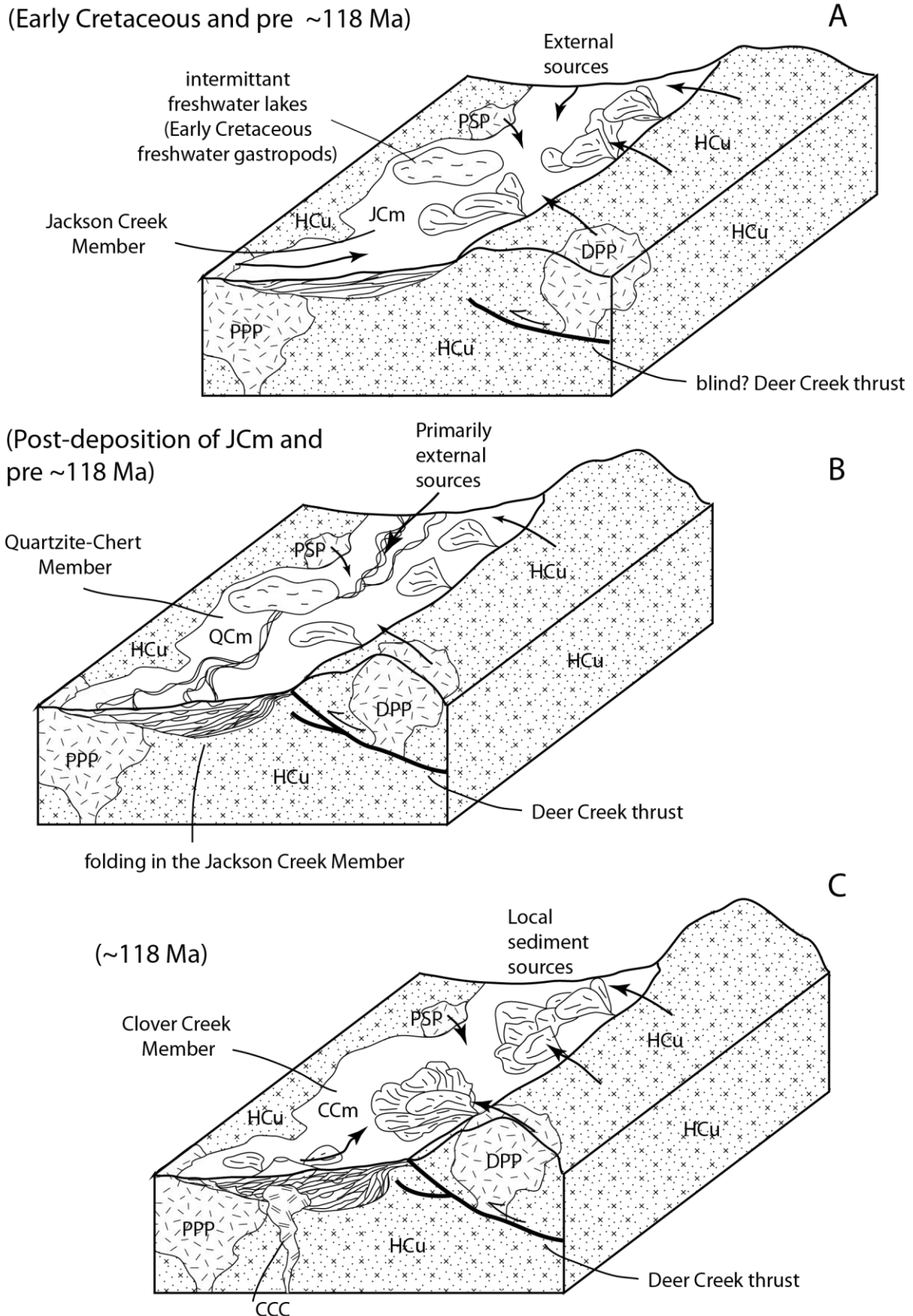


Figure 2.14. Stratigraphic and Structural Model for the Deposition of the King Lear Formation Associated with Early Cretaceous Movement Along the Deer Creek Thrust. Arrows indicate sediment source regions and pathways. For all diagrams: HCu = Happy Creek undivided, PPP = Parrot Peak Pluton, DPP = DeLong Peak Pluton, PSP = Prospect Springs Pluton, CCC = Clover Creek Complex. Members of the King Lear Formation include: JCm = Jackson Creek Member, QCm = Quartzite-Chert Member, and CCm = Clover Creek Member.

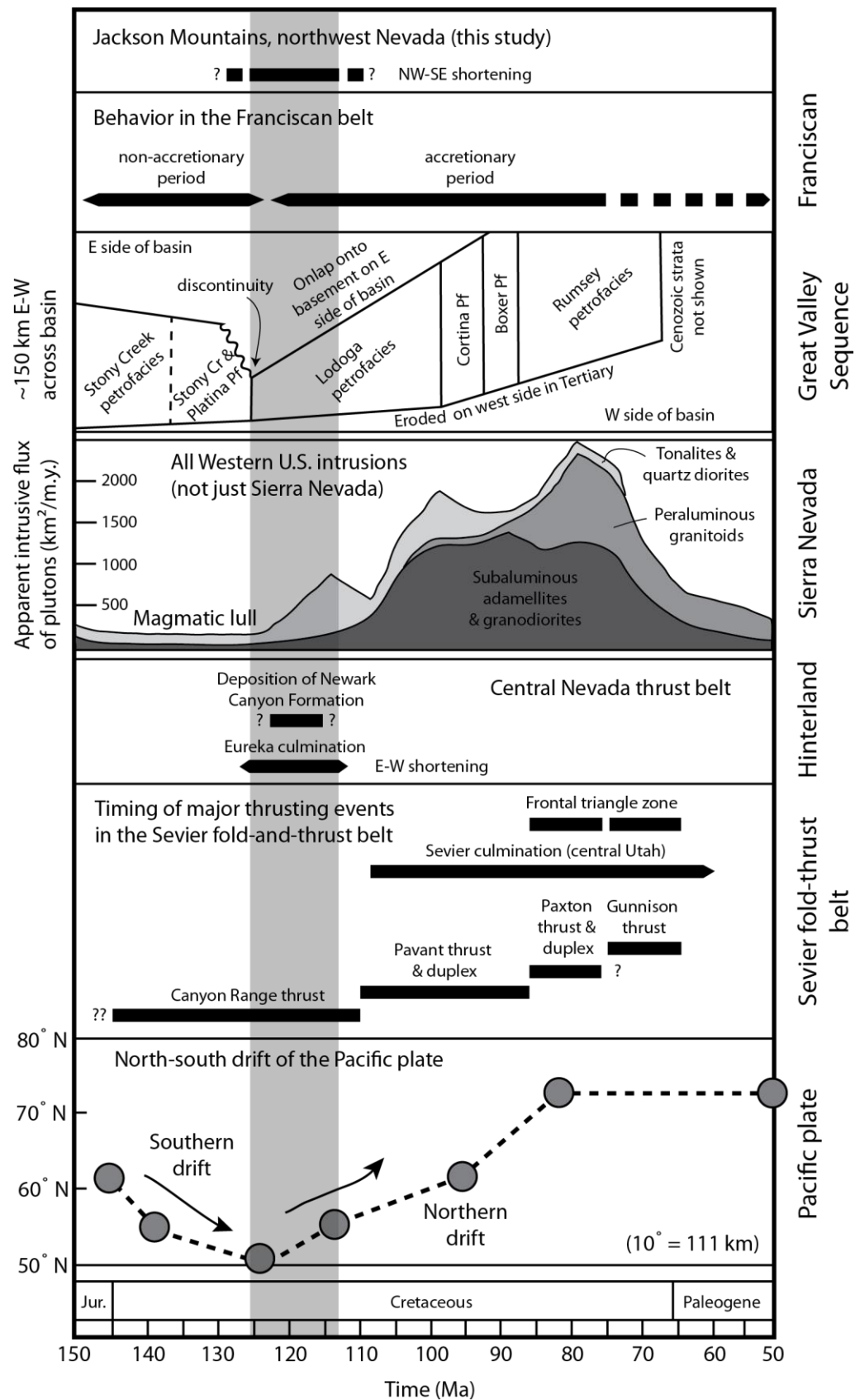


Figure 2.15. Summary of the Timing of Major Events in the Cordilleran Arc and Retroarc System. Modified from DeCelles & Coogan (2006), Dumitru et al. (2010), and Long et al. (2014). Emphasis is placed on Early Cretaceous events to compare with documented shortening in the Jackson Mountains (this study). Grey vertical bar shows how shortening in the Jackson Mountains compares temporally with events in other portions of the system. Data sources include: Franciscan belt = Dumitru et al. (2010), Great Valley = Constenius et al. (2000), Intrusions = Barton et al. (1998), Newark Canyon Fm = Druschke et al. (2010), Eureka culmination = Long et al. (2014), Sevier belt = DeCelles & Coogan (2006), Pacific plate = Sager (2007).

References

- Armstrong, R. L., and P. L. Ward (1993), Late Triassic to earliest Eocene magmatism in the North American Cordillera: Implications for the Western Interior Basin, in *Evolution of the Western Interior Basin, Geol. Assoc. Can. Spec. Pap.*, vol. 39, edited by W. G. E. Caldwell and E.G. Kauffman, pp. 49–72.
- Barton, M. D., D. A. Battles, G. E. Bebout, R. C. Capo, J. N. Christensen, S. R. Davis, R. B. Hanson, C. J. Michelsen, and H. E. Trim (1988), Mesozoic contact metamorphism in the western United States, in *Metamorphism and Crustal Evolution of the Western United States*, edited by W.G. Ernst, pp. 110–178, Prentice Hall, Englewood Cliffs, N. J.
- Burchfiel, B. C., D. S. Cowan, and G. A. Davis (1992), Tectonic overview of the Cordilleran orogen in the western United States, in *The Cordilleran orogen: Conterminous U.S.*, Geological Society of America, Geology of North America, vol. G-3, edited by B. C. Burchfiel et al., pp. 407–480, Boulder, CO.
- Burchfiel, B. C., and G. A. Davis (1972), Structural framework and evolution of the southern part of the Cordilleran orogen, western United States, *Amer. Jour. of Sci.*, 272, 97–118.
- Constenius, K. N., R. A. Johnson, W. R. Dickinson, and T. A. Williams (2000), Tectonic evolution of the Jurassic-Cretaceous Great Valley forearc, California: Implications for the Franciscan thrust-wedge hypothesis, *Geol. Soc. Am. Bull.*, 112, 1703–1723.
- Cowan, D. S., and R. L. Bruhn (1992), Late Jurassic to early Late Cretaceous geology of the U.S. Cordillera, in *The Cordilleran Orogen: Conterminous U.S.*, Geological Society of America, Geology of North America, vol. G-3, edited by B. C. Burchfiel et al., pp. 169–203, Boulder, CO.
- Dayyдов, В. И., J. L. Crowley, M. D. Schmitz, and V. I. Poletaev (2010), High-precision U-Pb zircon age calibration of the global Carboniferous time scale and Milankovitch band cyclicity in the Donets Basin, eastern Ukraine, *Geochem.*

- Geophys. Geosys.*, 11, 1, 22 p.
- DeCelles, P. G., and J. C. Coogan (2006), Regional structure and kinematic history of the Sevier fold-and-thrust belt, central Utah, *Geol. Soc. of Amer. Bull.*, 118, 841–864.
- DeCelles, P. G., T. F. Lawton, and G. Mitra (1995), Thrust timing, growth of structural culminations, and synorogenic sedimentation in the type Sevier orogenic belt, western United States, *Geology*, 23, 699–702.
- DeCelles, P. G. (2004), Late Jurassic to Eocene evolution of the Cordilleran thrust belt and foreland basin system, western U.S.A., *Amer. Jour. of Sci.*, 304, 105–168.
- Dickinson, W. R. (2004), Evolution of the North American Cordillera, *Ann. Rev. of Earth and Plan. Sci.*, 32, 13–45.
- Druschke, P., A. D. Hanson, M. L. Wells, G. E. Gehrels, and D. Stockli (2011), Paleogeographic isolation of the Cretaceous to Eocene Sevier hinterland, east-central Nevada: Insights from U-Pb and [U-Th]/He detrital zircon ages of hinterland strata, *Geol. Soc. of Amer. Bull.*, 123, 1141–1160.
- Ducea, M. (2001), The California arc: Thick granitic batholiths, eclogitic residues, lithospheric-scale thrusting, and magmatic flare-ups, *GSA Today*, 11[11], 4–10.
- Dumitru, T. A., J. Wakabayashi, J. E. Wright, and J. L. Wooden (2010), Early Cretaceous transition from nonaccretionary behavior to strongly accretionary behavior within the Franciscan subduction complex, *Tectonics*, 29, TC5001.
- Ernst, W. G. (1970), Tectonic contact between the Franciscan mélange and the Great Valley Sequence, crustal expression of a late Mesozoic Benioff Zone, *J. Geophys. Res.*, 75, 886–901.
- Fouch, T. D., J. M. Hanley, and R. M. Forester (1979), Preliminary correlation of Cretaceous and Paleogene lacustrine and related nonmarine sedimentary and volcanic rocks in parts of the Great Basin of Nevada and Utah, in *Basin and Range Symposium and Great Basin field conference: Rocky Mountain Association*

- of Petroleum Geologists and Utah Geological Association*, edited by G. W. Newman, and H. D. Goode, p. 305–312.
- Gehrels, G. (2012), Detrital zircon U-Pb geochronology: current methods and new opportunities, in *Tectonics of sedimentary basins: Recent advances*, edited by C. Busby, and A. Azor Perez, Hoboken: Blackwell Publishing Ltd, 1st edition.
- Ingersoll, R. V. (1983), Petrofacies and provenance of late Mesozoic forearc basin, northern and central California, *AAPG Bull.*, 67, 1125–1142.
- Katz, Y., R. Weinberger, and A. Aydin (2004), Geometry and kinematic evolution of Riedel shear structures, Capitol Reef National Park, Utah, *Jour. of Struct. Geol.*, 26, 491-501.
- Krogh, T. E. (1973), A low contamination method for hydrothermal decomposition of zircon and extraction of U and Pb for isotopic age determination, *Geochim. Cosmochim. Acta*, 37, 485–494.
- Logan, J. M., M. Friedman, N. Higgs, D. Dengo, and T. Shimamoto (1979), Experimental studies of simulated gouge and their application to studies of natural fault zones, in *Analysis of Actual Fault Zones in Bedrock*, U.S. Geol. Surv., Open-file Rept. 79-1239, p. 305-343.
- Long, S. P., C. D. Henry, J. L. Muntean, G. P. Edmondo, and E. J. Cassel (2014), Early Cretaceous construction of a structural culmination, Eureka, Nevada, U.S.A.: Implications for out-of-sequence deformation in the Sevier hinterland, *Geosphere*, 10, 3, 564-584.
- MacNeil, F. S. (1939), Fresh-water invertebrates and land plants of Cretaceous age from Eureka, Nevada, *Jour. of Paleont.*, 13, 355–360.
- Maher, K. A. (1989), Geology of the Jackson Mountains, northwest Nevada, Ph.D. thesis, *Calif. Inst. of Tech.*, Pasadena, 491 p.
- Martin, A. J., S. J. Wyld, J. E. Wright, and J. H. Bradford (2010), The Lower Cretaceous King Lear Formation, northwest Nevada: Implications for Mesozoic orogenesis in the western U.S. Cordillera, *Geol. Soc. of Amer. Bull.*, 122, 537–562.

- Mattinson, J. M. (2005), Zircon U-Pb chemical abrasion [“CA-TIMS”] method: Combined annealing and multi-step partial dissolution analysis for improved precision and accuracy of zircon ages, *Chem. Geol.*, 220, 47-66.
- Nolan, T. B. (1962), The Eureka mining district, Nevada, *U.S. Geol. Surv. Prof. Paper* 406, 78 p.
- Oldow, J. S., A. W. Bally, H. G. Ave Lallement, and W. P. Leeman (1989), Phanerozoic evolution of the North American Cordillera: United States and Canada, in *The geology of North America—An overview*, Geological Society of America, *Geology of North America*, vol. A, edited by A. W. Bally and A. R. Palmer, p. 139–232, Boulder, CO.
- Quinn, M. J. (1996), Pre-Tertiary stratigraphy, magmatism, and structural history of the central Jackson Mountains, Humboldt County, Nevada, Ph.D. thesis, Rice Univ., Houston, TX, 243 p.
- Quinn, M. J., J. E. Wright, and S. J. Wyld (1997), Happy Creek igneous complex and tectonic evolution of the early Mesozoic arc in the Jackson Mountains, northwest Nevada, *Geol. Soc. Of Amer. Bull.*, 109, 461-482.
- Riedel, W. (1929). Zur Mechanik Geologischer Brucherscheinungen. *Zentral-blatt fur Mineralogie, Geologie und Paleontologie*, B, 354–368.
- Rivera, T. A., M. D. Schmitz, B. R. Jicha, and J. L. Crowley (2016), Zircon petrochronology and $^{40}\text{Ar}/^{39}\text{Ar}$ sanidine dates for the Mesa Falls Tuff; crystal-scale records of magmatic evolution and the short lifespan of a large Yellowstone magma chamber, *Jour. of Petr.*, 57.9, 1677-1704.
- Russell, B. J. (1981), Pre-Tertiary paleogeography and tectonic history of the Jackson Mountains, northwestern Nevada, Ph.D. thesis, Northwestern Univ., Evanston, Illinois, 205 p.
- Russell, B. J. (1984), Mesozoic geology of the Jackson Mountains, northwestern Nevada, *Geol. Soc. Of Amer. Bull.*, 95, 313–323.

- Sager, W. W. (2007), Divergence between paleomagnetic and hotspot-model–predicted polar wander for the Pacific plate with implications for hotspot fixity, in *Plates, Plumes, and Planetary Processes*, edited by G. R. Foulger, and D. M. Jurdy, Spec. Pap. Geol. Soc. Am., 430, 335–357.
- Smith, J. F., and K. B. Ketner (1976), Stratigraphy of Post-Paleozoic rocks and summary of resources in the Carlin-Pinon Range area, Nevada, *U.S. Geol. Surv. Prof. Paper, 867-B*, 48 p.
- Snoke, A. W. (2005), Southern Cordillera, in *Encyclopedia of Geology*, edited by R. C. Selley, L. R. M. Cocks, and I. R. Plimer, vol. 4: Academic Press, p. 48–61.
- Swain, F. M. (1999), Fossil nonmarine Ostracoda of the United States, *Amsterdam, Elsevier Science*, 401 p.
- Taylor, W. J., J. M. Bartley, J. E. Fryxell, J. Schmitt, and D. S. Vandervoort (1993), Mesozoic central Nevada thrust belt, in *Crustal evolution of the Great Basin and the Sierra Nevada: Geological Society of America Cordilleran/Rocky Mountain Sections Field Trip Guidebook*, edited by M. M. Lahren et al., Reno, University of Nevada Mackay School of Mines, p. 57–96.
- Vandervoort, D. S. (1987), Sedimentology, provenance, and tectonic implications of the Cretaceous Newark Canyon Formation, east-central Nevada, M.S. thesis, Montana State University, Bozeman, 145 p.
- Willden, R. (1958), Cretaceous and Tertiary orogeny in Jackson Mountains, Humboldt County, Nevada, *Amer. Assoc. of Petr. Geol. Bull.*, 42, 2378–2398.
- Willden, R., (1963), General Geology of the Jackson Mountains, Humboldt County, Nevada, *U.S. Geol. Surv. Bull. 1141-D*, 65 p.
- Wyld, S. J., J. W. Rogers, and P. Copeland (2003), Metamorphic evolution of the Luning-Fencemaker fold-thrust belt, Nevada: Illite crystallinity, metamorphic petrology, and $^{40}\text{Ar}/^{39}\text{Ar}$ geochronology, *The Jour. of Geol.*, 111, 17–38.

CHAPTER THREE: U-PB ZIRCON GEOCHRONOLOGY PROVIDES INSIGHT
INTO THE MESOZOIC TECTONIC EVOLUTION, PALEOGEOGRAPHY, AND
STRUCTURAL ARCHITECTURE OF THE JACKSON MOUNTAINS, NORTHWEST
NEVADA, USA

Abstract

New detrital zircon U-Pb geochronology provides insight into the maximum depositional age, provenance, structural architecture, and paleogeography of the Late Triassic-Early Jurassic Boulder Creek Beds. Using a combination of LA-ICPMS and CA-IDTIMS, the Boulder Creek Beds represent a sequence of Norian (~215 Ma) to Sinemurian (~195 Ma) volcanogenic, marine rocks. All analyzed subunits show a single major Triassic to Early Jurassic mode with minimal input of older grains. Considering the texturally immature, volcanogenic, marine lithologies, these new data support marine deposition adjacent to an active Triassic and Jurassic volcanic arc with minimal input from other sources. Combined with regional geologic relationships, these new data are consistent with Triassic-Early Jurassic reconstructions in which the Black Rock area was separated from the continent by a deep-marine basin. Furthermore, these new data are consistent with reconstructions of the Black Rock and Olds Ferry terranes representing fragments of the same early Mesozoic fringing arc later separated by ~400 km of dextral translation.

Our data suggests that between the middle Early Jurassic and early Late Jurassic (post ~189 Ma and pre ~162 Ma) NW-SE shortening resulted in the production of thrust faults and local folding, regional-scale folding, and associated cleavage development. Similarities in timing, structural style, and shortening direction implies that Jurassic shortening in the Jackson Mountains was associated with the development of the adjacent Luning Fencemaker fold-and-thrust belt and closure of the early Mesozoic marine basin that culminated in the eastward thrusting of the arc terrane over the basinal terrane.

Introduction

Distributed throughout the North American Cordillera are isolated fragments and belts of Paleozoic and Mesozoic volcanic arc terranes (Fig. 3.1) (e.g. Burchfiel, Cowan, & Davis, 1992; Miller et al., 1992; Saleeby & Busby-Spera, 1992; Dickinson, 2004; Dickinson, 2006; Colpron, Nelson, & Murphy, 2007; Lund et al., 2015). Some represent intraoceanic arcs that evolved at unknown distances from the continent (i.e. the Wallowa terrane) while others may have formed continental (i.e. eastern California-Arizona) or continental-fringing arcs (i.e. the Quesnellia terrane, Olds Ferry terrane, and the Eastern Klamath-Northern Sierra terranes) (e.g. Goldstrand, 1994; Vallier, 1995; Dickinson, 2004; Stevens, Stone, & Miller, 2005; Wyld, Umhoefer, & Wright, 2006; Tumpane, 2010; Kurz, 2010; LaMaskin et al., 2011; Tosdal & Wooden, 2015; Kurz et al., 2016). Collectively, these arc terranes represent times of volcanism and accretion that led to the overall westward growth of the North American continent during the Phanerozoic.

While our understanding of these Cordilleran arc terranes continues to evolve and improve, many questions remain regarding their pre- and post-accretion paleogeography, tectonics, and potential correlations with other arc assemblages. Though correlations have

been suggested (e.g. Wyld & Wright, 2001; Dickinson, 2004; Wyld et al., 2006; Dorsey & LaMaskin, 2007; Dorsey & LaMaskin, 2008; LaMaskin et al., 2011; Lund et al., 2015; Kurz et al., 2016), in most cases the lack of robust biostratigraphy, geochronology, geochemistry, and structural data limits these interpretations. The Jackson Mountains, located in the Black Rock Desert region of northwest Nevada, contain a package of Paleozoic and Mesozoic arc-related rocks that represent an important locality in these terrane analyses (Figs. 3.1 and 3.2).

Geographically, due to Cenozoic cover, rocks of the Black Rock Desert region represent the first exposure of Paleozoic and Mesozoic basement to the south (i.e. Blue Mountains) and east (i.e. Klamath and Sierra Nevada Mountains) of other well-documented arc assemblages (Fig. 3.1). Additionally, the Jackson Mountains are located inboard of major Cretaceous strike-slip faults (Fig. 3.1), thus are essentially in place with respect to the North American continent. Therefore, the Jackson Mountains can act as potential tie between the continent and other outboard terranes when assessing the role and magnitude of strike-slip displacement along the margin. Finally, the Jackson Mountains are located adjacent and directly outboard of the Luning-Fencemaker fold-and-thrust belt. As such, the Jackson Mountains provide an important spatiotemporal link when investigating how deformation associated with the Luning-Fencemaker fold-and-thrust belt relates to the paleogeography and tectonics to the west. Along these lines, structural relationships in the Jackson Mountains provide important temporal constraints on the development and evolution of the Luning-Fencemaker fold-and-thrust belt. For these reasons, a comprehensive understanding of the geology and tectonics of the Jackson

Mountains is vital in evaluations of terrane relationships and assessing the role of horizontal translations within the Cordillera.

Several previous studies have looked at the geology of the Jackson Mountains and provide the foundation for this study (Willden, 1958; Willden, 1963; Russell, 1981; Russell, 1984; Maher, 1989; Quinn, 1996; Quinn, Wright, & Wyld, 1997; Martin et al., 2010). Here, we take a more detailed look at the Late Triassic to Early Jurassic volcanogenic strata of the Boulder Creek Beds. While previous studies have documented the petrology of the Boulder Creek Beds, uncertainty remains about their depositional age, sedimentary provenance, and early Mesozoic paleogeography, and specifically questions of how the depositional history of the Boulder Creek Beds compares with that of other Triassic and Jurassic Cordilleran strata.

In this paper, we use new U-Pb zircon geochronology of Triassic and Jurassic sedimentary and igneous rocks from the Jackson Mountains to assess the age, provenance, and paleogeography of this section of the North American Cordillera. Our objectives are to: 1) provide constraints on the age, provenance, and paleogeography of early Mesozoic sedimentary units in the Jackson Mountains, 2) use these new controls to investigate relationships with other arc fragments and, 3) investigate the structural architecture and evolution of the Jackson Mountains with respect to the development of the Luning-Fencemaker fold-and-thrust belt.

Using both laser ablation-inductively coupled plasma mass spectrometry (LA-ICPMS) and chemical abrasion-isotope dilution thermal ionization mass spectrometry (CA-IDTIMS) in tandem we show that the Boulder Creek Beds represent a Norian (~215 Ma) to Sinemurian (~195 Ma) succession of strongly volcanogenic, marine rocks

deposited adjacent to an active Triassic-Early Jurassic volcanic arc. Furthermore, these new data confirm correlations of the Olds Ferry and Black Rock terranes as fragments of the same early Mesozoic fringing arc separated from the continent by a deep-marine basin that was later fragmented and displaced by ~400 km of dextral translation. Additionally, our new data from the Jackson Mountains suggest that middle Early Jurassic to early Late Jurassic NW-SE shortening associated with the development of the Luning-Fencemaker fold-and-thrust belt resulted in the structural closure of the early Mesozoic marine basin and accretion of the Black Rock terrane to the North American margin.

Background

Regional Geology

Mesozoic Marine Province

Triassic and Jurassic strata in western Nevada have been broadly subdivided into three coeval to penecontemporaneous lithologic assemblages that together form the Mesozoic Marine Province (MMP) (Figs. 3.1 and 3.2) (e.g. Burke and Silberling, 1973; Silberling, 1973; Nichols and Silberling, 1977; Speed, 1978a; Speed, 1978b; Oldow, 1984; Manuszak, Satterfield, & Gehrels, 2000; Wyld, 2000). From east to west these assemblages include: 1) a “shelf terrane” containing a succession of carbonate rich, shallow-marine rocks 2) a “basinal terrane” containing a package of fine-grained, dominantly siliciclastic, deep marine rocks, and 3) a volcanic and volcaniclastic-rich marine succession (i.e. Black Rock arc terrane) to the west (Fig. 3.2) (e.g. Speed, 1978a; Wyld, 2000). The Black Rock arc terrane, which includes the Jackson Mountains, represents one of the early Mesozoic Cordilleran arc terranes (Fig. 3.1) (e.g. Burchfiel et

al., 1992; Wyld, 1996; Wyld, 2000). The overall history of the MMP is interpreted to document Early to Late Triassic regional extension that culminated in the opening of a wide, deep-marine basin (i.e. basinal terrane) situated between the shelf (i.e. shelf terrane) and a volcanic arc (i.e. Black Rock arc) (Wyld, 2000). While this early Mesozoic marine basin was geographically located in a back-arc position, it was likely floored by attenuated continental crust and did not involve sea-floor spreading (e.g. Burke and Silberling, 1973; Nichols and Silberling, 1977; Speed, 1978a; Speed, 1978b; Oldow, 1984; Wyld, 2000). Following extension in the Triassic, a major change to regional shortening in the Jurassic resulted in the structural closure of this early Mesozoic marine basin during the development of the Luning-Fencemaker fold-and-thrust belt (e.g. Oldow, 1984; Wyld, 2000; Wyld, Rogers, & Wright, 2001; Wyld, 2002).

Luning-Fencemaker Fold-And-Thrust Belt

The Luning-Fencemaker fold-and-thrust belt (LFTB) of central Nevada is one of several major structural belts of the North American Cordillera (Fig. 3.2). Deformation associated with the LFTB is primarily confined to rocks of the basinal terrane, except in the south, where deformation affected rocks associated with both the early Mesozoic arc and shelf terranes (Fig. 3.2) (e.g. Wyld, 2002). From early studies of the LFTB, Oldow (1984) recognized 4 distinct phases of shortening that involved the development of folds and/or reverse faults and cleavage. While the relative ages of these deformation phases were well established, the scarcity of geochronologic constraints unfortunately hindered his ability to tightly constrain the absolute timing and duration of each phase.

Nevertheless, Oldow (1984) proposed the following structural evolution for the LFTB based on the available ages of rocks involved and temporally constrained crosscutting

relationships. Beginning in the Late Triassic or Middle Jurassic, initiation of the LFTB began with the development of minor, locally developed NW-trending folds (D_1) forming during the deposition of arc rocks in the Black Rock terrane (Russell, 1981; Oldow, 1984). This minor phase was then followed by the main phase of LFTB shortening (D_2), active in the Middle or Late Jurassic to the Early Cretaceous. This major phase of NW-SE directed shortening resulted in the development of NE-trending folds, thrust imbrication, and thrust transport (Oldow, 1984). Following these phases were two other minor phases of NW-trending folds (D_3) and NS- and EW-trending folds (D_4) developed after the earlier phases (i.e. D_1 and D_2) and either prior to the intrusion of ~90 Ma crosscutting plutons (D_3) or after (D_4) (Oldow, 1984).

More recent studies in the northern and central LFTB were able to expand on this history and further constrain the timing of shortening associated with the development of the LFTB (e.g. Elison & Speed, 1989; Oldow, Bartel, & Gelber, 1990; Quinn, 1996; Rogers, 1999; Wyld et al., 2001; Wyld, 2002; Martin et al., 2010; Wilkins, 2010).

Structural analysis from the Santa Rosa Range (Wyld et al., 2001), Blue Mountain area (Wyld, 2002), and northern East Range (Elison & Speed, 1989) has been interpreted to provide evidence for at least one and maybe two phases of Jurassic shortening associated with the LFTB. D_1 involved tight to isoclinal folding, cleavage development, and reverse faulting that has been interpreted to accommodate from ~50–75% NW-SE shortening (Wyld et al., 2001; Wyld, 2002). Several lines of evidence constrain the timing of D_1 deformation to the Early and/or Middle Jurassic. In the west Humboldt Range, the youngest rocks involved in D_1 style deformation are late Early Jurassic (Speed, 1974).

Whole-rock $^{40}\text{Ar}/^{39}\text{Ar}$ analyses of slates and phyllites in the Santa Rosa Range indicate

that D₁ occurred prior to ~140 Ma (Wyld, Copeland, & Rogers, 1999). Furthermore, Wyld and Wright (2000) report a U-Pb zircon age of 165 Ma for a pluton cutting D₁ fabrics in the west Humboldt Range. It is important to point out that D₁ from these authors overall corresponds structurally and temporally with D₂ of Oldow (1984). D₂ is documented in the Santa Rosa Range and northern East Range and resulted in structures with a similar orientation to D₁ but with considerably less strain (Elison & Speed, 1989; Wyld et al., 2001). D₂ is constrained to the Middle and/or Late Jurassic (pre ~153 Ma) and was probably associated with late-phase thrusting on the eastern margin of the LFTB (Elison & Speed, 1989; Wyld et al., 2001; Wyld, 2002). Recent work in the northern East Range, suggests that significant shortening associated with the LFTB occurred prior to 161.8 Ma based on high-precision U-Pb geochronology of a crosscutting intrusive body (Wilkins, 2010). Further documentation of one and perhaps two minor phases of much younger Middle to Late Cretaceous NE-SW shortening that have been suggested to be related to pluton intrusion and far-field Sevier stresses (Wyld et al., 2001; Wyld, 2002). Therefore, the development of the LFTB is interpreted to have occurred primarily during the D₁ and D₂ phases of deformation associated with significant NW-SE shortening. Based on that conclusion, the LFTB is interpreted to have developed exclusively within the Jurassic and involved the structural closure of the early Mesozoic marine basin and juxtaposition of the arc, basinal, and shelf terranes discussed in the previous section (e.g. Oldow, 1984; Wyld et al., 2001; Wyld, 2002).

Geology of the Jackson Mountains

The Jackson Mountains are a ~50 km long N-NE oriented mountain range in the Black Rock Desert region of northwestern Nevada (Fig. 3.2). Overall, the geology of the

Jackson Mountains (Fig. 3.3) is dominated by four main rock groups: 1) a Paleozoic section of metasedimentary and metavolcanic rocks, 2) a Late Triassic-Early Jurassic succession of pelagic, carbonate, and volcanogenic rocks (the Boulder Creek Beds), 3) a package of Early Jurassic mafic to intermediate volcanic and intrusive rocks (the Happy Creek Igneous Complex) and associated Early and Late Jurassic plutons of the Early Mesozoic Intrusive Suite, and 4) Early Cretaceous sedimentary rocks of the King Lear Formation (e.g. Willden, 1958; Willden, 1963; Russell, 1981; Russell, 1984; Maher, 1989; Quinn, 1996; Quinn et al., 1997). For the purposes of this manuscript, we will discuss the geology of the Boulder Creek Beds, Happy Creek Igneous Complex, and Early Mesozoic Intrusive Suite.

Boulder Creek Beds

Russell (1981; 1984) was first to define the Boulder Creek Beds (BCB) as a Middle (?) to Late Triassic sequence of nine subunits that generally consist of: 1) interbedded thin pelitic rocks, chert, and calcarenite, 2) clastic carbonate rocks, 3) platform and slope carbonate deposits, and 4) volcanogenic sedimentary rocks with locally intercalated volcanic rocks. Later work by Quinn (1996) and Quinn et al. (1997) used mappable changes in clast composition and sedimentologic characteristics to arrive at five strongly volcanogenic subunits, two on the west side of the Jackson Mountains and three on the east side of the range (Fig. 3.3). These units are closely related to the BCB of Russell (1981, 1984) and therefore have kept the same name. As others authors have pointed out, the complicated stratigraphy and structure of the BCB has led to various interpretations about those lithologies to include within the unit, and its internal and external contact relationships (e.g. Russell, 1981, 1984; Maher, 1989; Quinn, 1996;

Quinn et al., 1997). We use the naming and subdivision of the BCB from Quinn (1996) and Quinn et al. (1997) in all upcoming discussions of the geology and tectonics of the Jackson Mountains.

Subunit BCB-1 outcrops on the west side of the Jackson Mountains and is generally composed of a volcanogenic, lithic-rich sequence of sandstone, siltstone, argillite, and conglomerate, with thin horizons of dark limestone and limestone megaclasts (Fig. 3.3; Table 3.1) (Quinn, 1996). Detailed work on the texture and composition of the sandstones reveal a large proportion of unstable lithic clasts, moderate to poor sorting, and abundant angular to subangular grains of quartz, feldspar, and quartzose lithics (Quinn, 1996). From these characteristics, Quinn (1996) interpreted a relatively short transport history and minimal reworking in a slope-associated debris-apron environment. Age constraints for BCB-1 are based on the recovery of mostly reworked late Paleozoic and Late Triassic (Carnian to Norian) fossils in the vicinities of Alaska and Bliss Canyons (Table 3.1) (Russell, 1981; Maher, 1989).

Subunit BCB-2 is also found on the west side of the range, to the north and east of subunit BCB-1 (Fig. 3.3). This subunit is almost entirely of volcanogenic origin with an abundance of massive debris flow, volcanic-lithic breccia, and sandstone with >95% volcanic and volcanioclastic clasts (Table 3.1) (Quinn, 1996). Quinn (1996) interpreted a slope-apron depositional environment adjacent to an active volcanic edifice for BCB-2 based on the increase in volcanic input and abundant debris flow to turbidite lithologies. No fossils have been recovered from subunit BCB-2 and age constraints are based on regional relationships that suggest a Late Triassic age (Table 3.1) (e.g. Russell, 1981; Maher, 1989; Quinn, 1996).

The following 3 subunits of the BCB are found on the east side of the Jackson Mountains and correspond to subunits 3A, 3B, and 3C from Quinn (1996) and subunits 3, 4, and 5 from Quinn et al. (1997) (Fig. 3.3). For the following section, we use the naming of Quinn et al. (1997), which is generally consistent with the naming of Russell (1981; 1984).

Subunit BCB-3 is composed of a heterogeneous sequence of volcanogenic clastic rocks that include abundant lithic-rich sandstone, conglomerate, and siltstone with minor shale and debris-flow diamictite (Table 3.1) (Quinn, 1996). Generally, the coarser grained lithologies are massive to well-stratified and at times present graded bedding and flame structures that demonstrate the upright orientation. The finer grained lithologies primarily include thin-bedded to massive siltstone (Quinn, 1996). Based on the abundance of debris flow lithologies with carbonate clasts and olistoliths, Quinn (1996) interprets a proximal slope-apron environment with adjacent active volcanism for subunit BCB-3. Age constraints for subunit BCB-3 are based primarily on resedimented and reworked Permian and Middle to Late Triassic fossils from blocks and/or clasts (Table 3.1) (Quinn, 1996). Therefore, the youngest such fossils are suggestive of a Norian maximum depositional age for subunit BCB-3 (Russell, 1981; Maher, 1989; Quinn, 1996).

Subunit BCB-4 is almost exclusively composed of volcanic and volcanogenic detritus of basaltic to basaltic andesite composition with common lithologies of basaltic andesite breccia and crystal-rich sandstone (Table 3.1) (Quinn, 1996). Sandstones from BCB-4 are poorly sorted with angular to subrounded clasts. No age constraints are reported for subunit BCB-4 (Table 3.1).

Subunit BCB-5 is similar in texture and composition to subunit BCB-3, although finer-grained and better stratified (Quinn, 1996). Common lithologies in this subunit include interbedded fine-grained sandstone and siltstone with lesser amounts of coarse sandstone and pebble conglomerate (Table 3.1) (Quinn, 1996). Where discernable, clasts consist of both volcanic and sedimentary lithics (Quinn, 1996). Due to the finer-grained, better-stratified character compared to BCB-3, Quinn (1996) interprets a more distal portion of the slope-apron setting for subunit BCB-5. Age constraints on BCB-5 are based on the recovery of upper middle to upper Norian conodonts from a limestone clast (Table 3.1) (Maher, 1989). This Norian age therefore represents a measure of the maximum depositional age of subunit BCB-5.

On the basis of sedimentology, composition, lithology, and general biostratigraphy, Quinn (1996) attempted to correlate the Boulder Creek Beds to similar aged strata documented in the Pine Forest Range (Fig. 3.4) (e.g. Wyld, 1991). Middle to Late Triassic strata in the Pine Forest Range includes, in stratigraphic order, the Bishop Canyon Formation, Dyke Canyon Formation, and the Cherry Creek Formation (Fig. 3.4) (Wyld, 1991). Using the above criteria, Quinn (1996) correlates subunits BCB-3, 4, and 5 to the Cherry Creek Formation, subunit BCB-2 to the Dyke Canyon Formation, and subunit BCB-1 to the Bishop Canyon Formation (Fig. 3.4).

Happy Creek Igneous Complex

There are several interpretations regarding which rocks and rock types are included in the Happy Creek Igneous Complex (Willden, 1958; Willden, 1963; Russell, 1981; Russell, 1984; Maher, 1989; Quinn, 1996; Quinn et al., 1997). Initial studies by Willden (1958; 1963) described the Happy Creek Igneous Complex as a Permian or older

volcanic and volcaniclastic succession of basaltic to andesitic flows, flow breccias, and volcaniclastic rocks. Russell (1981; 1984) viewed the Happy Creek Igneous Complex instead as a Mesozoic succession of compositionally similar intrusive, extrusive, and volcaniclastic rocks. While Maher (1989) agreed with the Mesozoic age of the Happy Creek Igneous Complex, he instead considered the unit to be entirely composed of volcanic and sedimentary strata. More recently, Quinn (1996) and Quinn et al. (1997) interpreted the Happy Creek Igneous Complex to represent a latest Triassic-Early Jurassic mix of hypabyssal basaltic to andesitic intrusions and intrusion breccias with minor supracrustal strata. Here, we use a combination of earlier descriptions and describe the Happy Creek Igneous Complex to include a succession of dominantly Early Jurassic mafic to intermediate volcanic, volcaniclastic, and intrusive rocks that generally lie within the center of the Jackson Range (Fig. 3.3). Rock types in this sequence include a package of subgreenschist-facies fine-grained volcanic and intrusive rocks ranging in composition from basaltic andesite to andesite in addition to packages of volcaniclastic strata that include conglomerate, breccia, sandstone, and mudstone (Russell, 1981; 1984; Quinn, 1996; Quinn et al., 1997).

Early Mesozoic Intrusive Suite

The Early Mesozoic Intrusive Suite is composed of several epizonal plutons, stocks, and dikes intruding into the Happy Creek Igneous Complex and Boulder Creek Beds (Fig. 3.3). Compositionally, rocks within the Early Mesozoic Intrusive Suite range from gabbro to granodiorite with the most common lithologies of quartz diorite to diorite (e.g. Russell, 1981; Maher, 1989; Quinn, 1996). Major, trace, and REE data for the Early Mesozoic Intrusive Suite are similar to basalts and basaltic andesites of the Happy Creek

Igneous Complex (e.g. Russell, 1981; Quinn, 1996; Quinn et al., 1997). These data show the Early Mesozoic Intrusive Suite as a package of high-K calc-alkaline intrusions that are genetically related to the Happy Creek Igneous Complex (Maher, 1989; Quinn, 1996). Together with the Happy Creek Igneous Complex, these rocks are interpreted to reflect Mesozoic arc volcanism in either a continental (Quinn, 1996; Quinn et al., 1997) or intraoceanic arc setting (Russell, 1981; 1984). U-Pb zircon geochronology presented by Quinn (1996) and Quinn et al. (1997) shows two general age groupings in the Early Jurassic and Late Jurassic for plutons of the Early Mesozoic Intrusive Suite.

Here, we provide brief descriptions of the Willow Creek pluton and Harrison Grove pluton to complement our new U-Pb zircon geochronology presented later. The Willow Creek pluton (WCP) is found on the eastern side of the range and is generally composed of two distinct phases (Fig. 3.3). The more common phase is a hornblende monzodiorite to monzonite with the less common phase consisting of a hornblende-pyroxene diorite (Quinn, 1996). The Harrison Grove pluton (HGP) is found on the western side of the Jackson Mountains and generally ranges in composition from diorite to quartz monzodiorite (Fig. 3.3) (Quinn, 1996).

Structural Geology of the Jackson Mountains

Structurally, the Jackson Mountains have experienced at least one, and perhaps multiple episodes of Mesozoic shortening that have resulted in the production of folds, cleavage, and/or thrusts. In light of this complicated history, previous work in the Jackson Mountains has resulted in several interpretations regarding the structural history (Fig. 3.5) (Russell, 1981; 1984; Maher, 1989; Quinn, 1996; Quinn et al., 1997). In the

following section, we review the proposed structural histories from these authors highlighting the orientation and type of structures.

Early detailed work by Russell (1981; 1984) concluded that several episodes of Mesozoic shortening affected the rocks of the Jackson Mountains between the Middle Jurassic and mid-Cretaceous (Fig. 3.5). The earliest phase (D_1) resulted in the production of “cryptic”, large-scale (0.5-1 km wavelength) NW or SE trending open folds (Fig. 3.5) (Russell, 1981). This period of NE-SW shortening was constrained to between the Middle Jurassic and Early Cretaceous (Fig. 3.5) (Russell, 1981). Following D_1 , and by far the best documented, a period of NW-SE shortening (D_2) resulted in the production of thrust faults, NE trending folds, and a steeply dipping, NE striking axial planar cleavage (Fig. 3.5) (Russell, 1981). Following these events, an Early to mid-Cretaceous phase of thrusting (D_3) affected those earlier D_1 and D_2 structures (Fig. 3.5) (Russell, 1981; 1984). Maher (1989) concluded that a period of Middle Jurassic sinistral wrench faulting (D_1) was followed by late Middle to Late Jurassic E-vergent folding and thrusting (D_2) (Fig. 3.5). This was then followed by a period of late-Early Cretaceous W and E-vergent thrusting (D_3) (Fig. 3.5) (Maher, 1989).

More recent work by Quinn (1996) and Quinn et al. (1997) concluded that all shortening deformation in the Jackson Mountains was pre-Cretaceous (Fig. 3.5). Like Russell (1981), these authors recognized an early period (D_1) of NE-SW shortening that resulted in NW-trending folds and a poorly developed axial planar cleavage (Fig. 3.5). Overprinting and cutting this earlier fabric is the widespread and strongly developed NE-trending folds and cleavage (D_2) recognized by previous workers (Fig. 3.5) (Quinn, 1996). Based on the conclusion that the D_2 fabric is exclusively developed in rocks older

than the King Lear Formation, this later phase of NW-SE shortening was constrained to post-late Early Jurassic and pre-Early Cretaceous (Fig. 3.5) (Quinn, 1996; Quinn et al., 1997).

Sample Collection and Analytical Procedures

Boulder Creek Beds Detrital Zircon

Sample collection for U-Pb zircon geochronology was aimed at documenting the age and provenance for each of the five stratigraphic subunits of the Boulder Creek Beds as subdivided by Quinn (1996). As such, we collected ~4-5 kg of fine- to coarse-grained sandstone (samples BCB-1, 2, 3, and 5) and volcaniclastic breccia (BCB-4) samples from these subunits (Figs. 3.3 and 3.4; Table 3.2). Unfortunately, due to its mafic composition, no zircons were recovered from subunit BCB-4. U-Pb detrital zircon data for four sandstone samples were obtained using laser ablation-inductively coupled plasma-mass spectrometry (LA-ICPMS) at Boise State University following the methods of Rivera et al. (2013). In order to tightly constrain the maximum depositional age of the samples, we plucked and analyzed several of the youngest zircons from each sample using chemical abrasion-isotope dilution thermal ionization mass spectrometry (CA-IDTIMS) at Boise State University following the methods of Davydov et al. (2010) and Rivera et al. (2016).

To calculate a maximum depositional age from the tandem use of LA-ICPMS and CA-IDTIMS, we advocate for the following protocol. Using LA-ICPMS, measure the dates of 100 or more grains to isolate the tail of the youngest subpopulation. From this tail, select grains to be further processed by chemical abrasion in concentrated HF to remove damaged zones and areas that may have experienced Pb loss. Assuming chemical abrasion has negated any problems associated with Pb loss, isolate the youngest sample

from the CA-IDTIMS dates by outlier rejection of older grains. We suggest the mean age of this youngest sample is a more robust measure of the maximum depositional age than using LA-ICPMS alone.

Happy Creek Igneous Complex

To resolve the age of the Happy Creek Igneous Complex, we collected and processed three (~4-5 kg) samples of intermediate to mafic volcanic and intrusive rocks. Unfortunately, probably due to this unit's composition, we were only able to recover zircons from one sample of a basaltic andesite to andesitic flow (sample HC-JM-1) (Fig. 3.3). As with the Boulder Creek Beds samples, U-Pb data for this sample was first obtained using LA-ICPMS, followed by CA-IDTIMS.

Early Mesozoic Intrusive Suite

To investigate the emplacement age of the Willow Creek pluton (WCP) and Harrison Grove pluton (HGP), we collected one (~4-5 kg) sample of each for processing and analysis at Boise State University following the methods described above for the Happy Creek Igneous Complex and Boulder Creek Beds (Fig. 3.3; Table 3.2).

Results

Detrital Zircon Analysis

BCB-1

BCB-1 contains a single major distribution of Middle to Late Triassic (ca. 240–202 Ma) grains with a mode at ~213 Ma and grains as young as ~202 Ma, and only eight grains scattered between 280-250 Ma (Permian) (Fig. 3.6a) and one grain at 1.85 Ga. Five grains were then selected from the tail of the youngest subpopulation for CA-IDTIMS to constrain the maximum depositional age. Four successfully analyzed grains

yielded dates of 216.34 ± 0.35 Ma, 215.39 ± 0.15 Ma, 215.30 ± 0.36 Ma, and 215.08 ± 1.43 Ma (Fig. 3.6b).

BCB-2

Sample BCB-2 contains a single major distribution of Late Triassic-Early Jurassic (ca. 178-223 Ma) zircon grains with a mode at ~195 Ma and grains as young as ~178 Ma, as well as nine grains scattered between 293-228 Ma (Permian-Triassic) (Fig. 3.6c).

Sample BCB-2 contains no other Paleozoic zircons and no Precambrian zircons. Five grains were then selected from the tail of the youngest subpopulation for CA-IDTIMS to constrain the maximum depositional age. Four successfully analyzed grains yielded dates of 195.87 ± 0.16 Ma, 195.71 ± 0.12 Ma, 195.26 ± 0.15 , and 195.24 ± 0.21 Ma (Fig. 3.6d).

BCB-3

Sample BCB-3 contains a single major distribution of Late Triassic-Early Jurassic (ca. 245-190 Ma) grains with a mode at ~204 Ma and grains as young as ~190 Ma. Six additional grains are scattered between 337-276 Ma (Carboniferous-Permian) (Fig. 3.7a), with a single grain at 1.58 Ga. Seven grains were then selected from the tail of the youngest subpopulation for CA-IDTIMS to constrain the maximum depositional age. Six successfully analyzed grains yielded dates of 202.04 ± 0.70 Ma, 201.32 ± 0.17 Ma, 201.31 ± 0.34 Ma, 201.26 ± 0.26 Ma, 201.18 ± 0.18 Ma, and 201.12 ± 0.59 Ma (Fig. 3.7b).

BCB-5

BCB-5 contains a single major distribution of Late Triassic-Early Jurassic (ca. 239–189 Ma) grains with a mode at ~205 Ma and grains as young as ~189 Ma, with three grains scattered between 257–249 Ma (Permian-Triassic) (Fig. 3.7c) and two grains at

1.76 Ga. Five grains were selected from the tail of the youngest subpopulation for CA-IDTIMS and yielded dates of 208.04 ± 0.96 Ma, 207.42 ± 0.26 Ma, 206.68 ± 0.28 Ma, 206.35 ± 0.20 Ma, and 205.03 ± 0.16 Ma (Fig. 3.7d).

Magmatic Zircon Analysis

Happy Creek Igneous Complex

Sample HC-JM-1 yields a date of 191.9 ± 1.9 Ma from 17 analyses using LA-ICPMS (Fig. 3.8). From these grains, seven were selected for further processing using CA-IDTIMS (e.g. Krogh, 1973; Mattinson, 2005). In selecting these grains, we targeted the younger tail of LA-ICPMS data and used cathodoluminescence (CL) images to identify grains with relatively simple growth histories while avoiding grains with obvious cores and complicated growth zones. Six yielded concordant and equivalent isotope ratios with a weighted mean $^{206}\text{Pb}/^{238}\text{U}$ date of 190.29 ± 0.06 Ma (2σ , MSWD = 0.36, prob. fit = 0.875) (Fig. 3.8; Table 3.2). One grain yielded a slightly older (190.61 ± 0.14 Ma) date suggesting minor inheritance or magma residence (Fig. 3.8).

Harrison Grove Pluton

Our analysis of the Harrison Grove Pluton yields a date of 188.7 ± 1.2 Ma from 53 analyses using LA-ICPMS (Fig. 3.9). From these grains, five were selected for further processing using CA-IDTIMS (e.g. Krogh, 1973; Mattinson, 2005). We selected grains in the same manner described for the Happy Creek Igneous Complex. All five grains yielded concordant and equivalent isotope ratios with a weighted mean $^{206}\text{Pb}/^{238}\text{U}$ date of 189.32 ± 0.07 Ma (2σ , MSWD = 1.3, prob. fit = 0.2539) (Fig. 3.9; Table 3.2).

Willow Creek Pluton

Our analysis of the Willow Creek Pluton yields a date of 159.95 ± 0.93 Ma from 70 analyses using LA-ICPMS (Fig. 3.10). From these grains, five were selected for further processing using CA-IDTIMS (e.g. Krogh, 1973; Mattinson, 2005). We selected grains in the same manner described for the Happy Creek Igneous Complex and Harrison Grove pluton. All five grains yielded concordant and equivalent isotope ratios by CA-IDTIMS, with a weighted mean $^{206}\text{Pb}/^{238}\text{U}$ date of 161.81 ± 0.07 Ma (2σ , MSWD = 0.27, prob. fit = 0.8976) (Fig. 3.10; Table 3.2).

Discussion

Boulder Creek Beds Provenance and Paleogeography

In all analyzed subunits of the Boulder Creek Beds, the common result for detrital zircon data is a single Triassic to Early Jurassic mode with minimal input from older grains (Figs. 3.6, 3.7, 3.11a). Considering the strongly volcanogenic, texturally immature, marine lithologies described previously (e.g. Russell, 1981; Quinn, 1996), these new detrital zircon data from the BCB are consistent with and support a model of marine deposition adjacent to an active Triassic and Early Jurassic volcanic arc with minimal input from other sources. Furthermore, the lack of significant proportions of older grains (Fig. 3.11a) implies that deposition of the BCB did not occur directly adjacent to the continent where we would expect a large influx of older, craton-derived grains. Along these lines, the minor input of older grains are best explained through recycling of Paleozoic arc and basement sources upon which these volcanic edifices were built, rather than being directly derived from the continent. These data are therefore consistent with

reconstructions of Late Triassic-Early Jurassic paleogeography in which the Black Rock area was separated from the continent by a deep-marine basin (e.g. Wyld, 2000).

Comparison to detrital zircon from Late Triassic strata deposited in the deep-marine basin inboard of the Jackson Mountains provides further insight into the Late Triassic-Early Jurassic paleogeography and detrital zircon provenance. To the south of the Jackson Mountains, the Pine Nut Assemblage is composed of Late Triassic volcanogenic siliciclastic rocks and limestone deposited in a shallow marine environment (e.g. Oldow, 1984; Proffett & Dilles, 1984; Oldow, Satterfield, & Silberling, 1993). The detrital zircon signature from this assemblage (Fig. 3.11b), though a little older, is very similar to that of the BCB and has been interpreted as proximal back-arc sedimentation with detritus being shed from active Sierra-Klamath eruptive centers (Manuszak et al., 2000). As with the BCB, the lack of older, continentally derived zircons supports the presence of a deep-marine basin separating the arc from the continent. To the east of the Pine Nut Assemblage, the Luning Assemblage displays a similar Late Triassic mode (~223 Ma) interpreted as derived from active arc sources but additionally records contribution from continental or continental-margin sources (Fig. 3.11b) (Manuszak et al., 2000). This relationship suggests the Luning Assemblage was deposited closer to the continental margin allowing input from both the active arc from the west and the continent from the east. Finally, the Lovelock Assemblage represents more inboard strata deposited closer to the continental margin. Detrital zircon from this assemblage records a very minor Late Triassic (~227 Ma) mode with primarily Paleozoic and Precambrian zircons likely derived from the continent (Fig. 3.11b) (Manuszak et al., 2000). Taken together, these detrital zircon data from Late Triassic assemblages of the basinal terrane

support the presence of a deep-marine basin separating an active arc to the west and the North American continent to the east.

Considering the location of the Boulder Creek Beds with respect to these other Triassic successions deposited in the backarc region, the BCB along with the Pine Nut Assemblage could represent the westernmost portion of this marine basin that received significant amounts of material from the active arc. In this model, detritus being shed from the continent would be caught in the basinal and shelf successions like the Luning and Lovelock Assemblages to the south and east, among others (e.g. Manuszak et al., 2000). Further detrital zircon work on the Triassic successions of Nevada could be used to test this model. Furthermore, constraining the amount of continental and arc derived material in various positions of the backarc could provide further insight into the Triassic paleogeography and later reorganization along inferred strike slip faults such as the Pine Nut fault (e.g. Oldow, 1984). Alternatively, the BCB could represent an intra-arc succession within the Black Rock terrane. This model would satisfy both the lack of continentally derived zircons and abundance of arc derived material in the BCB.

Comparison to Olds Ferry terrane

Late Triassic paleogeographic reconstructions have suggested that the Olds Ferry and Black Rock terranes could represent fragments of the same early Mesozoic fringing arc that were then separated and displaced by ~400 km of Early to mid-Cretaceous dextral strike-slip translation (e.g. Wyld & Wright, 2001; LaMaskin et al., 2011; LaMaskin et al., 2015). In this model, the Mojave-Snow Lake Fault (MSLF), the Western Nevada Shear Zone (WNSZ), and the Western Idaho Shear Zone (WISZ) may represent strands of a major Cretaceous fault zone that translated outboard terranes to their current

positions ~400 km to the north of their Triassic-Jurassic positions (Fig. 3.1). If this translation model is correct, we would predict similar geologic and tectonic histories preserved in the Black Rock and Olds Ferry terranes.

Our new detrital zircon data from the Boulder Creek Beds when compared to detrital zircon data from sediments deposited in the forearc of the Olds Ferry terrane (i.e. the Weatherby Formation) provide insight into this possible correlation and paleogeographic configuration. Sandstones from the Weatherby Formation yield a major Late Triassic to Early Jurassic mode with no input from older grains (Fig. 3.11c) (LaMaskin et al., 2011). These detrital zircon signatures are remarkably similar to those documented in the BCB and suggest derivation from active arc sources with no input from older, continentally derived material. Furthermore, recent geochronology of intrusive and volcanic rocks from the Olds Ferry terrane reveals abundant Late Triassic-Early Jurassic (~228 Ma to ~187 Ma) magmatism (e.g. Kurz, 2010; Tumpane, 2010; Kurz et al., 2016). These ages overlap with detrital zircon ages from the BCB and suggest a possible source. While these new data do not unequivocally prove the correlation between the Black Rock and Olds Ferry terranes, the strong similarity in detrital zircon provenance does support a paleogeographic linkage between these geographically separated arc fragments. Additionally, similarities in deformation history and provenance geochemistry support this connection (e.g. Wyld, Quinn, & Wright, 1996; LaMaskin, Dorsey, & Vervoort, 2008; LaMaskin et al., 2011).

Together, new detrital zircon data from the Jackson Mountains, when compared to the Olds Ferry terrane provide support for the correlation of these two arc terranes as representing fragments of the same early Mesozoic fringing arc that was later fragmented

by ~400 km of dextral strike-slip motion. Restoring that motion provides the following simplified Late Triassic to Early Jurassic paleogeography (Fig. 3.12) of the Olds Ferry and Black Rock terranes representing fragments of the same early Mesozoic fringing arc shedding material into the forearc (i.e. Weatherby Formation) and the BCB. Additionally, detrital zircon from the Jackson Mountains when compared to the Late Triassic assemblages of western Nevada provide support for the existence of a deep marine basin separating the arc from the North American continent (Fig. 3.12).

Correlation With Strata in the Pine Forest Range?

Previous studies have suggested a correlation between the BCB in the Jackson Mountains and similar aged strata in the Pine Forest Range (Fig. 3.4) (e.g. Quinn, 1996). However, a comparison of our new data with published detrital zircon data in the Pine Forest Range does not support this interpretation. To date, the only Triassic unit in the Pine Forest Range that has been analyzed using detrital zircon is a medium-grained sandstone from the Bishop Canyon Formation (Darby, Wyld, & Gehrels, 2000). As mentioned earlier, Quinn (1996) correlates the Bishop Canyon Formation with subunit BCB-1 in the Jackson Mountains. Detrital zircon analysis of 29 zircons yielded 11 that are younger than 450 Ma with the remainder between 1.1 to 3.1 Ga and the most dominant peaks at 326 Ma, 341 Ma, 366 Ma, and 1900 Ma (Fig. 3.13) (Darby et al., 2000). When compared to the detrital zircon data for sample BCB-1 (Figs. 3.6a and 3.11a), the differences become immediately clear. As discussed before, BCB-1 contains a single major distribution of Middle to Late Triassic grains with a mode at ~213 Ma, eight Permian grains (Fig. 3.6a), and one Paleoproterozoic grain. This is in clear contrast to detrital zircon from the Bishop Canyon Formation that contains exclusively Paleozoic

and Precambrian zircons (Fig. 3.13). As such, a direct correlation between BCB-1 and the Bishop Canyon Formation seems implausible at this time. Future sampling should target other Triassic units in the Pine Forest Range (i.e. Dyke Canyon Formation and Cherry Creek Formation) to test the possible correlation to strata in the Jackson Mountains.

Boulder Creek Beds Maximum Depositional Age

Previous age constraints on subunits of the BCB have been based on the recovery of partially recrystallized fossils found primarily in clasts and olistostromal blocks (Table 3.1) (e.g. Willden, 1963; Russell, 1981; Maher, 1989; Quinn, 1996). While beneficial, these detrital faunal ages could not be used to tightly constrain the depositional age of the BCB. First, the partial recrystallization and deformation of many fossils has in some cases made confident identification difficult. Second, many of these fossils were recovered from clasts and/or blocks and therefore represent a maximum age that ranges from the late Paleozoic (?) to Norian (Late Triassic). As such, the BCB has come to be thought of as a Carnian to Norian succession (e.g. Russell, 1981; Maher, 1989; Quinn, 1996).

New high-precision U-Pb zircon geochronology on detrital zircon grains from the tail of the youngest subpopulations provides important refinements to the maximum depositional age of subunits of the BCB. These new age constraints demonstrate that the BCB is younger than previously thought with maximum depositional ages ranging from the Sinemurian (Early Jurassic) to the middle Norian (Late Triassic) (Figs. 3.6 and 3.7). Therefore, the BCB now represents a Late Triassic (Norian) to Early Jurassic (Sinemurian) sequence of volcanogenic marine rocks deposited adjacent to an active Triassic and Early Jurassic volcanic arc.

While these ages for the BCB represent maximum depositional ages, they are rather close to the true depositional age for several reasons. All analyzed samples consist of one dominant mode with very little to no older material (Figs. 3.6 and 3.7). This relationship advocates for a proximal, single source of sediment. That source was likely an active arc as discussed previously, a scenario that is strongly supported by the lithology and petrography of the BCB and interbedded volcanics (e.g. Russell, 1981; Quinn, 1996). The zircons could have been delivered directly by ash-fall and pyroclastic flows or indirectly through the subaerial or subaqueous weathering and erosion of flows and/or ash. In either case, the grains were delivered over short travel times and distances such that magmatism and deposition were roughly coeval. Therefore, we believe the maximum depositional ages reported here are very close to the true depositional ages for subunits of the BCB.

LA-ICPMS and CA-IDTIMS

An important product of this study relates to the importance of using caution when selecting which dates to use in the interpretation of the maximum depositional age from LA-ICPMS detrital zircon data. Several different approaches have been suggested and used in the literature with varying degrees of success (e.g. Tyler, Page, & Griffin, 1999; Carter & Bristow, 2000; Nelson, 2001; Barth et al., 2003; Barth et al., 2004; Dickinson & Gehrels, 2009; Gehrels, 2012). In general, the use of multiple youngest grain ages or the youngest peak of ages has been suggested to provide more reliable results compared to the use of the youngest detrital zircon age (e.g. Dickinson & Gehrels, 2009).

In all subunits from the BCB reported here, the common characteristic is a dominant Late Triassic to Early Jurassic mode with tails defined by grains with apparent dates as much as 13-17 Ma younger than the dominant mode (Figs. 3.6 and 3.7). When several of those youngest grains are analyzed using the more precise CA-IDTIMS, the resulting ages are up to ~17 My older than when analyzed using LA-ICPMS and generally overlap with the primary youngest mode of LA-ICPMS data (Figs. 3.6 and 3.7). This relationship suggests that portions of those youngest grains have experienced varying degrees of Pb loss, that when chemically abraded in concentrated HF, the portion of the grains with the loss is removed. Therefore, an interpretation of maximum depositional age using those youngest grains analyzed by LA-ICPMS would be biased by as much as 17 My younger than the true geological age due to Pb loss. While in some scenarios this may not be a significant issue, in the Jackson Mountains it would suggest that deposition of the BCB is actually coeval and possibly younger than the Happy Creek Igneous Complex and plutons of the Early Mesozoic Intrusive Suite, a scenario that is incompatible with field relationships. These results support the use of the youngest mode from LA-ICPMS data as a more accurate measure of the maximum depositional age (e.g. Dickinson & Gehrels, 2009; LaMaskin et al., 2015). Furthermore, we strongly discourage the use of the youngest detrital zircon age and/or several ages when investigating the maximum depositional age due to problems associated with Pb loss. If possible, the tandem use of LA-ICPMS and CA-IDTIMS is a more robust tool to investigate the maximum depositional age of sedimentary rocks.

Jurassic Structural Evolution

Several interpretations regarding the structural architecture and evolution of the Jackson Mountains have been suggested by previous workers (Fig. 3.5) (e.g. Willden, 1958; Russell, 1981; Maher, 1989; Quinn, 1996). The contact relationships between the Boulder Creek Beds and other rock units (i.e. Paleozoic section, Happy Creek Igneous Complex, and Early Mesozoic Intrusive Suite) are a critical issue with respect to these structural interpretations. These relationships have been interpreted as either thrust faults placing the BCB over the Happy Creek Igneous Complex and Early Mesozoic Intrusive Suite (Russell, 1981; Maher, 1989) or as the Happy Creek Igneous Complex and plutons of the Early Mesozoic Intrusive Suite intruding into the BCB (Quinn, 1996). These alternative interpretations have then led to considerably different estimates of the amount and timing of Mesozoic shortening in the Jacksons. As discussed here, new age constraints, when combined with existing structural observations, provide evidence for thrust faulting, folding, and cleavage development associated with NW-SE shortening between the middle Early to early Late Jurassic.

Our new constraints on the maximum depositional age of the BCB suggest that several older over younger relationships exist within the eastern and western packages of the BCB (Figs. 3.3, 3.4, 3.6, and 3.7). Furthermore, the Paleozoic section apparently overlies the BCB and the BCB overlies the Early Jurassic (190.29 ± 0.06 Ma) Happy Creek Igneous Complex and Harrison Grove Pluton (189.32 ± 0.07 Ma) (Figs. 3.3, 3.8, and 3.9). Where exposed, field evidence strongly supports a thrust relationship to explain the juxtaposition of older over younger rocks. For example, in the vicinity of Alaska Canyon, an examination of the contact between a massive limestone of BCB-1 and the

Happy Creek Igneous Complex reveals a ~30 cm thick, highly sheared and brecciated zone (Fig. 3.14). While Quinn (1996) interprets this relationship to be intrusive, the lack of any significant thermal alteration expected with intrusion into a limestone does not support this conclusion. Furthermore, within the Happy Creek Igneous Complex, a well-documented NE trending axial planar cleavage becomes stronger and more closely spaced when nearing contacts inferred as thrust faults (e.g. Russell, 1981; Maher, 1989; Quinn, 1996). Within the BCB, identification of clear brecciation and planar shear fabrics along subunit contacts support the interpretation of internal thrusts (Maher, 1989). Together, these observations provide evidence for significant thrust faulting both within the BCB and between the Paleozoic section, BCB, and Happy Creek Igneous Complex. These thrust faults have translated the Paleozoic section over the BCB, older subunits of the BCB over younger subunits, and the BCB over the Happy Creek Igneous Complex and Early Jurassic plutons of the Early Mesozoic Intrusive Suite (Figs. 3.3 and 3.15).

On the geologic map (Fig. 3.3), these thrust faults are found on the east and west sides of the Jackson Mountains and generally dip away from the center of the range (Fig. 3.15). This observation led previous authors to conclude that the Jackson Mountains contains two thrust systems with opposing vergence, a western belt of east vergent thrusts and an eastern belt of west vergent thrusts (Russell, 1981; Maher, 1989). However, the likelihood of two roughly coeval opposing thrust systems is difficult to reconcile. We instead suggest these two thrust systems are actually part of a single belt of E-SE vergent thrust faults that were folded into a large, N-NE trending antiform during a period of NW-SE shortening (Figs. 3.3, 3.15, and 3.16). Furthermore, based on the timing, shortening direction, and geographic location of the Jackson Mountains, these data imply

that thrusting and folding was associated with the development of the adjacent Luning-Fencemaker fold-and-thrust belt and SE-vergent thrusting of the arc over the basinal terrane.

Based on available structural data and our new geochronology, the following structural model is proposed. We would also like to note that while the internal structure and stratigraphy of the BCB are difficult to constrain, the overall picture of a Paleozoic section thrust over the BCB, and the BCB thrust over the Happy Creek Igneous Complex and Early Jurassic plutons of Early Mesozoic Intrusive Suite is clear.

Early development (post ~189 Ma) of the thrust belt involved E-SE vergent thrusting of the Paleozoic section over younger units, duplexing and thrusting of subunits of the BCB, and thrusting of the Paleozoic section/BCB over the Happy Creek Igneous Complex and Early Jurassic plutons of the Early Mesozoic Intrusive Suite (Fig. 16a). We suggest that duplexing of the BCB best explains the complicated geometry of thrust faults within the BCB pinching out on the west side of the range but still observable on the east side (Figs. 3.3 and 3.15). The timing of this thrusting can be constrained using our new geochronology data, as the thrust faults must postdate the youngest units involved. In this case, the BCB and Paleozoic section are thrust over the Harrison Grove Pluton (~189 Ma) and require that thrusting initiated after the Early Jurassic intrusion of the HGP (Figs. 3.3 and 3.9). The minimum age of thrusting is constrained on the east side of the Jackson Mountains where the Willow Creek pluton (~162 Ma) stitches a thrust fault bringing the Boulder Creek Beds over the Happy Creek Igneous Complex (Figs. 3.3 and 3.10). Therefore, movement along the thrust faults is constrained to between the middle Early Jurassic and earliest Late Jurassic (post ~189 Ma and pre ~162 Ma).

Subsequently, the thrust belt was folded into a large, N-NE trending antiformal structure coupled with the development of the pervasive N-NE striking, steeply dipping axial planar cleavage found throughout the range (Figs. 3.3, 3.15, and 3.16b). Though more difficult to constrain the timing of the large-scale fold, several observations suggest that folding was probably prior to the intrusion of the Willow Creek pluton. First, the Early Cretaceous (~118 Ma) King Lear Formation lacks the penetrative NE-trending fabric and metamorphism that is found in all older units (Quinn, 1996; Quinn et al., 1997; Martin et al., 2010; Chapter 2). Furthermore, the King Lear Formation is only locally folded near younger thrust faults and is not incorporated into the large-scale N-NE trending antiform. Additionally, the King Lear Formation is unconformably deposited on the Happy Creek Igneous Complex. This relationship demands that a period of erosion and denudation must have stripped away the Paleozoic section and BCB prior to deposition of the King Lear Formation. These observations demonstrate that large-scale folding of the Jurassic thrust belt must have been prior to the Aptian (~118 Ma) deposition of the King Lear Formation (Chapter 2).

While the Willow Creek pluton (WCP; Fig. 3.3) stitches the thrust belt and provides a minimum age for the thrust faults, it unfortunately does not constrain the timing of the fold. As such, the WCP could have intruded before or after folding. However, previous studies from elsewhere in the LFTB suggests that significant crustal shortening was complete by the Middle to Late Jurassic (~162 Ma) (e.g. Elison & Speed, 1989; Wyld et al., 2001; Wyld, 2002; Wilkins, 2010). Therefore, if the thrust faults and large-scale folding were associated with the development of the LFTB, the WCP likely intrudes after the development of the N-NE trending antiform (Fig. 3.16c). Together, our

preferred model for the Jurassic structural evolution of the Jackson Mountains includes significant thrust faulting, folding, and cleavage development that formed during a single period of NW-SE shortening associated with the development of the LFTB. Specifically, Early to Middle Jurassic (post ~189 Ma and pre ~162 Ma) E-SE vergent thrusting and duplexing was followed by the large-scale folding of the thrust belt prior to ~162 Ma.

After folding, erosion and denudation developed the paleosurface on which the Early Cretaceous King Lear Formation was deposited (Figs. 3.16d). Early Cretaceous (~118 Ma) deposition of the King Lear Formation associated with movement along the NW-vergent Deer Creek thrust completes the Mesozoic contractional history of the Jackson Mountains (Fig. 3.16e) (e.g. Willden, 1958; Colby et al., 2016; Chapter 2).

Latest Triassic to Early Jurassic Shortening

Previous authors have suggested that significant shortening in the Black Rock Desert region is constrained to the latest Triassic to Early Jurassic (e.g. Wyld, 1996; Quinn, 1996). These relations have been best documented in the Pine Forest Range and involved the development of a ductile shear zone with an associated strain gradient of increasing cleavage, tightening of folds, and increasing metamorphism toward the shear zone (Wyld, 1996). Based on the textural relationships of syn- and post-tectonic intrusions and U-Pb zircon geochronology, Wyld (1996) concluded that regional shortening was ongoing at ~201 Ma and over by ~185 Ma. In the Jackson Mountains, Quinn (1996) correlates NW-trending folds and axial planar cleavage to this same latest Triassic-Early Jurassic event in the Pine Forest Range. Quinn (1996) further presented $^{40}\text{Ar}/^{39}\text{Ar}$ geochronology of hornblende that yielded ages between ~201 Ma and ~190 Ma. However, a review of these structural data and $^{40}\text{Ar}/^{39}\text{Ar}$ geochronology reveal that

both are from the Paleozoic section exposed on the western side of the Jackson Mountains (e.g. Russell, 1981; Maher, 1989; Quinn, 1996). As documented here, the timing of major shortening in the Jackson Mountains is constrained to between the middle Early Jurassic and early Late Jurassic (post ~189 Ma and pre ~162 Ma). Together, these observations suggest distinct and unrelated tectonic histories preserved in the Pine Forest Range/Jackson Mountains Paleozoic section and the Jackson Mountains Mesozoic section. Therefore, within the Jackson Mountains, the western thrust fault that brings the Paleozoic section over the Mesozoic section may be a significant boundary as suggested by several previous authors (e.g. Russell, 1981; Silberling et al., 1987; Jones, 1990) (Fig. 3.3). These relationships could help explain the differences presented earlier in detrital zircon provenance of Late Triassic strata between the ranges.

Summary and Conclusions

New U-Pb detrital zircon geochronology provides insight into the maximum depositional age and provenance of the Late Triassic-Early Jurassic Boulder Creek Beds in the Jackson Mountains. Through the combination of LA-ICPMS and CA-IDTMS, we have shown the BCB to be younger than previously thought and represent a sequence of Norian to Sinemurian volcanogenic, marine rocks deposited adjacent to an active volcanic arc. Furthermore, our data supports the use of the youngest age mode rather than the age of the youngest grain from LA-ICPMS data as a more reliable and robust measure of the maximum depositional age (e.g. Dickinson & Gehrels, 2009; LaMaskin et al., 2015). However, if possible, we advocate for the tandem use of LA-ICPMS and CA-IDTMS when investigating the maximum depositional age of clastic rocks.

Our detrital zircon data is consistent with reconstructions of Triassic-Early Jurassic paleogeography in which the Black Rock area was separated from the continent by a deep-marine basin (i.e. basinal terrane) (Wyld, 2000). Comparison to detrital zircon in the Blue Mountains Province is consistent with paleogeographic reconstructions suggesting ties between the Black Rock and Olds Ferry terranes as a series of early Mesozoic fringing arcs separated and displaced by ~400 km of later dextral translation (e.g. Wyld & Wright, 2001; LaMaskin et al., 2011; LaMaskin et al., 2015).

Detrital zircon data combined with new geochronology of the Happy Creek Igneous Complex and plutons of the Early Mesozoic Intrusive Suite provides insight into the structural architecture and timing of major shortening in the Jackson Mountains. Between the middle Early Jurassic and early Late Jurassic (post ~189 Ma and pre ~162 Ma) NW-SE shortening resulted in the production of major thrust faults, folding, and cleavage development. Given the geographic proximity to the Luning-Fencemaker fold-and-thrust belt, strong similarities in timing, structural style, and shortening direction suggests that Jurassic shortening in the Jackson Mountains was associated with the development of the LFTB and closure of the early Mesozoic marine basin that culminated in the eastward thrusting of the arc terrane over the basinal terrane.

Acknowledgements

Work related to this study was partially funded by Willis and Rose Burnham Graduate Student Research Grant of the Department of Geosciences, Boise State University.

Table 3.1. Summary of Dominant Lithology and Published Age Constraints for Subunits of the Boulder Creek Beds. Modified from tables in Quinn (1996).

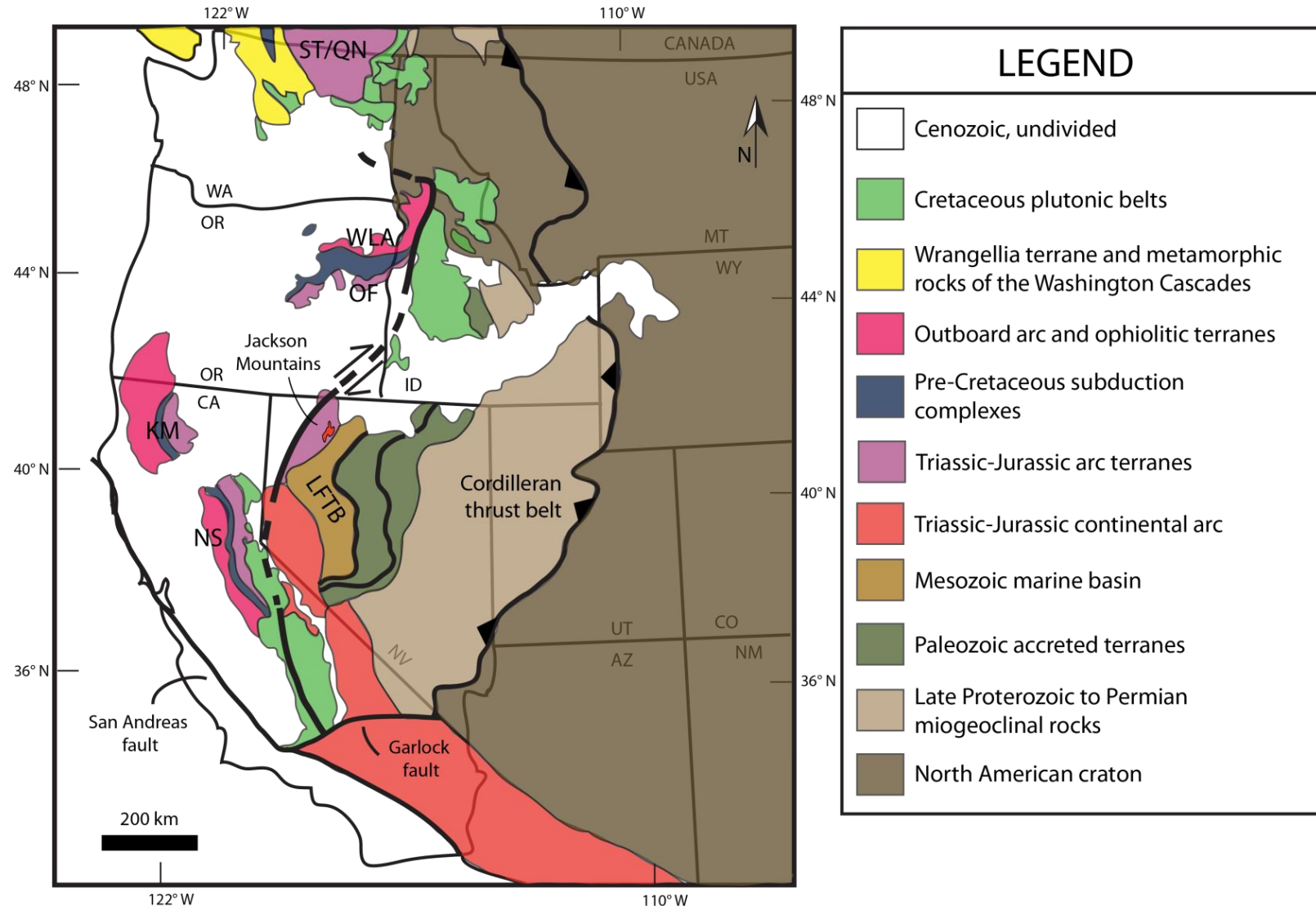
Subunit	Dominant lithology	Diagnostic fossil	Occurrence	Age	Reference
BCB-1	Volcanogenic, lithic rich sandstone, siltstone, argillite, and conglomerate, thin horizons of dark limestone and limestone megaclasts	Brachiopod: <i>Derbia</i> and other reworked late Paleozoic fauna	calcareous sandstone	Late Paleozoic	Russell (1981)
		Radiolarians	bedded chert and cherty limestone	Early Mesozoic (Triassic?)	Russell (1981)
		Bivalve: <i>Halobia cf. H. cordillerana</i>	pelitic rock	lower Carnian to middle Norian	Russell (1981)
		Coral	carbonate clast in conglomerate	Mesozoic	Russell (1981)
		Fusulinid	silicified limestone pebble	Late Paleozoic	Russell (1981)
		Bivalves: <i>Halobia cf. H. superba</i> and/or <i>Halobia cf. H. austriaca</i>	calcareous mudrocks	Carnian	Fuller (1986)
		Ammonites: <i>Arcestes pacificus</i> and <i>Discotropites mojsvarensis</i>	quartzose wackestone/packstones	Carnian	Fuller (1986)
		Conodonts: <i>Epigondolella primitia</i> or <i>E. postera</i>	massive limestone block	lower to middle Norian	Maher (1989)
		Ammonite: <i>Juvavites</i>	not specified	late early or early middle Norian	Maher (1989)
		Belemnite: <i>Aulacocera</i>	not specified	late Carnian to Norian	Maher (1989)
		Pectenacid bivalves	not specified	possibly Late Triassic	Maher (1989)

Table 3.1. continued

Subunit	Dominant lithology	Diagnostic fossil	Occurrence	Age	Reference
BCB-2	Volcaniclastic breccia, conglomerate, crystal-rich sandstone	No fossils recovered			
BCB-3	Lithic-rich sandstone, conglomerate, and siltstone with minor shale and debris-flow diamictite	Fusulinids Conodonts: <i>Neogondolella navicula</i> and <i>Epigondolella multidenta</i> Conodonts: <i>Epigondolella mungoensis</i> and <i>Neospathodus</i> Ammonite: <i>Joannites</i> Bivalves: <i>Halobia</i> or <i>Daomella</i>	limestones interpreted as olistoliths carbonate clasts in sandstone block of interbedded limestone and silicified mudstone block of interbedded limestone and silicified mudstone not specified	Permian Norian late Ladinian/early Carnian late Ladinian/early Carnian Middle or Late Triassic	Willden (1963) Russell (1981) Russell (1981) Russell (1981) Maher (1989)
BCB-4	Volcaniclastic breccia, conglomerate, crystal-rich sandstone	No fossils recovered			
BCB-5	Mudstone, sandstone, conglomerate, diamictite	Conodonts: <i>Epigondolella humboldtensis</i> or <i>Epigondolella postera</i>	carbonate clast in conglomerate	upper middle or upper Norian	Maher (1989)

Table 3.2. Summary of Samples and Corresponding $^{206}\text{Pb}/^{238}\text{U}$ ages

Sample Name	Geologic Map Unit	UTM Coordinates	$^{206}\text{Pb}/^{238}\text{U}$ Age (Ma)	MSWD	Prob. Of Fit	n
BCB-1	Boulder Creek Beds - subunit 1	11T 369962 E 4570340 N				
BCB-2	Boulder Creek Beds - subunit 2	11T 372261 E 4575070 N				
BCB-3	Boulder Creek Beds - subunit 3	11T 386124 E 4572609 N				
BCB-5	Boulder Creek Beds - subunit 5	11T 386905 E 4571537 N				
HC-JM-1	Happy Creek Igneous Complex	11T 375522 E 4573869 N	190.29 ± 0.06	0.36	0.875	6
HGP-1	Harrison Grove pluton	11T 372979 E 4575936 N	189.32 ± 0.07	1.3	0.2539	5
WCP-1	Willow Creek pluton	11T 382647 E 4567544 N	161.81 ± 0.07	0.27	0.8976	5



LEGEND

- [White square] Cenozoic, undivided
- [Light green square] Cretaceous plutonic belts
- [Yellow square] Wrangellia terrane and metamorphic rocks of the Washington Cascades
- [Pink square] Outboard arc and ophiolitic terranes
- [Dark blue square] Pre-Cretaceous subduction complexes
- [Purple square] Triassic-Jurassic arc terranes
- [Red square] Triassic-Jurassic continental arc
- [Brown square] Mesozoic marine basin
- [Dark green square] Paleozoic accreted terranes
- [Light brown square] Late Proterozoic to Permian miogeoclinal rocks
- [Dark brown square] North American craton

Figure 3.1. Simplified Geotectonic Assemblages of the Western United States. Modified from LaMaskin et al. (2011). ST/QN = Stikinia/Quesnellia terranes, WLA = Wallowa terrane, OF = Olds Ferry terrane, KM = Klamath Mountains, BR = Black Rock, NS = Northern Sierra, LFTB = Luning-Fencemaker fold-and-thrust belt.

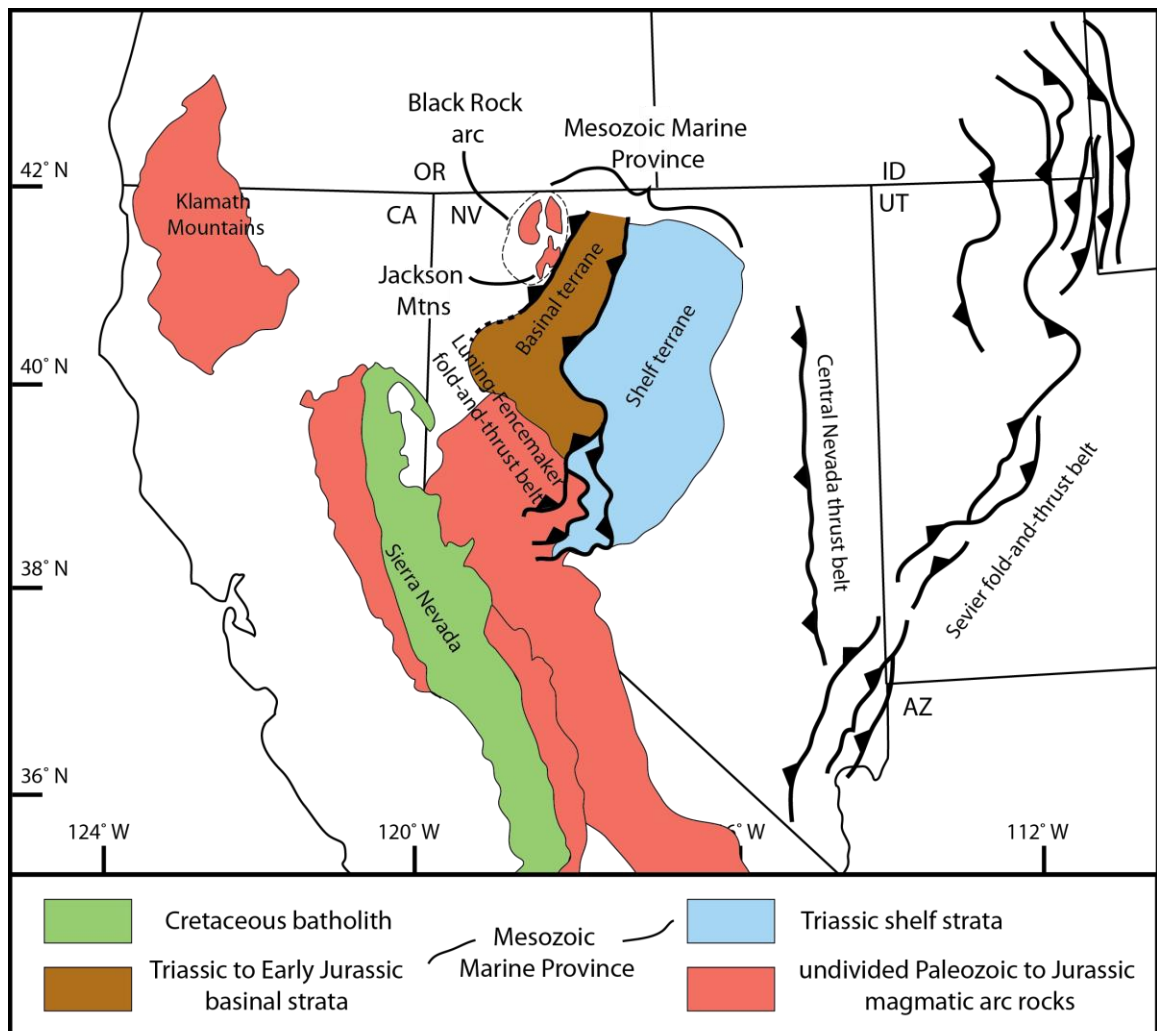


Figure 3.2. Simplified Map of the Great Basin and Western United States. Drafted to highlight the location of the Mesozoic Marine Province and Luning-Fencemaker fold-and-thrust belt in relation to Paleozoic and Mesozoic arc rocks. Modified after Wyld (2002).

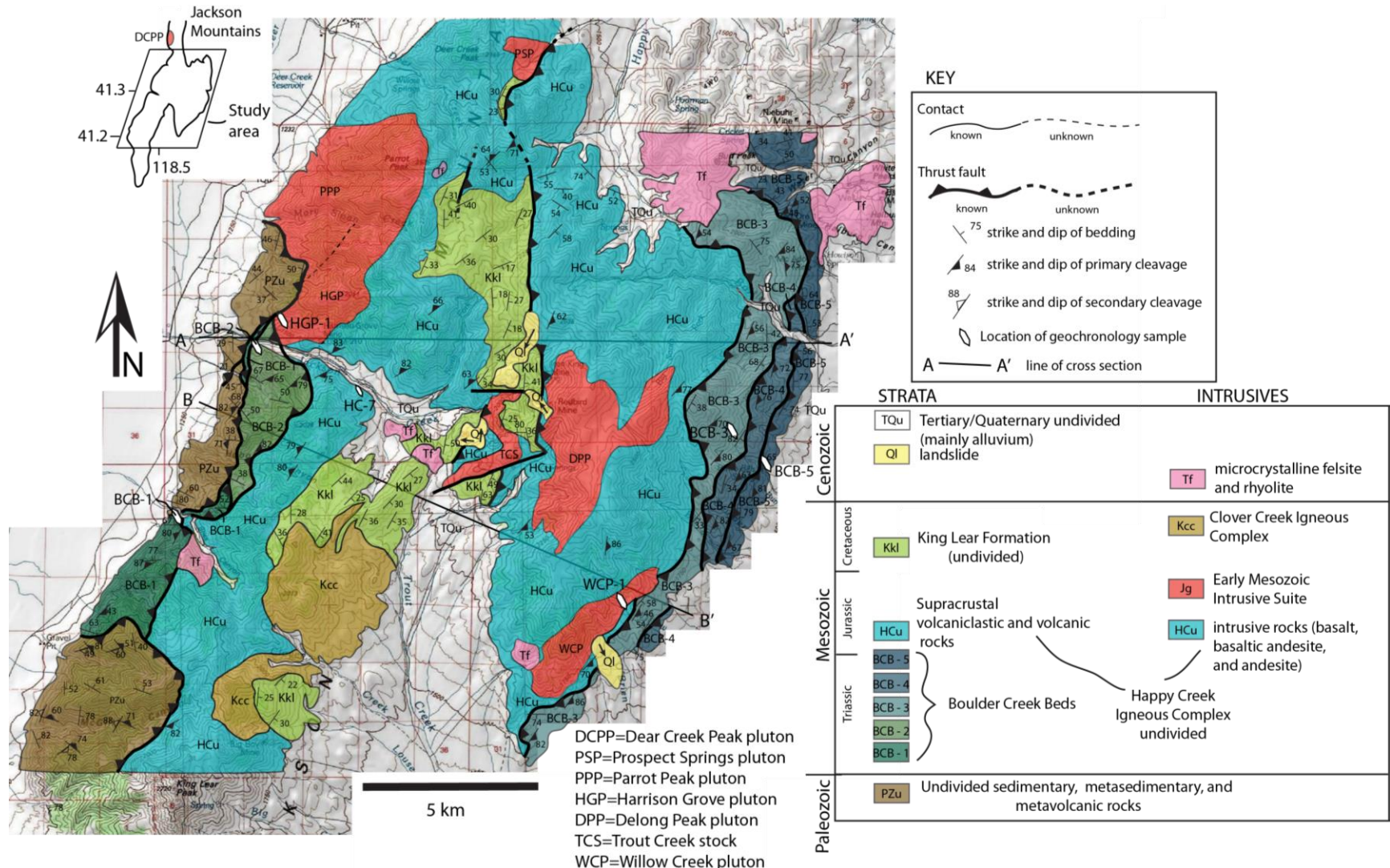


Figure 3.3. Geologic Map of the Central Jackson Mountains. Results from new geologic mapping and compilation from Russell (1981; 1984), Maher (1989), Quinn (1996), and Quinn et al. (1997).

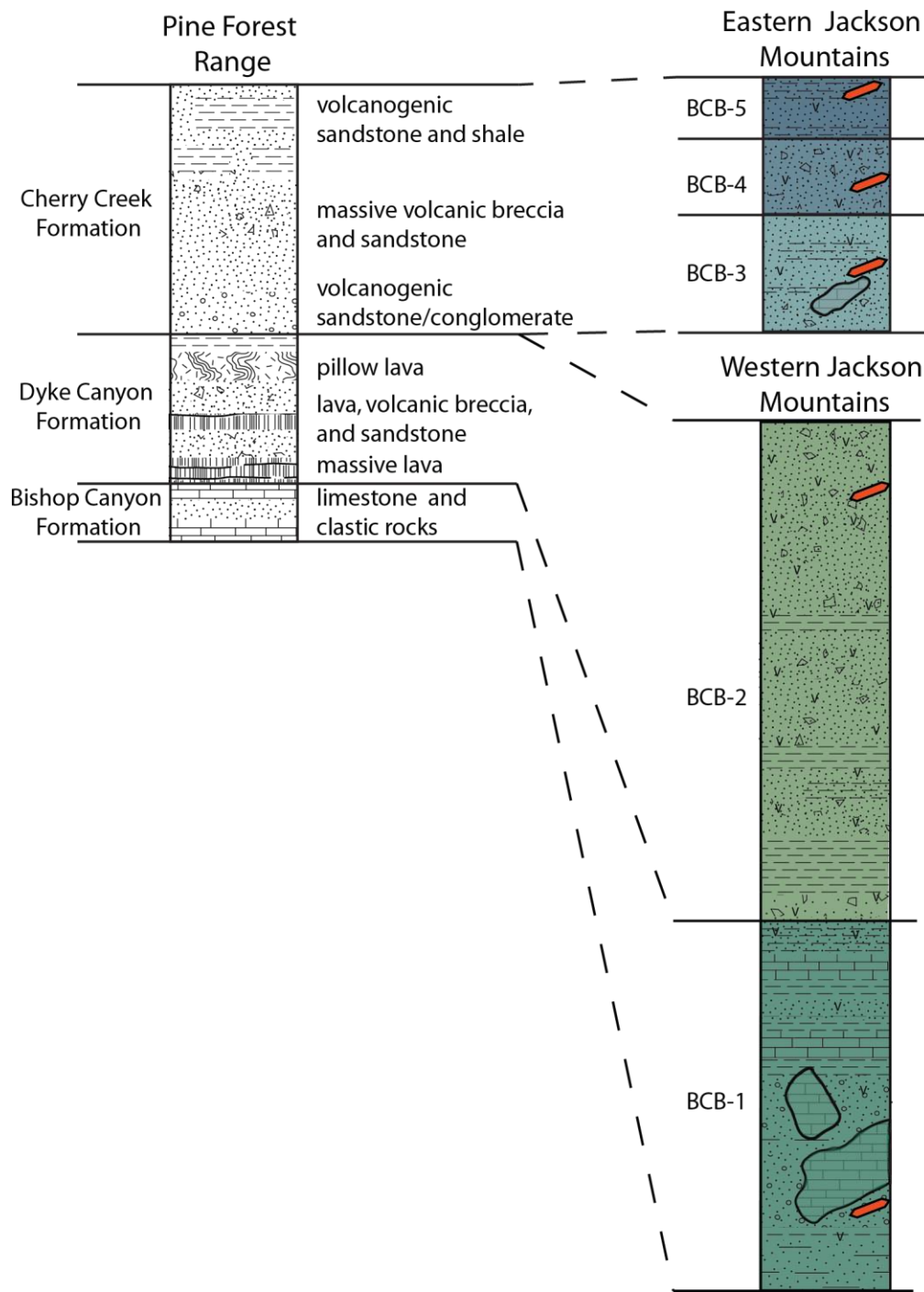


Figure 3.4. Simplified Stratigraphic Columns for Apparent Triassic Strata of the Pine Forest Range and Jackson Mountains. Refer to text and Table 3.1 for descriptions of subunits of the Boulder Creek Beds. Modified from Quinn (1996). Correlations of strata are from Quinn (1996). Red zircons mark the location of detrital zircon samples in this study.

		Russell (1981; 1984)	Maher (1989)	Quinn (1996); Quinn et al. (1997)
CRETACEOUS	LATE			
	EARLY	D ₃ Thrusting D ₂ NW-SE shortening (cleavage, thrusts, folds)	D ₃ W & E-vergent thrusts	(no Cretaceous shortening)
JURASSIC	LATE	D ₁ NE-SW shortening ("cryptic" large open folds)	D ₂ E-vergent folds & thrusts D ₁ Sinistral wrench faulting	D ₂ NW-SE shortening (NE-trending folds, cleavage)
	MIDDLE			
	EARLY			D ₁ NE-SW shortening (NW-trending folds, cleavage)
TRIASSIC	LATE			

Figure 3.5. Summary of Interpreted Mesozoic Structural History of the Jackson Mountains.

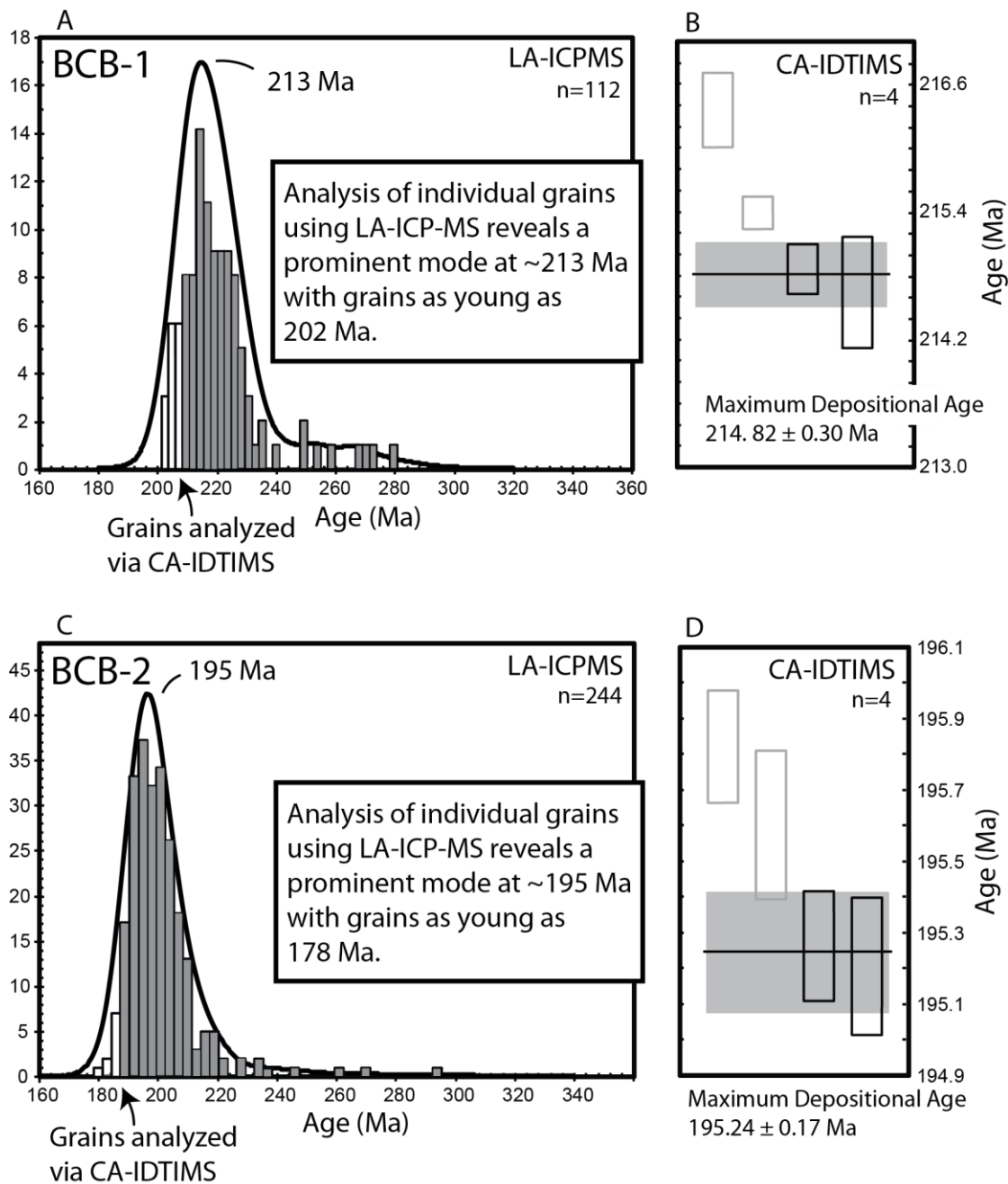


Figure 3.6. Relative Probability Plots, Histograms, and Ranked Age Plots for Detrital Zircons for Sandstones of BCB-1 and BCB-2. (A) and (C) represent dates obtained using LA-ICPMS. Curves represent the summation of individual detrital zircon ages and associated 2σ Gaussian errors; associated y-axes represent relative probability. Histograms are based on individual detrital zircon grain ages and do not incorporate errors; associated y-axes represent number of grains in a given age bin. (B) and (D) are CA-IDTIMS dates from the tail of the youngest detrital zircon subpopulation from LA-ICPMS. Ranked age charts show the distribution of $^{206}\text{Pb}/^{238}\text{U}$ ages from those grains. Bar heights depict their associated 2σ uncertainties. Grey horizontal bar and black line represent calculated maximum depositional age

from black analyses. Grey analyses were not used in calculation of maximum depositional age.

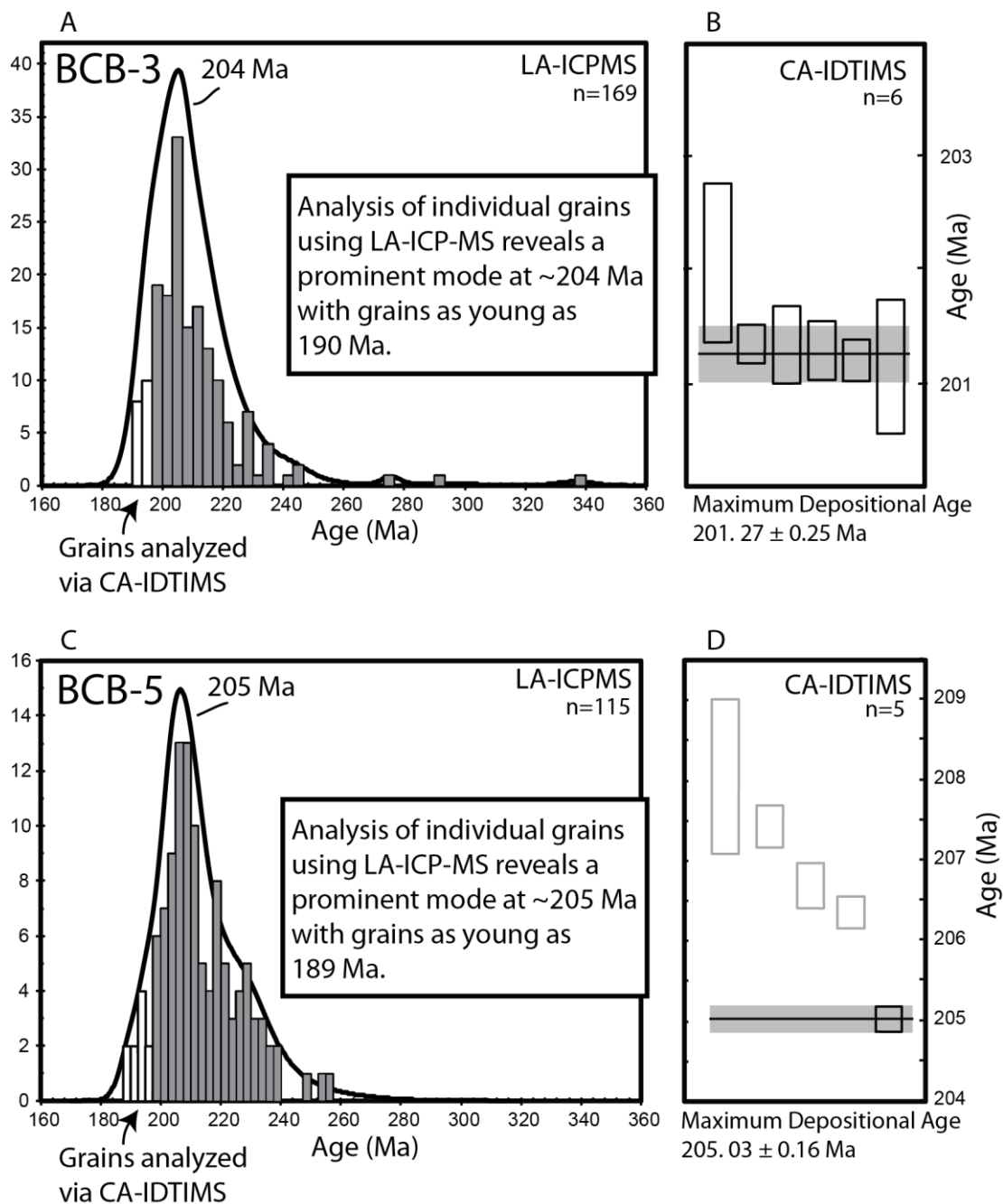


Figure 3.7. Relative Probability Plots, Histograms, and Ranked Age Plots for Detrital Zircons for Sandstones of BCB-3 and BCB-5. (A) and (C) represent dates obtained using LA-ICPMS. Curves represent the summation of individual detrital zircon ages and associated 2σ Gaussian errors; associated y-axes represent relative probability. Histograms are based on individual detrital zircon grain ages and do not incorporate errors; associated y-axes represent number of grains in a given age bin. (B) and (D) are CA-IDTIMS dates from the tail of the youngest detrital zircon subpopulation from LA-ICPMS. Ranked age charts show the distribution of $^{206}\text{Pb}/^{238}\text{U}$ ages from those grains. Bar heights depict their associated 2σ uncertainties. Grey horizontal bar and black line represent calculated maximum depositional age

from black analyses. Grey analyses were not used in calculation of maximum depositional age.

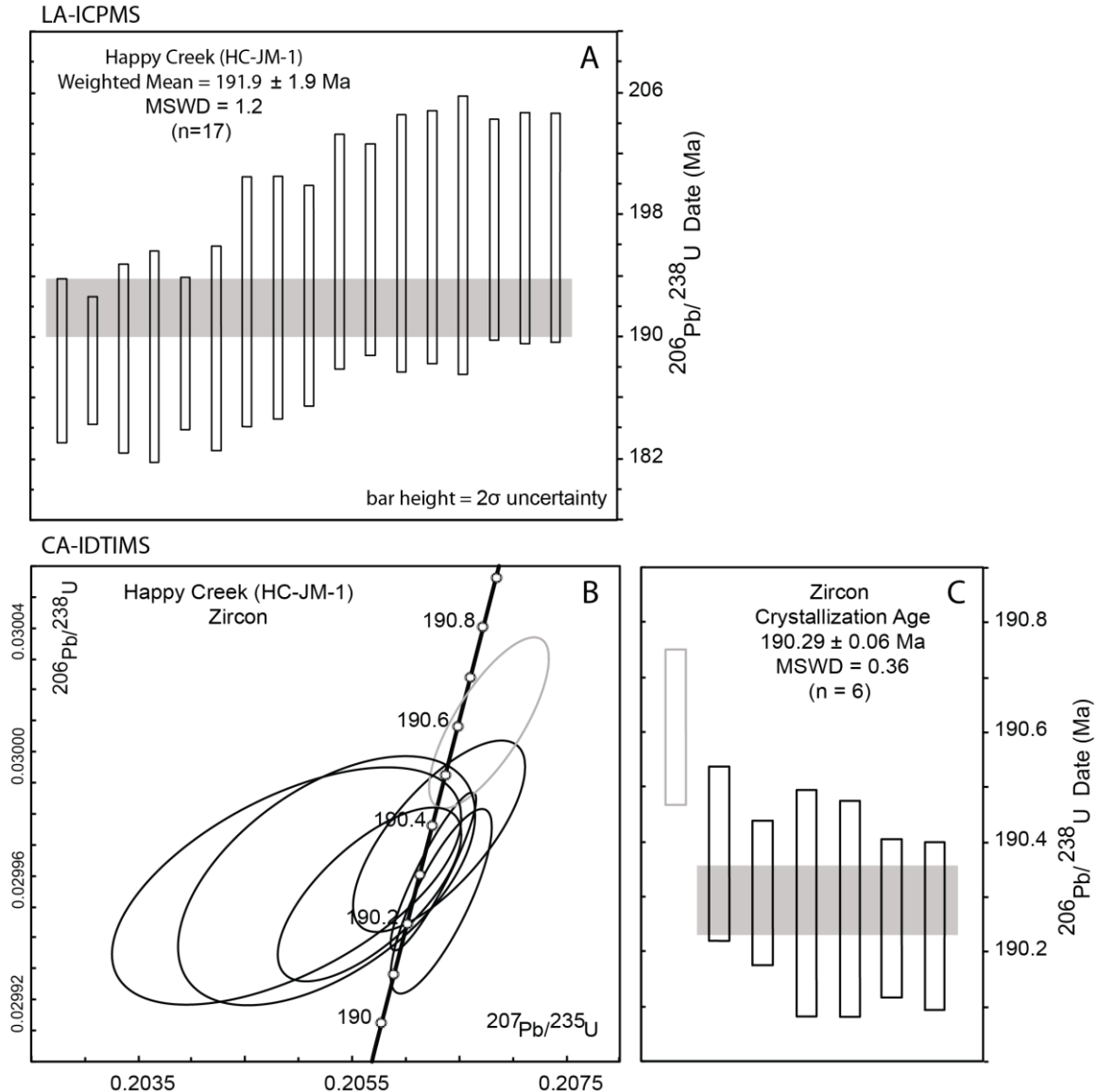


Figure 3.8. Results of U-Pb Zircon Geochronology Using Both LA-ICPMS (A) and CA-IDTIMS (B, C) of Magmatic Zircon From the Happy Creek Igneous Complex (HC-JM-1). For CA-IDTIMS results, zircon analyses included in the weighted mean $^{206}\text{Pb}/^{238}\text{U}$ crystallization age are represented by solid bold ellipses (B). Gray outlined ellipses were not used in any age calculation (B). Ranked age charts (C) located to the right of the concordia diagram show the distribution of $^{206}\text{Pb}/^{238}\text{U}$ ages. Bar heights depict their associated 2σ uncertainties. The gray band set behind the group represents the weighted mean of those analyses where the height illustrates the related uncertainty. Line-type designations on bar charts mimic those described for the concordia diagrams. MSWD—mean squared weighted deviation.

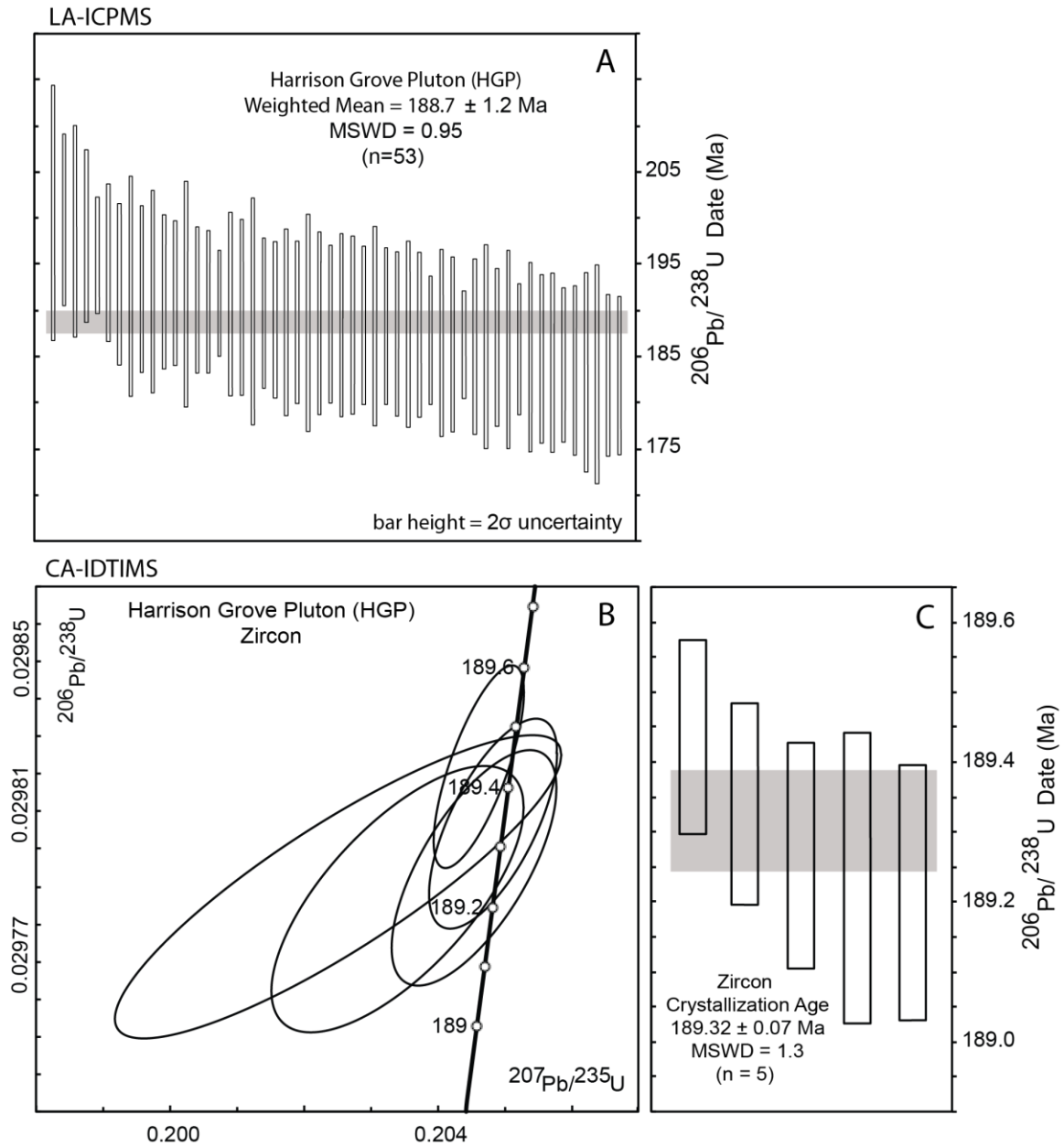


Figure 3.9. Results of U-Pb Zircon Geochronology Using Both LA-ICPMS (A) and CA-IDTIMS (B, C) of Magmatic Zircon From the Harrison Grove Pluton (HGP-1). For CA-IDTIMS results, zircon analyses included in the weighted mean $^{206}\text{Pb}/^{238}\text{U}$ crystallization age are represented by solid bold ellipses (B). Ranked age charts (C) located to the right of the concordia diagram show the distribution of $^{206}\text{Pb}/^{238}\text{U}$ ages. Bar heights depict their associated 2σ uncertainties. The gray band set behind the group represents the weighted mean of those analyses where the height illustrates the related uncertainty. Line-type designations on bar charts mimic those described for the concordia diagrams. MSWD—mean squared weighted deviation.

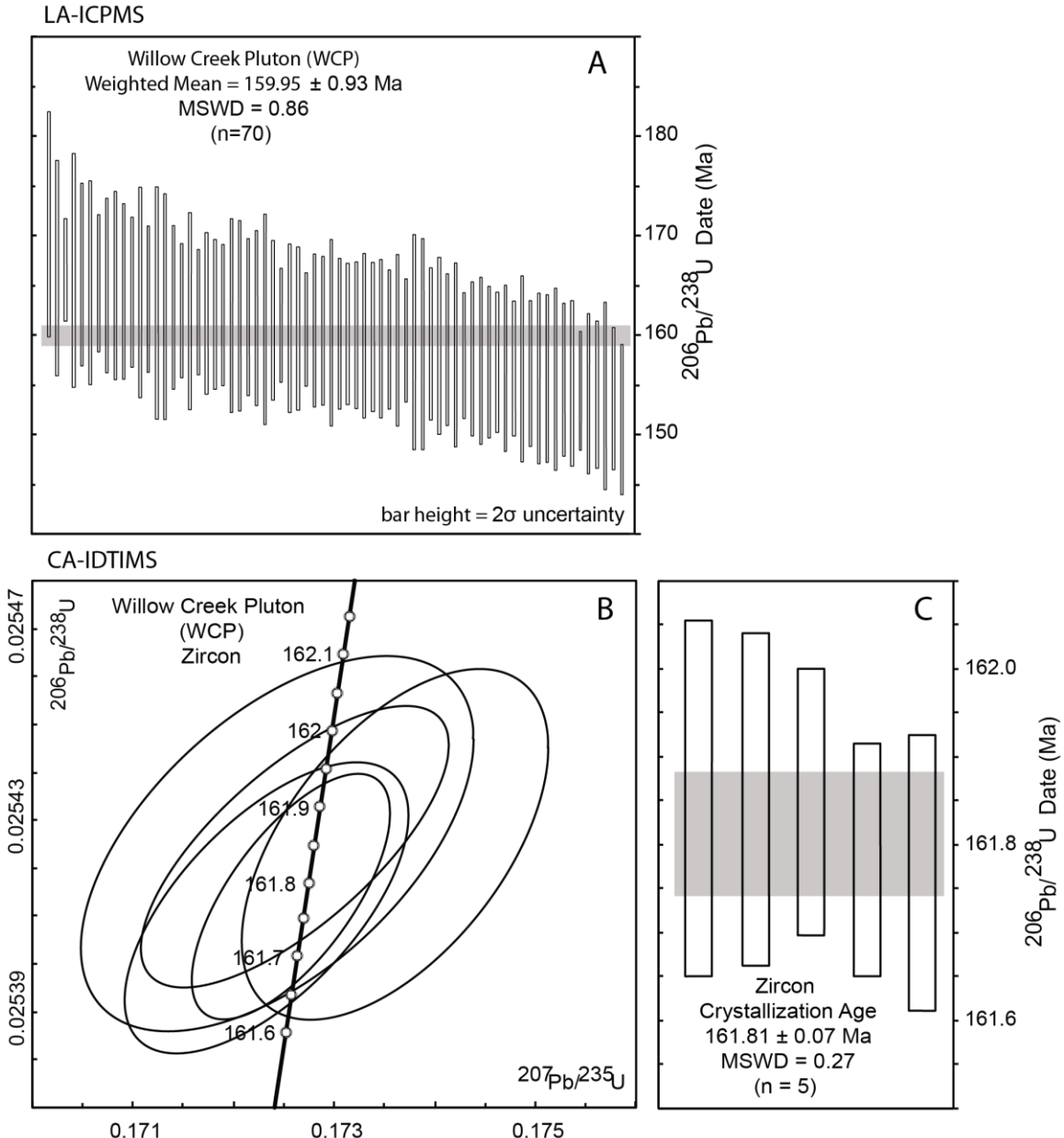


Figure 3.10. Results of U-Pb Zircon Geochronology Using Both LA-ICPMS (A) and CA-IDTIMS (B, C) of Magmatic Zircon From the Willow Creek Pluton (WCP-1). For CA-IDTIMS results, zircon analyses included in the weighted mean $^{206}\text{Pb}/^{238}\text{U}$ crystallization age are represented by solid bold ellipses (B). Ranked age charts (C) located to the right of the concordia diagram show the distribution of $^{206}\text{Pb}/^{238}\text{U}$ ages. Bar heights depict their associated 2σ uncertainties. The gray band set behind the group represents the weighted mean of those analyses where the height illustrates the related uncertainty. Line-type designations on bar charts mimic those described for the concordia diagrams. MSWD—mean squared weighted deviation.

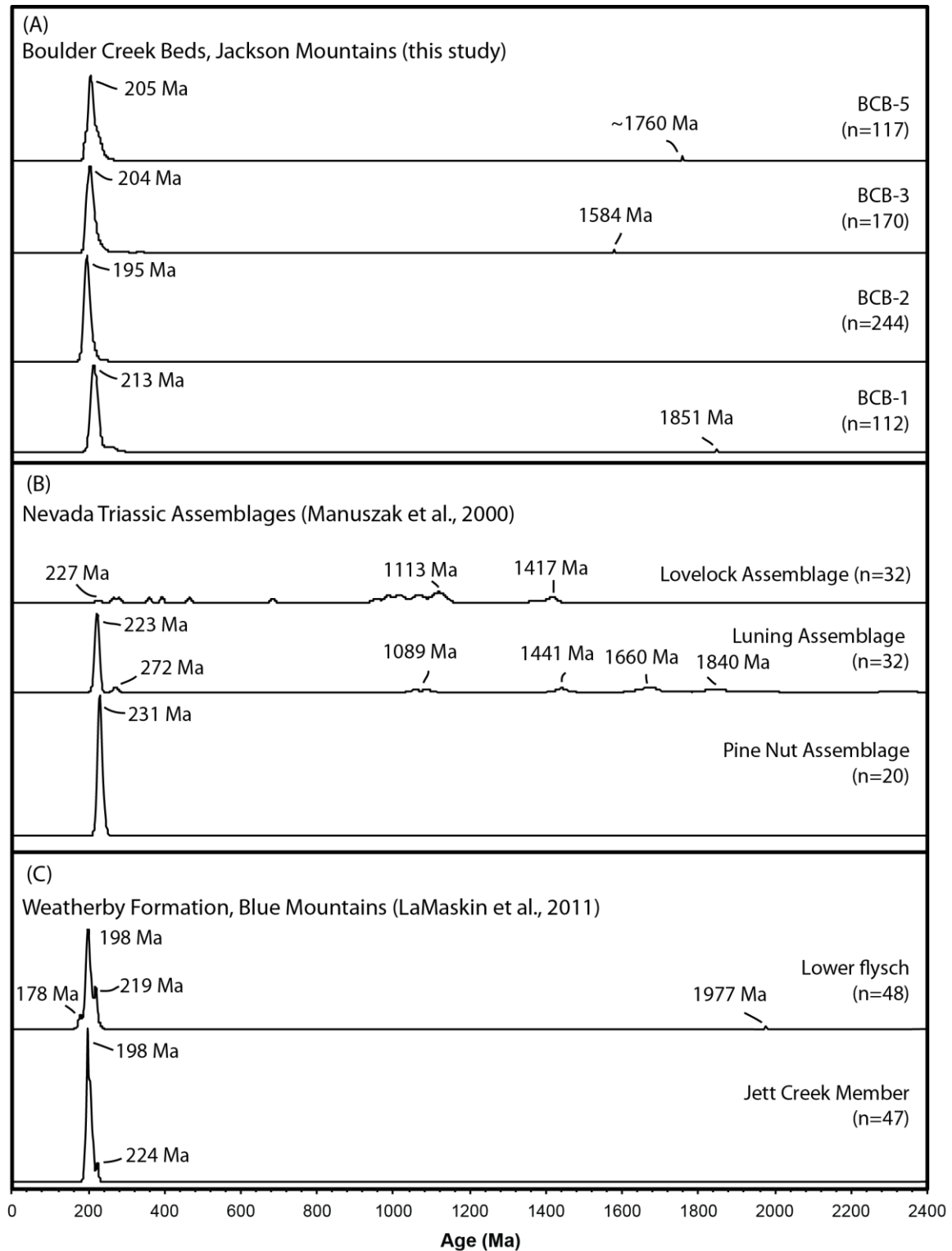


Figure 3.11. Compilation and Comparison of Triassic-Jurassic Arc-Related Strata of the Western United States. All plots have equal areas under the curve for comparison.

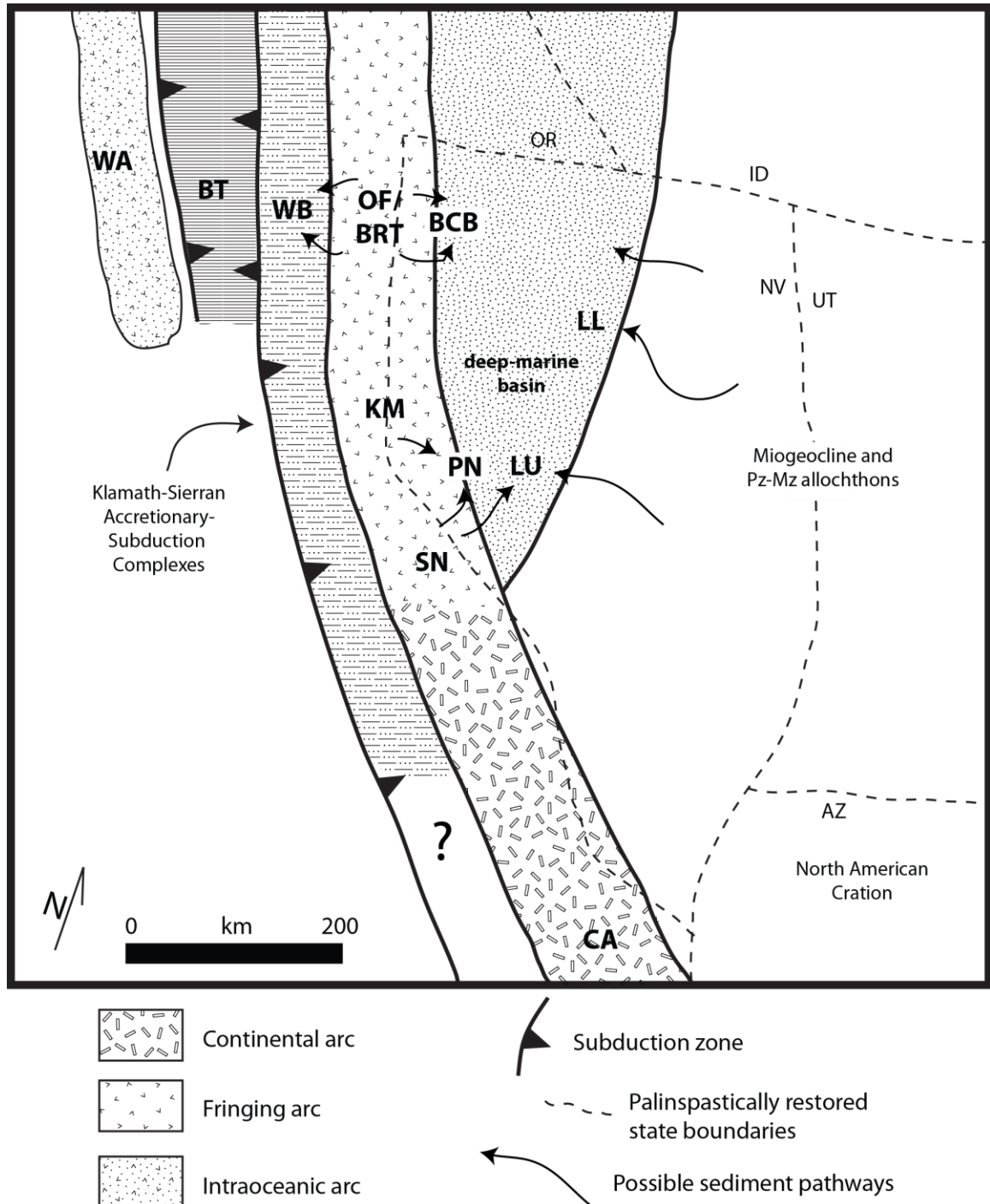


Figure 3.12. Late Triassic Reconstruction of the Western Margin of North America. Possible paleogeography following the restoration of ~400 km of dextral strike-slip motion in Cretaceous time. Modified from LaMaskin et al. (2011) and Manuszak et al. (2000). WA = Wallowa terrane, BT = Baker terrane, WB = Weatherby Formation, OF/BRT = Olds Ferry/Black Rock terrane, BCB = Boulder Creek Beds, KM = Klamath Mountains, SN = Sierra Nevada, CA = Cordilleran arc, PN = Pine Nut assemblage, LU = Luning assemblage, LL = Lovelock assemblage.

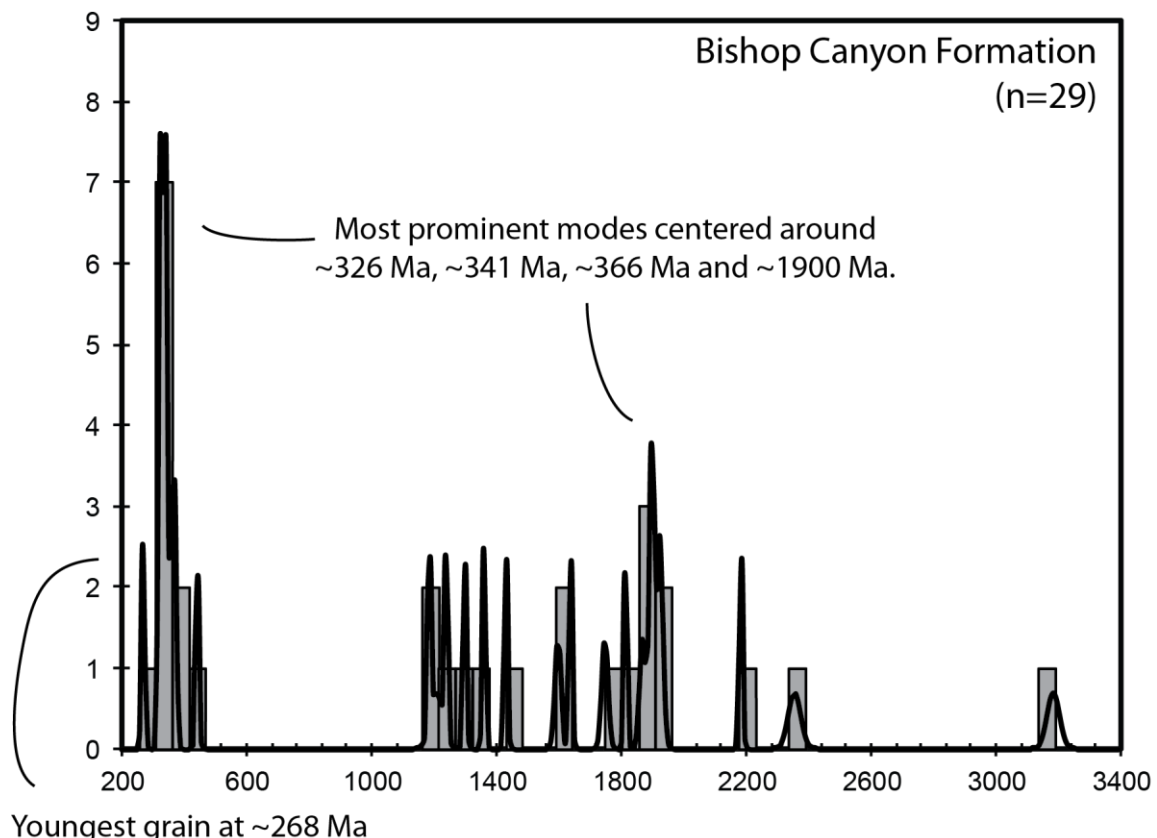


Figure 3.13. Relative Probability Plot and Histogram for Detrital Zircons From the Bishop Canyon Formation. Data from Darby et al. (2000). Curves represent the summation of individual detrital zircon ages and associated 2σ Gaussian errors; associated y-axes represent relative probability. Histograms are based on individual detrital zircon grain ages and do not incorporate errors; associated y-axes represent number of grains in a given age bin.

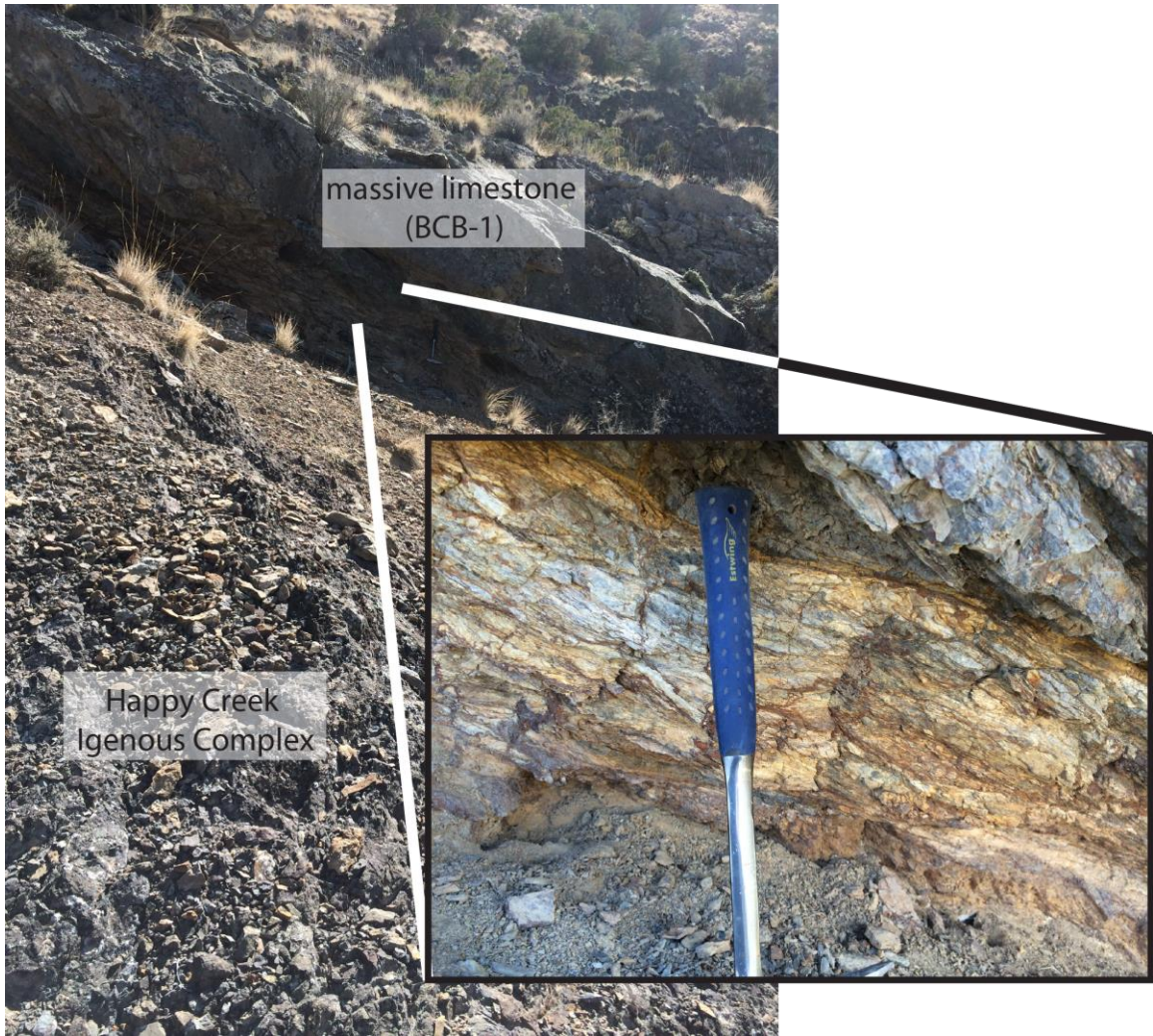


Figure 3.14. Field Photographs of the Contact Between the Happy Creek Igneous Complex and Massive Limestone From BCB-1. Note the highly sheared and brecciated zone behind the hammer handle.

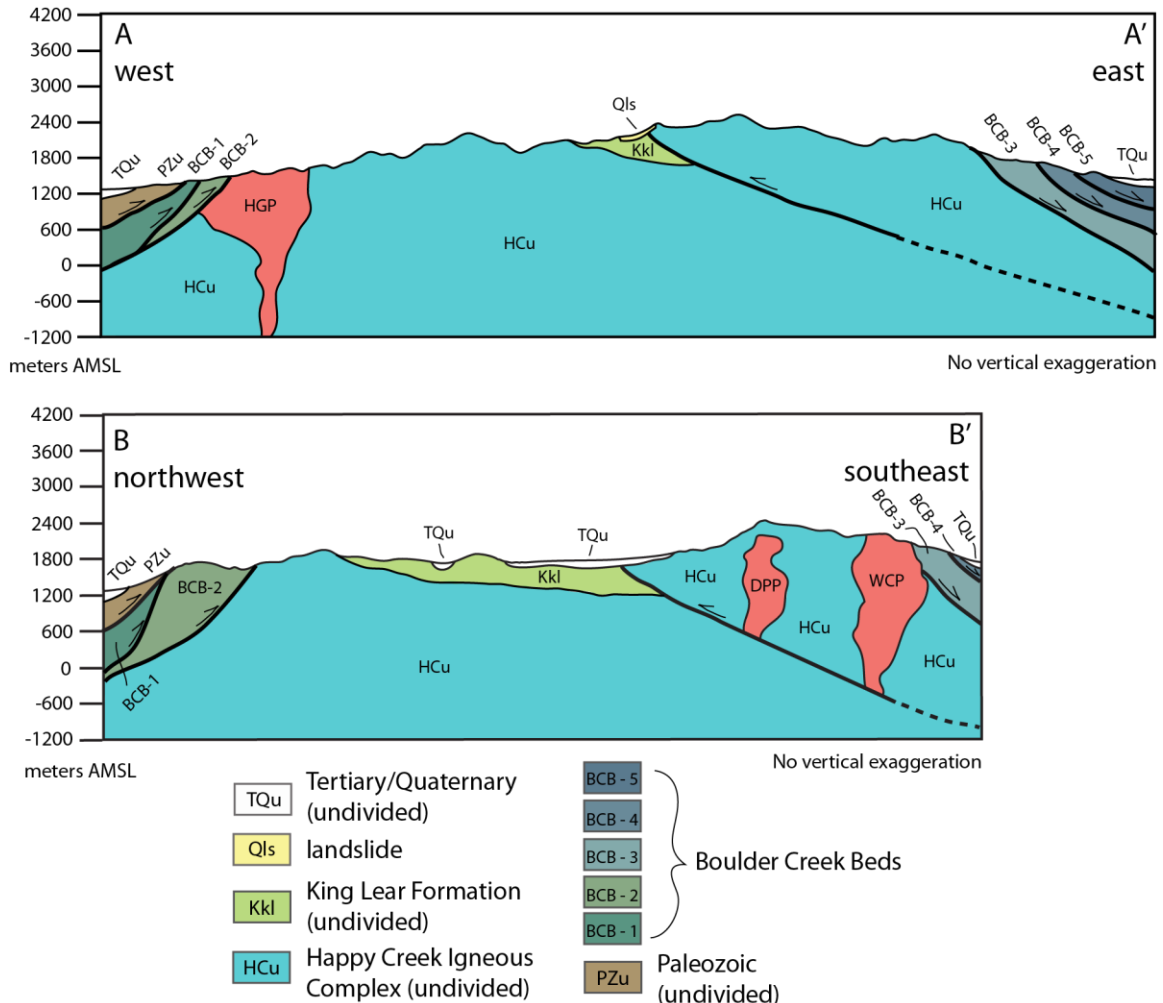


Figure 3.15. Geologic Cross Sections A-A' and B-B' of the Central Jackson Mountains. Refer to Figure 3.3 for location of cross sections. HGP=Harrison Grove pluton, DPP=Delong Peak pluton, WCP=Willow Creek pluton.

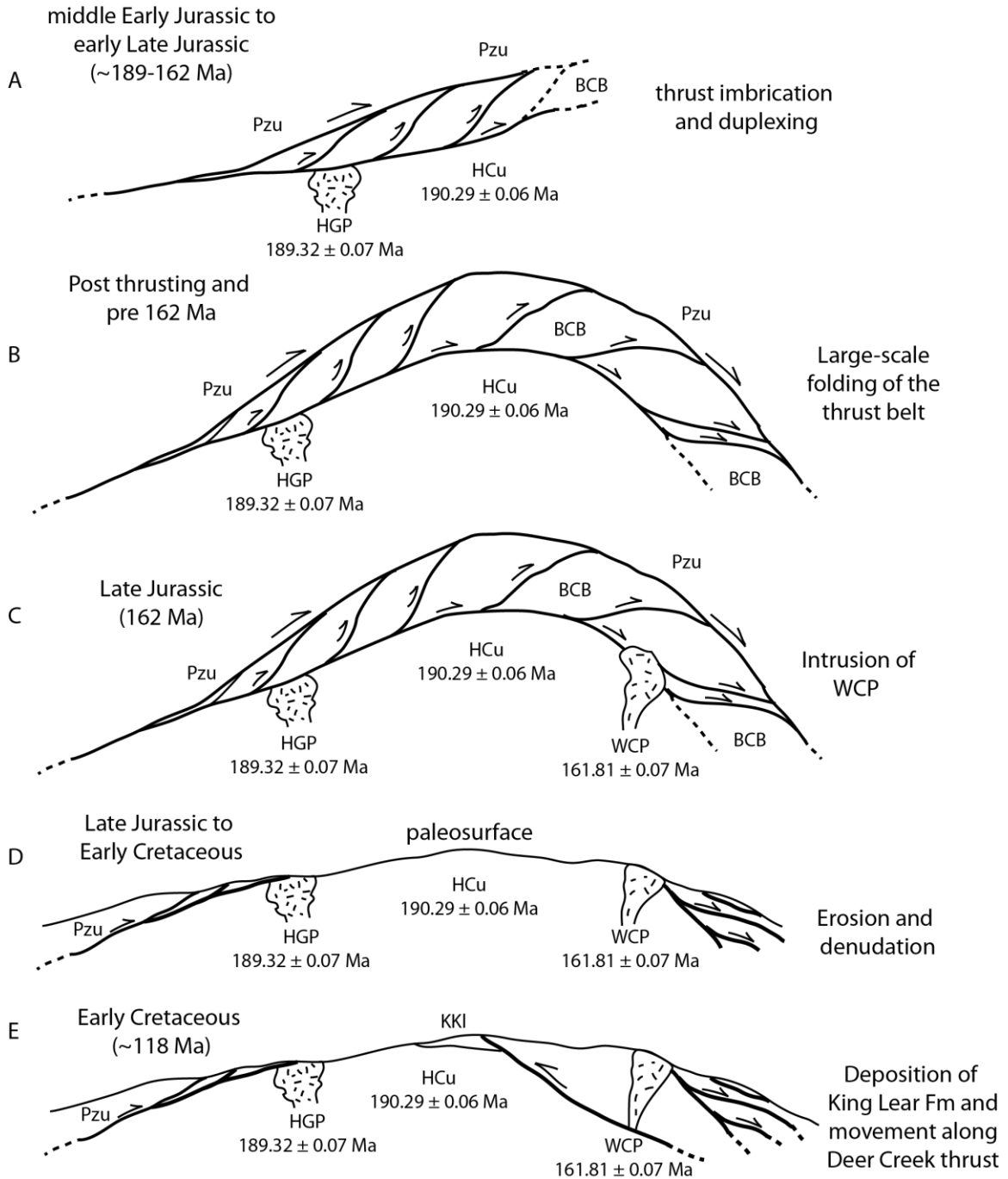


Figure 3.16. Summary of the Mesozoic Structural History of the Jackson Mountains. A) Thrust imbrication and duplexing between the middle Early Jurassic and early Late Jurassic. B) Large-scale folding of the thrust belt prior to intrusion of the Willow Creek pluton (WCP). C) Late Jurassic (162 Ma) intrusion of the WCP records the minimum age of Jurassic shortening in the Jackson Mountains. D) Erosion and denudation expose the paleosurface for deposition of the King Lear Formation. E) Early Cretaceous (~118 Ma) movement along the Deer Creek thrust and syncontractional deposition of the King Lear Formation. Abbreviations are as follows: Pzu=Paleozoic section undivided, BCB=Boulder Creek Beds, HGP=Harrison

Grove pluton, HCu=Happy Creek Igneous Complex undivided, WCP=Willow Creek pluton.

References

- Barth, A.P., Wooden, J.L., Grove, M., Jacobson, C.E., and Pedrick, J.N., 2003, U-Pb zircon geochronology of rocks in the Salinas Valley region of California: A reevaluation of the crustal structure and origin of the Salinian block: *Geology*, v. 31, n. 6, p. 517-520.
- Barth, A.P., Wooden, J.L., Jacobson, C.E., and Probst, K., 2004, U-Pb geochronology and geochemistry of the McCoy Mountains Formation, southeastern California: A Cretaceous retroarc foreland basin: *Geological Society of America Bulletin*, v. 116, n. 1-2, 142-153.
- Burchfiel, B.C., Cowan, D.S., and Davis, G.A., 1992, Tectonic overview of the Cordilleran orogen in the western United States, *in* Burchfiel, B.C., et al., eds., The Cordilleran orogen: Conterminous U.S.: Boulder, Colorado, Geological Society of America, *Geology of North America*, v. G-3, p. 407–480.
- Burke, D.B., and Silberling, N.J., 1973, The Auld Lang Syne Group of Late Triassic and Jurassic (?) Age, North-Central Nevada: U.S. Geological Survey Bulletin 1394-E, 14 p.
- Carter, A., and Bristow, C.S., 2000, Detrital zircon geochronology: enhancing the quality of sedimentary source information through improved methodology and combined U-Pb and fission-track techniques: *Basin Research*, v. 12, n. 1, p. 47-57.
- Colby, T.A., Northrup, C.J., Snyder, W.S., and Schmitz, M.D., 2016, Post-Early Cretaceous shortening in the Jackson Mountains, northwest Nevada: *Geological Society of America Abstracts with Programs*, vol. 48, no. 6.
- Colpron, M., Nelson, J.L., Murphy, D.C., 2007, Northern Cordilleran terranes and their interactions through time: *Geological Society of America Today*, v. 17, no. 4/5.
- Darby, B.J., Wyld, S.J., and Gehrels, G.E., 2000, Provenance and paleogeography of the Black Rock terrane, northwestern Nevada: Implications of U-Pb detrital zircon geochronology, *in* Soreghan, M.J., and Gehrels, G.E., eds., Paleozoic and Triassic

- paleogeography and tectonics of western Nevada and northern California: Boulder, Colorado, Geological Society of America Special Paper 347, p. 77-87.
- Davydov, V.I., Crowley, J.L., Schmitz, M.D., and Poletaev, V.I., 2010, High-precision U-Pb zircon age calibration of the global Carboniferous time scale and Milankovitch band cyclicity in the Donets Basin, eastern Ukraine: *Geochemistry Geophysics Geosystems*, v. 11, n. 1, 22 p.
- Dickinson, W.R., and Gehrels, G.E., 2009, U-Pb ages of detrital zircons in Jurassic eolian and associated sandstones of the Colorado Plateau: Evidence for transcontinental dispersal and intraregional recycling of sediment: *Geological Society of America Bulletin*, v. 121, p. 408-433.
- Dickinson, W.R., 2004, Evolution of the North American Cordillera: *Annual Review of Earth and Planetary Sciences*, v. 32, p. 13–45.
- Dickinson, W.R., 2006, Geotectonic evolution of the Great Basin: *Geosphere*, v. 2, p. 353–368.
- Dorsey, R.J., and LaMaskin, T.A., 2007, Stratigraphic record of Triassic-Jurassic collisional tectonics in the Blue Mountains Province, northeastern Oregon: *American Journal of Science*, v. 307, p. 1167–1193.
- Dorsey, R.J., and LaMaskin, T.A., 2008, Mesozoic collision and accretion of oceanic terranes in the Blue Mountains Province of northeastern Oregon: New insights from the stratigraphic record, *in* Spencer, J.E., and Titley, S.R., eds., *Circum-Pacific Tectonics, Geologic Evolution, and Ore Deposits*: Arizona Geological Society Digest, v. 22, p. 325–332.
- Elison, M.W., Speed, R.C., 1989, Structural development during flysch basin collapse: the Fencemaker allochthon, East Range, Nevada: *Journal of Structural Geology*, v. 11, p. 523-538.
- Gehrels, G., 2012, Detrital zircon U-Pb geochronology: current methods and new opportunities, *in* Busby, C., Azor Perez, A., eds., *Tectonics of sedimentary basins: Recent advances*, Hoboken: Blackwell Publishing Ltd, 1st edition.

- Goldstrand, P.M., 1994, The Mesozoic geologic evolution of the northern Wallowa Terrane, Northeastern Oregon and Western Idaho, *in* T.L. Vallier and H.C. Brooks, eds., Geology of the Blue Mountains Region of Oregon, Idaho, and Washington: U.S. Geological Survey Professional Paper 1439, p. 29-53.
- Jones, A.E., 1990, Geology and tectonic significance of terranes near Quinn River Crossing, Nevada, *in* Harwood, D.S. and Miller, M.M., eds., Late Paleozoic and early Mesozoic paleogeographic relations: Klamath Mountains, Sierra Nevada, and related terranes: Geological Society of America Special Paper 255, p. 239-254.
- Krogh, T.E., 1973, A low contamination method for hydrothermal decomposition of zircon and extraction of U and Pb for isotopic age determination: *Geochimica et Cosmochimica Acta*, v. 37, p. 485-494.
- Kurz, G.A., 2010, Geochemical, isotopic, and U-Pb geochronologic investigations of intrusive basement rocks from the Wallowa and Olds Ferry arc terranes, Blue Mountains province, Oregon-Idaho [PhD thesis]: Boise State University, Boise, Idaho.
- Kurz, G.A., Schmitz, M.D., Northrup, C.J., and Vallier, T.L., 2016, Isotopic compositions of intrusive rocks from the Wallowa and Olds Ferry arc terranes of northeastern Oregon and western Idaho: Implications for Cordilleran evolution, lithospheric structure, and Miocene magmatism: *Lithosphere* L550.1.
- LaMaskin, T.A., Dorsey, R.J., and Vervoort, J.V., 2008, Tectonic controls on mudrock geochemistry, Mesozoic rocks of eastern Oregon and western Idaho, U.S.A.: implications for Cordilleran tectonics: *Journal of Sedimentary Research*, v. 78, p. 765-783.
- LaMaskin, T.A., Vervoort, J.D., Dorsey, R.J., Wright, J.E., 2011, Early Mesozoic paleogeography and tectonic evolution of the western United States: insights from detrital zircon U-Pb geochronology of the Blue Mountains province, northeastern Oregon, U.S.A.: *Geological Society of America Bulletin*, v. 123, p. 1939-1965.

- LaMaskin, T.A., Dorsey, R.J., Vervoort, J.D., Schmitz, M.D., Tumpane, K.P., and Moore, N.O., 2015, Westward growth of Laurentia by Pre-Late Jurassic terrane accretion, Eastern Oregon and Western Idaho, United States: *The Journal of Geology*, v. 123, p. 000-000.
- Lund, K., Box, S.E., Holm-Denoma, C.S., San Juan, C.A., Blakely, R.J., Saltus, R.W., Anderson, E.D., DeWitt, E.H., 2015, Basement domain map of the conterminous United States and Alaska: U.S. Geological Survey Data Series 898, 48 p.
- Maher, K.A., 1989, Geology of the Jackson Mountains, northwest Nevada [Ph.D. thesis]: Pasadena, California Institute of Technology, 491 p.
- Manuszak, J.D., Satterfield, J.I., and Gehrels, G.E., 2000, Detrital zircon geochronology of Upper Triassic strata in western Nevada, *in* Soreghan, M.J., and Gehrels, G.E., eds., Paleozoic and Triassic paleogeography and tectonics of western Nevada and northern California: Boulder, Colorado, Geological Society of America Special Paper 347, p. 109-118.
- Martin, A.J., Wyld, S.J., Wright, J.E., and Bradford, J.H., 2010, The Lower Cretaceous King Lear Formation, northwest Nevada: Implications for Mesozoic orogenesis in the western U.S. Cordillera: *Geological Society of America Bulletin*, v. 122, p. 537–562.
- Mattinson, J.M., 2005, Zircon U-Pb chemical abrasion [“CA-TIMS”] method: Combined annealing and multi-step partial dissolution analysis for improved precision and accuracy of zircon ages: *Chemical Geology*, v. 220, p. 47-66.
- Miller, E.L., Miller, M.M., Stevens, C.H., Wright, J.E., and Madrid, R., 1992, Late Paleozoic paleogeographic and tectonic evolution of the western U.S. Cordillera, *in* Burchfiel, B.C., Lipman, P.W., and Zoback, M.L., eds., *The Cordilleran Orogen: Conterminous U.S.*: Boulder, Colorado, Geological Society of America, *Geology of North America*, v. G-3.
- Nelson, D.R., 2001, An assessment of the determination of depositional ages for Precambrian elastic sedimentary rocks by U-Pb dating of detrital zircons: *Sedimentary Geology*, v. 141, p. 37-60.

- Nichols, K.M., and Silberling, N.J., 1977, Stratigraphy and depositional history of the Star Peak Group (Triassic), northwestern Nevada: Geological Society of America Special Paper 178, 73 p.
- Oldow, J.S., Satterfield, J.I., and Silberling, N.J., 1993, Jurassic to Cretaceous transpressional deformation in the Mesozoic marine province of northwestern Great Basin, *in* Lahren, M.M., Trexler, J.H., Jr. and Spinoza, C., eds., Crustal Evolution of the Great Basin and Sierra Nevada: Cordilleran/Rocky Mountain Section, Geological Society of America Guidebook, Department of Geological Sciences, University of Nevada, Reno, p. 129-166.
- Oldow, J.S., 1984, Tectonic implications of a late Mesozoic fold and thrust belt in northwestern Nevada: *Geology*, v. 11, p. 542-546.
- Proffett, J.M., Jr., and Dilles, J.H., 1984, Geologic map of the Yerington district, Nevada: Nevada Bureau of Mines and Geology Map 77, scale 1:24,000.
- Quinn, M.J., 1996, Pre-Tertiary stratigraphy, magmatism, and structural history of the central Jackson Mountains, Humboldt County, Nevada [Ph.D. thesis]: Houston, Texas, Rice University, 243 p.
- Quinn, M.J., Wright, J.E., and Wyld, S.J., 1997, Happy Creek igneous complex and tectonic evolution of the early Mesozoic arc in the Jackson Mountains, northwest Nevada: *Geological Society of America Bulletin*, v. 109, p. 461-482.
- Rivera, T.A., Storey, M., Schmitz, M.D., and Crowley, J.L., 2013, Age intercalibration of $^{40}\text{Ar}/^{39}\text{Ar}$ sanidine and chemically distinct U/Pb zircon populations from the Alder Creek Rhyolite Quaternary geochronology standard: *Chemical Geology*, v. 345, p. 87-98.
- Rivera, T.A., Schmitz, M.D., Jicha, B.R., and Crowley, J.L., 2016, Zircon petrochronology and $^{40}\text{Ar}/^{39}\text{Ar}$ sanidine dates for the Mesa Falls Tuff; crystal-scale records of magmatic evolution and the short lifespan of a large Yellowstone magma chamber: *Journal of Petrology*, v. 57.9, p. 1677-1704.

- Rogers, J.W., 1999, Jurassic-Cretaceous deformation in the Santa Rosa Range, Nevada: implications for the development of the northern Luning-Fencemaker fold-and-thrust belt [M.S. thesis]: University of Georgia, Athens.
- Russell, B.J., 1981, Pre-Tertiary paleogeography and tectonic history of the Jackson Mountains, northwestern Nevada [Ph.D. thesis]: Evanston, Illinois, Northwestern University, 205 p.
- Russell, B.J., 1984, Mesozoic geology of the Jackson Mountains, northwestern Nevada: Geological Society of America Bulletin, v. 95, p. 313–323.
- Saleeby, J.B., and Busby-Spera, C., 1992, Early Mesozoic tectonic evolution of the western U.S. Cordillera, *in* Burchfiel, B.C., Lipman, P.W., and Zoback, M.L., eds., The Cordilleran Orogen: Conterminous U.S.: Boulder, Colorado, Geological Society of America, Geology of North America, v. G-3, p. 107-168.
- Silberling, N.J., 1973, Geologic events during Permian-Triassic time along the Pacific margin of the United States: Alberta Society of Petroleum Geologists Memoir 2, p. 345.
- Silberling, N.J., Jones, D.L., Blake, M.C., Jr., and Howell, D.G., 1987, Lithotectonic terrane map of the western conterminous United States, *in* Lithotectonic terrane maps of the North American Cordillera: U.S. Geological Survey Map MF-1874-C, scale 1:2,500,000.
- Speed, R.C., 1978a, Paleogeographic and plate tectonic evolution of the early Mesozoic marine province of the western Great Basin, *in* Howell, D.G., and McDougall, K.A., eds., Mesozoic paleogeography of the western U.S.: Pacific Section, Society of Economic Paleontologists and Mineralogists, Pacific Coast Paleogeography Symposium 2, p. 253–270.
- Speed, R.C., 1978b, Basinal terrane of the early Mesozoic marine province of the western Great Basin, *in* Howell, D.G., and McDougall, K.A., eds., Mesozoic paleogeography of the western U.S.: Pacific Section, Society of Economic Paleontologists and Mineralogists, Pacific Coast Paleogeography Symposium 2, p. 237–252.

- Stevens, C.H., Stone, P., and Miller, J.S., 2005, A new reconstruction of the Paleozoic continental margin of southwestern North America: Implications for the nature and timing of continental truncation and the possible role of the Mojave-Sonora megashear, *in* Anderson, T.H., Nourse, J.A., McKee, J.W., and Steiner, M.B., eds., The Mojave-Sonora Megashear Hypothesis: Development, Assessment, and Alternatives: Geological Society of America Special Paper 393, p. 597–618.
- Tosdal, R.M., and Wooden, J.L., 2015, Construction of the Jurassic magmatic arc, southeast California and southwest Arizona, *in* Anderson, T.H., Didenko, A.N., Johnson, C.L., Khanchuk, A.I., and MacDonald, J.H., Jr., eds., Late Jurassic Margin of Laurasia—A record of faulting accommodating plate rotation: Geological Society of America Special Paper 513.
- Tumpane, K.P., 2010, Age and isotopic investigations of the Olds Ferry terrane and its relation to other terranes of the Blue Mountains province, eastern Oregon and west-central Idaho [M.S. thesis]: Boise, Idaho, Boise State University, 220 p.
- Tyler, I.M., Page, R.W., and Griffin, T.J., 1999, Depositional age and provenance of the Marboo Formation from SHRIMP U-Pb zircon geochronology: Implications for the early Palaeoproterozoic tectonic evolution of the Kimberley region, Western Australia: Precambrian Research, v. 95, n. 3-4, p. 225-243.
- Vallier, T.L., 1995, Petrology of pre-Tertiary igneous rocks in the Blue Mountains region of Oregon, Idaho, and Washington: Implications for the geologic evolution of a complex island arc, *in* Vallier, T.L., and Brooks, H.C., eds., Geology of the Blue Mountains region of Oregon, Idaho, and Washington; petrology and tectonic evolution of pre-Tertiary rocks of the Blue Mountains region: U.S. Geological Survey Professional Paper 1438, p. 125-209.
- Wilkins, J.D., 2010, Structural and stratigraphic age constraints of the Inskip Formation, East Range, Nevada: Implications for Mesozoic tectonics of western North American [M.S. thesis]: Boise State University, Boise, Idaho.

- Willden, R., 1958, Cretaceous and Tertiary orogeny in Jackson Mountains, Humboldt County, Nevada: American Association of Petroleum Geologists Bulletin, v. 42, p. 2378–2398.
- Willden, R., 1963, General Geology of the Jackson Mountains, Humboldt County, Nevada: U.S. Geological Survey Bulletin 1141-D, 65 p.
- Wyld, S.J., 1991, Geology and geochronology of the Pine Forest Range, northwest Nevada: Stratigraphic, structural and magmatic history, and regional implications [Ph.D. thesis]: Stanford University, Stanford, California, 429 p.
- Wyld, S.J., 1996, Early Jurassic deformation in the Pine Forest Range, northwest Nevada, and implications for Cordilleran tectonics: *Tectonics*, v. 15, p. 566–583.
- Wyld, S.J., 2000, Triassic evolution of the arc and back-arc of northwest Nevada, and evidence for extensional tectonism, in Soreghan, M.J., and Gehrels, G.E., eds., Paleozoic and Triassic Paleogeography and Tectonic Evolution of Western Nevada and Northern California: Boulder, Colorado, Geological Society of America Special Paper 347, p. 1-23.
- Wyld, S.J., 2002, Structural evolution of a Mesozoic back-arc fold-and-thrust belt in the U.S. Cordillera: New evidence from northern Nevada: *Geological Society of America Bulletin*, v. 114, p. 1452–1468.
- Wyld, S.J., and Wright, J.E., 2000, Timing of deformation in the Mesozoic Luning-Fencemaker fold-thrust belt, Nevada: *Geological Society of America Abstracts with Programs*, v. 32, n. 7, A169-A170.
- Wyld, S.J., and Wright, J.E., 2001, New evidence for Cretaceous strike-slip faulting in the United States Cordillera and implications for terrane-displacement, deformation patterns, and plutonism: *American Journal of Science*, v. 301, p. 150–181.
- Wyld, S.J., Copeland, P., Rogers, J.W., 1999, $^{40}\text{Ar}/^{39}\text{Ar}$ whole rock phyllites ages from the Mesozoic Luning-Fencemaker thrust belt of central Nevada: *EOS, Transactions of the American Geophysical Union*, v. 80, n. 46, F977.

- Wyld, S.J., Quinn, M.J., and Wright, J.E., 1996, Anomalous(?) Early Jurassic deformation in the western United States Cordillera: *Geology*, v. 24, p. 1037–1040.
- Wyld, S.J., Rogers, J.W., and Wright, J.E., 2001, Structural evolution within the Luning-Fencemaker fold-thrust belt, Nevada: Progression from back-arc basin collapse to intra-arc shortening: *Journal of Structural Geology*, v. 23, p. 1971–1995.
- Wyld, S.J., Umhoefer, P.J., and Wright, J.E., 2006, Reconstructing northern Cordilleran terranes along known Cretaceous and Cenozoic strike-slip faults: Implications for the Baja British Columbia hypothesis and other models, *in* Haggart, J.W., Enkin, R.J., and Monger, J.W.H., eds., *Paleogeography of the North American Cordillera: Evidence For and Against Large-Scale Displacements*: Geological Association of Canada Special Paper 46, p. 277–298.

CHAPTER FOUR: PB, SR, AND ND ISOTOPIC DATA AND U-PB ZIRCON
GEOCHRONOLOGY OF JURASSIC INTRUSIVE ROCKS IN THE JACKSON
MOUNTAINS, NORTHWEST NEVADA: IMPLICATIONS FOR MESOZOIC
PALEOGEOGRAPHY, TERRANE CORRELATION, AND LUNING-FENCEMAKER
FOLD-AND-THRUST BELT DEFORMATION

Abstract

High-precision U-Pb zircon geochronology and isotope geochemistry of Jurassic intrusive rocks from the Jackson Mountains provide constraints on the duration, age, and paleogeography of Mesozoic magmatism and correlation to other arc terranes. The magmatic record of the Jackson Mountains involves Late Triassic (~215 Ma) to Early Jurassic (~195 Ma) marine sedimentation adjacent to an active arc followed by Early Jurassic (~193-189 Ma) eruption and emplacement of the Happy Creek Igneous Complex and plutons of the Early Mesozoic Intrusive Suite. Pb, Sr, and Nd isotopic data imply some interaction with enriched continental material. Combined with regional geology, these data support reconstructions of the Jackson Mountains representing an early Mesozoic fringing arc separated from the continent by a deep-marine basin (basinal terrane). This timing overlaps with magmatism in the Olds Ferry terrane of the Blue Mountains Province. Isotopic data from the Jackson Mountains consistently plot within the field of intrusive rocks from the Olds Ferry terrane. Combined with similarities in lithology and structure, these new data provide compelling evidence for the correlation of

Triassic-Jurassic arc-affinity rocks of the Jackson Mountains and the Olds Ferry terrane as fragments of an early Mesozoic fringing arc that was later separated and displaced by ~400 km of dextral translation.

Late Jurassic intrusive rocks of the Jackson Mountains are more isotopically enriched and radiogenic when compared to Early Jurassic intrusive rocks. We argue these differences are the result of crustal shortening and eastward movement of the upper crust during development of the Luning-Fencemaker fold-and-thrust belt, whereby younger intrusions are sourced from and travel through a more eastern crustal column.

Introduction

Following the introduction and acceptance of plate tectonic theory and the terrane concept, research in North American Cordillera has highlighted the importance of our understanding of the abundant Paleozoic and Mesozoic accreted volcanic arc terranes (Fig. 4.1) (e.g. Irwin, 1972; Monger, Souther, and Gabrielse, 1972; Coney, Jones, and Monger, 1980; Jones et al., 1982; Jones et al., 1983; Howell, 1989; Vallier, 1995; Sneeke and Barnes, 2006). While it is generally accepted that these terranes record Mesozoic accretion and westward growth of the North American continent, controversy remains regarding the age, origin, timing of accretion, and correlation to one another (e.g. Harper and Wright, 1984; Wright and Fahan, 1988; Oldow et al., 1989; McLlland, Gehrels, and Saleeby, 1992; Hacker et al., 1995; Moores, Wakabayashi, and Unruh, 2002; Dorsey and LaMaskin, 2007; Dickinson, 2004; Dickinson, 2008; Ernst, Snow, and Scherer, 2008; Schwartz et al., 2010; LaMaskin et al., 2015). Piecing together the geologic and tectonic histories of individual terranes is vital to our understanding of the assembly and subsequent shuffling of the Cordilleran orogen. Only with a detailed understanding of

individual terranes will we develop a more complete picture of Cordilleran evolution and the growth and assembly of the western margin of North America.

The Jackson Mountains, located in the Black Rock Desert region of northwest Nevada, contain a package of Paleozoic and Mesozoic arc-related rocks that represent an important locality in these terrane analyses (Figs. 4.1 and 4.2). Geographically, due to Cenozoic cover, rocks of the Black Rock Desert region represent the first exposure of Paleozoic and Mesozoic basement to the south (i.e. Blue Mountains) and east (i.e. Klamath and Sierra Nevada Mountains) of other well-documented arc assemblages (Fig. 4.1). Additionally, the Jackson Mountains are located inboard of major Cretaceous strike-slip faults (Fig. 4.1), thus are essentially in place with respect to the North American continent. As such, the Jackson Mountains provide a possible link between the continent and other outboard terranes when assessing the role and magnitude of strike-slip displacement along the margin. Finally, the Jackson Mountains are located adjacent and directly outboard of the Luning-Fencemaker fold-and-thrust belt. Therefore, the Jackson Mountains provide an important spatiotemporal link when investigating how deformation associated with the Luning-Fencemaker fold-and-thrust belt relates to the paleogeography and tectonics to the west. Along these lines, structural relationships in the Jackson Mountains provide insight into the development and evolution of the Luning-Fencemaker fold-and-thrust belt. For these reasons, a comprehensive understanding of the geology and tectonics of the Jackson Mountains is vital in evaluations of terrane relationships and assessing the role of horizontal translations within the Cordillera.

Several previous authors have examined the general geology of the Jackson Mountains (Willden, 1958; Willden, 1963; Russell, 1981; Russell, 1984; Maher, 1989;

Quinn, 1996; Quinn, Wright, and Wyld, 1997; Martin et al., 2010). These studies have documented the Jackson Mountains to contain a large exposure of volcanic, intrusive, and volcaniclastic rocks of apparent volcanic arc affinity. However, questions remain regarding the paleogeographic setting of magmatism, the precise timing and duration of magmatism, and the relationship to other arc terranes of the Cordillera. In this study, we take a closer look at the intrusive, volcanic, and volcaniclastic rocks that record early Mesozoic arc magmatism in the region. Paleozoic rocks are exposed in several small fault-bounded blocks on the west side of the range and are not discussed in this study.

Previous authors have suggested a possible paleogeographic relationship and correlation between volcanic arc rocks of the Black Rock Desert region and the Olds Ferry terrane of the Blue Mountains Province (Fig. 4.1) (e.g. Wyld and Wright, 2001; Wyld, Umhoefer, and Wright, 2006; LaMaskin et al., 2011). In this model, the Olds Ferry and Black Rock terranes may represent portions of the same early Mesozoic arc that was later fragmented and displaced by ~400 km of dextral translation (e.g. Wyld and Wright, 2001; Wyld et al., 2006; LaMaskin et al., 2011). While general similarities and relationships could be drawn, these correlations have been hindered by insufficient geochronologic, isotopic, and structural constraints in the Black Rock Desert region and specifically the Jackson Mountains. Moreover, recent high-precision U-Pb geochronology and isotope geochemistry in the Blue Mountains Province offers a new and exciting opportunity to test this potential correlation (e.g. Tumpane, 2010; Kurz, 2010; Northrup et al., 2011; Kurz et al., 2016). Additionally, new detrital zircon U-Pb geochronology in the Jackson Mountains offers a more complete look into the structural

and stratigraphic history that greatly enhances our understanding of early Mesozoic paleogeography (Chapter 3).

In this study, we present new high-precision U-Pb zircon geochronology coupled with Pb, Sr, and Nd isotopic data from Jurassic intrusive rocks of the Jackson Mountains. These data, when combined with detrital zircon data (Chapter 3), provide precise constraints on the age and duration of magmatic activity in the Jackson Mountains. Isotopic data provide insight into the paleogeography and tectonic affinity of Mesozoic arc magmatism. Together, these new data allow for a better comparison to magmatism in the Olds Ferry terrane and support models suggesting ~400 km of Cretaceous dextral translation displacing these Cordilleran arc assemblages. Additionally, isotopic data from Jurassic intrusive rocks of the Jackson Mountains provide insight into the magnitude of crustal shortening and movement of the upper crust during the development of the adjacent Luning-Fencemaker fold-and-thrust belt.

Background

Regional Geology

Triassic to Early Jurassic paleogeographic reconstructions of western Nevada emphasize three related geotectonic provinces that evolved together along the western margin of North America (Fig. 4.2) (e.g. Burke and Silberling, 1973; Silberling, 1973; Nichols and Silberling, 1977; Speed, 1978a; Speed, 1978b; Oldow, 1984; Manuszak, Satterfield, and Gehrels, 2000; Wyld, 2000; Wyld, 2002). To the east is a carbonate rich, shallow-marine succession known as the “shelf terrane” (Fig. 4.2). Located to the west of the shelf terrane is a fine-grained, dominantly siliciclastic, deep marine succession known as the “basinal terrane” (Fig. 4.2). Finally, west of the basinal terrane is a volcanic and

volcaniclastic-rich marine succession that includes the Black Rock arc terrane (Fig. 4.2).

The Black Rock arc terrane, which includes the Jackson Mountains, represents a fragment of the early Mesozoic arc sequences found throughout the North American Cordillera (Fig. 4.1) (e.g. Snyder and Brueckner, 1989; Burchfiel, et al., 1992; Wyld, 1996; Wyld, 2000).

The general history of these Triassic-Jurassic assemblages reflects Early to Late Triassic regional extension that culminated in the opening of a wide marine basin situated between the shelf and an offshore volcanic arc (e.g. Wyld, 2000). While this early Mesozoic marine basin was geographically located in a back-arc position, it was likely floored by attenuated continental crust and did not involve sea-floor spreading (e.g. Burke and Silberling, 1973; Nichols and Silberling, 1977; Speed, 1978a; Speed, 1978b; Oldow, 1984; Wyld, 2000). Following extension, regional shortening in the Jurassic resulted in the structural closure of this marine basin during the development of the Luning-Fencemaker fold-and-thrust belt (e.g. Oldow, 1984; Wyld, 2000; Wyld, Rogers, and Wright, 2001; Wyld, 2002).

The Luning-Fencemaker fold-and-thrust belt (LFTB) of central Nevada is one of the major structural belts of the North American Cordillera (Fig. 4.2) (e.g. Oldow, 1984; Elison & Speed, 1989; Oldow, Bartel, and Gelber, 1990; Rogers, 1999; Wyld et al., 2001; Wyld, 2002). At least one, and perhaps several phases of Jurassic contractional deformation have been described and associated with the development of the LFTB. These phases span the Early and/or Middle Jurassic to Late Jurassic and resulted in the production of reverse faults, folding, and associated cleavage (e.g. Oldow, 1984; Elison & Speed, 1989; Oldow et al., 1990; Rogers, 1999; Wyld et al., 2001; Wyld, 2002).

Several detailed structural studies have provided a NW-SE shortening direction for the LFTB (e.g. Oldow, 1984; Wyld et al., 2001; Wyld, 2002). Timing relationships in the northern LFTB imply that significant regional shortening was complete by the earliest Late Jurassic (~165-162 Ma) (e.g. Elison and Speed, 1989; Wyld et al., 2001; Wyld, 2002; Wilkins, 2010; Chapter 3).

While deformation associated with the LFTB is primarily confined to rocks deposited in the early Mesozoic marine basin (i.e. basinal terrane), recent work in the Jackson Mountains has demonstrated that NW-SE shortening, resulting in thrusts, folds, and associated cleavage, affected the region sometime in the middle Early Jurassic to earliest Late Jurassic (post-189 Ma and pre-162 Ma) (Chapter 3). Based on the timing, geographic location, and kinematic compatibility, Jurassic contractional deformation in the Jackson Mountains is likely associated with the development of the LFTB.

Geology of the Jackson Mountains

Several reconnaissance and detailed studies have documented the geology of the Jackson Mountains and provide the foundations for this study (e.g. Willden, 1958; Willden, 1963; Russell, 1981; Russell, 1984; Maher, 1989; Quinn, 1996; Quinn et al., 1997; Chapters 2 and 3). Overall, four main assemblages comprise the Paleozoic to Mesozoic geology of the Jackson Mountains (Fig. 4.3). 1) The oldest rocks, found strictly on the western side of the range, are a Devonian to Early Permian sequence of metasedimentary and metavolcanic rocks named the Hobo Canyon and McGill Canyon blocks. These Paleozoic rocks are interpreted to either form the basement for Mesozoic rocks (e.g. Quinn, 1996) or represent a separate tectonostratigraphic assemblage distinct from younger rocks (e.g. Russell, 1981; Silberling et al., 1987; Jones, 1990). 2) A Late

Triassic to Early Jurassic succession of volcanogenic marine rocks named the Boulder Creek Beds. 3) An Early Jurassic assemblage of mafic to intermediate volcanic and intrusive rocks composed of the Happy Creek Igneous Complex and plutons of the Early Mesozoic Intrusive Suite. 4) Early Cretaceous sedimentary rocks of the King Lear Formation.

The Boulder Creek Beds, Happy Creek Igneous Complex, and Early Jurassic plutons from the Early Mesozoic Intrusive Suite are interpreted to reflect a period of Late Triassic to Early Jurassic arc magmatism in an intraoceanic or marginal continental setting (e.g. Russell, 1981; 1984; Maher, 1989; Quinn, 1996; Quinn et al., 1997). In this model, deposition of the Boulder Creek Beds preceded the eruption and emplacement of the mafic to intermediate Happy Creek Igneous Complex which was then followed by intrusion of the more silicic, later-stage Jurassic plutons (Quinn, 1996; Quinn et al., 1997). Earlier work by Russell (1981; 1984) named this sequence the “Jackson Mountains Unit” and interpreted it to reflect Triassic deposition on a starved lower-slope basinal margin (i.e. Boulder Creek Beds) that transitioned into the eruption of a Late Triassic to Middle Jurassic intraoceanic magmatic arc (i.e. Happy Creek Igneous Complex). For the purposes of this manuscript, we will briefly discuss the geology and timing of these early Mesozoic units; however further descriptions of these and other units can be found in the aforementioned references.

Boulder Creek Beds

Early geologic mapping in the Jackson Mountains identified and described the Boulder Creek Beds (BCB) as a sequence of Middle (?) to Late Triassic volcanogenic sedimentary and volcanic rocks (Russell, 1981; Russell, 1984). These authors divided the

BCB into nine structurally controlled subunits that generally consist of the following lithologies: 1) interbedded thin pelitic rocks, chert, and calcarenite, 2) clastic carbonate rocks, 3) platform and slope carbonate deposits, and 4) volcanogenic sedimentary rocks with locally intercalated volcanic rocks. Based on mappable changes in clast composition and sedimentologic characteristics, later work by Quinn (1996) and Quinn et al. (1997) divided the BCB into five strongly volcanogenic subunits, two on the west side of the Jackson Mountains and three on the east side of the range (Fig. 4.3). These units are closely related to the BCB of Russell (1981, 1984) and therefore have kept the same name. In Chapter 3, we presented new detrital zircon geochronology for subunits 1, 2, 3, and 5. These data show that the BCB are younger than previously thought with maximum depositional ages ranging from the Norian (~215 Ma) to the Sinemurian (~195 Ma) (Chapter 4.3). Furthermore, detrital zircon provenance confirms paleogeographic reconstructions that place a deep-marine basin between a continental-fringing arc (i.e. Black Rock terrane) and the North American continent to the east (Chapter 3).

Happy Creek Igneous Complex

Several interpretations have been offered regarding which rocks and rock types are included in the Happy Creek Igneous Complex (Willden, 1958; Willden, 1963; Russell, 1981; Russell, 1984; Maher, 1989; Quinn, 1996; Quinn et al., 1997). In early reconnaissance studies, Willden (1958; 1963) described the Happy Creek Igneous Complex as a Permian or older volcanic and volcaniclastic succession of basaltic to andesitic flows, flow breccias, and volcaniclastic rocks. Russell (1981; 1984) instead considered the Happy Creek Igneous Complex as a Mesozoic succession of compositionally similar intrusive, extrusive, and volcaniclastic rocks. Russell (1981)

further presented a whole-rock Rb-Sr isochron age of 160 ± 35 Ma (1σ). Later work by Maher (1989) agreed with the Mesozoic age of the Happy Creek Igneous Complex, but instead considered the unit to be entirely composed of volcanic and sedimentary strata. Most recently, Quinn (1996) and Quinn et al. (1997) interpreted the Happy Creek Igneous Complex to represent a latest Triassic-Early Jurassic mix of hypabyssal basaltic to andesitic intrusions and intrusion breccias with minor supracrustal strata.

Here, we use a combination of earlier interpretations and describe the Happy Creek Igneous Complex to include a succession of Early Jurassic mafic to intermediate volcanic, volcaniclastic, and intrusive rocks that generally lie within the center of the Jackson Mountains (Fig. 4.3). Rock types in this sequence include a package of subgreenschist-facies fine-grained volcanic and intrusive rocks ranging in composition from basaltic andesite to andesite in addition to packages of volcaniclastic strata that include conglomerate, breccia, sandstone, and mudstone (e.g. Russell, 1981; 1984; Quinn, 1996; Quinn et al., 1997). In Chapter 3, we presented a new high-precision weighted mean $^{206}\text{Pb}/^{238}\text{U}$ age of 190.29 ± 0.06 Ma (2σ) for a sample of the Happy Creek Igneous Complex.

Early Mesozoic Intrusive Suite

Originally named by Maher (1989), the Early Mesozoic Intrusive Suite (EMIS) is a suite of plutons, stocks, and dikes intruding into the Happy Creek Igneous Complex and Boulder Creek Beds (Fig. 4.3). Compositionally, these epizonal intrusions range from gabbro to granodiorite with the most common lithologies of quartz diorite to diorite (Table 4.1) (e.g. Russell, 1981; Maher, 1989; Quinn, 1996). Major, trace, and REE data for the EMIS are similar to basalts and basaltic andesites of the Happy Creek Igneous

Complex (e.g. Russell, 1981; Quinn, 1996; Quinn et al., 1997). These data show the EMIS as a sequence of high-K calc-alkaline intrusions that are genetically related to the Happy Creek Igneous Complex (Maher, 1989; Quinn, 1996).

Previous geochronology of the EMIS include two U-Pb and one Rb-Sr ages reported by Maher (1989) and a more comprehensive U-Pb zircon assessment by Quinn (1996) and Quinn et al. (1997) (Table 4.1). The results of these analyses show two general age clusters in the Early Jurassic (~196-187 Ma) and Middle to Late Jurassic (~170-163 Ma). However, the majority of these ages were obtained from 3-12 mg bulk samples of zircon (Quinn, 1996; Quinn et al., 1997). Consequently, the reported ages could include inherited cores and grains that may have experienced significant Pb loss. Furthermore, Quinn (1996) and Quinn et al. (1997) reported the $^{207}\text{Pb}/^{206}\text{Pb}$ ages whereas the $^{206}\text{Pb}/^{238}\text{U}$ ages are more appropriate for evaluating Mesozoic rocks (e.g. Gehrels, 2012). As shown in Table 4.1, these reported ages differ by as much as ~50 million years for any single sample. In light of these complications, more precise geochronology of the EMIS is needed to investigate the timing of magmatism in the Jackson Mountains and to make meaningful correlations to other arc systems of the Cordillera.

Sample Collection and Analytical Procedures

To constrain the age and isotopic composition of Jurassic magmatism in the Jackson Mountains, we collected one (~4-5 kg) sample from all previously documented plutons within the Early Mesozoic Intrusive Suite (Fig. 4.3; Tables 2.1, 3.2, and 4.2) (e.g. Russell, 1981; 1984; Maher, 1989; Quinn, 1996; Quinn et al., 1997; Chapters 2 and 3). Additionally, one sample from the newly mapped Prospect Springs Pluton was collected and analyzed for geochronology (Chapter 2). Geochronology for the Prospect

Springs Pluton and Parrot Peak Pluton are presented in Chapter 2. Geochronology for the Harrison Grove Pluton and Willow Creek Pluton are presented in Chapter 3. For rocks previously dated by Quinn (1996) and Quinn et al. (1997), our sample collection attempted to best match the location to aid in the comparison of interpreted ages.

U-Pb Zircon Geochronology

Zircons were extracted from samples using standard crushing, density, and magnetic separation techniques in the Isotope Geology Laboratory at Boise State University. Following separation, the zircons were annealed at ~900°C for 60 hours in a muffle furnace. The annealed zircons were handpicked, mounted in epoxy, and polished to expose their centers. Using cathodoluminescence (CL), the polished grain mounts were imaged and used to identify preferred laser spot locations for laser ablation-inductively coupled plasma-mass spectrometry (LA-ICPMS). Analyses were performed on a Thermo Scientific X Series 2 quadrupole ICPMS coupled to a New Wave UP213 Laser Ablation System at Boise State University. For increased precision, samples were further analyzed using chemical abrasion-isotope dilution thermal ionization mass spectrometry (CA-IDTIMS). In this case, five or more grains were plucked from their epoxy mounts, chemically abraded in concentrated HF, spiked with a BSU mixed ^{233}U - ^{235}U - ^{205}Pb tracer solution, and dissolved (e.g. Mattison, 2005). In selecting these grains, we targeted the younger tail of LA-ICPMS data and used cathodoluminescence (CL) images to identify grains with relatively simple growth histories while avoiding grains with obvious cores and complicated growth zones. U and Pb were then separated using an HCl-based anion exchange chromatographic procedure (e.g. Krogh, 1973). U and Pb were then loaded

onto a single outgassed Re filament and analyzed on an IsotopX Isoprobe-T multicollector thermal ionization mass spectrometer (TIMS) at Boise State University.

Isotope Geochemistry

Pb Isotopic Analysis

Initial Pb isotopic ratios were determined from ~100 mg samples of primarily K-feldspar obtained from whole-rock separates using standard crushing, density, and magnetic separation techniques. Feldspar separates were sequentially leached in 1 M HF following the methods of Housh and Bowring (1991). Samples were collected from the fourth and fifth leach steps. From these leach steps, Pb was separated by anion exchange in dilute HBr medium. Pb samples were then loaded onto outgassed Re center filaments and analyzed using an IsotopX Isoprobe-T multicollector thermal ionization mass spectrometer (TIMS) at Boise State University. U-Th-Pb ratios were measured in aliquots of each leach step using solution ICPMS at Boise State University. Using these ratios and the interpreted age, the measured Pb ratios were corrected for any ingrowth of radiogenic Pb.

Sr and Nd Isotopic Analysis

Initial Sr and Nd isotopic compositions were determined on ~100 mg samples of whole-rock powders. Powders were first spiked with a mixed ^{150}Nd - ^{149}Sm tracer solution. The spiked powders were then dissolved in 29 M HF + 15 M HNO₃, dried, and redissolved in 6 M HCl. A 10% aliquot of that solution was then spiked with ^{87}Rb and ^{84}Sr tracers. Rb, Sr, and bulk REE were separated using standard dilute HCl and HNO₃ cation exchange chemistry. The Rb fraction was further purified by ion exchange in 0.6M HCl. Sm and Nd were separated from other REE by reverse phase HDEHP

chromatography (Pin and Zalduegui, 1997). Rb, Sr, and Sm were each loaded onto individual outgassed Re center filaments in 0.1N H₃PO₄ along with a tantalum oxide emitter solution (R. Creaser, pers. comm.). Nd was loaded onto single outgassed Re side filaments in 1M HNO₃. Rb, Sr, Sm, and Nd isotopic ratios were then measured on the IsotopX Isoprobe-T TIMS in the Boise State University Isotope Geology Laboratory.

Results

U-Pb Zircon Geochronology

Deer Creek Peak Pluton

Single grain analysis of the Deer Creek Peak Pluton (DCPP) reveals a date of 196.5 ± 1.1 Ma from 77 analyses using LA-ICPMS (Fig. 4.4). From these grains, five were selected for further processing using CA-IDTIMS (e.g. Krogh, 1973; Mattinson, 2005). Four grains yielded concordant and equivalent isotope ratios with a weighted mean ²⁰⁶Pb/²³⁸U date of 192.89 ± 0.07 Ma (2σ , MSWD = 0.30, prob. fit = 0.83) (Fig. 4.4). One grain yielded a slightly older (193.24 ± 0.17 Ma) date that suggests minor inheritance or magma residence. Therefore, we interpret the Early Jurassic weighted mean date as the emplacement age of the DCPP.

Mary Sloan Dikes

Our analysis of the Mary Sloan Dikes (MSD) reveals a date of 194.0 ± 3.1 Ma from 20 analyses using LA-ICPMS (Fig. 4.5). From these grains, eight were selected for further processing using CA-IDTIMS (e.g. Krogh, 1973; Mattinson, 2005). Six grains yielded concordant and equivalent isotope ratios with a weighted mean ²⁰⁶Pb/²³⁸U date of 189.94 ± 0.06 Ma (2σ , MSWD = 1.6, prob. fit = 0.17) (Fig. 4.5). Two younger dates of 189.35 ± 0.12 Ma and 188.86 ± 0.18 Ma imply a variable amount of Pb loss resistant to

removal by chemical abrasion (Fig. 4.5). We interpret the Early Jurassic weighted mean date as the emplacement age of the MSD.

Trout Creek Stock

Zircons extracted from the Trout Creek Stock (TCS) were unfortunately too small to mount and analyze using LA-ICPMS. Therefore, seven grains were examined using CA-IDTIMS (e.g. Krogh, 1973; Mattinson, 2005). Four grains yielded concordant and equivalent isotope ratios with a weighted mean $^{206}\text{Pb}/^{238}\text{U}$ date of 161.88 ± 0.11 Ma (2σ , MSWD = 0.77, prob. fit = 0.51) (Fig. 4.6). One grain yielded a slightly younger date (161.53 ± 0.19 Ma) that implies a small amount of Pb loss (Fig. 4.6). Two grains yielded older dates (~193-194 Ma) that imply inheritance from the Early Jurassic volcanic and intrusive rocks of the Jackson Mountains. These three analyses were not included in the final weighted mean calculation. Therefore, we interpret the earliest Late Jurassic weighted mean date as the emplacement age of the TCS.

Delong Peak Pluton

Similar to the TCS, zircons from the Delong Peak Pluton (DPP) were too small to mount and analyze using LA-ICPMS. Therefore, six grains were examined using CA-IDTIMS (e.g. Krogh, 1973; Mattinson, 2005). Five grains yielded concordant and equivalent isotope ratios with a weighted mean $^{206}\text{Pb}/^{238}\text{U}$ date of 161.63 ± 0.18 Ma (2σ , MSWD = 0.58, prob. fit = 0.68) (Fig. 4.7). One grain yielded an older date (192.53 ± 0.81 Ma) that implies inheritance from the Early Jurassic volcanic and intrusive rocks in the Jackson Mountains.

Other Intrusions of the EMIS

New high-precision U-Pb ages for other intrusions of the EMIS are presented in Chapters 2 and 3. For a complete picture of the timing of EMIS magmatism, we summarize those results here and in Table 4.1. The Prospect Springs pluton yielded five grains with concordant and equivalent isotope ratios with a weighted mean $^{206}\text{Pb}/^{238}\text{U}$ date of 160.72 ± 0.06 Ma (2σ , MSWD = 1.36, prob. fit = 0.2454) (Fig. 2.13 of Chapter 2). The Parrot Peak pluton yielded five grains with concordant and equivalent isotope ratios with a weighted mean $^{206}\text{Pb}/^{238}\text{U}$ date of 190.28 ± 0.07 Ma (2σ , MSWD = 1.14, prob. fit = 0.3347) (Fig. 2.12 of Chapter 2). The Willow Creek pluton yielded five grains with concordant and equivalent isotope ratios with a weighted mean $^{206}\text{Pb}/^{238}\text{U}$ date of 161.81 ± 0.07 Ma (2σ , MSWD = 0.27, prob. fit = 0.8976) (Fig. 3.9 of Chapter 3). The Harrison Grove pluton yielded five grains with concordant and equivalent isotope ratios with a weighted mean $^{206}\text{Pb}/^{238}\text{U}$ date of 189.32 ± 0.07 Ma (2σ , MSWD = 1.3, prob. fit = 0.2539) (Fig. 3.10 of Chapter 3).

Isotope Geochemistry

Plutonic rocks from the Early Mesozoic Intrusive Suite exhibit initial $^{87}\text{Sr}/^{86}\text{Sr}$ ratios that range from 0.7034 to 0.7046, and positive initial ϵ_{Nd} values between +3.4 and +4.89 (Table 4.3). No systematic change or trend in initial $^{87}\text{Sr}/^{86}\text{Sr}$ or initial ϵ_{Nd} is seen with respect to emplacement age. Initial $^{206}\text{Pb}/^{204}\text{Pb}$, $^{207}\text{Pb}/^{204}\text{Pb}$, and $^{208}\text{Pb}/^{204}\text{Pb}$ common Pb ratios range from 18.539 to 18.960, 15.599 to 15.634, and 38.310 to 39.092, respectively (Table 4.3). Common Pb isotope ratios show an increase from the Early Jurassic to Late Jurassic plutons (Table 4.3).

Discussion

Timing of Mesozoic Magmatism in the Jackson Mountains

New high-precision U-Pb zircon geochronology data when combined with recent detrital zircon data provide constraints on the timing of Mesozoic arc magmatism in the Jackson Mountains. Plutonic rocks of the Early Mesozoic Intrusive Suite (EMIS) yield two highly restricted age groups in the Jurassic Period. The older group consisting of the DCPP, PPP, HGP, and MSD form a tight cluster in Early Jurassic time between 192.89 ± 0.07 Ma and 189.32 ± 0.07 Ma (Fig. 4.8). The younger group consisting of DPP, TCS, PSP, and WCP form an even tighter cluster in earliest Late Jurassic time between 161.88 ± 0.11 Ma and 160.72 ± 0.06 Ma (Fig. 4.8). A single age (190.29 ± 0.06 Ma) from the Happy Creek Igneous Complex falls within the Early Jurassic range of EMIS magmatism (Fig. 4.8; Chapter 3). As mentioned previously, major, trace, and REE data for plutons from the EMIS and rocks of the Happy Creek Igneous Complex are essentially indistinguishable and indicate that they are genetically related (e.g. Russell, 1981; Quinn, 1996). These new age constraints presented here confirm this interpretation and identify the Happy Creek Igneous Complex and Early Jurassic plutons of the EMIS to represent a temporally restricted package of volcanic, intrusive, and volcaniclastic rocks of obvious arc-affinity. As suggested by previous workers (Quinn, 1996; Quinn et al., 1997), Late Jurassic plutons of the EMIS are significantly younger and must represent a separate period of magmatism – an interpretation that is supported by Pb isotopic data discussed later.

The Happy Creek Igneous Complex is an areally extensive unit (Fig. 4.3). Therefore, we cannot rule out the possibility of older and/or younger ages being

recovered from other portions of this unit. Several unsuccessful attempts were made to extract zircons from different portions of the assemblage (Chapter 3). However, the monotonous character and relatively uniform lithologies for the majority of this unit strongly suggests similar conditions and processes during eruption and emplacement. Given the strongly variable nature and environments of volcanic arcs, these relationships lend support to the temporally restricted, interpreted age of the Happy Creek Igneous Complex.

Considering that the Boulder Creek Beds, Happy Creek Igneous Complex, and Early Jurassic plutons of the EMIS represent a single period of Late Triassic to Early Jurassic arc magmatism, new detrital zircon geochronology from the Boulder Creek Beds helps to constrain the older periods of Mesozoic magmatism in the Jackson Mountains (Chapter 3). In Chapter 3, we presented new high-precision U-Pb geochronologic constraints on the maximum depositional age of the Boulder Creek Beds. These data demonstrate that the Boulder Creek Beds represent a Norian (~215 Ma) to Sinemurian (~195 Ma) succession of strongly volcanogenic marine rocks deposited adjacent to active volcanic arc. As such, arc magmatism in the Black Rock Desert region must have extended to older periods and at least the Late Triassic, though intrusive and volcanic rocks of this age are not exposed and/or documented in the Jackson Mountains. Additionally, though not abundant, the presence of Early and Middle Triassic detrital zircon grains may suggest that active arc magmatism may extend back even later (Chapter 3).

Taken together, these new geochronology data provide a precise and more complete timeline for arc magmatism in the Jackson Mountains that includes Late

Triassic (or older) to Early Jurassic (~215-195 Ma) marine deposition adjacent to an active volcanic arc that culminated in the eruption and emplacement of the Early Jurassic Happy Creek Igneous Complex and Early Jurassic plutons from the Early Mesozoic Intrusive Suite (~193-189 Ma) (Fig. 4.8).

Assessment of Magma Source Reservoirs and Paleogeography

In the following section, we discuss new Pb, Sr, and Nd isotopic data from intrusive rocks of the Early Mesozoic Intrusive Suite to evaluate possible source reservoirs and the possible role of crust-mantle mixing in the generation of magmas. Together, these data provide insight into the Late Triassic-Early Jurassic paleogeography and setting of magmatism in the Jackson Mountains.

To explore the possible interaction and mixing of mantle components in the production of arc magmas, we limit our discussion to the following known end-member mantle components: 1) depleted MORB mantle or “DMM”, 2) enriched mantle I or “EMI”, 3) enriched mantle II or “EMII”, and 4) high- μ mantle or “HIMU” (e.g. Zindler and Hart, 1986; Hart, 1988; Salters and Hart, 1991; Shirley and Walker, 1998). Here, we provide a brief summary of those end-member mantle components along with their present day isotopic ratios. These data can also be found in Table 4.4. DMM is interpreted as the source for MORB’s and is characterized by average Sr, Nd, and Pb isotope ratios of $^{87}\text{Sr}/^{86}\text{Sr} = 0.7026$, $^{143}\text{Nd}/^{144}\text{Nd} = 0.51311$, $^{206}\text{Pb}/^{204}\text{Pb} = 18.00$, $^{207}\text{Pb}/^{204}\text{Pb} = 15.43$, and $^{208}\text{Pb}/^{204}\text{Pb} = 37.70$ (Salters and Stracke, 2004). EMI is interpreted as a mixture of DMM and between ~5-10% subducted, pelagic sediments (Zindler and Hart, 1986; Weaver, 1991; Eisele et al., 2002; Stracke, Bizimis, and Salters, 2003). The EMI source exhibits Sr, Nd, and Pb isotope ratios of $^{87}\text{Sr}/^{86}\text{Sr} = 0.7053$,

$^{143}\text{Nd}/^{144}\text{Nd} = 0.51236$, $^{206}\text{Pb}/^{204}\text{Pb} = 17.65$, $^{207}\text{Pb}/^{204}\text{Pb} = 15.475$, and $^{208}\text{Pb}/^{204}\text{Pb} = 38.14$ (Eisele et al., 2002; Stracke et al., 2003). EMII is interpreted as a mixture of depleted mantle and a similar amount as EMI (~5-10%) of continentally derived, terrigenous sediment and ancient recycled oceanic crust (Zindler and Hart, 1986; Weaver, 1991; Workman et al., 2004). Sr, Pb, and Nd isotope ratios of EMII are $^{87}\text{Sr}/^{86}\text{Sr} = 0.7090$, $^{143}\text{Nd}/^{144}\text{Nd} = 0.5125$, $^{206}\text{Pb}/^{204}\text{Pb} = 19.00$, $^{207}\text{Pb}/^{204}\text{Pb} = 15.675$, and $^{208}\text{Pb}/^{204}\text{Pb} = 38.86$ (Zindler and Hart, 1986; Workman et al., 2004). Finally, the HIMU end-member is characterized by low $^{87}\text{Sr}/^{86}\text{Sr} = 0.703$, high $^{143}\text{Nd}/^{144}\text{Nd} = 0.5129$, and high Pb ratios of $^{206}\text{Pb}/^{204}\text{Pb} = 21.00$, $^{207}\text{Pb}/^{204}\text{Pb} = 15.85$, and $^{208}\text{Pb}/^{204}\text{Pb} = 39.75$ (Zindler and Hart, 1986; Stracke, Hofmann, and Hart, 2005). The high Pb isotope ratios in the HIMU source requires high time-integrated U/Pb and Th/Pb ratios that has been interpreted to represent the input of ancient recycled oceanic crust without a significant contribution of subducted sediment (Zindler and Hart, 1986; Weaver, 1991; Stracke et al., 2005).

These Sr, Nd, and Pb isotope ratios and end-member components are derived from modern OIB's. Therefore, when utilizing these end-member mantle components in assessments of ancient rocks (i.e. Mesozoic intrusive rocks), we must account for time-integrated isotopic evolution through the continual formation of each systems respective radiogenic daughter nuclides. Therefore, using parent/daughter (P/D) ratios compiled from the literature, we have “back-evolved” the average present-day isotopic compositions (discussed above) for each end-member to their respective Early Jurassic (~190 Ma) isotopic ratio. These back-evolved isotope ratios can be found in Table 4.4.

Additionally, we have calculated mixing relationships to explore the possible contribution and interaction of mantle-derived melts with enriched continental crust. To

provide an estimate of the possible isotopic composition of continental crust at the latitude of the Jackson Mountains, we compiled initial Sr, Nd, and Pb isotope ratios from Jurassic plutons from eastern Nevada and western Utah (e.g. Zartman, 1974; Stacey and Zartman, 1978; Lee, 1984; Kistler and Lee, 1989; Wright and Wooden, 1991; Wooden, Kistler, and Tosdal, 1998; Wooden, Kistler, and Tosdal, 1999). As these plutons intruded inboard of the interpreted western edge of the North American craton (e.g. Kistler and Peterman, 1973; Kistler and Peterman, 1978; Kistler, 1983; Kistler, 1991; Elison, Speed, and Kistler, 1990), their average, most radiogenic isotopic ratios provide an indirect measure of the predicted isotopic composition of the underlying crustal column. For use in mixing relationships, Sr, Nd, and Pb trace element concentrations were compiled from the literature for typical upper crustal values (e.g. Taylor, McLennan, and McCulloch, 1983; Weaver and Tarney, 1984; Shaw et al., 1986; Rudnick and Goldstein, 1990; Condie, 1993; Taylor and McLennan, 1995; Wedepohl, 1995; Kemp and Hawkesworth, 2004; Rudnick and Gao, 2004). These estimated isotopic ratios and trace element concentrations are shown in Table 4.4. To provide an estimate of the isotopic composition of mantle-derived melts, we used a MORB-like reservoir and a mafic intraoceanic arc reservoir. For the MORB reservoir, we used the back-evolved Sr, Nd, and Pb isotopic ratios from DMM with average trace element concentrations for MORB from the literature (Table 4.4) (e.g. Hofmann, 1988; Hart et al., 1999; Keleman, Hanghoj, and Greene, 2004; Klein, 2004; Salters and Stacke, 2004). To provide a measure of expected isotopic composition for eruptive products of an intraoceanic arc we used the isotope ratios and trace element concentrations from the Wallowa arc of the Blue Mountains Province (Table 4.4) (Kurz, 2010; Kurz et al., 2016). Late Triassic-Early

Jurassic paleography places the Wallowa arc outboard of the North American margin (e.g. Schwartz et al., 2010; Kurz et al., 2016) and therefore magmatism within the arc provides a measure of eruptive products of an intraoceanic arc located in the paleo-Pacific. Therefore, mixing relationships between the Wallowa arc and the North American continent provide insight into the interaction of mantle-derived volcanic arc products and enriched continental crust.

As shown in Figure 4.9, binary mixing of DMM and EMII end-member mantle components best describes the range of Sr, Nd, and Pb isotope ratios from Early Jurassic intrusive rocks of the Early Mesozoic Intrusive Suite. Late Jurassic intrusive rocks from the Jackson Mountains generally plot near this mixing trend but display elevated and more radiogenic Pb isotope ratios suggesting some contribution of a more enriched source (Figs. 4.9a–4.9e). Additionally, as shown in Figure 4.9e, $^{208}\text{Pb}/^{204}\text{Pb}$ ratios exceed those established for the EMII end-member and require a contribution from another, more enriched source. This enriched composition of Late Jurassic intrusive rocks will be discussed in more detail in the following sections.

Returning to the Early Jurassic intrusive rocks of the Jackson Mountains, in $^{87}\text{Sr}/^{86}\text{Sr}$ - $^{206}\text{Pb}/^{204}\text{Pb}$ space, binary mixing of DMM and EMII end member mantle components predicts between ~6-20% contribution of the EMII source (Fig. 4.9a). Mixing in ϵNd - $^{206}\text{Pb}/^{204}\text{Pb}$ space suggests a greater contribution of up to ~40% EMII (Fig. 4.9b). In Pb-Pb space (Figs. 4.9c–4.9e), binary mixing of DMM and EMII is compatible with predictions from $^{87}\text{Sr}/^{86}\text{Sr}$ - $^{206}\text{Pb}/^{204}\text{Pb}$ space and suggests between ~4-20% contribution from EMII. Binary mixing in ϵNd - $^{87}\text{Sr}/^{86}\text{Sr}$ space does not completely predict the compositions of Early Jurassic intrusive rocks but does follow the overall

trend and suggests between ~2-6% contribution from the EMII source (Fig. 4.9f). These results indicate that Early Jurassic magmatism in the Jackson Mountains involved some mixture of a depleted and enriched mantle component. Furthermore, modeling suggests that between ~2-20% and up to ~40% EMII is needed to explain the array of Pb, Sr, and Nd isotope ratios. Considering that EMII represents some mixture of depleted mantle and subducted, continentally derived sediment, these data are consistent with and support models that suggest a continental fringing-arc setting for Triassic-Early Jurassic magmatism in the Jackson Mountains (e.g. Wyld, 2002; Chapter 3).

Late Jurassic intrusive rocks of the Jackson Mountains are characterized by more enriched and radiogenic Pb isotope ratios when compared to Early Jurassic intrusive rocks (Figs. 4.9a–4.9e). As shown in Figure 4.9, the trend from Early to Late Jurassic plutons in the Jackson Mountains generally follows the binary mixing relationships between a mantle-derived component (MORB or WA) and the isotopically enriched continental crust (CC). This relationship implies that Late Jurassic intrusive rocks had an increased interaction with continental crust in the production of melts. In the following section, we will explore this enriched isotopic signature further with respect to regional tectonic relationships and the development of the Luning-Fencemaker fold-and-thrust belt.

Isotopic Signature of Early and Late Jurassic Plutons

As discussed previously, plutonic rocks from the Jackson Mountains occur in two distinct age groups: an Early Jurassic group between ~193-189 Ma and a Late Jurassic group between ~162-161 Ma (Fig. 4.8). Initial $^{87}\text{Sr}/^{86}\text{Sr}$ and εNd isotopic ratios are essentially the same between Early and Late Jurassic plutons (Figs. 4.9f; Table 4.3).

Furthermore, initial $^{87}\text{Sr}/^{86}\text{Sr}$ and ϵNd show no consistent relationship with emplacement age (Table 4.3). By contrast, initial Pb isotopic ratios of Late Jurassic plutons are consistently elevated and more radiogenic than Pb isotopic ratios for the Early Jurassic plutons (Figs. 4.9 and 4.10a-4.10d ; Table 4.3). Here, we will explore these systematics in initial Pb, $^{87}\text{Sr}/^{86}\text{Sr}$, and ϵNd isotopic signatures with respect to crustal architecture and the production of melts.

Initial Pb isotope ratios in plutonic rocks are a function of the age and chemistry of the magma source region. Therefore, higher Pb ratios in plutonic rocks are attributed to older sources with higher time-integrated U/Pb, Th/Pb, and Th/U ratios. Along these lines, higher initial Pb ratios have been interpreted to indicate higher crust-to-mantle contributions in the production of melts (e.g. Doe, 1967; Armstrong, 1968; Armstrong and Hein, 1973; Doe, 1973; Zartman, 1974; Wright and Wooden, 1991; Wooden et al., 1998). In the western US Cordillera between $\sim 38^\circ\text{N}$ and $\sim 42^\circ\text{N}$ (Figs. 4.10 and 4.11), a compilation of existing data shows a consistent and systematic west to east increase in initial $^{208}\text{Pb}/^{204}\text{Pb}$, $^{207}\text{Pb}/^{204}\text{Pb}$, and $^{206}\text{Pb}/^{204}\text{Pb}$ ratios for plutons between the ages 165 and 150 Ma (Fig. 4.10f–4.10h) that is not strongly correlated with emplacement age (Fig. 4.10k–4.10m) (e.g. Zartman, 1974; Stacey and Zartman, 1978; Lee, 1984; Kistler and Lee, 1989; Wright and Wooden, 1991; Wooden et al., 1998; Wooden et al., 1999). Plutons of these ages were picked to investigate the Pb isotopic structure of the region during intrusion of Late Jurassic plutons in the Jackson Mountains. This strong correlation with longitude is consistent with an increasing interaction with thinned and highly extended continental crust when moving to the east (e.g. Bond and Kominz, 1984; Wright and Wooden, 1991; Wooden et al., 1998).

In Chapter 3, we provided evidence for SE-directed shortening in the Jackson Mountains after intrusion of the Early Jurassic plutons (~189 Ma) and prior to intrusion of the Late Jurassic plutons (~162 Ma). Based on the age, shortening direction, structural style, and geographic proximity, this episode of middle Early to earliest Late Jurassic shortening is likely associated with the development of the LFTB (Chapter 3). Structural studies in the northern LFTB have concluded anywhere from 50-75% shortening associated with the major phases of contractional deformation (e.g. Elison and Speed, 1989; Wyld et al., 2001; Wyld, 2002; Wyld et al., 2002). We argue that the systematic increase in initial Pb ratios observed in Late Jurassic plutons compared to Early Jurassic plutons is the product of crustal shortening associated with the LFTB. Along these lines, eastward, post-emplacement movement of the Jackson Mountains has occurred such that later plutons are sourced from and traveled through a more eastward crustal column that may include small amounts of thinned continental crust and previously accreted terranes (Fig. 4.12). Wright and Wooden (1991) suggested a similar phenomenon relating Sevier contraction to differences observed in isotopic data for Jurassic-Early Cretaceous plutons and Late Cretaceous plutons.

By fitting a linear trendline to Pb isotopic data for intrusive rocks from Figures 4.10f-4.10h, we calculate that between ~46–147 km (modern geography) of post-Early Jurassic eastward movement is needed to produce the average differences observed in Pb isotope ratios of Early and Late Jurassic plutons from the Jackson Mountains. While uncorrected for Cretaceous–Paleogene shortening associated with Sevier orogenesis and Cenozoic extension associated with the Basin and Range, the general magnitude is within reason for contractional orogenic belts and provides insight into the magnitude of

shortening associated with the development of the Luning-Fencemaker fold-and-thrust belt.

The initial $^{87}\text{Sr}/^{86}\text{Sr}$ ratio of eastern California, northern Nevada, and western Utah (165-150 Ma) exhibits much more variability with respect to longitude and shows no relationship with emplacement age (Figs. 4.10i, 4.10n, and 4.11). A consistent west to east trend is not as evident as with initial Pb ratios and given a narrow range of longitude, initial $^{87}\text{Sr}/^{86}\text{Sr}$ ratios can range from ~0.705 to ~0.710 (Fig. 4.10i). Therefore, given the variability, post Early Jurassic eastward movement of the Jackson Mountains does not demand a significant change in the initial $^{87}\text{Sr}/^{86}\text{Sr}$ ratio of later plutons. Furthermore, the Jackson Mountains lies to the west of the well-documented Sr-0.706 line that is thought to demarcate the edge of transitional North American continental crust (Fig. 4.2) (e.g. Kistler and Peterman, 1973; Kistler and Peterman, 1978; Kistler, 1983; Kistler, 1991; Elison et al., 1990). Given this geographic relationship, a significant increase in initial $^{87}\text{Sr}/^{86}\text{Sr}$ ratios is not expected in the Jackson Mountains. These data suggest that post-Early Jurassic contraction was not substantial enough to bring the Jackson Mountains over the edge of competent North American continental crust that is estimated by the Sr-0.706 line.

Though data limited, Middle to Late Jurassic intrusions of eastern California, northern Nevada, and western Utah do not show a consistent relationship between longitude or emplacement age and initial ϵNd (Fig. 4.10j and 4.10o). When combined with our new ϵNd data from the Jackson Mountains, a clear and significant decrease is visible to the east of the Jackson Mountains (Fig. 4.10j). Though difficult to constrain the exact location considering the data density, the general location corresponds with the

approximate location of the Sr-0.706 line. Therefore, the relationship in ϵ Nd mirrors that seen in initial $^{87}\text{Sr}/^{86}\text{Sr}$ ratios and suggests that eastward translation was not sufficient in bringing the Jackson Mountains over the edge of competent North American continental crust.

Correlation to the Olds Ferry Arc Terrane

Several authors have suggested a possible correlation between the Olds Ferry terrane of the Blue Mountains Province (BMP) and the Black Rock terrane of northwest Nevada (Fig. 4.1) (e.g. Dorsey and LaMaskin, 2007; Wyld and Wright, 2001; Wyld et al., 2006; LaMaskin et al., 2011). In this model, the Olds Ferry and Black Rock terranes may represent portions of the same early Mesozoic volcanic arc that was later fragmented and displaced by ~400 km of dextral translation (e.g. Wyld and Wright, 2001; Wyld et al., 2006; LaMaskin et al., 2011). In the following section, we first provide a brief summary of the timing and style of magmatism in the Olds Ferry terrane followed by a comparison to arc magmatism in the Jackson Mountains.

Geographically, the Olds Ferry terrane occupies the furthest inboard position of the BMP terranes (Fig. 4.1) and consists of a Middle Triassic to Early Jurassic plutonic, volcanic, and volcaniclastic succession (e.g. Brooks and Vallier, 1978; Brooks, 1979; Vallier, 1995; Tumpane, 2010; LaMaskin et al., 2008; LaMaskin et al., 2011; Kurz et al., 2016). The oldest known component of the Olds Ferry terrane is the Brownlee pluton; a trondhjemite dated at 237.68 ± 0.07 Ma (Kurz, 2010). Unconformably overlying the Brownlee pluton, and by far the most abundant exposure of the Olds Ferry terrane, is the volcanic, volcaniclastic, carbonate, and clastic sedimentary rocks of the Huntington Formation (e.g. Brooks, McIntyre, and Walker, 1976; Brooks, 1979; Dorsey and

LaMaskin, 2007; Tumpane, 2010; Northrup et al., 2011; Kurz et al., 2016). The Huntington Formation itself is subdivided into a lower and upper member each bound by unconformities (Juras, 1973; Collins, 2000; Dorsey and LaMaskin, 2007; LaMaskin et al., 2008; Tumpane, 2010). The lower member consists primarily of mafic to intermediate lava flows and sills, volcanic breccia, and tuff breccia with minor interstratified fine-grained volcaniclastic rocks and limestone (Northrup et al., 2011). U-Pb geochronology has constrained this cycle of magmatism to between 228.6 ± 0.1 Ma and 210.0 ± 0.1 Ma (Tumpane, 2010; Kurz et al., 2016). The upper member of the Huntington Formation is generally more silicic than the lower member and has a greater abundance of volcaniclastic and sedimentary rocks (e.g. Collins, 2000; Dorsey and LaMaskin, 2007; Tumpane, 2010; Northrup et al., 2011; Kurz et al., 2016). This cycle of Olds Ferry magmatism began sometime after 210.0 ± 0.1 Ma and lasted into the Early Jurassic Period (187.1 ± 0.1 Ma) (Tumpane, 2010; Kurz et al., 2016). Volcanic tuffs and detrital zircon in the Weatherby Formation indicate that Olds Ferry magmatism continued into but no later than the earliest Middle Jurassic Period (~170 Ma) (Tumpane, 2010; Northrup et al., 2011; Ware, 2013; Kurz et al., 2016).

Though of shorter duration, the timing of magmatism in the Jackson Mountains (~215-189 Ma) clearly overlaps with the timing of magmatism in the Olds Ferry terrane (~238-187 Ma) (Fig. 4.13). Additionally, though not abundant, the existence Early to Middle Triassic detrital zircons in the Boulder Creek Beds (Chapter 3) implies that magmatism in the Jackson Mountains may extend to older periods. As discussed in Chapter 3, well-dated volcanic and intrusive rocks of the Olds Ferry terrane could be a possible source of detrital zircon in the Boulder Creek Beds. The similarity of Pb, Sr, and

Nd isotopic data from intrusive rocks of the Olds Ferry arc and Early Jurassic plutons of the Jackson Mountains imply similar sources of magmatism within a fringing-arc setting (Fig. 4.9) (Kurz et al., 2016). The mafic to intermediate lava flows, sills, and volcanic breccia of the lower Huntington Formation are strikingly similar, though older, to those found in the Happy Creek Igneous Complex. The progression toward more silicic volcanism exhibited in the Huntington Formation also corresponds with an evolution to more silicic compositions from the Happy Creek Igneous Complex to Early Jurassic plutons of the Early Mesozoic Intrusive Suite in the Jackson Mountains. Geographically, both areas represent the furthest inboard Triassic-Jurassic arc terranes with respect to the North American continent (Fig. 4.1). These relationships strongly support a correlation between the Olds Ferry terrane and early Mesozoic arc-related rocks of the Jackson Mountains.

Though debated, accretion of the Olds Ferry terrane to North America occurred sometime in the Middle to Late Jurassic or Early Cretaceous (e.g. Lund and Snee, 1988; Walker, 1986; Vallier, 1995; Dorsey and LaMaskin, 2008; Schwartz et al., 2010; Northrup et al., 2011; LaMaskin et al., 2011; LaMaskin et al., 2015; Kurz et al., 2016). However, recent detrital zircon work by LaMaskin et al. (2015) provides compelling evidence for pre-Late Jurassic (~160 Ma) accretion in the Blue Mountains region. As presented here and in Chapter 3, significant middle Early to earliest Late Jurassic shortening in the Jackson Mountains was associated with the development of the LFTB. This contractional event resulted in the structural closure of the early Mesozoic marine basin and accretion of the Triassic-Jurassic arc (i.e. Jackson Mountains) to North America. This timing of accretion agrees with recent constraints in the Blue Mountains

Province and further supports a correlation between these geographically separated tectonic elements (Fig. 4.13).

Together, data presented here provide strong support for the correlation of the Olds Ferry terrane and arc-related rocks of the Jackson Mountains as representing fragments of the same Triassic-Early Jurassic fringing-arc separated from the continent by a deep-marine basin. Furthermore, the interpretations discussed here provide strong support for paleogeographic and tectonic models suggesting ~400 km of Cretaceous dextral translation separating these arc assemblages (e.g. Wyld and Wright, 2001; Wyld et al., 2006; LaMaskin et al., 2011).

A conclusion of Kurz et al. (2016) was for the correlation of the Olds Ferry terrane and the Quesnellia terrane of British Columbia on the basis of their inboard position, isotopic similarity, and coeval packages of similar rock assemblages. As presented here, our new data from the Jackson Mountains provide support for the correlation of the Olds Ferry terrane and Triassic-Jurassic arc-affinity rocks of the Jackson Mountains. Therefore, these data and interpretations suggest that the Jackson Mountains, Olds Ferry terrane, and Quesnellia terrane represent fragments of an early Mesozoic fringing-arc system (e.g. Miller, 1987). Additionally, Early Jurassic to earliest Late Jurassic estimates for the timing of accretion are compatible for these tectonic elements (e.g. Monger and Price, 2002; Dorsey and LaMaskin, 2008; LaMaskin et al., 2015; Chapter 3). Overall, these new conclusions bring the early Mesozoic paleogeography, tectonics, and geologic history of the western margin of North America into better focus and will help to provide constraints on later horizontal translations of the Cordilleran “collage”.

Summary and Conclusions

High-precision U-Pb zircon geochronology, coupled with detrital zircon data presented in Chapter 3, provides constraints on the duration and age of Mesozoic magmatism in the Jackson Mountains. These data provide a picture of Late Triassic to Early Jurassic (~215-195 Ma) marine sedimentation adjacent to an active arc (i.e. the Boulder Creek Beds) followed by the Early Jurassic (~193-189 Ma) eruption and emplacement of the Happy Creek Igneous Complex and associated plutons of the Early Mesozoic Intrusive Suite. Though of shorter duration, this timing overlaps with new constraints on the timing of magmatism in the Olds Ferry terrane (e.g. Tumpane, 2010; Kurz, 2010; Kurz et al., 2016). Pb, Sr, and Nd isotopic data from Early Jurassic intrusive rocks of the Jackson Mountains fall along a binary mixing trend between DMM and EMII end-member mantle components suggesting a minor contribution of enriched continental material in a fringing-arc setting. Additionally, these data consistently plot within the field of intrusive rocks from the Olds Ferry terrane of the Blue Mountains Province implying similar magma source regions and paleogeographic settings. Regional geologic and tectonic relations support this paleogeographic setting. Combined with lithologic similarities, these new data provide compelling evidence for the correlation of Triassic-Jurassic arc-affinity rocks of the Jackson Mountains and the Olds Ferry terrane and provide support for models suggesting ~400 km of later dextral translation separating these arc fragments. Considering recent correlations of the Olds Ferry and Quesnellia terranes (e.g. Kurz et al., 2016), these data indicate that the Jackson Mountains, Olds Ferry, and Quesnellia terranes represent fragments of an early Mesozoic fringing-arc

system that collapsed against the margin sometime in the Early Jurassic to earliest Late Jurassic.

Our isotopic data for intrusions from the Early Mesozoic Intrusive Suite reveal intriguing differences between Early Jurassic and Late Jurassic plutons of the Jackson Mountains. While initial $^{87}\text{Sr}/^{86}\text{Sr}$ and ϵNd exhibit no significant variation with emplacement age, initial Pb ratios are consistently elevated in Late Jurassic plutons. We argue that these changes are the result of crustal shortening and eastward movement of the upper crust during the development of the LFTB. In this model, younger intrusions are sourced from and travel through a more eastern crustal column that may include fragments of enriched continental material. Though an interaction with a more enriched source is needed to explain the higher Pb ratios, the lack of changes in initial $^{87}\text{Sr}/^{86}\text{Sr}$ and ϵNd imply that eastward movement was not sufficient to carry the Jackson Mountains over the edge of the Precambrian rifted margin of North America.

Acknowledgments

Work related to this study was partially funded by Willis and Rose Burnham Graduate Student Research Grant of the Department of Geosciences, Boise State University.

Table 4.1. Summary of Lithologies and Previously Reported Ages for Plutons from the Early Mesozoic Intrusive Suite.

Name	Lithology	Reported Ages (Ma)				
		Quinn (1996)		Maher (1989)		This study $\frac{206}{238}\text{Pb}$
		$\frac{206}{238}\text{Pb}$	$\frac{207}{235}\text{Pb}$	$\frac{207}{206}\text{Pb}$	(Rb-Sr)	
Parrot Peak pluton	hornblende biotite or hornblende pyroxene quartz diorite	142.8 157.1 159.1 144.3 144.5	145.7 159.3 161.3 147.1 147.3	192.5 ± 1.2 191.7 ± 1.1 194.3 ± 1.3 192.2 ± 2.1 192.3 ± 1.2	173.3 ± 14.3 (U-Pb)	190.28 ± 0.07
Mary Sloan dikes	granite to granodiorite	181.3 172.7	182.1 173.6	191.8 ± 2.6 186.7 ± 2.6	-	189.94 ± 0.06
Harrison Grove pluton	diorite to quartz monzodiorite	169.6 161.1 149.4	170.8 163.0 151.8	188.6 ± 1.4 191.4 ± 1.3 189.9 ± 1.3	187 ± 2 (U-Pb)	189.32 ± 0.07
Deer Creek Peak pluton	quartz diorite to granodiorite	191.2 189.1 187.8 190.0 181.8 183.4	191.5 189.5 188.3 190.4 182.8 184.4	194.4 ± 1.9 195.0 ± 1.4 193.8 ± 2.3 195.8 ± 2.3 195.4 ± 1.9 197.0 ± 1.9	-	192.89 ± 0.07
Willow Creek pluton	hornblende monzonite to monzodiorite	159.7 155.4 160.2 151.2	159.9 155.9 160.2 152.0	163.5 ± 21.9 163.3 ± 9.1 159.2 ± 6.7 164.8 ± 6.4	162 ± 1 (U-Pb)	161.81 ± 0.07
Trout Creek stock	diorite	147.4	148.6	168.8 ± 1.7	-	161.88 ± 0.11
Delong Peak pluton	clinopyroxene diorite	158.0	158.9	171.5 ± 2.6	-	161.63 ± 0.18
Prospect Springs pluton	granite to granodiorite	-	-	-	-	160.72 ± 0.06

Notes: Multiple ages reported from Quinn (1996) and Quinn et al. (1997) are from different zircon size fractions. Ages from ~3-12 mg bulk samples of zircon. Authors interpret the $^{207}\text{Pb}/^{206}\text{Pb}$ age as emplacement age. Ages reported from Maher (1989) using isotopic system in parentheses. Ages reported in this study from weighted mean of single grain analysis using CA-IDTIMS. Range of (n) between 4 and 6.

Table 4.2. Summary of Samples and Corresponding $^{206}\text{Pb}/^{238}\text{U}$ ages

Sample Name	Geologic Map Unit	UTM Coordinates	$^{206}\text{Pb}/^{238}\text{U}$ Age (Ma)	MSWD	Prob. Of Fit	n
DCPP-1	Deer Creek Peak pluton	11T 376914 E 4591513 N	192.89 ± 0.07	0.3	0.83	4
MSD-1	Mary Sloan dikes	11T 373370 E 4580118 N	189.94 ± 0.06	1.6	0.17	6
TCS-1	Trout Creek stock	11T 379297 E 4572623 N	161.88 ± 0.11	0.77	0.51	4
DPP-1	Delong Peak pluton	11T 381084 E 4573899 N	161.63 ± 0.18	0.58	0.68	5

Table 4.3. Summary of the Age and Pb, Sr, and Nd Isotopic Composition for Plutons of the Early Mesozoic Intrusive Suite

Sample	Age (Ma)	$\frac{^{206}\text{Pb}}{^{204}\text{Pb}_i}$	$\frac{^{207}\text{Pb}}{^{204}\text{Pb}_i}$	$\frac{^{208}\text{Pb}}{^{204}\text{Pb}_i}$	$\frac{^{87}\text{Sr}}{^{86}\text{Sr}_i}$	ϵNd_i
Deer Creek Peak pluton (DCPP)	192.89 ± 0.07	18.6501	15.6190	38.3616	0.7046	+3.40
Parrot Peak pluton (PPP)	190.28 ± 0.07	18.6361	15.6012	38.3098	0.7039	+4.41
Harrison Grove pluton (HGP)	189.32 ± 0.07	18.6365	15.5986	38.3129	0.7039	+3.87
Mary Sloan dikes (MSD)	189.94 ± 0.06	18.5393	15.6075	38.3837	0.7034	+4.6
Trout Creek stock (TCS)	161.88 ± 0.11	18.6948	15.6071	38.5804	0.7040	+4.89
Delong Peak pluton (DPP)	161.63 ± 0.18	18.7790	15.6077	38.5224	0.7040	+3.96
Willow Creek pluton (WCP)	161.81 ± 0.07	18.9598	15.6341	39.0917	0.7043	+3.96
Prospect Springs pluton (PSP)	160.72 ± 0.06	-	-	-	-	-

Table 4.4. Geochemical and Isotopic Parameters for Mantle and Binary Mixing Components.

Component	Daughter Trace Element (ppm)	Isotopic P/D Ratio	Isotopic Ratio (Present)	Isotopic Ratio (Initial)	Mean Value (Initial)
Nd	Nd	$\frac{^{147}\text{Sm}}{^{144}\text{Nd}}$	$\frac{^{143}\text{Nd}}{^{144}\text{Nd}}$	εNd (Initial)	$\frac{^{143}\text{Nd}}{^{144}\text{Nd}}$ εNd (Initial)
DMM	0.713	0.2387	0.51311	8.19	0.51281
EMI (high)		0.1900	0.51236	-5.26	0.51212
EMI (low)		0.1810	0.51236	-5.04	0.51213
EMII	0.6	0.1920	0.51250	-2.58	0.51226
HIMU (high)		0.2240	0.51290	4.45	0.51262
HIMU (low)		0.2090	0.51290	4.81	0.51264
Continental Crust	26.5			-8.00	0.51223
Wallowa Arc	9.31			8.00	0.51305
MORB	8.61	0.2387	0.51311	8.19	0.51281
Sr	Sr	$\frac{^{87}\text{Rb}}{^{86}\text{Sr}}$	$\frac{^{87}\text{Sr}}{^{86}\text{Sr}}$	$\frac{^{87}\text{Sr}}{^{86}\text{Sr}}$	$\frac{^{87}\text{Sr}}{^{86}\text{Sr}}$
DMM	9.8	0.0253	0.7026	0.7025	
EMI (high)		0.0852	0.7053	0.7051	0.7051
EMI (low)		0.0646	0.7053	0.7051	
EMII	20.044	0.2050	0.7090	0.7084	
HIMU (high)		0.0310	0.7030	0.7029	0.7029
HIMU (low)		0.0100	0.7030	0.7030	
Continental Crust	321.94			0.7100	
Wallowa Arc	282.75			0.7029	
MORB	124.44	0.0253	0.7026	0.7025	
^{206}Pb	Pb	$\frac{^{238}\text{U}}{^{206}\text{U}}$	$\frac{^{206}\text{Pb}}{^{204}\text{Pb}}$	$\frac{^{206}\text{Pb}}{^{204}\text{Pb}}$	$\frac{^{206}\text{Pb}}{^{204}\text{Pb}}$
DMM	0.0232	4.0590	18.0000	17.8786	
EMI (high)		7.3400	17.6500	17.4304	17.4605
EMI (low)		5.3300	17.6500	17.4906	
EMII	1	5.8460	19.0000	18.8251	
HIMU (high)		20.0000	21.0000	20.4018	20.4840
HIMU (low)		14.5000	21.0000	20.5663	
Continental Crust	17.14			19.7500	
Wallowa Arc	2.08			18.4442	
MORB	0.344	4.0590	18.0000	17.8786	
^{207}Pb	Pb	$\frac{^{235}\text{U}}{^{207}\text{Pb}}$	$\frac{^{207}\text{Pb}}{^{204}\text{Pb}}$	$\frac{^{207}\text{Pb}}{^{204}\text{Pb}}$	$\frac{^{207}\text{Pb}}{^{204}\text{Pb}}$
DMM	0.0232	0.0294	15.4300	15.4240	
EMI (high)		0.0532	15.4750	15.4640	15.4655
EMI (low)		0.0387	15.4750	15.4670	
EMII	1	0.0424	15.6750	15.6663	
HIMU (high)		0.1451	15.8500	15.8202	15.8243
HIMU (low)		0.1052	15.8500	15.8284	
Continental Crust	17.14			15.8300	
Wallowa Arc	2.08			15.5400	
MORB	0.344	0.0294	15.4300	15.4240	

Component		Daughter Trace Element (ppm)	Isotopic P/D Ratio	Isotopic Ratio (Present)	Isotopic Ratio (Initial)	Mean Value (Initial)
	^{208}Pb	Pb	$\frac{^{232}\text{U}}{^{208}\text{Pb}}$	$\frac{^{208}\text{Pb}}{^{204}\text{Pb}}$	$\frac{^{208}\text{Pb}}{^{204}\text{Pb}}$	$\frac{^{208}\text{Pb}}{^{204}\text{Pb}}$
DMM		0.0232	23.6300	37.7000	37.4768	
EMI (high)			22.8000	38.1400	37.9247	37.9960
EMI (low)			7.7000	38.1400	38.0673	
EMII		1	50.6220	38.8600	38.3819	
HIMU (high)			3.6000	39.7500	39.7160	39.7174
HIMU (low)			3.3000	39.7500	39.7188	
Continental Crust		17.14			40.2500	
Wallowa Arc		2.08			39.9172	
MORB		0.344	23.6300	37.7000	37.4768	

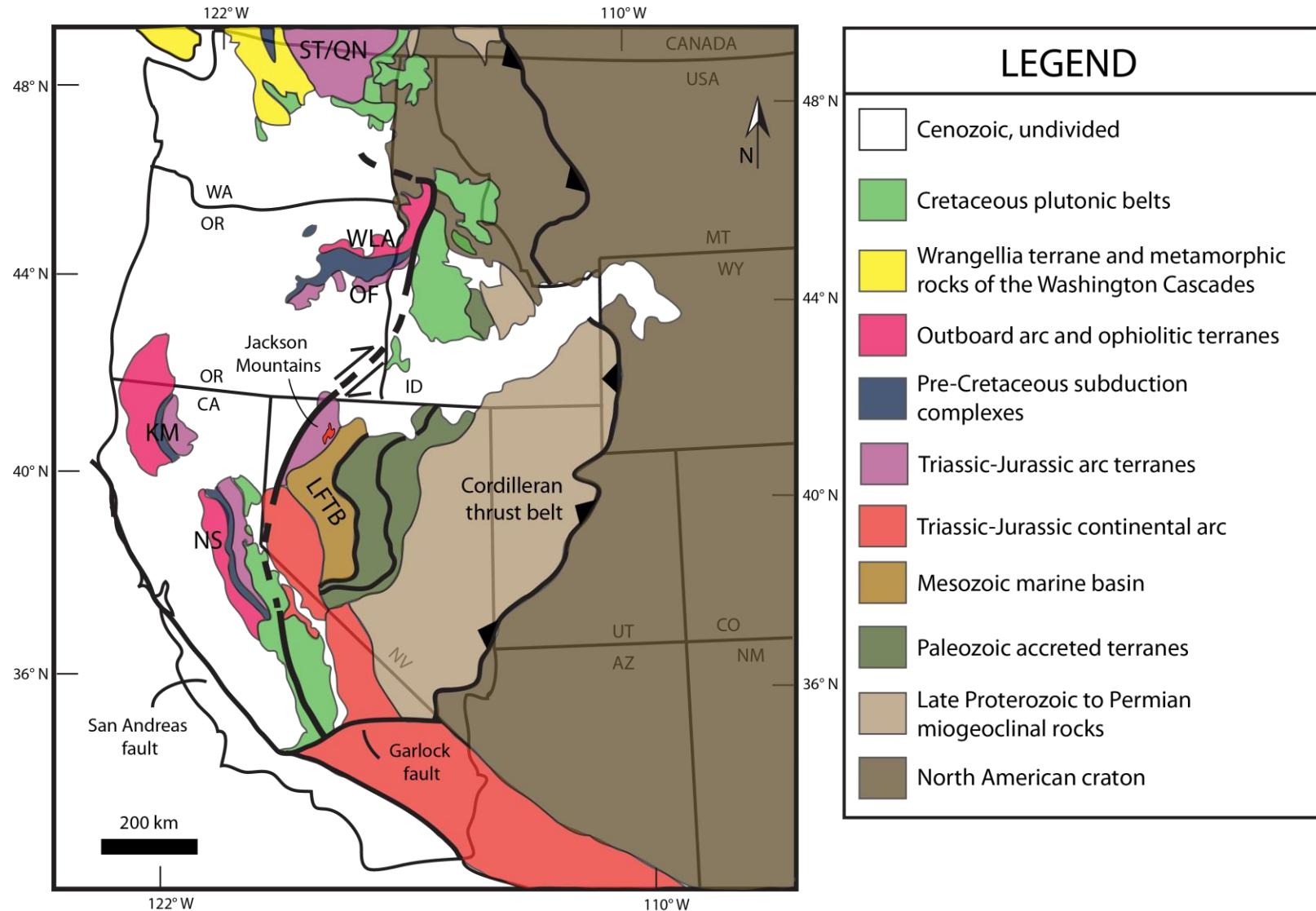


Figure 4.1. Simplified Geotectonic Assemblages of the Western United States. Modified from LaMaskin et al. (2011). ST/QN = Stikinia/Quesnellia terranes, WLA = Wallowa terrane, OF = Olds Ferry arc, KM = Klamath Mountains, NS = Northern Sierra, LFTB = Luning-Fencemaker fold-and-thrust belt.

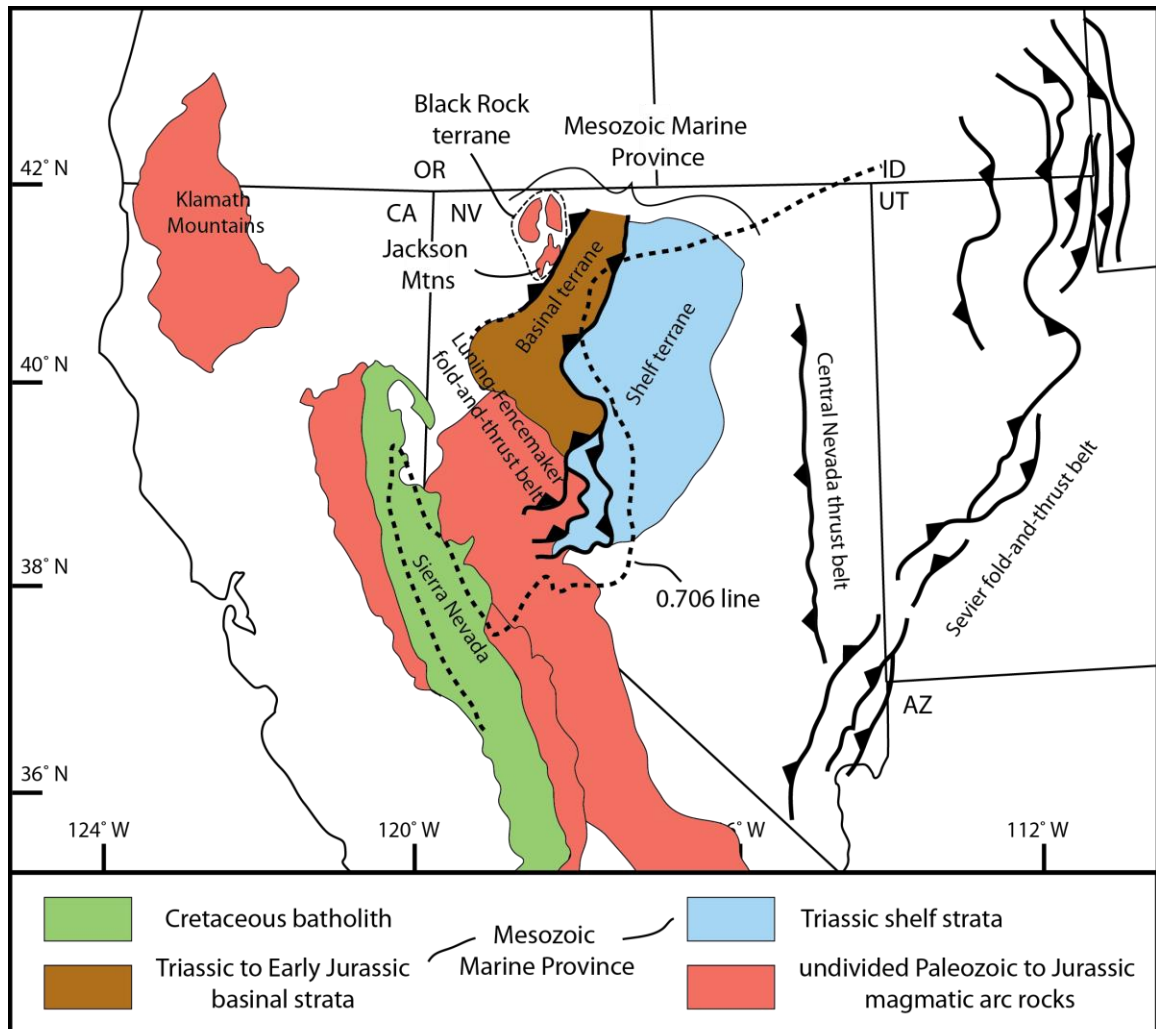


Figure 4.2. Simplified Map of the Great Basin and Western United States. Drafted to highlight the location of the Mesozoic Marine Province and Luning-Fencemaker fold-and-thrust belt in relation to Paleozoic and Mesozoic arc rocks. Modified after Wyld (2002). Initial $^{87}\text{Sr}/^{86}\text{Sr}$ 0.706 line from Elison et al. (1990).

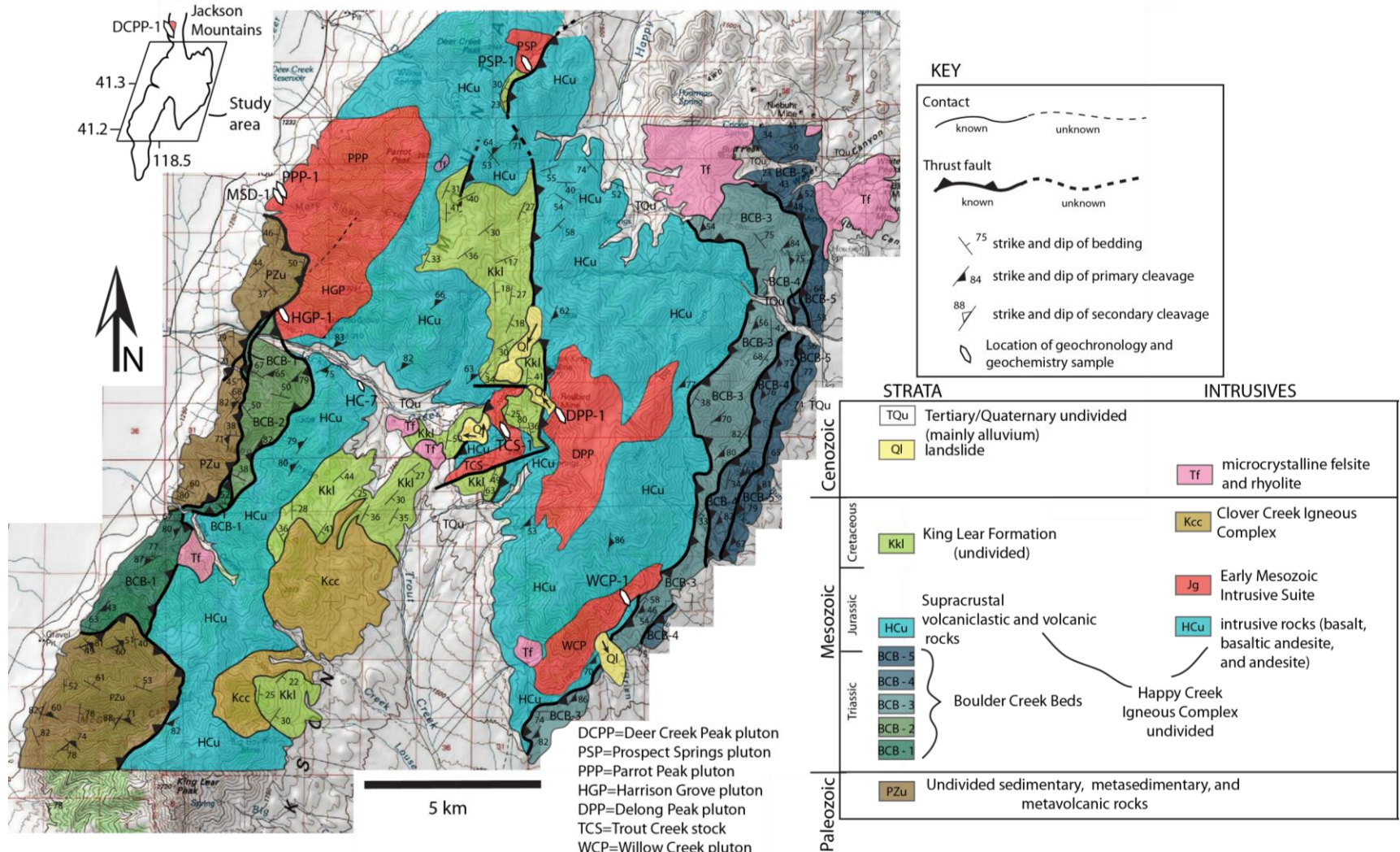


Figure 4.3. Geologic Map of the Central Jackson Mountains. Results from new geologic mapping and compilation from Willden (1958; 1963); Russell (1981; 1984), Maher (1989), Quinn (1996), and Quinn et al. (1997).

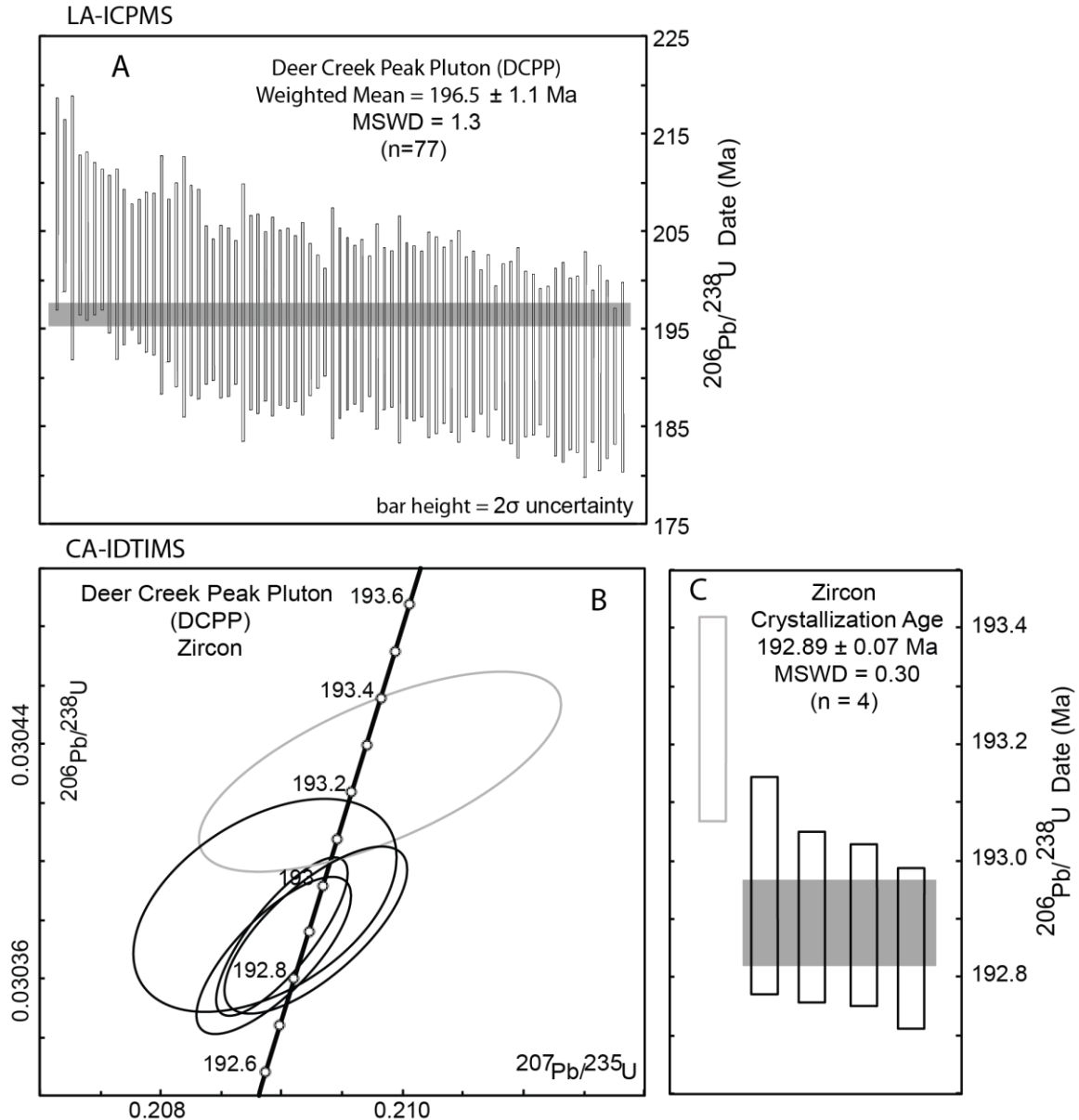


Figure 4.4. Results of U-Pb Zircon Geochronology Using Both LA-ICPMS (A) and CA-IDTIMS (B, C) of Magmatic Zircon from the Deer Creek Peak Pluton (DCPP). For CA-IDTIMS results, zircon analyses included in the weighted mean $^{206}\text{Pb}/^{238}\text{U}$ crystallization age are represented by solid bold ellipses (B). Gray outlined ellipses were not used in any age calculation (B). Ranked age charts located to the right of the concordia diagram show the distribution of $^{206}\text{Pb}/^{238}\text{U}$ ages (C). Bar heights depict their associated 2σ uncertainties. The gray band set behind the group represents the weighted mean of those analyses where the height illustrates the related uncertainty. Line-type designations on bar charts mimic those described for the concordia diagrams. MSWD mean squared weighted deviation.

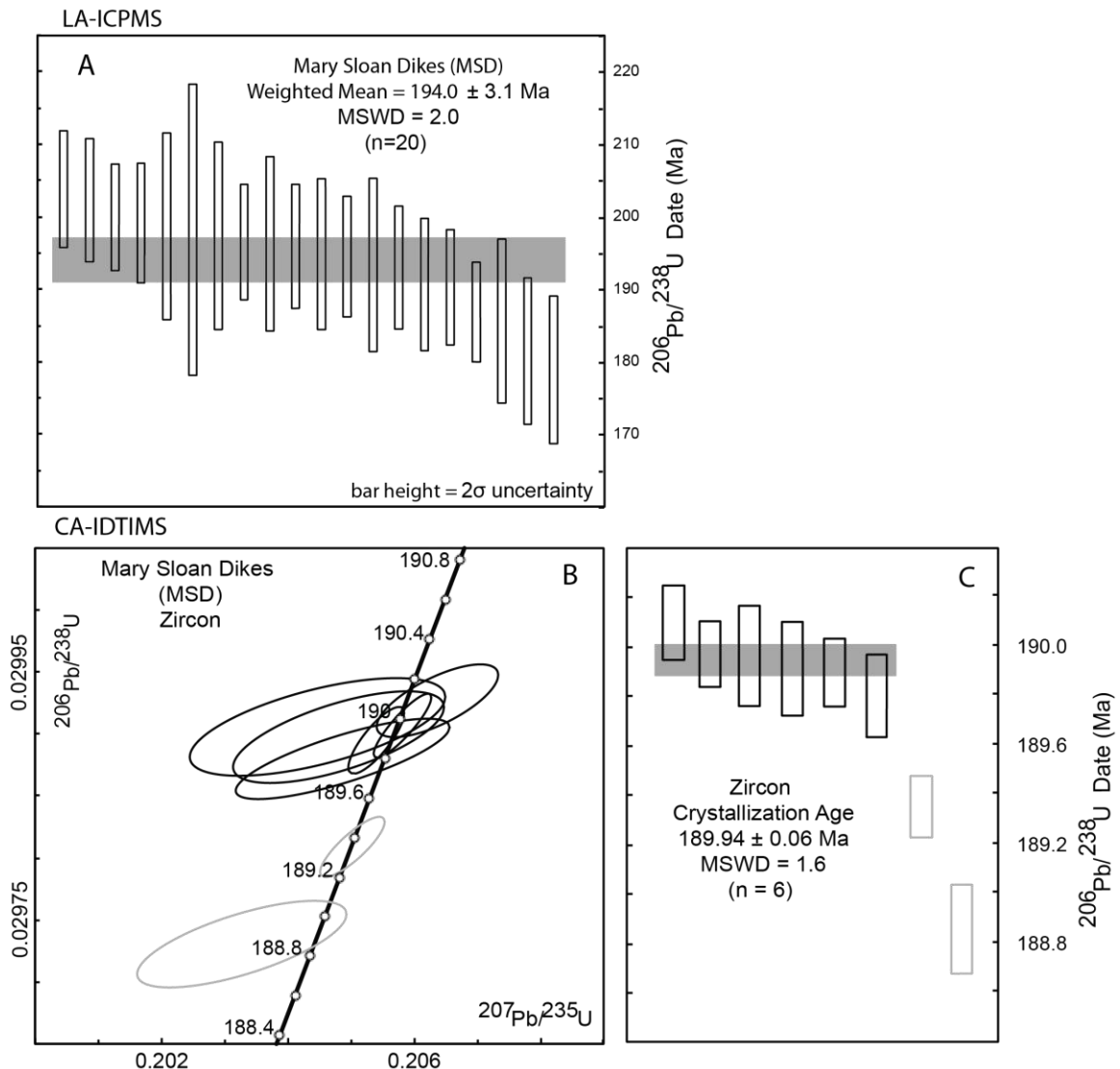


Figure 4.5. Results of U-Pb Zircon Geochronology Using Both LA-ICPMS (A) and CA-IDTIMS (B, C) of Magmatic Zircon from the Mary Sloan Dikes (MSD). For CA-IDTIMS results, zircon analyses included in the weighted mean $^{206}\text{Pb}/^{238}\text{U}$ crystallization age are represented by solid bold ellipses (B). Gray outlined ellipses were not used in any age calculation (B). Ranked age charts located to the right of the concordia diagram show the distribution of $^{206}\text{Pb}/^{238}\text{U}$ ages (C). Bar heights depict their associated 2σ uncertainties. The gray band set behind the group represents the weighted mean of those analyses where the height illustrates the related uncertainty. Line-type designations on bar charts mimic those described for the concordia diagrams. MSWD mean squared weighted deviation.

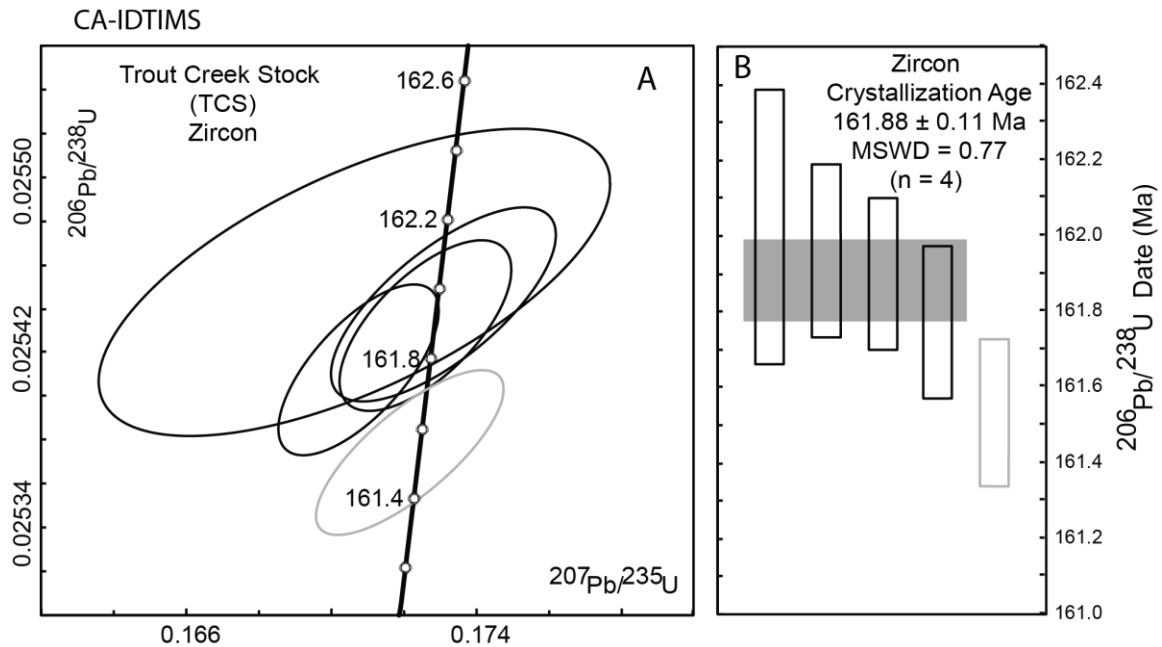


Figure 4.6. Results of U-Pb Zircon Geochronology Using CA-IDTIMS of Magmatic Zircon from the Trout Creek Stock (TCS). Zircon analyses included in the weighted mean $^{206}\text{Pb}/^{238}\text{U}$ crystallization age are represented by solid bold ellipses (A). Gray outlined ellipses were not used in any age calculation (A). Ranked age charts located to the right of the concordia diagram show the distribution of $^{206}\text{Pb}/^{238}\text{U}$ ages (B). Bar heights depict their associated 2σ uncertainties. The gray band set behind the group represents the weighted mean of those analyses where the height illustrates the related uncertainty. Line-type designations on bar charts mimic those described for the concordia diagrams. MSWD mean squared weighted deviation.

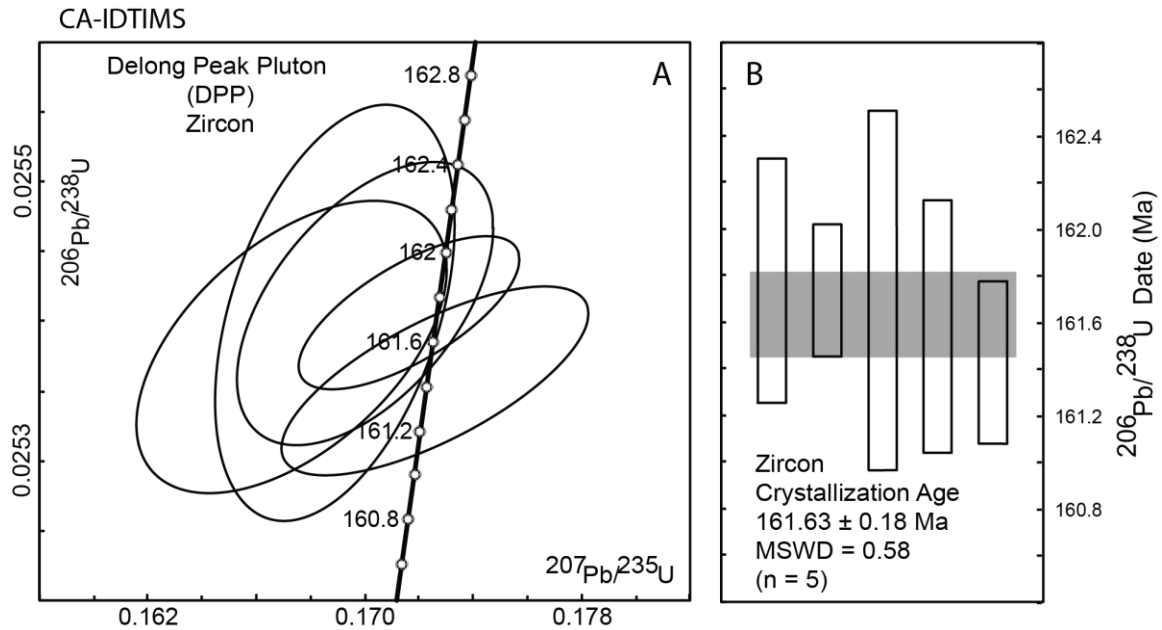


Figure 4.7. Results of U-Pb Zircon Geochronology Using CA-IDTIMS of Magmatic Zircon from the Delong Peak Pluton (DPP). Zircon analyses included in the weighted mean $^{206}\text{Pb}/^{238}\text{U}$ crystallization age are represented by solid bold ellipses (A). Ranked age charts located to the right of the concordia diagram show the distribution of $^{206}\text{Pb}/^{238}\text{U}$ ages (B). Bar heights depict their associated 2σ uncertainties. The gray band set behind the group represents the weighted mean of those analyses where the height illustrates the related uncertainty. Line-type designations on bar charts mimic those described for the concordia diagrams. MSWD mean squared weighted deviation.

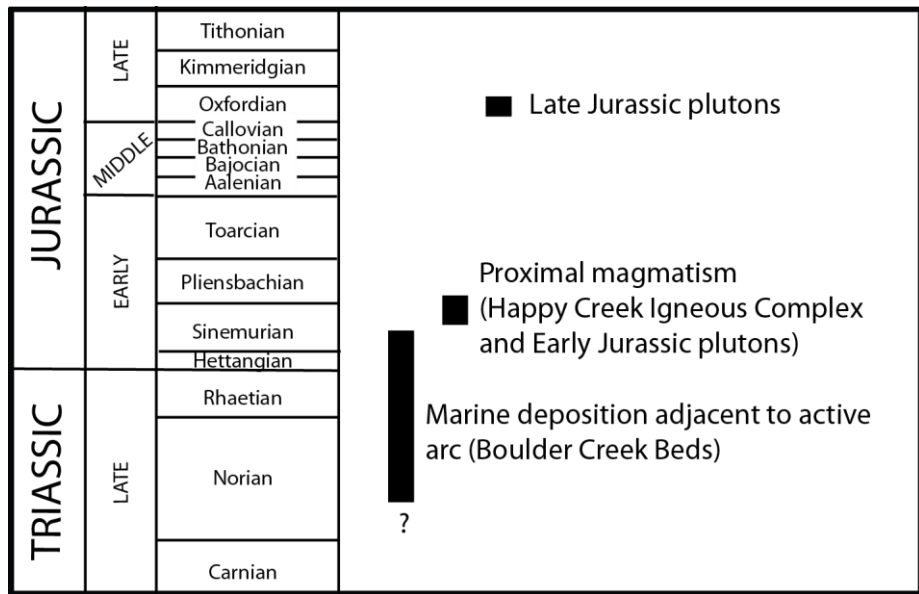


Figure 4.8. Simplified Summary of the Early Mesozoic Magmatic History of the Jackson Mountains.

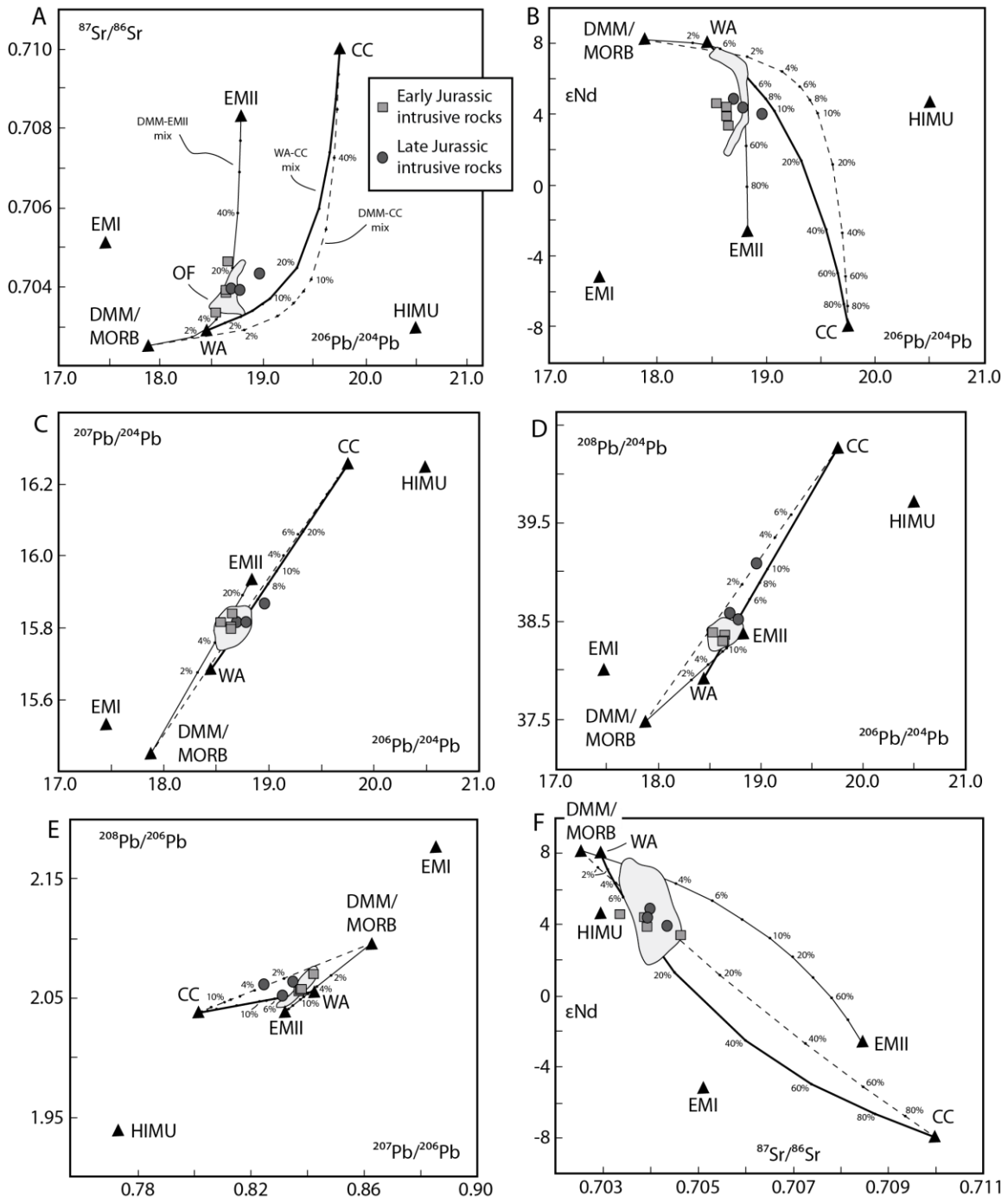


Figure 4.9. Sr, Nd, and Pb Isotopic Data for Intrusive Rocks of the Jackson Mountains. Panels B-F follow the same naming and coloring as Panel A. Solid circles are Late Jurassic intrusive rocks of the Jackson Mountains. Light colored squares are Early Jurassic intrusive rocks of the Jackson Mountains. Binary mixing line between DMM and CC is dashed line. Binary mixing line between DMM and EMII is lighter weight solid line. Binary mixing line between WA and CC is heavier weight, more bold solid line. Percentages represent the % contribution of the more enriched end-member (i.e. EMII or CC). Light grey field is for intrusive rocks of the Olds Ferry (OF) arc from Kurz et al., 2016. End member abbreviations as follows: DMM =

depleted MORB mantle, EMI = enriched mantle I, EMII = enriched mantle II, HIMU = high- μ mantle, WA = Wallowa mafic, CC = continental crust.

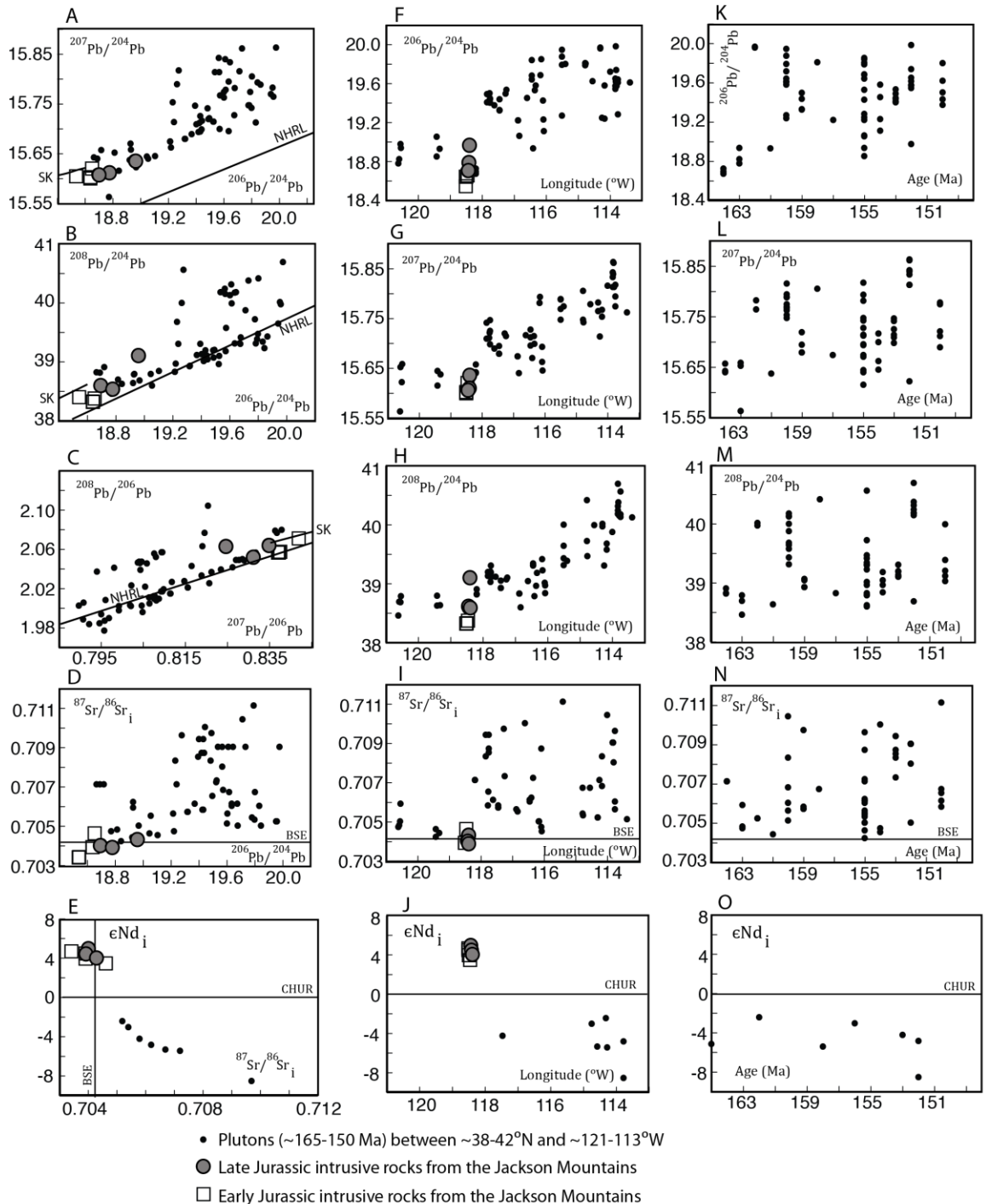


Figure 4.10. Sr, Nd, and Common Pb Isotope Diagrams for Intrusive Rocks of the Jackson Mountains Compared to Intrusive Rocks of Eastern California, Northern Nevada, and Western Utah. Panels A through E are isotope ratio vs isotope ratio plots. Panels F though J are isotope ratio plots against longitude. Panels K through O are isotope ratio plots against emplacement age. BSE=Bulk Silicate Earth, NHRL=Northern Hemisphere Reference Line, CHUR=Chondritic Uniform Reservoir, SK=Stacey and Kramers (1975) Pb evolution line curve. Data sources for western US intrusive rocks include Zartman, 1974; Stacey and Zartman, 1978;

Farmer and DePaolo, 1983; Lee, 1984; Kistler and Lee, 1989; Wright and Wooden, 1991; Wooden et al., 1998; Wooden et al., 1999; King et al., 2004.

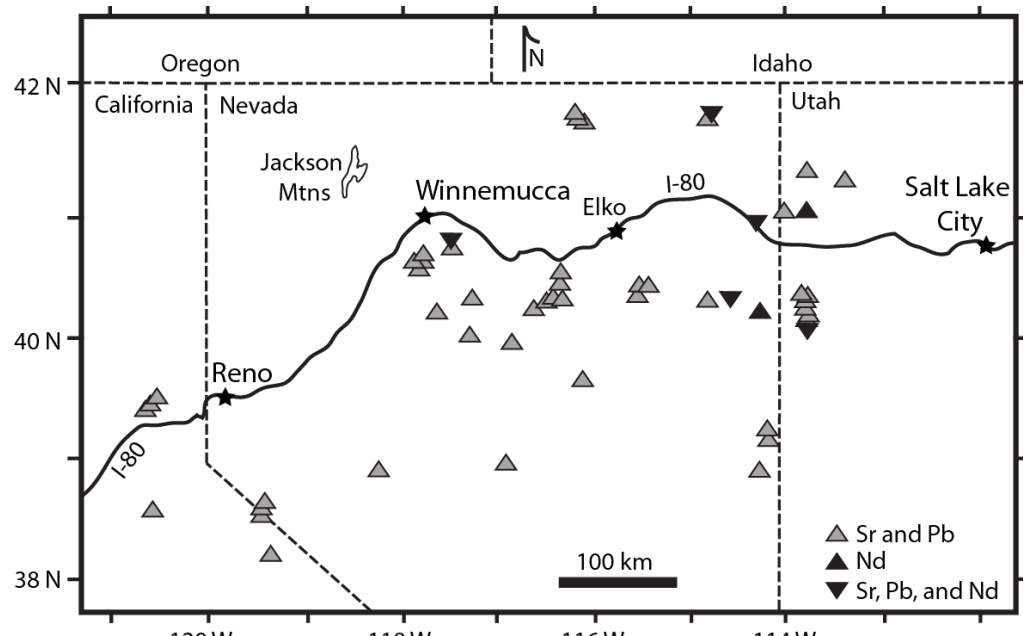


Figure 4.11. Sample Locations for Sr, Pb, and Nd Data Plotted in Figure 4.10.

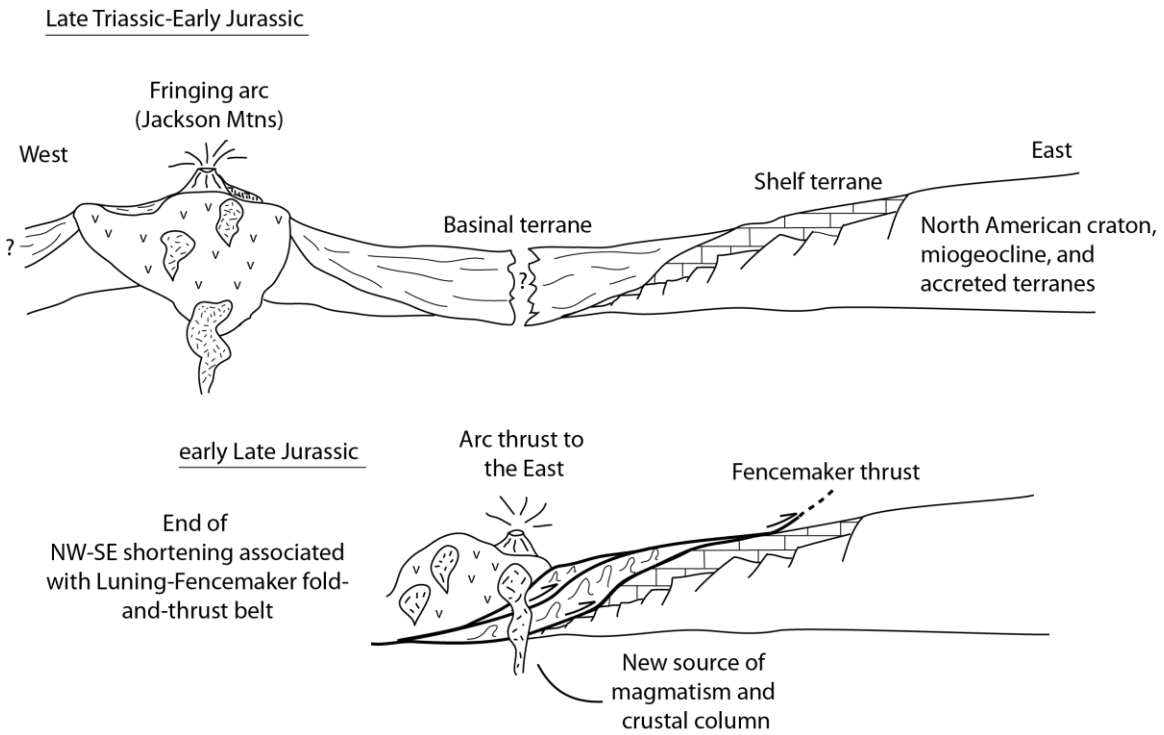


Figure 4.12. Simplified Triassic to Jurassic Tectonic Evolution of the Jackson Mountains and Adjacent Luning-Fencemaker Fold-and-Thrust Belt (LFTB). Late Triassic to Early Jurassic fringing-arc magmatism is followed by NW-SE shortening associated with the LFTB. Shortening results in eastward movement of the Jackson Mountains and thrusting over the basinal terrane and a more enriched crustal column that may include thinned fragments of continental crust and previously accreted terranes.

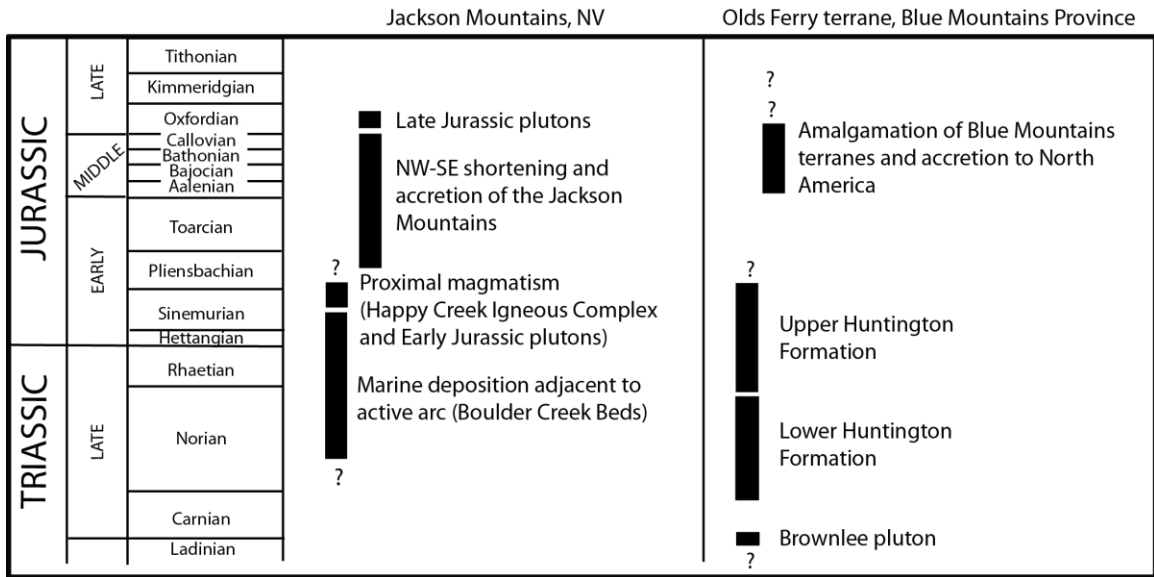


Figure 4.13. Comparison of the Triassic and Jurassic Magmatic and Tectonic History of the Jackson Mountains and Olds Ferry Terrane. See text for further descriptions and references to Olds Ferry terrane history.

References

- Armstrong, R.L., 1968, A model for the evolution of strontium and lead isotopes in a dynamic earth: *Reviews of Geophysics*, v. 6, p. 175–199.
- Armstrong, R.L., and Hein, S.M., 1973, Computer simulation of Pb and Sr isotope evolution of the earth's crust and upper mantle: *Geochimica Et Cosmochimica Acta*, v. 37, p. 1–18.
- Bond, G.C., and Kominz, M.A., 1984, Construction of tectonic subsidence curves for the early Paleozoic miogeocline, southern Canadian Rocky Mountains— Implications for subsidence mechanisms, age of breakup, and crustal thinning: *Geological Society of America Bulletin*, v. 100, p. 1909–1933.
- Brooks, H.C., and Vallier, T.L., 1978, Mesozoic rocks and tectonic evolution of eastern Oregon and western Idaho, *in* Howell, D.G., and McDougall, K.A., eds., *Mesozoic Paleogeography of the Western United States*: Society of Economic Paleontologists and Mineralogists, Pacific Section, *Paleogeography Symposium* 2, p. 133–145.
- Brooks, H.C., McIntyre, J.R., and Walker, G.W., 1976, Geology of the Oregon Part of the Baker 1-Degree by 2-Degree Quadrangle: Oregon Department of Geology and Mineral Industries Geologic Map Series GMS-7, scale 1:250,000, 1 sheet.
- Brooks, H.C., 1979, Geologic Map of the Huntington and Part of the Olds Ferry Quadrangles, Baker and Malheur Counties, Oregon: Oregon Department of Geology and Mineral Industries Geologic Map Series GMS-13, scale 1:62,500, 1 sheet.
- Burchfiel, B.C., Cowan, D.S., and Davis, G.A., 1992, Tectonic overview of the Cordilleran orogen in the western United States, *in* Burchfiel, B.C., et al., eds., *The Cordilleran orogen: Conterminous U.S.*: Boulder, Colorado, Geological Society of America, *Geology of North America*, v. G-3, p. 407–480.

- Burke, D.B., and Silberling, N.J., 1973, The Auld Lang Syne Group of Late Triassic and Jurassic (?) Age, North-Central Nevada: U.S. Geological Survey Bulletin 1394-E, 14 p.
- Collins, A.Q., 2000, Regional implications defined by the petrogenesis of the Huntington Formation, Olds Ferry terrane, Baker County, Oregon [B.S. thesis]: Boise, Idaho, Boise State University, 43 p.
- Condie, K.C., 1993, Chemical composition and evolution of the upper continental crust: contrasting results from surface samples and shales: Chemical Geology, v. 104, p. 1–37.
- Coney, P.L., Jones, D.L., and Monger, J.W.H., 1980, Cordilleran suspect terranes: Nature, v. 288, p. 329–333.
- Dickinson, W.R., 2004, Evolution of the North American Cordillera: Annual Review of Earth and Planetary Sciences, v. 32, p. 13–45.
- Dickinson, W.R., 2008, Accretionary Mesozoic-Cenozoic expansion of the Cordilleran continental margin in California and adjacent Oregon: Geosphere, v. 4, p. 329–353.
- Doe, B.R., 1967, The bearing of lead isotopes on the source of granitic magma: Journal of Petrology, v. 8, p. 51–83.
- Doe, B.R., 1973, Variations in lead-isotope compositions in Mesozoic granitic rocks of California – A preliminary investigation: Geological Society of America Bulletin, v. 84, p. 3513–3526.
- Dorsey, R.J., and LaMaskin, T.A., 2007, Stratigraphic record of Triassic-Jurassic collisional tectonics in the Blue Mountains Province, northeastern Oregon: American Journal of Science, v. 307, p. 1167–1193.
- Dorsey, R.J., and LaMaskin, T.A., 2008, Mesozoic collision and accretion of oceanic terranes in the Blue Mountains Province of northeastern Oregon: New insights from the stratigraphic record, *in* Spencer, J.E., and Titley, S.R., eds., Circum-Pacific Tectonics, Geologic Evolution, and Ore Deposits: Arizona Geological Society Digest, v. 22, p. 325–332.

- Eisele, J., Sharma, M., Galer, S.J.G., Blichert-Toft, J., Devey, C.W., and Hofmann, A.W., 2002, The role of sediment recycling in EM-1 inferred from Os, Pb, Hf, Nd, Sr isotope and trace element systematics of the Pitcairn hotspot: *Earth and Planetary Science Letters*, v. 196, p. 197–212.
- Elison, M.W., and Speed, R.C., 1989, Structural development during flysch basin collapse: the Fencemaker allochthon, East Range, Nevada: *Journal of Structural Geology*, v. 11, p. 523–538.
- Elison, M.W., Speed, R.C., and Kistler, R.W., 1990, Geologic and isotopic constraints on the crustal structure of the northern Great Basin: *Geological Society of America Bulletin*, v. 102, p. 1077–1092.
- Ernst, W. G., Snow, C. A., and Scherer, H. H., 2008, Mesozoic transpression, transtension, subduction, and metallogenesis in northern and central California: *Terra Nova*, v. 20, p. 394–413.
- Farmer, G.J., and DePaolo, D.J., 1983, Origin of Mesozoic and Tertiary granite in the western United States and implications for pre-Mesozoic crustal structure: 1. Nd and Sr isotopic studies in the geocline of the northern Great Basin: *Journal of Geophysical Research*, v. 88, p. 3379–3401.
- Hacker, B. R., Donato, M., Barnes, C., McWilliams, M. O., and Ernst, W. G., 1995, Timescales of orogeny: Jurassic construction of the Klamath Mountains: *Tectonics*, v. 14, p. 677–703.
- Harper, G. D., and Wright, J. E., 1984, Middle to Late Jurassic tectonic evolution of the Klamath Mountains, California-Oregon: *Tectonics*, v. 3, p. 759–772.
- Hart, S.R., 1988, Heterogeneous mantle domains: Signatures, genesis and mixing chronologies: *Earth and Planetary Science Letters*, v. 90, p. 273–296.
- Hart, S.R., Blusztajn, J., Dick, H.J.B., Meyer, P.S., and Muehlenbachs, K., 1999, The fingerprint of seawater circulation in a 500-meter section of ocean crust gabbros: *Geochimica et Cosmochimica acta*, v. 63, p. 4059–4080.

- Hofmann, A.W., 1988, Chemical differentiation of the Earth: the relationship between mantle, continental crust, and oceanic crust: *Earth and Planetary Science Letter*, v. 90, p. 297–314.
- Housh, T., Bowring, S.A., 1991, Lead isotopic heterogeneities within alkali feldspars: implications for the determination of initial lead isotopic compositions: *Geochimica Et Cosmochimica Acta*, v. 55, p. 2309–2316.
- Howell, D. G., 1989, *Tectonics of Suspect Terranes*: Chapman & Hall, New York, 232 p.
- Irwin, W. P., 1972, Terranes of the western Paleozoic and Triassic Belt in the southern Klamath Mountains, California: U.S. Geological Survey Professional Paper 800-C, p. 103–111.
- Jones, D.L., Cox, A., Coney, P.J., and Beck, M., 1982, The growth of Western North America: *Scientific American*, v. 247, p. 70-84.
- Jones, D.L., Howell, D.G., Coney, P.J., and Monger, J.W.H., 1983, Recognition character, and analysis of tectonostratigraphic terranes in western North America, in Hashimoto, M., and Uyeda, S., eds., *Advances in Earth and Planetary Sciences*: Terra Scientific Publication Company, Tokyo, p. 21-35.
- Jones, A.E., 1990, Geology and tectonic significance of terranes near Quinn River Crossing, Nevada, in Harwood, D.S. and Miller, M.M., eds., Late Paleozoic and early Mesozoic paleogeographic relations: Klamath Mountains, Sierra Nevada, and related terranes: *Geological Society of America Special Paper* 255, p. 239–254.
- Juras, D.S., 1973, Pre-Miocene Geology of the Northwest Part of the Olds Ferry Quadrangle, Washington County, Idaho [M.S. thesis]: Moscow, Idaho, University of Idaho, 82 p.
- Keleman, P.B., Hanghoj, K., and Greene, A.R., 2004, One view of the geochemistry of subduction-related magmatic arcs, with an emphasis on primitive andesite and lower crust, in, Holland, H.D. and Turekian, K.K., eds., *Treatise on Geochemistry*: Elsevier, Amsterdam, v. 3, p. 593–659.

- Kemp, A.I.S., and Hawkesworth, C.J., 2004, Granitic perspectives on the generation and secular evolution of the continental crust, *in*, Holland, H.D. and Turekian, K.K., eds., Treatise on Geochemistry, vol. 3, Elsevier, Amsterdam, p. 349-410.
- King, E.M., Valley, J.W., Stockli, D.F., and Wright, J.E., 2004, Oxygen isotope trends of granitic magmatism in the Great Basin: location of the Precambrian craton boundary as reflected in zircon: Geological Society of America Bulletin, v. 116, p. 451-462.
- Kistler, R.W., and Lee, D. E., 1989, Rubidium, strontium, and strontium isotopic data for a suite of granitoid rocks from the Basin and Range Province, Arizona, California, Nevada, and Utah: U. S. Geological Survey Open-File Report 89-199, 13 p.
- Kistler, R.W., and Peterman, Z.E., 1973, Variations in Sr, Rb, K, Na, and initial $^{87}\text{Sr}/^{86}\text{Sr}$ in Mesozoic granitic rocks and intruded wall rocks in central California: Geological Society of America Bulletin, v. 84, p. 3489-3512.
- Kistler, R.W., and Peterman, Z.E., 1978, Reconstruction of crustal blocks of California on the basis of initial strontium isotopic compositions of Mesozoic granitic rocks: U.S. Geological Survey Professional Paper 1071, 17 p.
- Kistler, R.W., 1983, Isotope geochemistry of plutons in the northern Great Basin: Geothermal Resources Council Special Report 13, p. 3-8.
- Kistler, R. W., 1991, Chemical and isotopic characteristics of plutons in the Great Basin: Geology and Ore Deposits of the Great Basin Symposium, Reno 1990, Proceedings, p. 107-109.
- Klein, E.M., 2004, Geochemistry of the igneous oceanic crust, *in*, Holland, H.D., and Turekian, K.K., eds., Treatise on Geochemistry: Elsevier, Amsterdam, v. 3, p. 433-463.
- Krogh, T.E., 1973, A low contamination method for hydrothermal decomposition of zircon and extraction of U and Pb for isotopic age determination: Geochimica Et Cosmochimica Acta, v. 37, p. 485-494.
- Kurz, G.A., 2010, Geochemical, isotopic, and U-Pb geochronologic investigations of intrusive basement rocks from the Wallowa and Olds Ferry arc terranes, Blue

- Mountains province, Oregon-Idaho [PhD thesis]: Boise State University, Boise, Idaho.
- Kurz, G.A., Schmitz, M.D., Northrup, C.J., and Vallier, T.L., 2016, Isotopic compositions of intrusive rocks from the Wallowa and Olds Ferry arc terranes of northeastern Oregon and western Idaho: Implications for Cordilleran evolution, lithospheric structure, and Miocene magmatism: *Lithosphere* L550.1.
- LaMaskin, T.A., Dorsey, R.J., and Vervoort, J.V., 2008, Tectonic controls on mudrock geochemistry, Mesozoic rocks of eastern Oregon and western Idaho, U.S.A.: implications for Cordilleran tectonics: *Journal of Sedimentary Research*, v. 78, p. 765–783.
- LaMaskin, T.A., Vervoort, J.D., Dorsey, R.J., and Wright, J.E., 2011, Early Mesozoic paleogeography and tectonic evolution of the western United States: insights from detrital zircon U-Pb geochronology of the Blue Mountains province, northeastern Oregon, U.S.A: *Geological Society of America Bulletin*, v. 123, p. 1939–1965.
- LaMaskin, T.A., Dorsey, R.J., Vervoort, J.D., Schmitz, M.D., Tumpane, K.P., and Moore, N.O., 2015, Westward growth of Laurentia by Pre-Late Jurassic terrane accretion, Eastern Oregon and Western Idaho, United States: *The Journal of Geology*, v. 123, p. 000-000.
- Lee, D. E., 1984, Analytical data for a suite of granitoid rocks from the Basin and Range Province: U. S. Geological Survey Bulletin 1602, 54 p.
- Lund, K., and Snee, L.W., 1988, Metamorphism, structural development, an age of the continent-island arc juncture, west-central Idaho, *in* Ernst, W.P., ed., *Metamorphism and Crustal Evolution of the Western United States*: Englewood Cliffs, New Jersey, Prentice-Hall, p. 296–331.
- Maher, K.A., 1989, Geology of the Jackson Mountains, northwest Nevada [Ph.D. thesis]: Pasadena, California Institute of Technology, 491 p.
- Manuszak, J.D., Satterfield, J.I., and Gehrels, G.E., 2000, Detrital zircon geochronology of Upper Triassic strata in western Nevada, *in* Soreghan, M.J., and Gehrels, G.E., eds., *Paleozoic and Triassic paleogeography and tectonics of western Nevada and*

- northern California: Boulder, Colorado, Geological Society of America Special Paper 347, p. 109-118.
- Martin, A.J., Wyld, S.J., Wright, J.E., and Bradford, J.H., 2010, The Lower Cretaceous King Lear Formation, northwest Nevada: Implications for Mesozoic orogenesis in the western U.S. Cordillera: Geological Society of America Bulletin, v. 122, p. 537–562.
- Mattinson, J.M., 2005, Zircon U-Pb chemical abrasion [“CA-TIMS”] method: Combined annealing and multi-step partial dissolution analysis for improved precision and accuracy of zircon ages: Chemical Geology, v. 220, p. 47-66.
- McClelland, W. C., Gehrels, G. E., and Saleeby, J. B., 1992, Upper Jurassic–lower Cretaceous basinal strata along the Cordilleran margin: implications for the accretionary history of the Alexander-Wrangellia-Peninsular terrane: Tectonics, v. 11, p. 832–835.
- Miller, M.M., 1987, Dispersed remnants of a northeast Pacific fringing arc – Upper Paleozoic island arc terranes of Permian McCloud faunal affinity, western U.S.: Tectonics, v. 6, p. 807-830.
- Monger, J., Souther, J., and Gabrielse, H., 1972, Evolution of the Canadian Cordillera: a plate tectonic model: American Journal of Science, v. 272, p. 577– 602.
- Monger, J., and Price, R., 2002, The Canadian Cordillera: Geology and tectonic evolution: Canadian Society of Exploration Geophysicists Recorder, 17 p.
- Moores, E. M., Wakabayashi, J., and Unruh, J. R., 2002, Crustal-scale cross-section of the U.S. Cordillera, California and beyond, its tectonic significance, and speculations on the Andean orogeny: International Geology Reviews, v. 44, p. 479–500.
- Nichols, K.M. and Silberling, N.J., 1977, Stratigraphy and depositional history of the Star Peak Group (Triassic), northwestern Nevada: Geological Society of America, Special Paper 178, 73 p.
- Northrup, C.J., Schmitz, M., Kurz, G., and Tumpane, K., 2011, Tectonomagmatic evolution of distinct arc terranes in the Blue Mountains Province, Oregon and

- Idaho, *in* Lee, J., and Evans, J.P., eds., Geologic Field Trips to the Basin and Range, Rocky Mountains, Snake River Plain, and Terranes of the U.S. Cordillera: Geological Society of America Field Guide 21, p. 67–88.
- Oldow, J.S., 1984, Tectonic implications of a late Mesozoic fold and thrust belt in northwestern Nevada: *Geology*, v. 11, p. 542–546.
- Oldow, J. S., Bally, A. W., Avé Lallement, H. G., and Leeman, W. P., 1989, Phanerozoic evolution of the North American Cordillera: United States and Canada: Boulder, Colorado, Geological Society of America, *Geology of North America*, v. A, p. 139–232.
- Oldow, J.S., Bartel, R.L., and Gelber, A.W., 1990, Depositional setting and regional relationships of basinal assemblages: Pershing Ridge Group and Fencemaker Canyon sequence in northwestern Nevada: *Geological Society of America Bulletin*, v. 102, p. 193–222.
- Pin, C., and Zalduogui, J.S., 1997, Sequential separation of light rare-earth elements, thorium and uranium by miniaturized extraction chromatography: application to isotopic analyses of silicate rocks: *Analytica Chimica Acta*, v. 339, p. 79–89.
- Quinn, M.J., 1996, Pre-Tertiary stratigraphy, magmatism, and structural history of the central Jackson Mountains, Humboldt County, Nevada [Ph.D. thesis]: Houston, Texas, Rice University, 243 p.
- Quinn, M.J., Wright, J.E., and Wyld, S.J., 1997, Happy Creek igneous complex and tectonic evolution of the early Mesozoic arc in the Jackson Mountains, northwest Nevada, *Geological Society of America Bulletin*, v. 109, p. 461–482.
- Rogers, J.W., 1999, Jurassic-Cretaceous deformation in the Santa Rosa Range, Nevada: implications for the development of the northern Luning-Fencemaker fold-and-thrust belt [M.S. thesis]: University of Georgia, Athens.
- Rudnick, R.L., and Gao, S., 2004, Composition of the continental crust, *in*, Holland, H.D., and Turekian, K.K., eds., *Treatise on Geochemistry*, vol. 3, Elsevier, Amsterdam, p. 1–64.

- Rudnick, R.L., and Goldstein, S.L., 1990, The Pb isotopic composition of lower crustal xenoliths and the evolution of lower crustal Pb: *Earth and Planetary Science Letter*, v. 98, p. 192–207.
- Russell, B.J., 1981, Pre-Tertiary paleogeography and tectonic history of the Jackson Mountains, northwestern Nevada [Ph.D. thesis]: Evanston, Illinois, Northwestern University, 205 p.
- Russell, B.J., 1984, Mesozoic geology of the Jackson Mountains, northwestern Nevada: *Geological Society of America Bulletin*, v. 95, p. 313–323.
- Salter, V.J.M., and Hart, S.R., 1991, The mantle sources of ocean ridges, islands and arcs; the Hf-isotope connection: *Earth and Planetary Science Letters*, v. 104, p. 364–380.
- Salter, V.J.M., and Stracke, A., 2004, Composition of the depleted mantle: *Geochemistry Geophysics Geosystems*, v. 5, p. 05004.
- Schwartz, J. J., Snock, A. W., Frost, C. D., Barnes, C. G., Gromet, L. P., and Johnson, K., 2010, Analysis of the Walla-Walla-Baker terrane boundary: implications for tectonic accretion in the Blue Mountains province, northeastern Oregon: *Geological Society of America Bulletin*, v. 122, p. 517–536.
- Shirely, S. B. and Walker, R. J., 1998, The Re-Os isotope system in cosmochemistry and high-temperature geochemistry: *Annual Reviews Earth and Planetary Sciences*, v. 26, p. 423–500.
- Silberling, N.J., 1973, Geologic events during Permian-Triassic time along the Pacific margin of the United States: *Alberta Society of Petroleum Geologists Memoir* 2, p. 345.
- Silberling, N.J., Jones, D.L., Blake, M.C., Jr., and Howell, D.G., 1987, Lithotectonic terrane map of the western conterminous United States, *in* *Lithotectonic terrane maps of the North American Cordillera: U.S. Geological Survey Map MF-1874-C*, scale 1:2,500,000.
- Shaw, D.M., Cramer, J.J., Higgins, M.D., and Truscott, M.G., 1986, Composition of the Canadian Precambrian shield and continental crust of the Earth, *in*, Dawson, J.D.,

- et al., eds., The nature of the lower continental crust: Geological Society Special Publications, Geological Society of London, v. 24, p. 275–282.
- Snoke, A., and Barnes, C., 2006, The development of tectonic concepts for the Klamath Mountains province, California and Oregon, *in* Snoke, A., and Barnes, C., eds., Geological studies in the Klamath Mountains province, California and Oregon: A volume in honor of William P. Irwin: Boulder, Colorado, Geological Society of America Special Paper, v. 410, p. 1-29.
- Snyder, W.S., and Brueckner, H.K., 1989, Permian-Carboniferous tectonics of the Golconda Allochthon; an accreted terrane in the Western United States: Compte Rendu 4 – XI Congres International de Stratigraphie et de Geologie du Carbonifere, p. 294-312.
- Speed, R.C., 1978a, Paleogeographic and plate tectonic evolution of the early Mesozoic marine province of the western Great Basin, *in* Howell, D.G., and McDougall, K.A., eds., Mesozoic paleogeography of the western U.S.: Pacific Section, Society of Economic Paleontologists and Mineralogists, Pacific Coast Paleogeography Symposium 2, p. 253–270.
- Speed, R.C., 1978b, Basinal terrane of the early Mesozoic marine province of the western Great Basin, *in* Howell, D.G., and McDougall, K.A., eds., Mesozoic paleogeography of the western U.S.: Pacific Section, Society of Economic Paleontologists and Mineralogists, Pacific Coast Paleogeography Symposium 2, p. 237–252.
- Stacey, J.S., and Kramers, J.D., 1975, Approximation of terrestrial lead isotope evolution by a two-stage model: Earth and Planetary Science Letters, v. 26, p. 207-221.
- Stacey, J. S., and Zartman, R. E., 1978, A lead and strontium isotopic study of igneous rocks and ores from the Gold Hill Mining district, Utah: Utah Geology, v. 5, p. 1-15.
- Stracke, A., Bizimis, M., and Salters, V.J.M., 2003, Recycling ocean crust: Quantitative constraints: Geochemistry Geophysics Geosystems, v. 4, p. Q08003.

- Stracke, A., Hofmann, A.W., and Hart, S.R., 2005, FOZO, HIMU, and the rest of the mantle zoo: *Geochemistry Geophysics Geosystems*, v. 6, p. Q05007.
- Taylor, S.R., and McLennan, S.M., 1995, The geochemical evolution of the continental crust: *Reviews in Geophysics*, v. 33, p. 241–265.
- Taylor, S.R., McLennan, S.M., and McCulloch, M.T., 1983, Geochemistry of loess, continental crustal composition and crustal model ages: *Geochimica et Cosmochimica Acta*, v. 47, p. 1897–1905.
- Tumpane, K.P., 2010, Age and isotopic investigations of the Olds Ferry terrane and its relation to other terranes of the Blue Mountains province, eastern Oregon and west-central Idaho [M.S. thesis]: Boise, Idaho, Boise State University, 220 p.
- Vallier, T.L., 1995, Petrology of pre-Tertiary igneous rocks in the Blue Mountains region of Oregon, Idaho, and Washington: Implications for the geologic evolution of a complex island arc, *in* Vallier, T.L., and Brooks, H.C., eds., *Geology of the Blue Mountains region of Oregon, Idaho, and Washington; petrology and tectonic evolution of pre-Tertiary rocks of the Blue Mountains region*, U.S. Geological Survey Professional Paper, v. 1438, p. 125-209.
- Walker, N.W., 1986, U/Pb Geochronologic and Petrologic Studies in the Blue Mountains Terrane, Northeastern Oregon and Westernmost-Central Idaho: Implications for Pre-Tertiary Tectonic Evolution [Ph.D. thesis]: Santa Barbara, California, University of California, Santa Barbara, 224 p.
- Ware, B.D., 2013, Age, Provenance and Structure of the Weatherby Formation, Eastern Izee Sub-Basin, Blue Mountains Province, Oregon and Idaho [M.S. thesis]: Boise, Idaho, Boise State University, 249 p.
- Wilkins, J.D., 2010, Structural and stratigraphic age constraints of the Inskip Formation, East Range, Nevada: Implications for Mesozoic tectonics of western North America [M.S. thesis]: Boise State University, Boise, Idaho.
- Willden, R., 1958, Cretaceous and Tertiary orogeny in Jackson Mountains, Humboldt County, Nevada: *American Association of Petroleum Geologists Bulletin*, v. 42, p. 2378–2398.

- Willden, R., 1963, General Geology of the Jackson Mountains, Humboldt County, Nevada: U.S. Geological Survey Bulletin 1141-D, 65 p.
- Weaver, B.L., 1991, Trace element evidence for the origin of ocean-island basalts: *Geology*, v. 19, p. 123–126.
- Weaver, B.L., and Tarney, J., 1984, Empirical approach to estimating the composition of the continental crust: *Nature*, v. 310, p. 575–577.
- Wedepohl, K.H., 1995, The composition of the continental crust: *Geochimica et Cosmochimica Acta*, v. 59, p. 1217–1239.
- Wooden, J. L., Kistler, R. W., and Tosdal, R. M., 1998, Pb isotopic mapping of crustal structure in the northern Great Basin and relationships to Au deposit trends: *in* Tosdal, R.M., Contributions to the gold metallogeny of northern Nevada: U.S. Geological Survey Open-File Report, 98-338, p. 20-33.
- Wooden, J.L., Kistler, R.W., and Tosdal, R.M., 1999, Strontium, Lead, and Oxygen isotopic data for granitoid and volcanic rocks from the northern Great Basin and Sierra Nevada, California, Nevada and Utah: U.S. Geological Survey Open-File Report, 99-569.
- Workman, R.K., Hart, S.R., Jackson, M., Regelous, M., Farley, K.A., Blusztajn, J., Kurz, M., and Staudigel, H., 2004, Recycled metasomatized lithosphere as the origin of the enriched mantle II (EM2) end-member: Evidence from the Samoan volcanic chain: *Geochemistry, Geophysics, Geosystems (G3)*, v. 5.
- Wright, J. E., and Fahan, M. R., 1988, An expanded view of Jurassic orogenesis in the western United States Cordillera: Middle Jurassic (pre-Nevadan) regional metamorphism and thrust faulting within an active arc environment, Klamath Mountains, California: *Geological Society of America Bulletin*, v. 100, p. 859–876.
- Wright, J.E., and Wooden, J.L., 1991, New Sr, Nd, and Pb isotopic data from plutons in the northern Great Basin: Implications for crustal structure and granite petrogenesis in the hinterland of the Sevier thrust belt: *Geology*, v. 19, p. 457-460.

- Wyld, S.J., and Wright, J.E., 2001, New evidence for Cretaceous strike-slip faulting in the United States Cordillera and implications for terrane-displacement, deformation patterns, and plutonism: *American Journal of Science*, v. 301, p. 150–181.
- Wyld, S.J., Rogers, J.W., and Wright, J.E., 2001, Structural evolution within the Luning-Fencemaker fold-thrust belt, Nevada: Progression from back-arc basin collapse to intra-arc shortening: *Journal of Structural Geology*, v. 23, p. 1971–1995.
- Wyld, S.J., Umhoefer, P.J., Wright, J.E., 2006, Reconstructing northern Cordilleran terranes along known Cretaceous and Cenozoic strike-slip faults: Implications for the Baja British Columbia hypothesis and other models, *in* Haggart, J.W., Enkin, R.J., and Monger, J.W.H., eds., *Paleogeography of the North American Cordillera: Evidence For and Against Large-Scale Displacements*: Geological Association of Canada Special Paper 46, p. 277–298.
- Wyld, S.J., 1996, Early Jurassic deformation in the Pine Forest Range, northwest Nevada, and implications for Cordilleran tectonics: *Tectonics*, v. 15, p. 566–583.
- Wyld, S.J., 2000, Triassic evolution of the arc and back-arc of northwest Nevada, and evidence for extensional tectonism, *in* Soreghan, M.J., and Gehrels, G.E., eds., *Paleozoic and Triassic Paleogeography and Tectonic Evolution of Western Nevada and Northern California*: Boulder, Colorado, Geological Society of America Special Paper 347, p. 1–23.
- Wyld, S.J., 2002, Structural evolution of a Mesozoic back-arc fold-and-thrust belt in the U.S. Cordillera: New evidence from northern Nevada: *Geological Society of America Bulletin*, v. 114, p. 1452–1468.
- Zartman, R. E., 1974, Lead isotopic provinces in the Cordillera of the western United States and their geologic significance: *Economic Geology*, v. 69, p. 792–805.
- Zindler, A., and Hart, S.R., 1986, Chemical dynamics: *Annual Review of Earth and Planetary Sciences*, v. 14, p. 493–571.

CHAPTER FIVE: CONCLUDING COMMENTS

In the preceding chapters, I have used a combination of new geologic mapping and structural analysis, high-precision U-Pb zircon geochronology, and isotope geochemistry to examine the magmatic, stratigraphic, and structural history of the Jackson Mountains of the Black Rock Desert region of northwest Nevada. While individual chapters are written as stand alone manuscripts dealing with specific problems, their combination provides the most comprehensive and complete picture of the Mesozoic geologic and tectonic history of the Jackson Mountains.

In Chapter Two, I documented and described the evidence for at least one phase of Early Cretaceous (~118 Ma) NW-SE shortening in the Jackson Mountains. Using a combination of new detailed mapping and U-Pb zircon geochronology, I provided strong support for movement along the Deer Creek thrust and syndepositional shortening of the King Lear basin. I then explored the possible driving mechanisms and place shortening in the Jackson Mountains into a more regional context. In this examination, it becomes apparent that significant, temporally overlapping changes in the forearc, arc, and retroarc regions correspond with a significant change in plate motions at the margin. As I argue, Early Cretaceous shortening in the Jackson Mountains may reflect internal shortening of the hinterland in response to a change in the Pacific-Farallon-North American velocity structure. In this model, the Deer Creek thrust represents an out-of-sequence back thrust that overall assisted in shortening the orogenic wedge. These results provide new insight into the structural evolution of the hinterland and back arc region and raises questions

concerning the regional extent and magnitude of Early Cretaceous shortening within the United States Cordillera. This study provides a foundation to investigate contractional deformation of this age and its significance in the evolution of the Cordillera. Furthermore, this study reinforces the importance of out-of-sequence contraction in the hinterland and is therefore important for those researching the spatial and temporal structural evolution and dynamics of fold-and-thrust belts in general.

In Chapter Three, I focused on the age, provenance, structure, and paleogeography of the volcanogenic, marine rocks of the Boulder Creek Beds (BCB). The results of new detrital zircon data from sandstones of the BCB reveal unimodal Late Triassic to Early Jurassic age peaks that imply derivation from an adjacent active arc source. Using single-grain analysis from LA-ICPMS and the more accurate and precise CA-IDTIMS in tandem, I have shown the BCB to be younger than previously thought and represent a Norian (~215 Ma) to Sinemurian (~195 Ma) succession. These data support the use of the youngest age mode rather than the youngest grain age from LA-ICPMS data as a more reliable and robust measure of the maximum depositional age. Additionally, we argue for the combined use of LA-ICPMS and CA-IDTIMS when investigating the maximum depositional age of clastic rocks. Together with regional geologic and tectonic relationships, these new data from the Boulder Creek Beds support paleogeographic reconstructions that place a deep marine basin between a fringing-arc (i.e. Jackson Mountains) and the continent. Furthermore, these new data from the Jackson Mountains provide strong support for the correlation of the Olds Ferry and Black Rock terranes as representing fragments of the same early Mesozoic fringing arc later separated and displaced by ~400 km of dextral translation. When combined with U-Pb

geochronologic constraints on intrusive rocks of the Jackson Mountains, these data provide strong support for a phase of NW-SE shortening between the middle Early Jurassic (post ~189 Ma) and earliest Late Jurassic (pre ~162 Ma). Based on overlap in timing, kinematic compatibility, and geographic proximity, this contractional event is likely associated with the development of the Luning-Fencemaker fold-and-thrust belt involving the closure of the early Mesozoic marine basin and thrusting of the fringing-arc over the basinal terrane. Together, the results from this study provide new insight into the early Mesozoic paleogeography and structural evolution of the Jackson Mountains.

In Chapter Four, I use a combination of high-precision U-Pb zircon geochronology and isotope geochemistry to investigate the age, duration, and paleogeographic setting of Mesozoic magmatism in the Jackson Mountains. The results of this study provide a picture of Late Triassic to Early Jurassic fringing-arc magmatism that correlates with the timing and chemistry of magmatism in the Olds Ferry terrane of the Blue Mountains Province. These data strongly support reconstructions that place the Jackson Mountains, Olds Ferry, and Quesnellia terranes as fragments of an early Mesozoic fringing-arc system that collapsed against the margin sometime in the Early Jurassic to earliest Late Jurassic. Furthermore, differences in the isotopic composition of Early and Late Jurassic intrusive rocks of the Jackson Mountains are consistent with crustal shortening and eastward movement of the upper crust during the development of the Luning-Fencemaker fold-and-thrust belt.

The results of this dissertation help immensely in our continuing understanding of Cordilleran terranes and their relationship to one another. Through decades of research in the Cordillera, it has become clear that our understanding of the assembly and subsequent

shuffling of the Cordilleran orogen hinges upon our ability to piece together the geologic and tectonic histories of individual terranes. Only with a more detailed understanding of individual terranes will we be able to develop a more complete picture of Cordilleran evolution and the growth and assembly of western North America. This refined and updated understanding of the geology and tectonics of the Jackson Mountains improves our understanding of Cordilleran magmatism, accretion, and paleogeography and provides insight into terrane correlations.

APPENDIX A

**U-Pb Isotopic Data for Magmatic and Detrital Zircon Analyzed By LA-ICPMS and
CA-IDTIMS From Chapter 2**

Table A.1. U-Pb Isotopic Data for Magmatic Zircon from the Jackson Mountains for Chapter 2

Samp.	Compositional Parameters					Radiogenic Isotope Ratios							Isotopic Ages						
	$^{206}\text{Pb}^*$ x10 ⁻¹³ mol	mol %	Pb^*	Pbc	^{206}Pb	^{208}Pb	^{207}Pb	% err	^{207}Pb	^{235}U	% err	^{206}Pb	corr.	^{207}Pb	^{235}U	^{207}Pb	^{235}U	^{206}Pb	^{238}U
(a)	(b)	(b)	(b)	(b)	(c)	(d)	(d)	(e)	(d)	(e)	(d)	(e)	(f)	(e)	(f)	(e)	(f)	(e)	
KLT-1 (King Lear Formation – volcanic tuff from the Clover Creek Member)																			
z1	0.431	99.1%	32	0.31	2076	0.083	0.048506	0.284	0.124503	0.332	0.018616	0.083	0.662	124.03	6.69	119.15	0.37	118.90	0.10
z2	0.509	98.5%	18	0.64	1210	0.077	0.048208	0.474	0.123377	0.536	0.018562	0.063	0.978	109.47	11.20	118.13	0.60	118.56	0.07
z3	1.428	99.6%	80	0.42	5154	0.081	0.048334	0.138	0.123763	0.191	0.018571	0.072	0.823	115.65	3.25	118.48	0.21	118.62	0.08
z4	0.947	99.5%	56	0.40	3565	0.091	0.048301	0.211	0.123598	0.259	0.018559	0.074	0.728	114.03	4.98	118.33	0.29	118.54	0.09
z5	1.706	99.3%	44	0.91	2847	0.088	0.048313	0.166	0.123640	0.213	0.018561	0.077	0.730	114.65	3.91	118.37	0.24	118.55	0.09
z6	1.131	98.9%	25	1.06	1629	0.083	0.048366	0.194	0.123998	0.245	0.018594	0.073	0.779	117.23	4.56	118.69	0.27	118.76	0.09
z7	1.127	99.2%	33	0.78	2186	0.079	0.048431	0.192	0.124173	0.241	0.018595	0.073	0.752	120.37	4.51	118.85	0.27	118.77	0.09
PPP-1 (Parrot Peak pluton)																			
z1	1.1306	99.6%	88	0.33	5141	0.201	0.049836	0.165	0.205754	0.215	0.029943	0.072	0.788	187.37	3.84	189.98	0.37	190.19	0.14
z2	0.5006	99.0%	32	0.40	1882	0.178	0.049746	0.407	0.205445	0.452	0.029953	0.083	0.613	183.16	9.47	189.72	0.78	190.25	0.16
z3	1.3696	99.6%	80	0.43	4837	0.153	0.049954	0.130	0.206452	0.185	0.029974	0.073	0.841	192.85	3.02	190.57	0.32	190.39	0.14
z4	0.2174	98.0%	15	0.37	891	0.177	0.049790	0.878	0.205595	0.942	0.029948	0.122	0.565	185.19	20.45	189.85	1.63	190.22	0.23
z5	3.6070	99.8%	165	0.59	9228	0.249	0.049853	0.092	0.205946	0.150	0.029961	0.071	0.892	188.16	2.15	190.14	0.26	190.30	0.13
PSP-1 (Prospect Springs pluton)																			
z1	2.0939	99.4%	62	1.10	2889	0.535	0.049221	0.124	0.171396	0.179	0.025255	0.071	0.859	158.35	2.90	160.63	0.27	160.78	0.11
z2	0.7711	98.7%	31	0.81	1450	0.527	0.049254	0.269	0.171347	0.318	0.025231	0.076	0.714	159.94	6.30	160.59	0.47	160.63	0.12
z3	0.2859	96.2%	10	0.94	478	0.531	0.049296	0.634	0.171691	0.698	0.025260	0.095	0.707	161.92	14.83	160.89	1.04	160.82	0.15
z4	0.4097	98.2%	22	0.61	1032	0.553	0.049298	0.440	0.171548	0.494	0.025238	0.084	0.689	162.01	10.29	160.76	0.73	160.68	0.13
z5	0.4805	98.5%	25	0.61	1210	0.504	0.049205	0.484	0.171285	0.537	0.025247	0.092	0.627	157.63	11.33	160.53	0.80	160.73	0.15

(a) z1, z2, etc., are labels for fractions composed of single zircon or fragments; all zircon fractions were annealed and chemically abraded after Mattinson (2005)

(b) Pb* and Pbc represent radiogenic and common Pb, respectively; mol % 206Pb* with respect to radiogenic, blank and initial common Pb.

(c) Measured ratio corrected for spike and fractionation only. Fractionation estimated at 0.17 ± 0.03 (1-sigma) %/amu for Daly analyses, based on analysis of NBS-981 and NBS-982.

(d) Corrected for fractionation, spike, and common Pb; all common Pb was assumed to be procedural blank: $206\text{Pb}/204\text{Pb} = 18.042 \pm 0.61\%$; $207\text{Pb}/204\text{Pb} = 15.537 \pm 0.52\%$;

$208\text{Pb}/204\text{Pb} = 37.686 \pm 0.63\%$ (all uncertainties 1-sigma).

(e) Errors are 2-sigma, propagated using the algorithms of Schmitz and Schoene (2007).

(f) Calculations are based on the decay constants of Jaffey et al. (1971). 206Pb/238U and 207Pb/206Pb ages corrected for initial disequilibrium in 230Th/238U using Th/U [magma] = 3.

Table A.2. U-Pb Isotopic Data for Detrital Zircon from the Jackson Mountains for Chapter 2

Samp.	Compositional Parameters					Radiogenic Isotope Ratios						Isotopic Ages							
	$^{206}\text{Pb}^*$ $\times 10^{-13}$ mol	mol %	$\frac{\text{Pb}^*}{\text{Pbc}}$	$\frac{\text{Pbc}}{\text{Pb}^*}$	$\frac{^{206}\text{Pb}}{^{204}\text{Pb}}$	^{208}Pb	^{207}Pb	$\frac{^{207}\text{Pb}}{^{235}\text{U}}$	^{206}Pb	$\frac{^{206}\text{Pb}}{^{238}\text{U}}$	corr.	^{207}Pb	$\frac{^{207}\text{Pb}}{^{235}\text{U}}$	^{206}Pb	$\frac{^{206}\text{Pb}}{^{238}\text{U}}$	\pm			
(a)	(b)	(b)	(b)	(c)	(d)	(d)	(e)	(d)	(e)	(d)	(e)	(f)	(e)	(f)	(e)	(f)	(e)		
KLS-1 (King Lear Formation – Clover Creek Member)																			
z2	0.5946	99.0%	29	0.52	1734	0.167	0.048305	0.216	0.123970	0.293	0.018613	0.055	1.311	114.24	5.10	118.66	0.33	118.89	0.06
z3	0.7688	99.3%	42	0.45	2561	0.138	0.048440	0.234	0.124361	0.284	0.018620	0.075	0.736	120.79	5.52	119.02	0.32	118.93	0.09
z4	1.1073	99.0%	30	0.88	1907	0.107	0.048329	0.234	0.123948	0.280	0.018601	0.075	0.698	115.40	5.53	118.64	0.31	118.81	0.09
z5	0.5052	98.8%	25	0.49	1566	0.137	0.048410	0.351	0.124383	0.402	0.018635	0.080	0.697	119.37	8.27	119.04	0.45	119.02	0.09

(a) z1, z2, etc., are labels for fractions composed of single zircon or fragments; all zircon fractions were annealed and chemically abraded after Mattinson (2005)

(b) Pb* and Pbc represent radiogenic and common Pb, respectively; mol % $^{206}\text{Pb}^*$ with respect to radiogenic, blank and initial common Pb.

(c) Measured ratio corrected for spike and fractionation only. Fractionation estimated at 0.17 ± 0.03 (1-sigma) %/amu for Daly analyses, based on analysis of NBS-981 and NBS-982.

(d) Corrected for fractionation, spike, and common Pb; all common Pb was assumed to be procedural blank: $^{206}\text{Pb}/^{204}\text{Pb} = 18.042 \pm 0.61\%$; $^{207}\text{Pb}/^{204}\text{Pb} = 15.537 \pm 0.52\%$;

$^{208}\text{Pb}/^{204}\text{Pb} = 37.686 \pm 0.63\%$ (all uncertainties 1-sigma).

(e) Errors are 2-sigma, propagated using the algorithms of Schmitz and Schoene (2007).

(f) Calculations are based on the decay constants of Jaffey et al. (1971). $^{206}\text{Pb}/^{238}\text{U}$ and $^{207}\text{Pb}/^{206}\text{Pb}$ ages corrected for initial disequilibrium in $^{230}\text{Th}/^{238}\text{U}$ using Th/U [magma] = 3.

Table A.3. Magmatic Zircon LA-ICPMS U-Pb Geochronology for Chapter 2

Analysis	Composition						Corrected isotope ratios						Apparent ages (Ma)											
	U ppm	Th ppm	Pb ppm	Th/U	$\frac{^{206}\text{Pb}}{^{204}\text{Pb}}$	$\frac{^{207}\text{Pb}}{^{235}\text{U}}$	$\pm 2s$ (%)	$\frac{^{206}\text{Pb}}{^{238}\text{U}}$	$\pm 2s$ (%)	error corr.	$\frac{^{238}\text{U}}{^{206}\text{Pb}}$	$\pm 2s$ (%)	$\frac{^{207}\text{Pb}}{^{206}\text{Pb}}$	$\pm 2s$ (%)	$\frac{^{207}\text{Pb}}{^{206}\text{Pb}}$ (abs)	$\pm 2s$ (%)	$\frac{^{207}\text{Pb}}{^{235}\text{U}}$ (abs)	$\pm 2s$ (%)	$\frac{^{206}\text{Pb}}{^{238}\text{U}}$ (abs)	$\pm 2s$ (%)	% disc.			
KLT-1 (King Lear Formation – King Lear tuff, Clover Creek Member)																								
KLT-1_L_93	290	82	6	0.28	223	0.126	10.7	0.0188	4.9	0.46	53.302	4.9	0.0486	9.5	128	223	120	12	120	6	7			
KLT-1_L_104	490	174	10	0.36	3531	0.119	8.5	0.0187	4.8	0.57	53.446	4.8	0.0461	7.0	4	169	114	9	120	6	-2949			
KLT-1_L_108	592	147	12	0.25	255	0.120	5.8	0.0183	3.7	0.65	54.691	3.7	0.0474	4.4	71	104	115	6	117	4	-64			
KLT-1_L_109	793	239	18	0.30	417	0.166	9.5	0.0185	5.4	0.57	54.100	5.4	0.0651	7.8	777	164	156	14	118	6	85			
KLT-1_L_110	809	250	17	0.31	120	0.125	7.8	0.0185	4.0	0.52	54.022	4.0	0.0488	6.7	140	157	119	9	118	5	16			
KLT-1_L_113	494	134	10	0.27	438	0.126	7.9	0.0183	3.7	0.47	54.652	3.7	0.0498	7.0	185	162	120	9	117	4	37			
KLT-1_L_114	259	45	6	0.17	869	0.236	18.2	0.0197	4.0	0.22	50.753	4.0	0.0869	17.7	1359	342	215	35	126	5	91			
KLT-1_L_115	521	292	12	0.56	1447	0.142	11.3	0.0186	4.6	0.41	53.788	4.6	0.0555	10.3	432	229	135	14	119	5	73			
KLT-1_L_116	861	287	18	0.33	2030	0.120	6.4	0.0186	4.0	0.63	53.648	4.0	0.0467	4.9	35	118	115	7	119	5	-236			
KLT-1_L_118	238	80	5	0.34	98	0.126	10.0	0.0196	4.3	0.43	51.043	4.3	0.0467	9.0	36	215	121	11	125	5	-245			
KLT-1_L_120	258	139	6	0.54	136	0.113	9.2	0.0180	4.0	0.44	55.535	4.0	0.0456	8.2	-26	200	109	9	115	5	550			
KLT-1_L_122	418	126	9	0.30	706	0.123	8.0	0.0189	4.4	0.55	53.002	4.4	0.0474	6.7	72	159	118	9	120	5	-68			
KLT-1_L_123	793	217	16	0.27	764	0.128	7.0	0.0184	3.8	0.54	54.217	3.8	0.0502	5.9	203	138	122	8	118	4	42			
KLT-1_L_124	353	90	7	0.25	470	0.127	9.1	0.0188	4.9	0.54	53.255	4.9	0.0490	7.6	148	179	121	10	120	6	19			
KLT-1_L_125	1002	275	21	0.27	971	0.131	6.9	0.0190	4.2	0.61	52.549	4.2	0.0500	5.5	195	127	125	8	122	5	38			
KLT-1_L_126	1035	367	22	0.35	2469	0.122	5.7	0.0181	4.2	0.74	55.268	4.2	0.0490	3.8	145	89	117	6	116	5	21			
KLT-1_L_133	511	142	11	0.28	272	0.135	8.1	0.0194	5.0	0.61	51.600	5.0	0.0506	6.4	224	149	129	10	124	6	45			
KLT-1_L_135	528	177	11	0.34	5946	0.131	8.4	0.0186	5.2	0.62	53.795	5.2	0.0511	6.6	243	152	125	10	119	6	51			
KLT-1_L_136	624	144	13	0.23	529	0.125	7.1	0.0189	3.9	0.55	52.916	3.9	0.0479	5.9	92	140	119	8	121	5	-31			
KLT-1_S_388	597	258	12	0.43	559	0.116	10.4	0.0179	5.8	0.56	55.928	5.8	0.0471	8.6	55	206	112	11	114	7	-108			
KLT-1_S_390	824	211	16	0.26	239	0.118	7.5	0.0177	5.2	0.70	56.552	5.2	0.0485	5.3	126	125	114	8	113	6	10			
KLT-1_S_391	875	213	17	0.24	487	0.117	9.4	0.0174	6.5	0.69	57.351	6.5	0.0487	6.8	133	161	112	10	111	7	16			
KLT-1_S_397	600	157	12	0.26	620	0.118	12.2	0.0176	7.9	0.65	56.872	7.9	0.0486	9.2	128	217	113	13	112	9	12			
KLT-1_S_400	684	191	14	0.28	746	0.125	7.2	0.0181	5.5	0.77	55.193	5.5	0.0499	4.6	188	108	119	8	116	6	39			
KLT-1_S_409	480	122	10	0.25	415	0.120	8.9	0.0187	5.9	0.66	53.436	5.9	0.0465	6.7	24	161	115	10	120	7	-401			
KLT-1_S_412	436	111	10	0.25	238	0.170	11.5	0.0192	5.9	0.51	52.130	5.9	0.0641	9.8	746	208	159	17	122	7	84			
KLT-1_M_469	512	248	10	0.49	2192	0.124	7.7	0.0180	3.2	0.41	55.566	3.2	0.0498	7.0	184	164	118	9	115	4	38			
KLT-1_M_470	661	241	14	0.36	318	0.122	11.8	0.0189	6.8	0.58	52.954	6.8	0.0470	9.7	47	231	117	13	121	8	-155			
KLT-1_M_471	584	285	12	0.49	2495	0.119	8.2	0.0186	3.9	0.48	53.680	3.9	0.0463	7.2	12	173	114	9	119	5	-915			
KLT-1_M_472	638	204	17	0.32	204	0.312	8.5	0.0200	5.2	0.62	50.066	5.2	0.1134	6.7	1854	121	276	21	127	7	93			

KLT-1_M_473	766	265	16	0.35	466	0.126	7.3	0.0189	4.7	0.64	52.971	4.7	0.0482	5.6	111	132	120	8	121	6	-9
KLT-1_M_474	774	269	16	0.35	1377	0.126	6.8	0.0189	4.7	0.69	53.026	4.7	0.0484	4.9	121	116	120	8	120	6	0
KLT-1_M_475	582	176	12	0.30	154	0.125	8.7	0.0190	4.8	0.55	52.585	4.8	0.0477	7.3	82	172	120	10	121	6	-48
KLT-1_M_476	506	171	10	0.34	64	0.126	7.6	0.0185	3.1	0.40	53.941	3.1	0.0494	7.0	168	163	121	9	118	4	30
KLT-1_M_478	531	258	11	0.49	2132	0.121	7.5	0.0187	4.7	0.62	53.613	4.7	0.0471	5.9	54	140	116	8	119	6	-120
KLT-1_M_483	696	318	15	0.46	787	0.126	6.8	0.0187	5.0	0.72	53.492	5.0	0.0490	4.7	148	110	121	8	119	6	20
KLT-1_M_484	482	168	10	0.35	890	0.129	7.8	0.0187	3.3	0.42	53.416	3.3	0.0501	7.0	199	164	123	9	120	4	40
KLT-1_M_485	469	226	10	0.48	240	0.119	11.0	0.0191	4.4	0.40	52.261	4.4	0.0450	10.1	-58	245	114	12	122	5	311
KLT-1_M_486	526	175	11	0.33	786	0.127	8.8	0.0188	4.1	0.47	53.199	4.1	0.0490	7.8	148	182	121	10	120	5	19
KLT-1_M_487	902	351	19	0.39	360	0.124	7.9	0.0186	3.6	0.45	53.743	3.6	0.0483	7.1	113	167	119	9	119	4	-5
KLT-1_M_488	472	152	10	0.32	525	0.124	11.7	0.0193	4.8	0.41	51.713	4.8	0.0466	10.7	29	256	119	13	123	6	-320
KLT-1_M_495	872	292	19	0.34	3340	0.139	6.2	0.0190	4.3	0.70	52.669	4.3	0.0533	4.4	340	100	133	8	121	5	64
KLT-1_M_499	545	230	12	0.42	1934230.166	10.2	0.0189	4.5	0.44	52.899	4.5	0.0637	9.1	732	193	156	15	121	5	84	
KLT-1_M_500	462	126	9	0.27	325	0.117	7.4	0.0184	4.8	0.64	54.397	4.8	0.0462	5.6	7	136	112	8	117	6	-1612
KLT-1_M_505	558	250	12	0.45	744	0.126	7.5	0.0186	4.4	0.59	53.625	4.4	0.0488	6.1	139	143	120	9	119	5	14
KLT-1_S_421	549	106	11	0.19	193	0.125	6.7	0.0180	3.5	0.51	55.630	3.5	0.0503	5.8	208	134	119	8	115	4	45
KLT-1_S_425	836	258	17	0.31	359	0.132	8.9	0.0184	4.4	0.49	54.270	4.4	0.0521	7.7	292	176	126	11	118	5	60
Analysis	Composition			Corrected isotope ratios										Apparent ages (Ma)							
	U	Th	Pb	$\frac{^{206}\text{Pb}}{^{204}\text{Pb}}$	$\frac{^{207}\text{Pb}}{^{235}\text{U}}$	$\pm 2\sigma$	$\frac{^{206}\text{Pb}}{^{238}\text{U}}$	$\pm 2\sigma$	error	$\frac{^{238}\text{U}}{^{206}\text{Pb}}$	$\pm 2\sigma$	$\frac{^{207}\text{Pb}}{^{206}\text{Pb}}$	$\pm 2\sigma$	$\frac{^{207}\text{Pb}}{^{206}\text{Pb}}$	$\pm 2\sigma$	$\frac{^{207}\text{Pb}}{^{235}\text{U}}$	$\pm 2\sigma$	$\frac{^{206}\text{Pb}}{^{238}\text{U}}$	$\pm 2\sigma$	%	
	ppm	ppm	ppm	Th/U	$\frac{^{204}\text{Pb}}{^{238}\text{U}}$	(%)	$\frac{^{238}\text{U}}{^{206}\text{Pb}}$	(%)	corr.	$\frac{^{206}\text{Pb}}{^{206}\text{Pb}}$	(%)	$\frac{^{206}\text{Pb}}{^{206}\text{Pb}}$	(abs)	$\frac{^{207}\text{Pb}}{^{206}\text{Pb}}$	(abs)	$\frac{^{207}\text{Pb}}{^{235}\text{U}}$	(abs)	$\frac{^{206}\text{Pb}}{^{238}\text{U}}$	(abs)	disc.	
PPP-1 (Parrot Peak pluton)																					
PPP_L_100	574	459	22	0.80	13241	0.204	5.8	0.0290	4.6	0.80	34.429	4.6	0.0510	3.5	239	80	189	10	185	8	23
PPP_L_101	440	259	16	0.59	775	0.204	6.9	0.0295	5.2	0.75	33.919	5.2	0.0502	4.5	207	105	189	12	187	10	9
PPP_L_102	747	701	30	0.94	526	0.198	5.5	0.0289	4.5	0.81	34.571	4.5	0.0498	3.2	184	75	184	9	184	8	0
PPP_L_103	1240	805	47	0.65	4106	0.202	5.0	0.0291	4.5	0.89	34.404	4.5	0.0504	2.3	214	53	187	9	185	8	14
PPP_L_104	472	281	17	0.60	767	0.206	8.2	0.0294	7.3	0.88	33.996	7.3	0.0509	3.9	236	89	191	14	187	13	21
PPP_L_105	970	896	38	0.92	684	0.200	5.9	0.0280	5.2	0.88	35.731	5.2	0.0519	2.8	282	65	185	10	178	9	37
PPP_L_106	249	229	10	0.92	245	0.192	7.0	0.0289	4.5	0.64	34.545	4.5	0.0481	5.4	105	127	178	12	184	8	-75
PPP_L_107	364	251	13	0.69	10327	0.196	6.7	0.0286	5.0	0.74	34.973	5.0	0.0497	4.5	180	104	182	11	182	9	-1
PPP_L_108	489	508	20	1.04	188	0.194	6.4	0.0286	5.1	0.80	34.995	5.1	0.0493	3.8	160	90	180	10	182	9	-14
PPP_L_109	242	220	9	0.91	831	0.197	7.7	0.0288	5.1	0.67	34.754	5.1	0.0496	5.7	175	133	182	13	183	9	-5
PPP_L_112	571	394	21	0.69	299	0.198	6.4	0.0286	5.4	0.85	34.997	5.4	0.0501	3.4	201	79	183	11	182	10	10
PPP_L_113	682	618	26	0.91	401	0.197	6.5	0.0277	5.2	0.80	36.062	5.2	0.0516	3.9	268	90	183	11	176	9	34
PPP_L_114	1743	2547	76	1.46	57970	0.188	5.1	0.0272	4.9	0.94	36.698	4.9	0.0501	1.7	197	40	175	8	173	8	12
PPP_L_115	1248	1650	53	1.32	4300	0.190	5.3	0.0275	4.6	0.87	36.386	4.6	0.0501	2.6	201	61	177	9	175	8	13
PPP_L_117	1251	1828	56	1.46	1801	0.197	5.9	0.0280	5.2	0.88	35.742	5.2	0.0510	2.8	239	64	182	10	178	9	26

PPP_M_340	1012	763	38	0.75	858	0.200	6.2	0.0291	5.6	0.91	34.374	5.6	0.0498	2.6	188	60	185	11	185	10	2
PPP_M_346	1254	668	47	0.53	3578	0.211	5.8	0.0301	4.6	0.78	33.193	4.6	0.0507	3.6	228	83	194	10	191	9	16
PPP_M_347	600	333	22	0.56	2652	0.201	6.2	0.0298	4.3	0.69	33.550	4.3	0.0488	4.5	139	105	186	11	189	8	-36
PPP_M_352	1531	1080	60	0.71	4470	0.216	4.9	0.0299	4.1	0.84	33.447	4.1	0.0523	2.7	299	61	198	9	190	8	36
PPP_M_353	983	696	38	0.71	1360	0.203	5.0	0.0295	4.4	0.88	33.857	4.4	0.0499	2.4	189	57	188	9	188	8	1
PPP_M_354	294	184	11	0.63	186	0.211	8.8	0.0307	5.8	0.66	32.558	5.8	0.0498	6.7	187	155	194	16	195	11	-4
PPP_M_355	705	416	26	0.59	297	0.199	6.9	0.0294	5.3	0.76	34.032	5.3	0.0490	4.5	148	106	184	12	187	10	-26
PPP_M_358	1334	990	53	0.74	1411	0.200	5.1	0.0300	4.1	0.79	33.348	4.1	0.0483	3.1	113	74	185	9	190	8	-69
PPP_M_359	2060	1727	87	0.84	27562	0.212	5.3	0.0306	4.7	0.88	32.646	4.7	0.0503	2.5	209	59	196	9	195	9	7
PPP_M_360	1499	1026	58	0.68	410	0.216	5.5	0.0296	4.7	0.86	33.727	4.7	0.0529	2.8	324	64	199	10	188	9	42
PPP_M_366	480	260	18	0.54	253	0.207	6.8	0.0303	4.3	0.63	33.033	4.3	0.0495	5.3	173	123	191	12	192	8	-11
PPP_M_367	457	180	16	0.39	411	0.196	8.0	0.0301	4.9	0.61	33.178	4.9	0.0472	6.3	59	150	182	13	191	9	-223
PPP_M_374	3108	2697	126	0.87	2458	0.199	6.3	0.0287	6.0	0.95	34.902	6.0	0.0504	2.0	215	46	185	11	182	11	15
PPP_M_378	1135	718	43	0.63	2855	0.213	4.8	0.0292	4.3	0.90	34.225	4.3	0.0529	2.1	327	47	196	9	186	8	43
PPP_M_379	259	113	9	0.44	353	0.217	8.2	0.0286	5.0	0.61	34.985	5.0	0.0549	6.5	410	146	199	15	182	9	56
PPP_M_380	1155	799	43	0.69	2666	0.196	5.5	0.0284	4.9	0.91	35.157	4.9	0.0500	2.3	197	54	182	9	181	9	8
PPP_M_381	1977	1557	78	0.79	9821	0.209	6.2	0.0289	5.4	0.87	34.586	5.4	0.0524	3.1	305	70	193	11	184	10	40
PPP_M_382	749	360	27	0.48	1106	0.205	7.0	0.0294	4.5	0.64	34.060	4.5	0.0506	5.4	223	124	189	12	187	8	17
PPP_M_385	708	262	25	0.37	574	0.214	5.8	0.0302	4.6	0.80	33.140	4.6	0.0515	3.5	264	81	197	10	192	9	27
PPP_M_386	1081	520	39	0.48	1134	0.201	4.6	0.0289	3.8	0.83	34.564	3.8	0.0505	2.6	218	59	186	8	184	7	16
PPP_M_388	807	424	29	0.53	1444	0.204	5.5	0.0288	4.7	0.86	34.663	4.7	0.0513	2.8	255	65	189	9	183	8	28
PPP_M_391	505	261	19	0.52	551	0.208	6.2	0.0298	4.6	0.75	33.509	4.6	0.0506	4.1	224	94	192	11	190	9	15
PPP_M_392	848	482	32	0.57	1378	0.212	8.6	0.0292	7.5	0.88	34.256	7.5	0.0526	4.1	310	93	195	15	185	14	40
PPP_M_398	2057	1598	82	0.78	2391	0.201	5.5	0.0294	5.0	0.90	34.067	5.0	0.0497	2.4	180	57	186	9	187	9	-3
PPP_M_400	832	444	31	0.53	787	0.201	6.0	0.0297	5.1	0.84	33.624	5.1	0.0489	3.3	144	77	186	10	189	9	-31
PPP_M_402	1375	1240	56	0.90	1542	0.224	8.0	0.0303	7.5	0.94	33.050	7.5	0.0537	2.8	360	63	205	15	192	14	47
PPP_M_406	1119	737	42	0.66	931	0.211	6.4	0.0295	5.0	0.77	33.929	5.0	0.0518	4.0	277	93	194	11	187	9	32
PPP_M_410	1188	642	42	0.54	12099	0.205	5.4	0.0289	4.5	0.84	34.659	4.5	0.0514	2.9	260	68	189	9	183	8	29
PPP_M_415	500	225	18	0.45	3659	0.198	6.2	0.0295	4.4	0.71	33.875	4.4	0.0486	4.4	129	104	183	10	188	8	-46
PPP_M_420	925	568	35	0.61	361	0.199	5.7	0.0292	4.8	0.85	34.242	4.8	0.0495	3.0	174	71	185	10	186	9	-7
PPP_M_423	1408	837	55	0.59	1888	0.212	5.7	0.0302	5.2	0.92	33.164	5.2	0.0509	2.3	236	52	195	10	192	10	19
PPP_M_426	759	408	27	0.54	674	0.200	5.6	0.0289	4.5	0.81	34.553	4.5	0.0502	3.3	205	76	185	9	184	8	10
PPP_M_429	1430	1084	57	0.76	1542	0.206	7.0	0.0295	6.2	0.89	33.844	6.2	0.0507	3.2	226	75	191	12	188	11	17
PPP_M_432	324	153	11	0.47	314	0.219	6.5	0.0290	4.6	0.70	34.502	4.6	0.0549	4.6	408	104	201	12	184	8	55
PPP_M_439	493	259	18	0.52	497	0.206	7.0	0.0296	4.7	0.68	33.734	4.7	0.0505	5.1	217	118	190	12	188	9	13
PPP_M_440	331	172	12	0.52	745	0.206	7.6	0.0297	5.5	0.73	33.687	5.5	0.0504	5.2	215	120	191	13	189	10	12
PPP_M_441	901	703	35	0.78	805	0.208	6.7	0.0293	5.4	0.80	34.144	5.4	0.0515	4.0	262	92	192	12	186	10	29

PPP_M_443	607	414	24	0.68	465	0.222	9.6	0.0302	7.2	0.75	33.088	7.2	0.0533	6.3	342	142	204	18	192	14	44
PPP_S_634	572	315	21	0.55	8684	0.193	7.4	0.0293	6.0	0.81	34.181	6.0	0.0478	4.4	90	103	179	12	186	11	-106
PPP_S_635	717	538	27	0.75	2875	0.200	7.4	0.0290	6.5	0.88	34.533	6.5	0.0501	3.5	199	81	185	13	184	12	7
PPP_S_641	904	457	33	0.50	450	0.209	5.6	0.0299	4.9	0.89	33.418	4.9	0.0508	2.6	230	60	193	10	190	9	17
PPP_S_646	629	359	22	0.57	488	0.204	6.3	0.0284	5.1	0.80	35.185	5.1	0.0519	3.8	283	86	188	11	181	9	36
PPP_S_647	751	448	27	0.60	541	0.205	6.0	0.0289	4.9	0.82	34.603	4.9	0.0513	3.4	257	77	189	10	184	9	28
PPP_S_649	1754	1393	70	0.79	6127	0.201	6.4	0.0287	6.0	0.93	34.811	6.0	0.0508	2.3	233	54	186	11	183	11	22
PPP_S_652	832	524	30	0.63	11957	0.199	5.9	0.0285	4.8	0.81	35.051	4.8	0.0506	3.4	221	79	184	10	181	9	18
PPP_S_653	784	489	29	0.62	1825	0.199	5.1	0.0287	4.3	0.84	34.790	4.3	0.0502	2.8	205	66	184	9	183	8	11
PPP_S_658	1445	1116	57	0.77	3386	0.205	7.6	0.0295	6.9	0.90	33.948	6.9	0.0505	3.3	218	77	189	13	187	13	14
PPP_S_659	950	527	37	0.56	1553	0.221	6.6	0.0305	6.1	0.93	32.770	6.1	0.0526	2.5	313	56	203	12	194	12	38
PPP_S_662	2683	2610	112	0.97	10830	0.199	8.3	0.0292	8.0	0.97	34.193	8.0	0.0494	2.1	169	49	185	14	186	15	-10
PPP_S_668	480	188	17	0.39	817	0.203	6.0	0.0300	4.0	0.67	33.317	4.0	0.0490	4.4	148	104	188	10	191	8	-29
Composition			Corrected isotope ratios												Apparent ages (Ma)						
Analysis	U	Th	Pb	$\frac{^{206}\text{Pb}}{^{204}\text{Pb}}$	$\frac{^{207}\text{Pb}}{^{235}\text{U}}$	$\pm 2\sigma$	$\frac{^{206}\text{Pb}}{^{238}\text{U}}$	$\pm 2\sigma$	error	$\frac{^{238}\text{U}}{^{206}\text{Pb}}$	$\pm 2\sigma$	$\frac{^{207}\text{Pb}}{^{206}\text{Pb}}$	$\pm 2\sigma$	$\frac{^{207}\text{Pb}}{^{206}\text{Pb}}$	$\pm 2\sigma$	$\frac{^{207}\text{Pb}}{^{235}\text{U}}$	$\pm 2\sigma$	$\frac{^{206}\text{Pb}}{^{238}\text{U}}$	$\pm 2\sigma$	%	
	ppm	ppm	ppm	Th/U	$\frac{^{204}\text{Pb}}{^{235}\text{U}}$	(%)	$\frac{^{238}\text{U}}{^{206}\text{Pb}}$	(%)	corr.	$\frac{^{206}\text{Pb}}{^{206}\text{Pb}}$	(%)	$\frac{^{206}\text{Pb}}{(\text{abs})}$	(%)	$\frac{^{207}\text{Pb}}{^{206}\text{Pb}}$	$\pm 2\sigma$	$\frac{^{207}\text{Pb}}{(\text{abs})}$	$\pm 2\sigma$	$\frac{^{206}\text{Pb}}{^{238}\text{U}}$	$\pm 2\sigma$	disc.	

PSP-1 (Prospect Springs pluton)

PSP_L_708	1959	3918	84	2.00	2619	0.159	4.0	0.0243	3.2	0.80	41.153	3.2	0.0475	2.4	75	56	150	6	155	5	-107
PSP_L_709	1810	3674	79	2.03	2516	0.166	4.5	0.0245	3.4	0.76	40.797	3.4	0.0492	2.9	159	67	156	6	156	5	2
PSP_L_710	1470	2848	62	1.94	994	0.171	4.7	0.0245	3.4	0.72	40.749	3.4	0.0505	3.2	219	75	160	7	156	5	29
PSP_L_711	1674	3334	74	1.99	11974	0.170	4.4	0.0254	2.7	0.60	39.354	2.7	0.0485	3.5	125	81	159	6	162	4	-29
PSP_L_712	1944	3522	75	1.81	2129	0.158	4.5	0.0238	3.7	0.82	41.991	3.7	0.0480	2.5	102	60	149	6	152	6	-49
PSP_L_713	1471	2496	57	1.70	1831	0.162	5.0	0.0246	3.8	0.77	40.729	3.8	0.0478	3.2	92	75	152	7	156	6	-71
PSP_S_653	2459	5086	129	2.07	7026	0.175	3.5	0.0260	2.6	0.74	38.428	2.6	0.0488	2.3	139	53	164	5	166	4	-19
PSP_S_654	1102	1385	44	1.26	2357	0.169	4.4	0.0248	3.5	0.80	40.326	3.5	0.0493	2.6	163	61	158	6	158	6	3
PSP_S_660	2384	4613	113	1.93	4046	0.172	4.1	0.0254	3.6	0.87	39.343	3.6	0.0491	2.0	154	46	161	6	162	6	-5
PSP_S_664	1648	3074	76	1.87	2069	0.167	4.9	0.0249	4.1	0.83	40.178	4.1	0.0488	2.7	138	63	157	7	158	6	-15

Notes: Isotope ratios and ages are reported without initial common Pb correction; gas blank-corrected mass 204 signals were generally irresolvable from zero.

Isotope ratio and apparent age errors do NOT include systematic calibration errors of 0.25% for the $^{207}\text{Pb}/^{206}\text{Pb}$ ratio, and 0.56% for the $^{206}\text{Pb}/^{238}\text{U}$ ratio (1s).

Trace element concentrations in ppm, calculated using the mean count rate method, internal standardization to ^{29}Si , and calibration to NIST 610 and 612 glass standards.

Ablation using a 213 nm wavelength laser, spot size of 25 microns, repetition rate of 10 Hz, and fluence of ~5 J/cm².

Table A.4. Detrital Zircon LA-ICPMS U-Pb Geochronology for Chapter 2

Analysis	Composition							Corrected isotope ratios							Apparent ages (Ma)						
	U ppm	Th ppm	Pb ppm	Th/U	$\frac{^{206}\text{Pb}}{^{204}\text{Pb}}$	$\frac{^{207}\text{Pb}}{^{235}\text{U}}$	$\pm 2\sigma$ (%)	$\frac{^{206}\text{Pb}}{^{238}\text{U}}$	$\pm 2\sigma$ (%)	error corr.	$\frac{^{238}\text{U}}{^{206}\text{Pb}}$	$\pm 2\sigma$ (%)	$\frac{^{207}\text{Pb}}{^{206}\text{Pb}}$	$\pm 2\sigma$ (%)	$\frac{^{207}\text{Pb}}{^{206}\text{Pb}}$ (abs)	$\pm 2\sigma$ (%)	$\frac{^{207}\text{Pb}}{^{235}\text{U}}$ (abs)	$\pm 2\sigma$ (%)	$\frac{^{206}\text{Pb}}{^{238}\text{U}}$ (abs)	$\pm 2\sigma$ (%)	% disc.
KLS-1 (King Lear Formation – Clover Creek Member)																					
KLS-1_L_1	255	116	8	0.46	199	0.172	11.6	0.0282	6.3	0.54	35.508	6.3	0.0443	9.7	-95	238	161	17	179	11	288
KLS-1_L_2	409	297	13	0.73	263	0.177	6.9	0.0256	4.1	0.60	39.029	4.1	0.0502	5.5	203	128	166	11	163	7	20
KLS-1_L_3	276	231	9	0.84	40614	0.154	8.8	0.0249	3.8	0.44	40.085	3.8	0.0448	7.9	-68	192	145	12	159	6	332
KLS-1_L_4	392	374	12	0.95	136	0.174	7.3	0.0251	4.0	0.55	39.769	4.0	0.0503	6.2	208	143	163	11	160	6	23
KLS-1_L_5	233	160	7	0.69	57	0.165	9.8	0.0251	5.2	0.53	39.767	5.2	0.0476	8.3	81	198	155	14	160	8	-97
KLS-1_L_6	312	142	9	0.45	115	0.163	10.1	0.0248	5.2	0.51	40.260	5.2	0.0477	8.7	83	206	154	14	158	8	-91
KLS-1_L_7	1420	1080	44	0.76	2927	0.165	5.1	0.0241	4.0	0.78	41.445	4.0	0.0496	3.2	175	75	155	7	154	6	12
KLS-1_L_8	210	113	6	0.54	130	0.165	9.4	0.0252	5.4	0.57	39.695	5.4	0.0476	7.7	81	184	155	14	160	9	-97
KLS-1_L_9	1075	1222	37	1.14	348	0.166	6.7	0.0247	5.8	0.86	40.504	5.8	0.0486	3.3	130	79	156	10	157	9	-21
KLS-1_L_10	390	483	13	1.24	618	0.172	6.4	0.0244	4.3	0.67	41.015	4.3	0.0513	4.7	254	109	162	9	155	7	39
KLS-1_L_11	835	789	27	0.95	374	0.166	6.9	0.0244	5.1	0.75	41.012	5.1	0.0494	4.6	168	107	156	10	155	8	8
KLS-1_L_12	1593	1831	54	1.15	2943	0.160	5.7	0.0234	5.0	0.87	42.755	5.0	0.0496	2.8	178	64	151	8	149	7	16
KLS-1_L_13	315	265	10	0.84	137	0.166	9.3	0.0255	6.0	0.65	39.152	6.0	0.0470	7.1	51	169	156	13	163	10	-220
KLS-1_L_14	1201	1066	39	0.89	1751	0.170	6.5	0.0246	5.2	0.80	40.709	5.2	0.0501	3.9	198	90	159	10	156	8	21
KLS-1_L_15	677	519	21	0.77	2416	0.165	8.0	0.0245	5.1	0.64	40.891	5.1	0.0488	6.1	139	144	155	11	156	8	-12
KLS-1_L_16	542	261	22	0.48	172	0.447	16.4	0.0273	7.2	0.44	36.686	7.2	0.1189	14.8	1940	264	375	51	173	12	91
KLS-1_L_17	292	209	11	0.71	470	0.252	16.6	0.0267	6.7	0.40	37.420	6.7	0.0685	15.2	884	313	229	34	170	11	81
KLS-1_L_18	491	379	15	0.77	293	0.177	6.7	0.0246	4.9	0.74	40.729	4.9	0.0524	4.5	301	102	166	10	156	8	48
KLS-1_L_19	613	463	20	0.76	1992	0.197	7.3	0.0259	5.2	0.72	38.681	5.2	0.0553	5.1	424	114	183	12	165	9	61
KLS-1_L_20	470	405	16	0.86	764	0.167	6.9	0.0256	4.6	0.66	39.125	4.6	0.0474	5.1	70	122	157	10	163	7	-131
KLS-1_L_21	652	509	20	0.78	2431	0.192	6.8	0.0233	4.7	0.70	42.974	4.7	0.0599	4.9	598	106	178	11	148	7	75
KLS-1_L_22	1359	1445	46	1.06	559	0.167	5.2	0.0244	4.2	0.81	41.004	4.2	0.0496	3.0	174	70	156	8	155	6	11
KLS-1_L_23	1856	1727	61	0.93	1861	0.165	4.8	0.0237	4.2	0.87	42.238	4.2	0.0506	2.3	222	54	155	7	151	6	32
KLS-1_L_24	397	339	13	0.85	245	0.198	8.2	0.0249	5.0	0.61	40.113	5.0	0.0576	6.5	513	142	183	14	159	8	69
KLS-1_L_25	1139	796	39	0.70	3157	0.187	5.9	0.0264	5.2	0.88	37.869	5.2	0.0515	2.8	263	64	174	9	168	9	36
KLS-1_L_26	487	412	16	0.85	517	0.167	5.5	0.0249	4.3	0.78	40.086	4.3	0.0486	3.4	128	80	157	8	159	7	-24
KLS-1_L_27	491	374	15	0.76	1642	0.167	7.3	0.0247	4.6	0.64	40.507	4.6	0.0492	5.6	157	132	157	11	157	7	0
KLS-1_L_28	414	285	15	0.69	1809	0.201	8.5	0.0281	6.7	0.78	35.588	6.7	0.0519	5.3	281	122	186	15	179	12	36
KLS-1_L_29	2170	3083	83	1.42	6061	0.165	5.5	0.0242	5.1	0.92	41.397	5.1	0.0496	2.2	176	51	155	8	154	8	12
KLS-1_L_30	539	495	18	0.92	160	0.188	6.7	0.0251	4.0	0.60	39.916	4.0	0.0544	5.4	386	121	175	11	160	6	59

KLS-1_L_31	406	219	12	0.54	135	0.167	7.1	0.0252	4.1	0.57	39.684	4.1	0.0482	5.8	109	138	157	10	160	6	-47
KLS-1_L_32	199	114	6	0.57	2045	0.205	9.1	0.0256	5.6	0.62	39.102	5.6	0.0580	7.1	531	156	189	16	163	9	69
KLS-1_L_33	438	417	15	0.95	161	0.174	8.1	0.0253	4.3	0.53	39.596	4.3	0.0500	6.8	196	158	163	12	160.8	7	18
KLS-1_L_34	539	429	17	0.80	232	0.170	7.6	0.0251	5.2	0.69	39.762	5.2	0.0490	5.5	147	129	159	11	160	8	-9
KLS-1_L_35	450	247	14	0.55	170	0.176	7.5	0.0253	5.1	0.69	39.579	5.1	0.0505	5.5	217	126	164	11	161	8	26
KLS-1_L_36	180	100	6	0.56	185	0.159	12.3	0.0250	5.2	0.42	39.935	5.2	0.0460	11.2	-2	270	150	17	159	8	8707
KLS-1_L_37	605	511	20	0.84	587	0.157	6.7	0.0250	4.4	0.66	39.974	4.4	0.0454	5.0	-36	122	148	9	159	7	549
KLS-1_L_38	258	132	8	0.51	225	0.173	7.0	0.0249	4.1	0.58	40.148	4.1	0.0503	5.7	210	132	162	10	159	6	25
KLS-1_L_39	443	290	14	0.66	407	0.174	7.4	0.0253	3.4	0.46	39.501	3.4	0.0499	6.6	189	153	163	11	161	5	15
KLS-1_L_40	2000	2493	70	1.25	1656	0.164	5.1	0.0243	3.9	0.77	41.200	3.9	0.0489	3.3	142	76	154	7	155	6	-9
KLS-1_L_41	174	83	5	0.48	621	0.185	8.0	0.0262	3.8	0.47	38.219	3.8	0.0514	7.1	259	162	173	13	167	6	36
KLS-1_L_42	1365	1493	46	1.09	1219	0.164	6.7	0.0244	4.7	0.70	40.970	4.7	0.0488	4.7	140	111	154	10	155	7	-11
KLS-1_L_43	396	296	13	0.75	25260	0.175	6.9	0.0261	4.1	0.60	38.368	4.1	0.0486	5.5	130	130	164	10	166	7	-28
KLS-1_L_44	246	167	7	0.68	134	0.172	9.0	0.0251	4.8	0.53	39.820	4.8	0.0496	7.6	174	177	161	13	160	8	8
KLS-1_L_45	306	300	10	0.98	308	0.168	9.1	0.0261	4.6	0.51	38.261	4.6	0.0466	7.9	29	189	158	13	166	8	-466
KLS-1_L_46	232	199	7	0.86	618	0.175	8.4	0.0250	4.3	0.51	39.962	4.3	0.0507	7.2	229	167	164	13	159	7	31
KLS-1_L_47	983	777	31	0.79	993	0.211	9.0	0.0243	4.1	0.45	41.208	4.1	0.0630	8.1	708	172	194	16	155	6	78
KLS-1_L_48	756	574	23	0.76	3173	0.178	6.9	0.0241	5.1	0.74	41.548	5.1	0.0536	4.6	353	104	166	11	153	8	57
KLS-1_L_49	282	165	8	0.58	97	0.161	10.4	0.0251	6.0	0.58	39.916	6.0	0.0466	8.4	30	202	152	15	160	10	-439
KLS-1_L_50	1072	1127	35	1.05	2990	0.169	6.3	0.0242	5.0	0.80	41.371	5.0	0.0507	3.8	228	87	159	9	154	8	32
KLS-1_L_51	981	811	30	0.83	2420	0.165	6.2	0.0241	5.0	0.81	41.509	5.0	0.0498	3.6	187	85	155	9	153	8	18
KLS-1_L_52	672	890	23	1.32	514	0.160	6.5	0.0238	3.9	0.60	42.033	3.9	0.0486	5.2	130	121	150	9	152	6	-16
KLS-1_L_53	474	490	15	1.04	399	0.172	8.0	0.0245	4.7	0.59	40.887	4.7	0.0509	6.5	235	150	161	12	156	7	34
KLS-1_L_55	697	263	29	0.38	346	0.253	4.5	0.0359	3.4	0.75	27.862	3.4	0.0511	3.0	247	68	229	9	227	8	8
KLS-1_L_56	304	202	9	0.66	693	0.163	10.2	0.0256	5.9	0.58	39.037	5.9	0.0461	8.4	4	202	153	15	163	10	-4377
KLS-1_L_57	486	331	16	0.68	423	0.173	7.2	0.0259	5.2	0.72	38.671	5.2	0.0484	5.0	121	117	162	11	165	8	-36
KLS-1_L_58	1744	1649	56	0.95	3674	0.168	5.5	0.0235	4.6	0.84	42.480	4.6	0.0516	3.0	268	68	157	8	150	7	44
KLS-1_L_60	1060	624	32	0.59	481	0.174	6.0	0.0247	4.6	0.77	40.550	4.6	0.0511	3.9	244	90	163	9	157	7	36
KLS-1_L_61	160	98	5	0.61	76	0.168	11.2	0.0255	4.9	0.44	39.290	4.9	0.0479	10.1	95	238	158	16	162	8	-70
KLS-1_L_62	263	180	8	0.69	110	0.172	7.4	0.0249	4.5	0.61	40.171	4.5	0.0502	5.9	206	136	162	11	159	7	23
KLS-1_L_63	226	117	7	0.52	817	0.164	9.8	0.0260	5.8	0.59	38.437	5.8	0.0458	7.9	-15	191	154	14	166	9	1224
KLS-1_L_64	526	383	17	0.73	1201	0.172	7.5	0.0250	4.1	0.54	40.004	4.1	0.0499	6.3	188	147	161	11	159	6	15
KLS-1_L_65	2167	2287	76	1.06	3367420	0.162	5.9	0.0240	5.2	0.88	41.649	5.2	0.0488	2.9	141	67	152	8	153	8	-9
KLS-1_L_66	343	330	11	0.96	114	0.165	7.9	0.0251	3.8	0.48	39.782	3.8	0.0477	6.9	86	164	155	11	160	6	-87
KLS-1_L_67	153	104	5	0.68	39	0.158	13.1	0.0258	5.3	0.40	38.826	5.3	0.0445	12.0	-85	293	149	18	164	9	292
KLS-1_L_68	446	250	16	0.56	354	0.248	11.9	0.0277	5.2	0.44	36.064	5.2	0.0650	10.7	774	225	225	24	176	9	77
KLS-1_L_69	2292	1979	75	0.86	942	0.161	5.6	0.0235	4.8	0.86	42.475	4.8	0.0497	2.8	182	66	152	8	150	7	18

KLS-1_L_70	727	432	22	0.59	1328	0.166	6.1	0.0250	4.8	0.79	39.959	4.8	0.0480	3.7	101	88	156	9	159	8	-58
KLS-1_L_71	370	207	11	0.56	291	0.163	11.3	0.0248	5.0	0.44	40.376	5.0	0.0476	10.1	80	240	153	16	158	8	-96
KLS-1_L_72	252	91	7	0.36	94	0.170	9.0	0.0257	3.8	0.42	38.889	3.8	0.0480	8.2	98	194	160	13	164	6	-67
KLS-1_L_73	1824	2163	66	1.19	1688	0.160	5.4	0.0240	4.4	0.82	41.638	4.4	0.0483	3.1	113	74	151	8	153	7	-35
KLS-1_L_74	652	462	22	0.71	1310	0.176	6.6	0.0264	4.7	0.71	37.923	4.7	0.0485	4.7	123	111	165	10	168	8	-37
KLS-1_L_75	957	958	34	1.00	1689	0.170	5.6	0.0250	4.6	0.81	39.939	4.6	0.0492	3.3	156	77	159	8	159	7	-2
KLS-1_L_76	109	55	3	0.50	255	0.154	18.5	0.0272	5.3	0.29	36.824	5.3	0.0410	17.7	-286	452	145	25	173	9	160
KLS-1_L_78	344	193	11	0.56	8934	0.187	7.6	0.0269	4.7	0.61	37.131	4.7	0.0504	6.0	214	140	174	12	171	8	20
KLS-1_L_79	491	266	15	0.54	136	0.190	5.7	0.0255	3.5	0.61	39.197	3.5	0.0541	4.5	374	102	177	9	162	6	57
KLS-1_L_80	797	628	25	0.79	395	0.166	5.3	0.0244	3.9	0.73	40.998	3.9	0.0495	3.6	172	85	156	8	155	6	10
KLS-1_L_81	403	264	12	0.65	272	0.172	7.7	0.0244	4.0	0.52	41.021	4.0	0.0512	6.6	248	151	161	11	155	6	38
KLS-1_L_82	298	127	9	0.42	908	0.182	7.4	0.0256	4.1	0.56	38.992	4.1	0.0516	6.1	266	141	170	12	163	7	39
KLS-1_L_83	273	92	6	0.34	4183	0.121	9.3	0.0196	4.9	0.52	50.922	4.9	0.0449	8.0	-63	194	116	10	125	6	298
KLS-1_L_84	427	178	9	0.42	209	0.127	7.6	0.0185	3.4	0.45	54.177	3.4	0.0497	6.8	181	158	121	9	118	4	35
KLS-1_L_85	419	437	14	1.04	1450	0.167	8.5	0.0253	4.8	0.56	39.601	4.8	0.0479	7.1	95	168	157	12	161	8	-70
KLS-1_L_86	1271	872	40	0.69	956	0.171	5.5	0.0244	4.5	0.81	40.997	4.5	0.0508	3.3	233	75	160	8	155	7	33
KLS-1_L_87	410	254	13	0.62	4737	0.166	8.0	0.0251	6.2	0.77	39.865	6.2	0.0481	5.1	102	121	156	12	160	10	-57
KLS-1_L_88	468	367	16	0.79	322	0.172	9.8	0.0262	5.0	0.51	38.169	5.0	0.0477	8.4	85	200	161	15	167	8	-95
KLS-1_L_89	1255	1332	45	1.06	1838	0.169	4.6	0.0253	3.8	0.82	39.542	3.8	0.0486	2.6	127	62	159	7	161	6	-27
KLS-1_L_90	1143	917	46	0.80	455	0.247	9.3	0.0280	6.7	0.72	35.744	6.7	0.0641	6.5	745	137	224	19	178	12	76
KLS-1_L_91	418	239	13	0.57	413	0.173	8.5	0.0261	4.5	0.52	38.359	4.5	0.0481	7.3	105	172	162	13	166	7	-58
KLS-1_M_570	461	296	15	0.64	1114	0.188	8.2	0.0272	4.8	0.59	36.734	4.8	0.0502	6.7	202	155	175	13	173	8	14
KLS-1_M_571	357	263	11	0.74	241	0.169	9.6	0.0251	4.2	0.44	39.844	4.2	0.0489	8.7	142	204	159	14	160	7	-12
KLS-1_M_572	372	394	12	1.06	523	0.174	11.0	0.0247	5.2	0.47	40.432	5.2	0.0509	9.7	236	223	162	17	157	8	33
KLS-1_M_573	71	103	57	1.44	2442	12.492	5.1	0.5045	4.7	0.92	1.982	4.7	0.1796	2.0	2649	32	2642	47	2633	101	1
KLS-1_M_574	256	132	8	0.52	132	0.171	10.0	0.0270	5.0	0.50	36.994	5.0	0.0459	8.7	-10	210	160	15	172	8	1858
KLS-1_M_575	297	141	7	0.48	118	0.129	12.9	0.0191	5.8	0.45	52.262	5.8	0.0490	11.5	146	270	123	15	122	7	16
KLS-1_M_576	363	311	14	0.86	795	0.228	11.3	0.0280	5.8	0.52	35.669	5.8	0.0591	9.7	569	210	209	21	178	10	69
KLS-1_M_578	587	746	20	1.27	760	0.179	5.2	0.0250	3.3	0.65	40.022	3.3	0.0519	3.9	280	90	167	8	159	5	43
KLS-1_M_579	255	120	6	0.47	164	0.115	11.7	0.0198	3.9	0.33	50.582	3.9	0.0421	11.1	-223	279	110	12	126	5	157
KLS-1_M_580	485	436	15	0.90	393	0.168	7.1	0.0245	4.8	0.68	40.778	4.8	0.0497	5.2	179	121	158	10	156	7	13
KLS-1_M_581	883	57	142	0.07	32199	1.301	5.1	0.1303	4.8	0.95	7.673	4.8	0.0724	1.6	998	32	846	29	790	36	21
KLS-1_M_582	1265	2171	46	1.72	702	0.187	6.1	0.0236	3.5	0.58	42.316	3.5	0.0575	5.0	511	109	174	10	151	5	71
KLS-1_M_583	296	328	9	1.11	50	0.162	8.8	0.0238	4.2	0.48	42.096	4.2	0.0494	7.7	165	181	152	12	151	6	8
KLS-1_M_584	170	129	6	0.76	810	0.219	11.8	0.0262	3.9	0.33	38.205	3.9	0.0607	11.1	627	239	201	21	166.6	6	73
KLS-1_M_585	1296	1998	47	1.54	827	0.175	4.6	0.0242	3.5	0.76	41.239	3.5	0.0522	3.0	294	69	163	7	154	5	48
KLS-1_M_586	196	172	6	0.88	248	0.154	13.8	0.0245	5.0	0.36	40.822	5.0	0.0457	12.9	-16	311	146	19	156	8	1053

KLS-1_M_587	973	1492	35	1.53	799	0.174	5.4	0.0249	4.0	0.74	40.113	4.0	0.0507	3.7	228	84	163	8	159	6	30
KLS-1_M_588	362	393	12	1.08	78	0.171	9.4	0.0249	4.5	0.48	40.159	4.5	0.0498	8.3	184	192	160	14	159	7	14
KLS-1_M_589	311	354	10	1.14	325	0.171	9.7	0.0246	4.0	0.41	40.704	4.0	0.0504	8.9	212	206	160	14	156	6	26
KLS-1_M_590	385	208	20	0.54	1157	0.315	7.0	0.0434	4.3	0.62	23.029	4.3	0.0526	5.5	312	125	278	17	274	12	12
KLS-1_M_591	837	1496	33	1.79	386	0.175	5.2	0.0261	4.0	0.77	38.284	4.0	0.0486	3.3	130	77	164	8	166	7	-28
KLS-1_M_592	737	769	23	1.04	1212	0.164	5.8	0.0244	3.5	0.60	40.988	3.5	0.0486	4.6	129	108	154	8	155	5	-20
KLS-1_M_593	352	219	11	0.62	991	0.181	7.9	0.0258	4.9	0.61	38.699	4.9	0.0507	6.3	226	145	169	12	164	8	27
KLS-1_M_594	393	321	13	0.82	1381	0.175	7.7	0.0261	3.3	0.43	38.354	3.3	0.0488	6.9	137	162	164	12	166	5	-21
KLS-1_M_595	365	322	12	0.88	210	0.216	10.0	0.0259	4.3	0.43	38.563	4.3	0.0603	9.0	615	195	198	18	165	7	73
KLS-1_M_596	345	292	11	0.85	247	0.178	8.8	0.0249	4.0	0.45	40.116	4.0	0.0519	7.8	281	179	167	14	159	6	43
KLS-1_M_597	333	219	10	0.66	490	0.173	7.1	0.0260	5.0	0.71	38.414	5.0	0.0481	5.0	106	119	162	11	166	8	-57
KLS-1_M_598	422	574	14	1.36	215	0.163	9.4	0.0242	3.5	0.38	41.362	3.5	0.0489	8.7	142	203	153	13	154	5	-9
KLS-1_M_599	153	101	5	0.66	124	0.166	16.4	0.0268	5.6	0.34	37.379	5.6	0.0449	15.4	-59	374	156	24	170	9	389
KLS-1_M_600	501	424	16	0.85	463	0.181	6.4	0.0260	3.7	0.58	38.508	3.7	0.0505	5.2	217	120	169	10	165	6	24
KLS-1_M_601	331	301	11	0.91	633	0.167	9.7	0.0252	4.3	0.44	39.736	4.3	0.0481	8.7	102	205	157	14	160	7	-57
KLS-1_M_602	334	213	10	0.64	449	0.168	9.5	0.0247	4.1	0.43	40.437	4.1	0.0491	8.6	155	202	157	14	157	6	-2
KLS-1_M_603	490	360	15	0.74	414	0.174	8.8	0.0253	6.1	0.70	39.522	6.1	0.0499	6.3	189	146	163	13	161	10	15
KLS-1_M_604	389	202	12	0.52	306	0.184	8.9	0.0260	3.8	0.42	38.489	3.8	0.0514	8.0	258	185	172	14	165	6	36
KLS-1_M_605	280	224	8	0.80	5785	0.163	8.9	0.0248	4.2	0.47	40.298	4.2	0.0478	7.8	89	186	154	13	158	7	-78
KLS-1_M_606	259	127	6	0.49	58	0.141	10.6	0.0186	5.8	0.54	53.657	5.8	0.0551	8.9	414	199	134	13	119	7	71
KLS-1_M_607	387	249	12	0.64	694	0.170	8.4	0.0256	5.5	0.65	39.086	5.5	0.0482	6.4	110	150	160	12	163	9	-48
KLS-1_M_608	467	340	15	0.73	275	0.179	6.4	0.0252	5.0	0.79	39.738	5.0	0.0515	3.9	263	90	167	10	160	8	39
KLS-1_M_609	333	264	11	0.79	2371	0.203	10.2	0.0259	6.1	0.59	38.564	6.1	0.0567	8.2	478	181	187	17	165	10	66
KLS-1_M_610	293	265	9	0.90	140	0.144	11.2	0.0234	4.9	0.43	42.757	4.9	0.0446	10.1	-79	248	136	14	149	7	288
KLS-1_M_611	865	428	26	0.49	1305	0.169	6.5	0.0244	4.8	0.74	40.948	4.8	0.0502	4.3	205	101	159	9	156	7	24
KLS-1_M_612	501	340	18	0.68	537	0.287	5.8	0.0270	3.6	0.62	37.082	3.6	0.0771	4.5	1125	90	256	13	172	6	85
KLS-1_M_614	2060	2893	75	1.40	12465	0.168	5.1	0.0237	4.0	0.79	42.112	4.0	0.0512	3.1	252	71	157	7	151	6	40
KLS-1_M_615	241	132	7	0.55	354	0.185	11.7	0.0254	4.5	0.38	39.411	4.5	0.0530	10.8	327	246	173	19	162	7	51
KLS-1_M_616	259	146	8	0.56	108	0.179	11.2	0.0260	4.4	0.40	38.388	4.4	0.0498	10.3	184	239	167	17	166	7	10
KLS-1_M_617	1295	1202	42	0.93	1610	0.163	5.9	0.0246	4.1	0.69	40.721	4.1	0.0483	4.3	112	101	154	8	156	6	-40
KLS-1_M_618	168	98	5	0.58	67	0.188	9.7	0.0257	4.3	0.44	38.910	4.3	0.0529	8.7	326	196	175	15	164	7	50
KLS-1_M_620	176	92	5	0.52	113	0.179	12.0	0.0252	5.9	0.49	39.760	5.9	0.0517	10.5	273	240	168	19	160	9	41
KLS-1_M_621	244	146	7	0.60	169	0.156	9.2	0.0246	5.5	0.59	40.626	5.5	0.0461	7.4	2	178	148	13	157	8	-6931
KLS-1_M_622	573	430	18	0.75	344	0.177	7.1	0.0252	5.5	0.78	39.608	5.5	0.0509	4.5	237	103	166	11	161	9	32
KLS-1_M_623	336	196	10	0.58	961	0.170	7.7	0.0252	5.1	0.66	39.658	5.1	0.0490	5.8	147	136	160	11	161	8	-10
KLS-1_M_624	775	469	29	0.61	492	0.404	7.8	0.0257	4.2	0.54	38.880	4.2	0.1139	6.5	1863	118	345	23	164	7	91
KLS-1_M_625	370	274	11	0.74	504	0.157	9.4	0.0238	4.0	0.42	42.063	4.0	0.0480	8.6	98	203	148	13	151	6	-55

KLS-1_M_626	232	179	8	0.77	295	0.185	10.7	0.0269	4.9	0.46	37.214	4.9	0.0498	9.5	188	222	172	17	171	8	9
KLS-1_M_627	615	403	20	0.65	1079	0.174	8.1	0.0265	5.6	0.69	37.696	5.6	0.0476	5.9	79	139	163	12	169	9	-112
KLS-1_M_628	358	246	11	0.69	455	0.165	9.4	0.0249	4.6	0.49	40.135	4.6	0.0481	8.2	103	193	155	14	159	7	-54
KLS-1_M_629	650	977	25	1.50	445	0.176	7.5	0.0257	4.6	0.61	38.948	4.6	0.0497	6.0	182	139	165	11	163	7	10
KLS-1_M_630	175	95	9	0.54	1014	0.808	10.6	0.0301	4.1	0.38	33.194	4.1	0.1946	9.8	2781	161	601	48	191	8	93
KLS-1_M_631	336	257	11	0.77	460	0.170	9.0	0.0254	4.9	0.54	39.324	4.9	0.0486	7.6	128	179	160	13	162	8	-26
KLS-1_M_632	307	154	9	0.50	250	0.166	8.8	0.0252	4.5	0.51	39.690	4.5	0.0477	7.5	86	178	156	13	160	7	-86
KLS-1_M_633	292	164	9	0.56	234	0.197	10.0	0.0250	3.8	0.37	39.981	3.8	0.0572	9.3	498	205	183	17	159	6	68
KLS-1_M_634	486	347	15	0.71	790	0.160	7.9	0.0255	4.0	0.51	39.207	4.0	0.0454	6.8	-36	166	150	11	162	6	554
KLS-1_M_635	519	386	16	0.74	516	0.177	7.8	0.0252	6.1	0.78	39.665	6.1	0.0510	4.9	239	113	166	12	161	10	33
KLS-1_M_636	794	600	24	0.76	594	0.160	6.3	0.0244	4.4	0.71	40.979	4.4	0.0474	4.5	71	106	150	9	155	7	-119
KLS-1_M_637	826	1008	27	1.22	2467	0.168	5.4	0.0241	3.6	0.66	41.457	3.6	0.0505	4.1	217	95	158	8	154	5	29
KLS-1_M_638	838	679	25	0.81	1442	0.168	6.1	0.0239	4.4	0.72	41.857	4.4	0.0510	4.3	240	98	158	9	152	7	37
KLS-1_M_639	227	176	7	0.77	223	0.151	10.8	0.0247	4.7	0.44	40.506	4.7	0.0442	9.7	-98	238	142	14	157	7	260
KLS-1_M_641	530	409	12	0.77	151	0.135	10.3	0.0179	4.5	0.44	55.754	4.5	0.0544	9.2	390	207	128	12	115	5	71
KLS-1_M_642	849	855	28	1.01	5426	0.172	6.7	0.0251	3.6	0.53	39.858	3.6	0.0499	5.7	188	133	162	10	160	6	15
KLS-1_M_643	190	132	6	0.69	149	0.179	10.0	0.0265	4.9	0.49	37.676	4.9	0.0490	8.7	149	203	168	15	169	8	-13
KLS-1_M_644	552	480	17	0.87	530	0.170	6.9	0.0247	4.3	0.62	40.486	4.3	0.0499	5.5	192	127	159	10	157	7	18
KLS-1_M_645	221	29	24	0.13	327	0.835	5.8	0.0997	4.3	0.74	10.030	4.3	0.0607	3.9	630	83	616	27	613	25	3
KLS-1_M_646	162	106	5	0.65	710	0.175	11.0	0.0259	4.5	0.41	38.553	4.5	0.0488	10.1	140	236	163	17	165	7	-18
KLS-1_M_647	206	144	6	0.70	209	0.163	11.1	0.0258	3.8	0.34	38.708	3.8	0.0458	10.4	-14	251	153	16	164	6	1273
KLS-1_M_648	202	128	63	0.63	5986	3.129	5.7	0.2482	4.8	0.84	4.028	4.8	0.0914	3.1	1455	58	1440	44	1429	61	2
KLS-1_M_649	186	93	6	0.50	475	0.200	9.9	0.0273	4.7	0.48	36.607	4.7	0.0531	8.7	332	196	185	17	174	8	48
KLS-1_M_650	322	215	10	0.67	108	0.167	8.2	0.0255	3.7	0.45	39.187	3.7	0.0473	7.4	66	176	156	12	162	6	-147
KLS-1_M_651	261	175	8	0.67	429	0.166	10.5	0.0248	3.1	0.29	40.333	3.1	0.0486	10.1	127	237	156	15	158	5	-25
KLS-1_M_653	320	237	10	0.74	365	0.172	8.9	0.0256	4.2	0.47	39.048	4.2	0.0488	7.9	140	184	162	13	163	7	-16
KLS-1_M_654	1007	1454	36	1.44	793	0.168	5.5	0.0254	3.4	0.62	39.350	3.4	0.0480	4.3	98	103	158	8	162	5	-64
KLS-1_M_655	333	197	8	0.59	969	0.195	19.7	0.0199	5.4	0.27	50.278	5.4	0.0711	18.9	960	386	181	33	127	7	87
KLS-1_M_656	810	1056	28	1.30	350	0.168	6.9	0.0250	4.7	0.68	40.011	4.7	0.0488	5.1	140	120	158	10	159	7	-14
KLS-1_M_657	626	471	19	0.75	436	0.174	7.2	0.0243	4.5	0.62	41.097	4.5	0.0518	5.6	276	129	163	11	155	7	44
KLS-1_M_658	1539	2469	57	1.60	820	0.165	6.5	0.0245	5.1	0.78	40.897	5.1	0.0490	4.1	146	97	155	9	156	8	-6
KLS-1_M_659	640	545	20	0.85	77705	0.172	5.8	0.0256	4.6	0.78	38.999	4.6	0.0486	3.6	130	85	161	9	163	7	-26
KLS-1_M_660	313	276	10	0.88	269	0.172	11.6	0.0262	6.4	0.55	38.196	6.4	0.0478	9.7	89	230	162	17	167	11	-88
KLS-1_M_661	834	1104	29	1.32	296	0.181	8.7	0.0252	8.0	0.91	39.751	8.0	0.0521	3.6	291	83	169	14	160	13	45
KLS-1_M_662	189	151	6	0.80	234	0.154	11.6	0.0256	5.1	0.44	39.020	5.1	0.0437	10.4	-128	257	146	16	163	8	228
KLS-1_M_663	1351	1333	42	0.99	1306	0.158	5.4	0.0230	4.5	0.82	43.559	4.5	0.0500	3.1	195	72	149	8	146	6	25
KLS-1_M_664	336	270	11	0.80	519	0.197	11.6	0.0242	5.8	0.50	41.374	5.8	0.0593	10.1	576	220	183	19	154	9	73

KLS-1_M_665	188	120	6	0.64	107	0.176	9.9	0.0251	4.9	0.49	39.770	4.9	0.0506	8.6	224	200	164	15	160	8	29
KLS-1_M_666	665	537	22	0.81	454	0.205	7.5	0.0257	5.4	0.72	38.979	5.4	0.0581	5.2	533	114	190	13	163	9	69
KLS-1_M_667	250	159	7	0.64	360	0.163	8.3	0.0247	5.8	0.70	40.430	5.8	0.0477	6.0	86	142	153	12	158	9	-82
KLS-1_M_668	353	172	11	0.49	1134	0.198	8.5	0.0260	4.9	0.58	38.409	4.9	0.0551	6.9	418	155	183	14	166	8	60
KLS-1_M_669	1394	1824	50	1.31	4933	100.166	5.4	0.0246	4.2	0.78	40.608	4.2	0.0489	3.4	145	79	156	8	157	6	-8
KLS-1_M_671	3017	5384	121	1.78	23296	0.172	5.1	0.0232	3.0	0.60	43.040	3.0	0.0537	4.1	358	92	161	8	148	4	59
KLS-1_M_672	676	738	23	1.09	1108	0.167	6.1	0.0245	4.2	0.68	40.755	4.2	0.0493	4.5	164	105	157	9	156	6	5
KLS-1_M_673	715	649	24	0.91	552	0.165	6.9	0.0251	4.1	0.59	39.787	4.1	0.0475	5.6	74	133	155	10	160	6	-116
KLS-1_M_674	825	842	27	1.02	1908	0.160	7.0	0.0244	4.6	0.65	41.041	4.6	0.0477	5.3	85	126	151	10	155	7	-83
KLS-1_M_675	353	228	11	0.65	735	0.163	8.8	0.0258	4.8	0.54	38.828	4.8	0.0459	7.4	-5	179	153	13	164	8	3153
KLS-1_M_676	943	501	70	0.53	1151	0.437	4.9	0.0589	4.1	0.82	16.972	4.1	0.0538	2.8	363	63	368	15	369	15	-2
KLS-1_M_677	404	106	28	0.26	610	0.457	6.4	0.0612	5.7	0.89	16.343	5.7	0.0542	2.9	378	64	382	20	383	21	-1
KLS-1_M_678	228	108	7	0.47	301	0.175	8.2	0.0243	5.1	0.62	41.111	5.1	0.0520	6.4	287	146	163	12	155	8	46
KLS-1_M_679	233	131	7	0.56	1801	0.184	9.0	0.0250	4.5	0.50	40.047	4.5	0.0533	7.8	343	177	171	14	159	7	54
KLS-1_M_680	317	161	9	0.51	317	0.171	9.5	0.0247	4.0	0.43	40.477	4.0	0.0501	8.6	198	199	160	14	157	6	20
KLS-1_M_681	242	171	8	0.71	380	0.165	11.2	0.0256	5.7	0.51	39.007	5.7	0.0465	9.6	26	231	155	16	163	9	-530
KLS-1_M_682	257	158	8	0.61	376	0.183	8.7	0.0252	5.2	0.59	39.723	5.2	0.0527	7.0	317	160	171	14	160	8	49
KLS-1_M_683	247	156	8	0.63	1809	0.161	8.3	0.0251	4.1	0.50	39.886	4.1	0.0466	7.2	27	172	152	12	160	6	-493
KLS-1_M_684	456	261	14	0.57	210	0.171	7.8	0.0248	4.8	0.61	40.266	4.8	0.0498	6.1	186	143	160	11	158	7	15
KLS-1_M_685	212	117	6	0.55	10943	0.160	11.7	0.0259	5.3	0.45	38.663	5.3	0.0448	10.4	-66	254	151	16	165	9	350
KLS-1_M_686	181	113	6	0.63	223	0.169	14.3	0.0264	6.0	0.42	37.865	6.0	0.0463	13.0	12	312	158	21	168	10	-1256
KLS-1_M_687	467	298	15	0.64	1212	0.165	9.5	0.0257	5.4	0.57	38.958	5.4	0.0465	7.7	25	186	155	14	163	9	-546
KLS-1_M_688	473	659	20	1.39	2437	0.188	9.6	0.0285	6.6	0.69	35.107	6.6	0.0478	7.0	90	166	175	15	181	12	-101
KLS-1_M_689	510	461	18	0.90	115	0.192	9.4	0.0266	4.5	0.48	37.635	4.5	0.0524	8.2	301	188	178	15	169	8	44
KLS-1_M_690	423	405	15	0.96	530	0.213	6.6	0.0270	4.6	0.70	37.049	4.6	0.0572	4.7	501	104	196	12	172	8	66
KLS-1_M_691	880	956	32	1.09	475	0.203	4.9	0.0259	2.4	0.48	38.613	2.4	0.0570	4.3	491	95	188	8	165	4	66
KLS-1_M_692	386	307	12	0.80	147	0.180	6.6	0.0250	3.4	0.51	40.075	3.4	0.0523	5.6	299	129	168	10	159	5	47
KLS-1_M_694	222	127	7	0.57	363	0.173	9.4	0.0263	4.5	0.48	38.090	4.5	0.0477	8.2	82	195	162	14	167	7	-103
KLS-1_M_695	305	263	10	0.86	1941	0.174	7.2	0.0254	3.7	0.52	39.296	3.7	0.0497	6.2	179	144	163	11	162	6	10
KLS-1_M_696	514	519	18	1.01	821	0.174	6.6	0.0264	3.7	0.57	37.894	3.7	0.0478	5.4	89	129	163	10	168	6	-88
KLS-1_M_697	241	143	8	0.59	276	0.176	9.8	0.0263	4.5	0.46	38.080	4.5	0.0487	8.7	132	205	165	15	167	7	-26
KLS-1_M_698	1086	1171	37	1.08	2833	0.169	5.6	0.0249	4.8	0.85	40.096	4.8	0.0490	2.9	148	69	158	8	159	8	-7
KLS-1_M_699	231	129	5	0.56	119	0.104	15.3	0.0194	4.7	0.31	51.673	4.7	0.0391	14.5	-408	379	101	15	124	6	130
KLS-1_M_700	189	112	6	0.59	106	0.180	7.0	0.0265	5.1	0.74	37.791	5.1	0.0493	4.7	160	110	168	11	168	9	-5
KLS-1_M_701	676	592	23	0.88	17518	0.234	9.1	0.0256	4.7	0.52	39.103	4.7	0.0664	7.8	819	164	214	18	163	8	80
KLS-1_M_702	718	685	23	0.95	969	0.162	6.3	0.0250	3.7	0.59	39.954	3.7	0.0470	5.1	47	122	152	9	159	6	-241
KLS-1_M_703	603	472	20	0.78	2000	0.182	6.1	0.0266	4.4	0.72	37.633	4.4	0.0497	4.3	182	99	170	10	169	7	7

KLS-1_M_704	410	377	14	0.92	1010	0.178	8.1	0.0266	4.5	0.56	37.652	4.5	0.0486	6.7	131	158	166	12	169	8	-29
KLS-1_M_705	1310	1922	48	1.47	1396	0.173	5.0	0.0252	3.7	0.74	39.705	3.7	0.0497	3.3	181	77	162	7	160	6	11
KLS-1_M_706	136	106	4	0.78	84	0.185	11.5	0.0255	3.4	0.29	39.188	3.4	0.0525	11.0	309	251	172	18	162	5	47
KLS-1_M_707	610	698	20	1.14	276	0.172	4.9	0.0249	3.0	0.60	40.216	3.0	0.0501	3.9	200	91	161	7	158	5	21
KLS-1_M_708	610	636	20	1.04	815	0.172	6.0	0.0255	4.0	0.67	39.205	4.0	0.0490	4.4	149	104	162	9	162	6	-9
KLS-1_M_709	271	212	6	0.78	94	0.132	9.0	0.0192	4.7	0.52	52.188	4.7	0.0499	7.7	189	179	126	11	122	6	35
KLS-1_M_710	615	604	21	0.98	1182	0.173	5.9	0.0261	3.8	0.64	38.365	3.8	0.0480	4.5	101	107	162	9	166	6	-63
KLS-1_M_711	201	101	4	0.50	130	0.132	11.0	0.0189	4.6	0.42	52.942	4.6	0.0507	10.0	227	230	126	13	121	6	47
KLS-1_M_712	608	478	19	0.79	3726	0.164	6.2	0.0255	3.7	0.60	39.199	3.7	0.0466	4.9	31	118	154	9	162	6	-427
KLS-1_M_713	351	272	11	0.78	742	0.178	7.9	0.0253	3.9	0.49	39.472	3.9	0.0511	6.9	245	160	167	12	161	6	34
KLS-1_M_714	918	1066	32	1.16	1155	0.178	6.0	0.0264	4.5	0.75	37.881	4.5	0.0488	3.9	140	93	166	9	168	7	-20
KLS-1_M_715	404	307	13	0.76	1973	0.185	8.0	0.0254	4.8	0.60	39.386	4.8	0.0528	6.4	320	145	172	13	162	8	49
KLS-1_M_716	237	213	8	0.90	317	0.175	9.1	0.0252	4.9	0.54	39.635	4.9	0.0504	7.7	213	179	164	14	161	8	25
KLS-1_M_717	194	97	6	0.50	129	0.212	13.1	0.0268	4.8	0.37	37.304	4.8	0.0572	12.2	500	269	195	23	171	8	66
KLS-1_M_718	1725	2576	63	1.49	1442	0.175	5.4	0.0247	4.5	0.83	40.454	4.5	0.0514	3.0	259	70	164	8	157	7	39
KLS-1_M_720	512	569	18	1.11	956	0.198	10.9	0.0259	6.0	0.55	38.539	6.0	0.0554	9.1	427	203	183	18	165	10	61
KLS-1_M_721	365	234	11	0.64	443	0.184	8.5	0.0256	4.8	0.57	39.121	4.8	0.0522	7.0	295	159	172	13	163	8	45
KLS-1_M_722	595	497	19	0.83	709	0.168	6.9	0.0254	4.2	0.61	39.351	4.2	0.0479	5.5	93	130	157	10	162	7	-74
KLS-1_M_723	341	304	11	0.89	145	0.181	7.5	0.0245	5.5	0.72	40.871	5.5	0.0535	5.2	352	118	169	12	156	8	56
KLS-1_M_724	1508	1654	50	1.10	42402	0.167	5.5	0.0244	4.8	0.87	40.973	4.8	0.0497	2.7	182	63	157	8	155	7	15
KLS-1_M_725	202	175	6	0.87	94	0.178	10.6	0.0249	4.9	0.46	40.198	4.9	0.0520	9.4	287	216	167	16	158	8	45
KLS-1_M_726	250	177	8	0.71	402	0.185	7.6	0.0251	4.9	0.64	39.777	4.9	0.0535	5.8	349	131	173	12	160	8	54
KLS-1_M_727	68	29	15	0.43	446	2.215	6.1	0.1942	4.0	0.66	5.150	4.0	0.0827	4.6	1263	90	1186	43	1144	42	9
KLS-1_M_728	243	241	8	0.99	557	0.188	8.8	0.0265	5.5	0.63	37.742	5.5	0.0515	6.8	265	155	175	14	169	9	36
KLS-1_M_729	1594	1475	52	0.93	821	0.159	6.5	0.0239	4.9	0.75	41.856	4.9	0.0483	4.3	113	102	150	9	152	7	-35
KLS-1_M_730	90	44	11	0.48	1244	0.838	6.8	0.1020	5.0	0.74	9.800	5.0	0.0596	4.6	588	99	618	31	626	30	-7
KLS-1_M_731	620	953	23	1.54	1677	0.188	11.5	0.0237	5.9	0.51	42.161	5.9	0.0575	9.8	511	216	175	18	151	9	70
KLS-1_M_732	433	529	15	1.22	288	0.179	7.6	0.0251	5.1	0.67	39.894	5.1	0.0517	5.7	273	130	167	12	160	8	42
KLS-1_M_733	388	200	8	0.52	231	0.121	10.0	0.0182	3.3	0.33	55.066	3.3	0.0481	9.4	106	222	116	11	116	4	-10
KLS-1_M_734	292	118	6	0.41	437	0.122	11.4	0.0185	4.3	0.38	54.108	4.3	0.0477	10.6	84	251	116	13	118	5	-41
KLS-1_M_735	295	127	6	0.43	301	0.118	10.0	0.0182	5.0	0.50	55.087	5.0	0.0471	8.7	55	207	113	11	116	6	-109
KLS-1_M_736	631	722	23	1.14	520	0.192	5.7	0.0253	2.7	0.48	39.578	2.7	0.0551	5.0	416	111	178	9	161	4	61
KLS-1_M_737	285	127	9	0.45	118	0.195	8.5	0.0265	4.3	0.50	37.675	4.3	0.0533	7.4	340	167	181	14	169	7	50
KLS-1_M_738	145	69	5	0.48	107	0.177	13.2	0.0272	4.0	0.30	36.776	4.0	0.0472	12.6	59	301	165	20	173	7	-195
KLS-1_M_739	354	201	11	0.57	1029	0.176	9.0	0.0264	4.5	0.50	37.922	4.5	0.0484	7.8	120	185	165	14	168	7	-40
KLS-1_M_740	595	471	20	0.79	1084	0.181	6.0	0.0257	4.6	0.77	38.900	4.6	0.0512	3.9	248	89	169	9	164	7	34
KLS-1_M_741	303	205	9	0.68	1495	0.174	7.9	0.0253	4.5	0.58	39.523	4.5	0.0500	6.4	195	150	163	12	161	7	17

KLS-1_M_742	315	246	10	0.78	1229	0.175	8.4	0.0257	5.0	0.60	38.900	5.0	0.0494	6.7	165	156	164	13	164	8	1
KLS-1_M_743	410	225	15	0.55	234	0.329	14.6	0.0269	5.0	0.35	37.218	5.0	0.0888	13.7	1399	262	289	37	171	9	88
KLS-1_M_744	371	330	11	0.89	1043	0.159	7.4	0.0231	5.2	0.70	43.250	5.2	0.0498	5.3	185	124	150	10	147	8	20
KLS-1_M_745	1351	535	43	0.40	4347	0.185	5.6	0.0265	4.2	0.76	37.694	4.2	0.0505	3.7	220	85	172	9	169	7	23
KLS-1_M_746	453	340	14	0.75	1333	0.169	7.9	0.0237	4.3	0.55	42.181	4.3	0.0518	6.6	276	151	159	12	151	6	45
KLS-1_M_747	83	39	15	0.47	1799	1.381	7.1	0.1494	5.9	0.83	6.693	5.9	0.0671	4.0	839	83	881	42	898	49	-7
KLS-1_M_748	629	580	21	0.92	1421	0.169	5.2	0.0249	3.2	0.61	40.220	3.2	0.0492	4.1	157	96	158	8	158	5	-1
KLS-1_M_749	297	323	10	1.09	402	0.168	8.1	0.0245	3.3	0.41	40.899	3.3	0.0498	7.4	185	171	158	12	156	5	16
KLS-1_M_750	185	105	6	0.57	447	0.151	11.3	0.0251	3.5	0.31	39.812	3.5	0.0436	10.8	-133	266	143	15	160	6	220
KLS-1_M_751	227	192	7	0.85	218	0.180	9.3	0.0249	4.6	0.49	40.207	4.6	0.0525	8.1	308	184	168	14	158	7	49
KLS-1_M_752	530	316	16	0.60	1379	0.170	7.0	0.0247	4.3	0.61	40.562	4.3	0.0499	5.5	191	128	159	10	157	7	18
KLS-1_M_753	740	775	25	1.05	3065	0.171	6.6	0.0247	4.0	0.60	40.470	4.0	0.0502	5.3	203	123	160	10	157	6	22
KLS-1_M_754	127	69	4	0.54	306	0.173	13.1	0.0257	4.7	0.36	38.871	4.7	0.0488	12.2	137	287	162	20	164	8	-19
KLS-1_M_755	309	230	10	0.74	315	0.177	8.2	0.0250	4.5	0.55	39.960	4.5	0.0513	6.8	253	156	165	12	159	7	37
KLS-1_M_756	491	459	17	0.93	182	0.177	7.0	0.0257	4.3	0.62	38.881	4.3	0.0499	5.4	190	127	165	11	164	7	14
KLS-1_M_758	437	317	14	0.73	210	0.180	6.8	0.0257	3.7	0.54	38.979	3.7	0.0509	5.8	234	133	168	11	163	6	30
KLS-1_M_759	327	137	7	0.42	69	0.141	10.3	0.0186	3.8	0.37	53.819	3.8	0.0552	9.6	419	213	134	13	119	4	72
KLS-1_M_760	275	138	6	0.50	419	0.117	13.8	0.0188	3.8	0.27	53.234	3.8	0.0450	13.2	-54	322	112	15	120	4	321
KLS-1_M_761	225	152	7	0.68	419	0.175	9.1	0.0252	3.2	0.35	39.722	3.2	0.0505	8.5	219	197	164	14	160	5	27
KLS-1_M_763	666	267	130	0.40	2460	1.470	3.6	0.1470	3.1	0.84	6.802	3.1	0.0725	2.0	1000	40	918	22	884	25	12
KLS-1_M_764	223	136	7	0.61	414	0.192	6.8	0.0258	4.1	0.59	38.784	4.1	0.0539	5.5	368	124	178	11	164	7	55
KLS-1_M_765	235	220	8	0.94	78	0.164	6.7	0.0254	3.5	0.52	39.335	3.5	0.0467	5.7	32	138	154	10	162	6	-402
KLS-1_M_766	341	203	10	0.59	353	0.179	7.7	0.0259	3.6	0.47	38.648	3.6	0.0501	6.8	200	159	167	12	165	6	18
KLS-1_M_767	772	654	25	0.85	535	0.171	5.4	0.0255	2.9	0.53	39.278	2.9	0.0486	4.6	130	108	160	8	162	5	-25
KLS-1_M_768	245	185	8	0.75	361	0.195	9.3	0.0275	4.8	0.52	36.425	4.8	0.0515	7.9	262	182	181	15	175	8	33
KLS-1_M_769	314	227	10	0.72	1211	0.164	8.7	0.0253	5.1	0.58	39.597	5.1	0.0470	7.1	50	169	154	12	161	8	-221
KLS-1_M_770	524	366	17	0.70	918	0.179	6.6	0.0264	4.3	0.65	37.836	4.3	0.0493	5.0	160	116	168	10	168	7	-5
KLS-1_M_771	351	322	12	0.92	1624	0.227	8.5	0.0260	4.7	0.55	38.436	4.7	0.0633	7.1	717	150	208	16	166	8	77
KLS-1_M_772	398	312	13	0.78	1000	0.170	8.0	0.0264	3.8	0.48	37.867	3.8	0.0468	7.0	37	167	160	12	168	6	-357
KLS-1_M_773	1309	1465	44	1.12	5806	0.171	4.9	0.0250	2.9	0.60	40.041	2.9	0.0498	3.9	185	90	161	7	159	5	14
KLS-1_M_774	285	267	9	0.94	903	0.152	8.3	0.0263	2.9	0.35	38.012	2.9	0.0419	7.8	-232	197	144	11	167	5	172
KLS-1_M_775	586	598	20	1.02	1759	0.174	7.1	0.0264	3.8	0.54	37.860	3.8	0.0477	6.0	84	142	163	11	168	6	-99
KLS-1_M_776	397	446	13	1.12	1844	0.163	7.1	0.0251	3.6	0.50	39.852	3.6	0.0472	6.2	59	147	154	10	160	6	-173
KLS-1_M_777	881	980	30	1.11	3389	0.204	5.1	0.0248	2.6	0.51	40.391	2.6	0.0598	4.4	598	95	189	9	158	4	74
KLS-1_M_778	178	179	6	1.01	183	0.180	9.2	0.0268	3.1	0.34	37.349	3.1	0.0489	8.7	141	204	168	14	170	5	-21
KLS-1_M_779	369	389	12	1.05	2632	0.166	7.8	0.0259	3.3	0.43	38.545	3.3	0.0464	7.0	19	169	156	11	165	5	-749
KLS-1_M_780	544	438	18	0.81	15863	0.179	7.6	0.0261	4.2	0.55	38.337	4.2	0.0499	6.3	190	146	168	12	166	7	13

KLS-1_M_782	13822	23377	708	1.69	220	0.264	19.8	0.0314	5.4	0.27	31.845	5.4	0.0609	19.0	637	409	238	42	199	11	69
KLS-1_M_783	801	616	25	0.77	5007	0.175	7.0	0.0253	4.6	0.66	39.538	4.6	0.0501	5.2	199	121	163	11	161	7	19
KLS-1_M_784	1161	877	36	0.76	712	0.166	6.0	0.0249	4.3	0.71	40.193	4.3	0.0483	4.2	116	99	156	9	158	7	-37
KLS-1_M_785	421	293	13	0.70	566	0.179	9.3	0.0261	4.9	0.53	38.363	4.9	0.0497	7.9	182	185	167	14	166	8	9
KLS-1_M_786	809	740	26	0.91	6710	0.166	5.9	0.0249	4.1	0.70	40.214	4.1	0.0483	4.2	115	99	156	8	158	6	-37
KLS-1_M_787	162	109	5	0.67	559	0.181	10.3	0.0250	5.4	0.52	39.926	5.4	0.0525	8.8	308	201	169	16	159	9	48
KLS-1_M_788	146	93	4	0.64	120	0.168	11.2	0.0257	5.3	0.48	38.878	5.3	0.0474	9.8	69	234	158	16	164	9	-137
KLS-1_M_789	366	219	12	0.60	616	0.188	7.8	0.0275	5.1	0.66	36.364	5.1	0.0497	5.9	181	137	175	13	175	9	4
KLS-1_M_790	211	159	7	0.75	445	0.179	9.1	0.0258	3.3	0.36	38.750	3.3	0.0504	8.4	213	195	167	14	164	5	23
KLS-1_M_791	537	445	17	0.83	412	0.172	6.2	0.0257	3.8	0.62	38.890	3.8	0.0485	4.9	125	115	161	9	164	6	-30
KLS-1_M_792	207	144	7	0.69	551	0.174	8.4	0.0256	4.2	0.50	39.032	4.2	0.0494	7.3	165	170	163	13	163	7	1
KLS-1_M_793	260	153	8	0.59	15645	0.182	15.5	0.0259	5.5	0.36	38.563	5.5	0.0509	14.5	236	334	170	24	165	9	30
KLS-1_M_794	162	78	5	0.48	65	0.189	10.3	0.0255	4.8	0.47	39.279	4.8	0.0538	9.1	362	205	176	17	162	8	55
KLS-1_M_795	224	92	7	0.41	97	0.167	11.2	0.0261	5.7	0.51	38.291	5.7	0.0464	9.7	20	232	157	16	166	9	-726
KLS-1_M_796	191	117	6	0.61	215	0.177	9.9	0.0259	4.8	0.49	38.579	4.8	0.0495	8.7	171	202	165	15	165	8	3
KLS-1_M_797	444	340	15	0.77	453	0.184	8.3	0.0261	4.4	0.53	38.250	4.4	0.0511	7.0	247	161	172	13	166	7	33
KLS-1_M_798	2912	4276	112	1.47	19010	0.163	3.9	0.0237	3.4	0.86	42.165	3.4	0.0497	2.0	181	47	153	6	151	5	17
KLS-1_M_799	151	255	7	1.69	1983	0.237	10.8	0.0276	3.8	0.35	36.220	3.8	0.0621	10.1	679	216	216	21	176	7	74
KLS-1_M_800	163	95	5	0.58	186	0.177	9.9	0.0260	4.3	0.43	38.451	4.3	0.0493	8.9	161	208	165	15	166	7	-3
KLS-1_M_801	401	209	12	0.52	3281	0.164	7.7	0.0256	3.6	0.46	39.106	3.6	0.0465	6.8	25	164	154	11	163	6	-554
KLS-1_M_802	365	173	12	0.47	628	0.266	15.5	0.0268	3.1	0.20	37.245	3.1	0.0717	15.2	978	310	239	33	171	5	83
KLS-1_M_803	320	101	7	0.31	88	0.135	10.8	0.0187	5.2	0.48	53.475	5.2	0.0523	9.5	300	216	129	13	119	6	60
KLS-1_M_804	219	88	6	0.40	73	0.229	16.0	0.0194	5.9	0.37	51.446	5.9	0.0854	14.9	1324	288	209	30	124	7	91
KLS-1_M_805	314	254	10	0.81	951	0.174	7.8	0.0253	3.7	0.48	39.575	3.7	0.0500	6.8	193	159	163	12	161	6	17
KLS-1_M_806	542	775	23	1.43	626	0.187	6.9	0.0276	4.0	0.57	36.230	4.0	0.0491	5.7	155	133	174	11	176	7	-14
KLS-1_M_807	797	716	28	0.90	809	0.177	6.4	0.0262	3.4	0.54	38.136	3.4	0.0489	5.4	141	127	165	10	167	6	-18
KLS-1_M_808	420	312	14	0.74	199	0.175	8.2	0.0264	5.6	0.69	37.909	5.6	0.0482	5.9	110	140	164	12	168	9	-53
KLS-1_M_809	364	178	11	0.49	593	0.171	8.7	0.0256	5.0	0.57	39.023	5.0	0.0483	7.2	114	169	160	13	163	8	-43
KLS-1_M_810	362	191	11	0.53	219	0.191	7.4	0.0262	3.7	0.50	38.237	3.7	0.0529	6.4	323	145	177	12	166	6	49
KLS-1_M_811	148	73	5	0.49	565	0.197	12.8	0.0257	3.5	0.27	38.895	3.5	0.0555	12.3	432	274	182	21	164	6	62
KLS-1_M_812	344	322	13	0.94	202	0.266	10.1	0.0260	4.3	0.43	38.521	4.3	0.0744	9.1	1052	184	240	22	165	7	84
KLS-1_M_813	711	689	25	0.97	4228	0.212	5.7	0.0255	3.6	0.63	39.163	3.6	0.0603	4.4	614	96	195	10	163	6	74
KLS-1_M_814	915	562	29	0.61	5383	0.186	5.9	0.0251	3.1	0.52	39.847	3.1	0.0538	5.1	361	114	173	9	160	5	56
KLS-1_M_815	300	176	9	0.59	93	0.180	9.0	0.0254	4.2	0.47	39.302	4.2	0.0514	8.0	260	184	168	14	162	7	38
KLS-1_M_816	255	139	7	0.54	200	0.294	16.2	0.0198	5.8	0.36	50.623	5.8	0.1080	15.1	1766	276	262	37	126	7	93
KLS-1_M_818	1525	1271	47	0.83	770	0.207	7.4	0.0228	5.1	0.69	43.854	5.1	0.0657	5.3	796	112	191	13	145	7	82
KLS-1_M_819	932	153	23	0.16	8549	0.162	6.6	0.0228	4.6	0.69	43.778	4.6	0.0514	4.8	257	111	152	9	146	7	43

KLS-1_M_820	203	219	7	1.08	283	0.199	11.6	0.0252	4.4	0.38	39.636	4.4	0.0571	10.7	494	235	184	19	161	7	67
KLS-1_M_821	663	415	14	0.63	807	0.120	6.2	0.0183	3.4	0.55	54.516	3.4	0.0473	5.2	65	123	115	7	117	4	-79
KLS-1_M_822	156	143	5	0.91	231	0.163	13.0	0.0259	4.6	0.36	38.613	4.6	0.0455	12.1	-27	293	153	18	165	8	703
KLS-1_M_823	264	265	9	1.00	3344	0.189	7.9	0.0270	5.0	0.64	37.014	5.0	0.0508	6.0	233	139	176	13	172	9	26
KLS-1_M_824	401	270	13	0.67	5064	0.177	6.9	0.0263	3.5	0.51	37.961	3.5	0.0486	5.9	129	138	165	10	168	6	-30
KLS-1_M_825	152	122	5	0.80	210	0.186	12.5	0.0266	5.3	0.42	37.656	5.3	0.0508	11.3	232	261	173	20	169	9	27
KLS-1_M_826	258	278	8	1.08	654	0.166	11.1	0.0246	4.6	0.42	40.575	4.6	0.0489	10.1	142	237	156	16	157	7	-11
KLS-1_M_827	207	92	8	0.45	491	0.332	17.6	0.0272	7.2	0.41	36.767	7.2	0.0885	16.1	1394	308	291	45	173	12	88
KLS-1_M_828	409	381	13	0.93	2049	0.168	7.5	0.0254	5.5	0.73	39.329	5.5	0.0480	5.2	101	123	158	11	162	9	-
	Composition						Corrected isotope ratios						Apparent ages (Ma)								
Analysis	U ppm	Th ppm	Pb ppm	Th/U	$\frac{^{206}\text{Pb}}{^{204}\text{Pb}}$	$\frac{^{207}\text{Pb}}{^{235}\text{U}}$	$\pm 2\sigma$ (%)	^{206}Pb ^{238}U	$\pm 2\sigma$ (%)	error corr.	^{238}U ^{206}Pb	$\pm 2\sigma$ (%)	^{207}Pb ^{206}Pb	$\pm 2\sigma$ (%)	^{207}Pb ^{206}Pb (abs)	$\pm 2\sigma$ (%)	^{207}Pb ^{235}U	$\pm 2\sigma$ (abs)	^{206}Pb ^{238}U	$\pm 2\sigma$ (abs)	% disc.
	KLS-2 (King Lear Formation – Jackson Creek Member)																				
KLS-2_L_1	451	186	14	0.41	888	0.198	5.3	0.0278	3.4	0.64	35.925	3.4	0.0517	4.0	270	92	184	9	177	6	34
KLS-2_L_2	87	40	3	0.46	64	0.247	8.8	0.0313	4.3	0.49	31.917	4.3	0.0572	7.6	499	168	224	18	199	8	60
KLS-2_L_3	189	76	10	0.40	1127	0.361	7.6	0.0500	4.7	0.62	20.006	4.7	0.0524	6.0	301	136	313	21	314	15	-4
KLS-2_L_4	60	15	2	0.25	69	0.208	15.9	0.0331	5.9	0.37	30.220	5.9	0.0456	14.7	-24	356	192	28	210	12	987
KLS-2_L_5	393	215	11	0.55	2388	0.183	7.6	0.0261	5.7	0.74	38.244	5.7	0.0507	5.1	228	118	170	12	166	9	27
KLS-2_L_6	546	266	15	0.49	2069	0.174	6.2	0.0249	4.6	0.73	40.130	4.6	0.0507	4.2	227	97	163	9	159	7	30
KLS-2_L_7	368	217	10	0.59	1474	0.172	6.4	0.0247	3.9	0.60	40.526	3.9	0.0505	5.1	218	118	161	10	157	6	28
KLS-2_L_8	257	175	7	0.68	615	0.174	6.4	0.0247	3.9	0.60	40.452	3.9	0.0510	5.1	239	118	163	10	157	6	34
KLS-2_L_10	93	45	5	0.49	318	0.370	9.8	0.0510	7.1	0.72	19.623	7.1	0.0527	6.8	314	155	320	27	320.4	22	-2
KLS-2_L_11	332	170	16	0.51	3190	0.299	6.0	0.0427	4.5	0.75	23.414	4.5	0.0508	3.9	233	90	266	14	270	12	-16
KLS-2_L_12	72	46	4	0.63	2183	0.427	9.4	0.0458	5.6	0.60	21.818	5.6	0.0675	7.5	855	155	361	28	289	16	66
KLS-2_L_13	173	75	8	0.44	6172	0.315	8.7	0.0432	3.6	0.41	23.133	3.6	0.0528	7.9	320	179	278	21	273	10	15
KLS-2_L_14	133	79	8	0.59	1380	0.363	8.5	0.0502	5.2	0.61	19.932	5.2	0.0525	6.8	307	154	315	23	316	16	-3
KLS-2_L_15	87	36	5	0.42	231	0.360	9.1	0.0497	5.1	0.56	20.101	5.1	0.0525	7.5	308	171	312	24	313	16	-1
KLS-2_L_16	317	40	11	0.13	1208	0.254	8.0	0.0337	5.1	0.63	29.658	5.1	0.0547	6.2	401	139	230	17	214	11	47
KLS-2_L_17	620	79	23	0.13	793	0.330	16.8	0.0339	5.8	0.34	29.514	5.8	0.0707	15.8	950	324	290	42	215	12	77
KLS-2_L_18	38	22	2	0.58	99	0.309	17.0	0.0458	7.3	0.43	21.829	7.3	0.0490	15.3	147	359	274	41	289	21	-96
KLS-2_L_19	32	17	2	0.54	69	0.310	18.2	0.0442	5.5	0.30	22.604	5.5	0.0508	17.3	233	400	274	44	279	15	-20
KLS-2_L_20	122	35	7	0.29	881	0.373	8.0	0.0517	5.2	0.65	19.361	5.2	0.0524	6.0	302	137	322	22	325	16	-8
KLS-2_L_21	68	22	4	0.33	638	0.440	10.2	0.0546	5.9	0.57	18.306	5.9	0.0585	8.4	547	183	370	32	343	20	37
KLS-2_L_22	152	70	9	0.46	1144	0.386	8.8	0.0565	5.9	0.66	17.684	5.9	0.0495	6.6	171	154	331	25	355	20	-108
KLS-2_L_23	115	58	7	0.50	2088	0.399	7.6	0.0582	5.3	0.70	17.181	5.3	0.0497	5.4	181	126	341	22	365	19	-102
KLS-2_L_24	50	16	3	0.32	195	0.382	14.2	0.0578	6.2	0.43	17.288	6.2	0.0479	12.8	96	303	329	40	362	22	-279

KLS-2_L_25	65	22	5	0.34	718	0.470	12.0	0.0677	7.9	0.66	14.772	7.9	0.0503	9.0	211	210	391	39	422	32	-100
KLS-2_L_26	101	40	5	0.40	386	0.323	10.5	0.0417	7.7	0.73	23.987	7.7	0.0562	7.2	460	159	284	26	263	20	43
KLS-2_L_27	106	41	6	0.38	175	0.373	7.3	0.0511	4.4	0.59	19.554	4.4	0.0529	5.9	326	134	322	20	322	14	1
KLS-2_L_28	471	182	14	0.39	1683	0.177	8.2	0.0266	5.4	0.65	37.646	5.4	0.0482	6.2	111	146	165	12	169	9	-52
KLS-2_L_29	258	144	8	0.56	438	0.182	10.7	0.0267	5.7	0.53	37.476	5.7	0.0495	9.1	171	212	170	17	170	10	0
KLS-2_L_30	105	30	5	0.28	341	0.379	9.2	0.0499	5.6	0.61	20.044	5.6	0.0551	7.2	417	162	326	26	314	17	25
KLS-2_L_31	228	135	7	0.59	530	0.200	8.3	0.0289	5.6	0.67	34.608	5.6	0.0502	6.1	203	141	185	14	184	10	10
KLS-2_L_32	252	161	7	0.64	333	0.166	8.3	0.0244	5.3	0.63	41.060	5.3	0.0496	6.4	175	150	156	12	155	8	11
KLS-2_L_33	137	137	7	1.00	681	0.286	13.2	0.0418	5.9	0.45	23.946	5.9	0.0497	11.8	181	275	256	30	264	15	-46
KLS-2_L_34	38	15	2	0.38	74	0.298	16.1	0.0413	4.4	0.27	24.201	4.4	0.0523	15.5	297	354	265	38	261	11	12
KLS-2_L_35	124	67	7	0.54	522	0.362	9.9	0.0531	5.0	0.50	18.839	5.0	0.0495	8.6	171	200	314	27	333	16	-95
KLS-2_L_36	131	45	7	0.35	0	0.383	6.9	0.0526	4.1	0.59	18.999	4.1	0.0528	5.5	322	126	330	19	331	13	-3
KLS-2_L_37	362	268	11	0.74	9967	0.162	10.1	0.0241	6.7	0.66	41.531	6.7	0.0488	7.5	138	176	152	14	153	10	-11
KLS-2_L_38	93	48	5	0.51	8366	0.369	9.4	0.0456	5.7	0.60	21.913	5.7	0.0586	7.5	553	164	319	26	288	16	48
KLS-2_L_39	145	64	5	0.44	272	0.211	9.3	0.0294	3.9	0.42	34.013	3.9	0.0521	8.4	288	192	194	16	187	7	35
KLS-2_L_40	128	55	4	0.43	433	0.216	9.2	0.0312	5.5	0.59	32.053	5.5	0.0502	7.4	203	172	198	17	198	11	3
KLS-2_L_41	116	30	20	0.26	2310	1.528	5.6	0.1546	4.5	0.78	6.467	4.5	0.0717	3.5	977	71	942	35	927	38	5
KLS-2_L_42	120	54	7	0.44	2042	0.454	8.0	0.0555	4.8	0.60	18.025	4.8	0.0594	6.3	580	138	380	25	348	16	40
KLS-2_L_43	60	29	3	0.48	120	0.345	12.8	0.0480	6.7	0.52	20.825	6.7	0.0521	10.9	289	249	301	33	302	20	-5
KLS-2_L_44	384	233	15	0.61	1217	0.233	8.1	0.0330	6.1	0.75	30.320	6.1	0.0512	5.3	251	123	213	16	209	13	17
KLS-2_L_45	379	29	10	0.08	368	0.180	7.7	0.0262	6.0	0.78	38.140	6.0	0.0497	4.8	182	112	168	12	167	10	9
KLS-2_L_46	164	64	6	0.39	158	0.214	8.9	0.0323	4.1	0.45	30.926	4.1	0.0480	7.9	100	187	197	16	205	8	-105
KLS-2_L_47	61	44	3	0.72	1346	0.282	13.4	0.0402	6.1	0.46	24.877	6.1	0.0509	11.9	237	274	252	30	254	15	-7
KLS-2_L_48	99	36	3	0.36	705	0.169	13.8	0.0253	5.4	0.39	39.458	5.4	0.0482	12.7	110	299	158	20	161	9	-46
KLS-2_L_49	472	245	13	0.52	978	0.176	9.6	0.0240	6.6	0.68	41.657	6.6	0.0531	7.0	333	158	164	15	153	10	54
KLS-2_L_50	60	20	3	0.33	353	0.440	11.0	0.0545	7.7	0.70	18.356	7.7	0.0586	7.8	552	171	370	34	342	26	38
KLS-2_L_51	88	33	5	0.37	165	0.420	9.6	0.0540	5.9	0.61	18.519	5.9	0.0564	7.7	468	169	356	29	339	19	28
KLS-2_L_52	152	70	10	0.46	332	0.548	8.0	0.0533	4.2	0.52	18.766	4.2	0.0746	6.8	1059	137	444	29	335	14	68
KLS-2_L_53	125	48	7	0.38	635	0.400	7.6	0.0505	4.5	0.59	19.819	4.5	0.0576	6.1	513	135	342	22	317	14	38
KLS-2_L_54	489	342	14	0.70	474	0.178	5.6	0.0257	3.0	0.53	38.868	3.0	0.0502	4.7	204	110	166	9	164	5	20
KLS-2_L_55	67	37	3	0.55	142	0.146	27.9	0.0364	5.7	0.20	27.474	5.7	0.0292	27.3	-1248	855	139	36	230	13	118
KLS-2_L_56	44	23	2	0.52	655	0.309	10.5	0.0418	4.4	0.42	23.942	4.4	0.0537	9.5	360	215	274	25	264	11	27
KLS-2_L_57	176	97	34	0.55	2080	1.690	5.4	0.1621	3.6	0.66	6.167	3.6	0.0756	4.0	1084	81	1005	35	969	33	11
KLS-2_L_58	463	183	20	0.40	561	0.277	5.8	0.0385	3.6	0.61	26.007	3.6	0.0522	4.6	293	104	248	13	243	9	17
KLS-2_L_59	222	104	6	0.47	718	0.187	9.8	0.0263	4.3	0.44	38.089	4.3	0.0516	8.8	269	201	174	16	167	7	38
KLS-2_L_60	359	81	9	0.23	875	0.175	8.6	0.0244	3.9	0.45	41.023	3.9	0.0520	7.7	287	176	164	13	155	6	46
KLS-2_L_61	57	23	3	0.41	161	0.367	12.0	0.0525	3.5	0.29	19.058	3.5	0.0507	11.4	227	264	317	33	330	11	-45

KLS-2_L_62	221	18	6	0.08	587	0.196	10.5	0.0279	5.4	0.51	35.880	5.4	0.0509	9.0	235	207	181	17	177	9	25
KLS-2_L_63	72	38	4	0.53	244	0.390	10.6	0.0506	4.8	0.45	19.774	4.8	0.0559	9.5	447	211	334	30	318	15	29
KLS-2_L_64	84	35	4	0.41	659	0.291	12.8	0.0431	3.5	0.27	23.181	3.5	0.0489	12.4	144	290	259	29	272	9	-89
KLS-2_L_65	80	27	5	0.34	357	0.407	10.1	0.0553	5.8	0.57	18.071	5.8	0.0534	8.3	345	187	347	30	347	20	-1
KLS-2_L_66	306	130	9	0.43	218	0.183	8.3	0.0254	5.6	0.67	39.321	5.6	0.0522	6.1	292	140	171	13	162	9	45
KLS-2_L_67	68	31	4	0.45	90	0.416	9.4	0.0554	5.3	0.56	18.063	5.3	0.0546	7.8	394	175	354	28	347	18	12
KLS-2_L_68	114	25	7	0.22	1743	0.377	7.9	0.0579	5.5	0.69	17.268	5.5	0.0473	5.7	63	135	325	22	363	19	-475
KLS-2_L_69	142	46	4	0.32	358	0.170	12.0	0.0268	5.0	0.41	37.353	5.0	0.0462	10.9	6	262	160	18	170	8	-2819
KLS-2_L_70	228	135	13	0.59	1217	0.368	6.8	0.0508	4.4	0.63	19.670	4.4	0.0525	5.2	305	120	318	19	320	14	-5
KLS-2_L_71	139	57	7	0.41	10263	0.372	7.8	0.0491	4.3	0.55	20.379	4.3	0.0549	6.5	409	145	321	21	309	13	25
KLS-2_L_72	170	135	5	0.79	254	0.178	9.6	0.0265	4.3	0.45	37.768	4.3	0.0487	8.5	133	201	166	15	168	7	-26
KLS-2_L_74	134	102	7	0.76	326	0.306	12.4	0.0453	6.2	0.50	22.072	6.2	0.0491	10.7	150	252	271	30	286	17	-90
KLS-2_L_75	84	35	2	0.42	145	0.210	10.9	0.0273	4.6	0.42	36.601	4.6	0.0558	9.9	445	219	194	19	174	8	61
KLS-2_L_76	119	78	3	0.66	1898	0.160	10.9	0.0250	6.0	0.55	39.973	6.0	0.0462	9.1	10	219	150	15	159	9	-1457
KLS-2_L_77	132	73	5	0.55	215	0.211	9.9	0.0317	4.1	0.41	31.501	4.1	0.0481	9.1	104	214	194	18	201	8	-94
KLS-2_L_78	86	33	5	0.38	320	0.405	12.0	0.0525	6.1	0.51	19.030	6.1	0.0559	10.3	448	228	345	35	330	20	26
KLS-2_L_79	356	104	11	0.29	8009	0.213	8.1	0.0304	4.3	0.53	32.898	4.3	0.0508	6.8	233	157	196	14	193	8	17
KLS-2_L_80	93	29	5	0.31	689	0.390	10.2	0.0525	4.1	0.40	19.045	4.1	0.0539	9.3	367	210	335	29	330	13	10
KLS-2_L_81	1045	275	38	0.26	5634	0.237	5.8	0.0315	3.6	0.61	31.737	3.6	0.0545	4.6	391	103	216	11	200	7	49
KLS-2_L_82	220	199	9	0.90	341	0.262	18.2	0.0305	6.2	0.34	32.797	6.2	0.0624	17.2	687	366	236	38	194	12	72
KLS-2_L_83	52	20	2	0.39	239	0.314	14.6	0.0455	6.0	0.41	21.974	6.0	0.0500	13.3	197	310	277	36	287	17	-46
KLS-2_L_84	315	248	15	0.79	4510	0.284	8.4	0.0396	6.0	0.71	25.245	6.0	0.0520	5.9	286	135	254	19	250	15	12
KLS-2_L_85	348	283	14	0.81	2878	0.214	10.1	0.0318	7.1	0.70	31.461	7.1	0.0489	7.2	145	169	197	18	202	14	-39
KLS-2_L_86	99	35	6	0.35	2712	0.423	10.5	0.0546	6.1	0.58	18.301	6.1	0.0561	8.6	457	190	358	32	343	20	25
KLS-2_L_87	181	59	5	0.33	2423	0.190	13.0	0.0270	5.8	0.45	36.988	5.8	0.0509	11.6	237	269	176	21	172	10	27
KLS-2_L_88	129	38	7	0.30	1675	0.354	9.5	0.0498	6.2	0.65	20.099	6.2	0.0517	7.2	271	164	308	25	313	19	-16
KLS-2_L_89	237	74	7	0.31	994	0.206	7.2	0.0293	3.6	0.49	34.137	3.6	0.0511	6.3	246	145	191	13	186	7	24
KLS-2_L_90	141	68	8	0.48	925	0.362	10.4	0.0519	6.9	0.66	19.279	6.9	0.0507	7.7	226	179	314	28	326	22	-44
KLS-2_L_92	108	36	34	0.33	10362	3.362	6.7	0.2664	5.6	0.82	3.753	5.6	0.0915	3.8	1457	72	1496	53	1523	76	-4
KLS-2_L_93	158	105	8	0.66	484	0.322	8.4	0.0442	5.4	0.64	22.646	5.4	0.0528	6.4	321	146	283	21	279	15	13
KLS-2_L_94	77	22	5	0.29	325	0.392	10.9	0.0575	6.6	0.61	17.395	6.6	0.0495	8.6	170	202	336	31	360	23	-112
KLS-2_L_95	269	144	8	0.54	219	0.182	8.4	0.0263	4.7	0.55	38.027	4.7	0.0502	7.0	203	162	170	13	167	8	18
KLS-2_L_96	225	110	6	0.49	4240	0.160	11.4	0.0248	7.4	0.64	40.276	7.4	0.0469	8.7	43	209	151	16	158	12	-270
KLS-2_L_97	118	50	7	0.42	587	0.419	9.1	0.0546	6.5	0.71	18.304	6.5	0.0556	6.3	437	140	355	27	343	22	22
KLS-2_L_98	78	26	3	0.33	623	0.221	13.5	0.0322	6.3	0.46	31.033	6.3	0.0498	11.9	186	278	203	25	204	13	-10
KLS-2_L_99	252	70	7	0.28	309	0.173	7.3	0.0249	5.3	0.72	40.165	5.3	0.0504	5.1	214	117	162	11	159	8	26
KLS-2_L_100	117	58	25	0.49	1439	1.995	6.5	0.1813	5.2	0.80	5.514	5.2	0.0798	3.9	1191	77	1114	44	1074	52	10

KLS-2_L_101	168	88	10	0.52	6742	0.401	7.8	0.0530	5.2	0.65	18.876	5.2	0.0549	5.9	409	132	342	23	333	17	19
KLS-2_L_102	117	65	7	0.56	10581	0.369	8.4	0.0512	3.4	0.39	19.550	3.4	0.0523	7.7	299	176	319	23	322	11	-8
KLS-2_L_103	286	143	10	0.50	656	0.239	8.7	0.0309	4.2	0.48	32.406	4.2	0.0561	7.6	456	168	217	17	196	8	57
KLS-2_L_104	300	119	10	0.40	612	0.198	7.2	0.0297	5.1	0.70	33.654	5.1	0.0483	5.1	114	121	183	12	189	9	-66
KLS-2_L_105	168	95	5	0.56	322	0.173	9.3	0.0245	5.0	0.53	40.867	5.0	0.0513	7.8	256	180	162	14	156	8	39
KLS-2_L_106	391	142	10	0.36	3413	0.162	6.8	0.0241	3.7	0.54	41.541	3.7	0.0488	5.7	140	133	153	10	153	6	-10
KLS-2_L_107	165	56	5	0.34	596	0.196	9.1	0.0310	4.3	0.47	32.250	4.3	0.0458	8.0	-13	194	182	15	197	8	1624
KLS-2_L_108	245	165	12	0.67	272	0.310	7.0	0.0430	4.5	0.64	23.248	4.5	0.0523	5.4	298	122	274	17	271	12	9
KLS-2_L_109	144	87	8	0.60	578	0.353	8.1	0.0500	3.7	0.45	20.005	3.7	0.0513	7.2	252	166	307	21	314	11	-25
KLS-2_L_110	171	52	10	0.30	728	0.404	7.7	0.0553	5.2	0.68	18.098	5.2	0.0530	5.6	328	127	344	22	347	18	-6
KLS-2_L_111	64	23	4	0.36	281	0.419	9.5	0.0593	5.8	0.61	16.853	5.8	0.0512	7.5	248	172	355	28	372	21	-50
KLS-2_L_112	111	27	7	0.24	151	0.453	6.9	0.0577	4.2	0.60	17.341	4.2	0.0570	5.5	492	121	380	22	361	15	27
KLS-2_L_113	60	22	4	0.37	3595	0.447	11.3	0.0659	5.4	0.48	15.180	5.4	0.0492	9.9	158	231	375	35	411	22	-161
KLS-2_L_114	61	19	4	0.31	3243	0.440	11.2	0.0589	6.5	0.57	16.983	6.5	0.0542	9.1	381	205	370	35	369	23	3
KLS-2_L_115	74	32	5	0.43	273	0.416	10.6	0.0576	5.5	0.51	17.357	5.5	0.0524	9.1	302	207	353	32	361	19	-19
KLS-2_L_116	89	39	3	0.44	2853	0.306	18.5	0.0328	5.4	0.29	30.490	5.4	0.0676	17.7	858	366	271	44	208	11	76
KLS-2_L_117	451	217	13	0.48	587	0.172	8.9	0.0255	5.8	0.65	39.261	5.8	0.0491	6.8	152	158	162	13	162	9	-7
KLS-2_L_118	447	225	23	0.50	1257	0.318	6.9	0.0446	5.5	0.80	22.443	5.5	0.0517	4.1	272	94	280	17	281	15	-3
KLS-2_L_119	57	21	3	0.36	73	0.424	14.5	0.0560	5.7	0.39	17.850	5.7	0.0549	13.3	407	298	359	44	351	20	14
KLS-2_L_120	460	1671	25	3.63	391	0.229	6.3	0.0250	3.6	0.56	39.950	3.6	0.0664	5.2	820	109	210	12	159	6	81
KLS-2_L_121	150	63	7	0.42	787	0.325	8.8	0.0444	5.4	0.60	22.499	5.4	0.0531	7.0	333	158	286	22	280	15	16
KLS-2_L_122	361	162	12	0.45	74039	0.214	7.8	0.0293	4.5	0.57	34.114	4.5	0.0528	6.4	322	145	197	14	186	8	42
KLS-2_L_123	128	46	26	0.36	1834	1.919	8.1	0.1821	7.2	0.88	5.492	7.2	0.0765	3.8	1107	76	1088	54	1078	71	3
KLS-2_L_124	395	112	13	0.28	1275	0.223	8.5	0.0313	6.2	0.72	31.996	6.2	0.0518	5.8	279	132	205	16	198	12	29
KLS-2_L_125	134	47	7	0.35	311	0.391	9.3	0.0486	6.4	0.68	20.575	6.4	0.0584	6.7	543	146	335	26	306	19	44
KLS-2_L_126	137	73	8	0.53	1065	0.370	6.5	0.0498	3.7	0.55	20.084	3.7	0.0540	5.3	370	120	320	18	313.2	11	15
KLS-2_L_127	502	133	13	0.26	3813	0.177	7.0	0.0252	5.0	0.70	39.613	5.0	0.0510	4.9	239	113	166	11	161	8	33
KLS-2_L_128	91	26	5	0.29	4732	0.377	11.1	0.0509	5.2	0.46	19.632	5.2	0.0537	9.8	358	222	325	31	320	16	11
KLS-2_L_129	80	34	3	0.43	243	0.221	13.0	0.0298	5.6	0.43	33.566	5.6	0.0539	11.7	367	263	203	24	189	10	48
KLS-2_L_130	25	6	1	0.26	90	0.309	17.7	0.0431	6.1	0.34	23.204	6.1	0.0520	16.6	287	380	274	42	272	16	5
KLS-2_L_131	44	9	2	0.21	159	0.305	13.1	0.0461	5.9	0.45	21.688	5.9	0.0480	11.7	100	277	270	31	291	17	-191
KLS-2_L_132	509	231	16	0.45	1729	0.203	5.9	0.0273	4.4	0.73	36.564	4.4	0.0538	3.9	361	89	187	10	174	8	52
KLS-2_L_133	436	191	13	0.44	2089	0.191	7.1	0.0274	5.5	0.76	36.443	5.5	0.0505	4.6	217	106	177	12	175	9	20
KLS-2_L_134	989	95	24	0.10	7742	0.159	7.7	0.0231	6.5	0.84	43.240	6.5	0.0497	4.1	182	96	149	11	147	9	19
KLS-2_L_135	426	230	25	0.54	1029	0.395	6.1	0.0500	4.7	0.76	19.989	4.7	0.0573	3.9	503	86	338	17	315	14	37
KLS-2_L_136	137	78	28	0.57	2628	1.797	5.5	0.1702	3.5	0.61	5.874	3.5	0.0766	4.3	1110	86	1044	36	1013	33	9
KLS-2_L_137	79	26	5	0.33	565	0.407	11.4	0.0533	6.5	0.56	18.749	6.5	0.0554	9.4	427	210	347	34	335	21	22

KLS-2_L_138	80	69	4	0.86	1681	0.248	12.3	0.0354	8.1	0.65	28.265	8.1	0.0508	9.3	231	216	225	25	224	18	3
KLS-2_L_139	126	73	7	0.57	1253	0.364	10.4	0.0487	6.5	0.62	20.542	6.5	0.0543	8.2	382	183	315	28	306	19	20
KLS-2_L_140	103	38	3	0.37	111	0.312	14.1	0.0263	6.6	0.46	38.034	6.6	0.0862	12.5	1342	242	276	34	167	11	88
KLS-2_L_141	189	78	5	0.41	0	0.172	11.9	0.0259	7.8	0.65	38.612	7.8	0.0480	9.0	101	212	161	18	165	13	-64
KLS-2_L_142	166	45	9	0.27	563	0.383	10.7	0.0531	7.1	0.66	18.848	7.1	0.0524	8.0	303	182	330	30	333	23	-10
KLS-2_L_143	128	60	7	0.47	2142	0.390	8.0	0.0526	6.0	0.74	19.007	6.0	0.0538	5.3	362	119	334	23	331	19	9
KLS-2_L_144	298	126	8	0.43	1061	0.165	10.2	0.0250	6.4	0.62	39.948	6.4	0.0477	8.0	85	189	155	15	159	10	-89
KLS-2_L_145	235	87	6	0.37	995	0.180	9.0	0.0258	4.2	0.46	38.775	4.2	0.0505	8.0	218	185	168	14	164	7	25
KLS-2_L_146	66	28	3	0.42	470	0.300	11.5	0.0435	3.5	0.29	22.999	3.5	0.0501	10.9	198	254	267	27	274	9	-38
KLS-2_L_147	1110	107	293	0.10	42148	0.957	13.7	0.0706	13.6	0.99	14.174	13.6	0.0983	1.8	1593	34	682	68	439	58	72
KLS-2_L_148	138	83	8	0.60	9201	0.369	8.6	0.0497	3.8	0.43	20.118	3.8	0.0539	7.7	367	174	319	24	313	12	15
KLS-2_L_149	75	24	4	0.32	201	0.404	8.9	0.0516	4.2	0.47	19.379	4.2	0.0567	7.8	480	172	344	26	324	13	32
KLS-2_L_150	346	239	10	0.69	468	0.175	6.9	0.0244	3.9	0.55	41.005	3.9	0.0519	5.7	282	130	163	10	155	6	45
KLS-2_L_151	59	24	3	0.41	410	0.288	15.6	0.0446	5.2	0.33	22.442	5.2	0.0468	14.7	40	352	257	35	281	14	-594
KLS-2_L_152	89	52	4	0.58	233	0.315	7.0	0.0436	4.2	0.60	22.917	4.2	0.0523	5.5	301	126	278	17	275	11	8
KLS-2_L_153	261	134	9	0.51	411	0.213	9.4	0.0307	6.2	0.66	32.522	6.2	0.0503	7.0	208	163	196	17	195	12	6
KLS-2_L_154	790	674	23	0.85	18167	0.159	6.4	0.0228	4.4	0.67	43.898	4.4	0.0505	4.6	219	107	150	9	145	6	34
KLS-2_L_155	68	22	4	0.32	220	0.433	11.2	0.0569	4.4	0.38	17.578	4.4	0.0551	10.3	418	231	365	34	357	15	15
KLS-2_L_156	96	36	6	0.37	514	0.508	8.8	0.0540	5.3	0.60	18.509	5.3	0.0683	7.0	876	145	417	30	339	18	61
KLS-2_L_157	75	25	4	0.33	318	0.399	9.6	0.0524	4.5	0.46	19.098	4.5	0.0553	8.5	423	189	341	28	329	14	22
KLS-2_L_158	199	92	6	0.46	325	0.196	10.7	0.0289	5.0	0.46	34.594	5.0	0.0491	9.5	152	222	181	18	184	9	-21
KLS-2_L_159	177	45	7	0.26	706	0.290	8.6	0.0409	4.1	0.46	24.451	4.1	0.0514	7.6	258	175	258	20	258	10	0
KLS-2_L_160	627	47	16	0.07	1066	0.169	7.2	0.0252	5.1	0.70	39.709	5.1	0.0486	5.1	126	120	158	11	160	8	-27
KLS-2_L_161	210	89	6	0.42	137	0.175	9.1	0.0267	4.6	0.49	37.495	4.6	0.0477	7.9	84	188	164	14	170	8	-103
KLS-2_L_162	164	41	10	0.25	2658	0.414	7.1	0.0576	4.0	0.55	17.375	4.0	0.0521	5.8	291	133	352	21	361	14	-24
KLS-2_L_163	128	84	10	0.66	896	0.534	7.2	0.0672	3.7	0.50	14.881	3.7	0.0576	6.1	514	135	434	25	419	15	18
KLS-2_L_164	42	21	2	0.49	194	0.273	13.7	0.0400	6.7	0.48	25.024	6.7	0.0495	12.0	171	280	245	30	253	17	-47
KLS-2_L_165	80	34	4	0.42	1887	0.315	12.1	0.0435	5.4	0.44	22.969	5.4	0.0524	10.8	303	246	278	29	275	15	9
KLS-2_L_166	61	20	3	0.33	652	0.386	10.0	0.0535	5.4	0.53	18.696	5.4	0.0523	8.4	300	192	331	28	336	18	-12
KLS-2_L_167	80	23	5	0.29	251	0.419	10.0	0.0580	5.6	0.56	17.249	5.6	0.0524	8.2	305	187	355	30	363	20	-19
KLS-2_L_168	418	759	14	1.82	684	0.146	8.3	0.0219	6.2	0.74	45.647	6.2	0.0484	5.5	119	130	139	11	140	9	-17
KLS-2_L_169	94	33	5	0.35	539	0.356	8.5	0.0478	5.1	0.59	20.931	5.1	0.0540	6.8	373	153	309	23	301	15	19
KLS-2_L_170	614	221	23	0.36	4096	0.237	6.5	0.0325	4.7	0.71	30.739	4.7	0.0528	4.5	322	103	216	13	206	9	36
KLS-2_L_171	196	64	7	0.33	1728	0.213	7.9	0.0309	5.4	0.68	32.344	5.4	0.0501	5.7	197	133	196	14	196	10	1
KLS-2_L_172	263	97	8	0.37	1080	0.191	8.8	0.0277	3.8	0.42	36.161	3.8	0.0501	8.0	198	185	177	14	176	7	11
KLS-2_L_173	109	53	5	0.49	817	0.289	9.5	0.0395	4.0	0.41	25.330	4.0	0.0531	8.6	334	194	258	22	250	10	25
KLS-2_L_174	210	72	5	0.35	1173	0.164	7.9	0.0243	5.3	0.67	41.077	5.3	0.0489	5.8	145	136	154	11	155	8	-7

KLS-2_L_175	96	43	5	0.45	296	0.385	9.0	0.0515	4.2	0.46	19.419	4.2	0.0542	7.9	378	178	330	25	324	13	14
KLS-2_L_176	112	51	4	0.45	180	0.196	9.7	0.0301	4.1	0.42	33.246	4.1	0.0473	8.7	66	208	182	16	191	8	-190
KLS-2_L_177	128	58	6	0.45	542	0.290	8.4	0.0407	3.7	0.43	24.577	3.7	0.0517	7.5	273	173	259	19	257	9	6
KLS-2_L_178	57	42	3	0.74	157	0.288	13.7	0.0397	6.3	0.45	25.203	6.3	0.0526	12.1	312	276	257	31	251	15	20
KLS-2_L_179	49	24	2	0.50	1867	0.268	17.6	0.0410	4.9	0.28	24.379	4.9	0.0474	16.8	69	401	241	38	259	12	-273
KLS-2_L_180	333	287	11	0.86	3679	0.168	7.5	0.0259	5.2	0.68	38.668	5.2	0.0470	5.4	50	130	157	11	165	8	-227
KLS-2_L_181	156	55	4	0.35	98	0.168	9.7	0.0242	6.1	0.62	41.394	6.1	0.0504	7.5	213	175	158	14	154	9	28
KLS-2_L_182	144	37	8	0.26	220	0.393	7.5	0.0526	4.2	0.55	19.015	4.2	0.0542	6.3	381	141	337	22	330	14	13
KLS-2_L_183	17	20	2	1.17	196	0.711	19.0	0.0886	5.4	0.28	11.283	5.4	0.0582	18.2	536	399	545	80	547	28	-2
KLS-2_L_184	445	158	12	0.36	577	0.183	7.9	0.0255	6.6	0.83	39.184	6.6	0.0521	4.3	290	97	171	12	162	11	44
KLS-2_L_185	54	29	3	0.54	52	0.412	8.7	0.0493	5.4	0.61	20.303	5.4	0.0607	6.8	628	147	350	26	310	16	51
KLS-2_L_186	358	168	10	0.47	504	0.171	8.2	0.0258	4.9	0.59	38.805	4.9	0.0483	6.5	112	154	161	12	164	8	-46
KLS-2_L_187	381	107	13	0.28	1734	0.209	10.7	0.0315	8.2	0.77	31.705	8.2	0.0480	6.8	100	162	193	19	200	16	-101
KLS-2_L_188	416	200	15	0.48	874	0.228	9.8	0.0312	8.4	0.85	32.083	8.4	0.0531	5.1	332	115	209	19	198	16	40
KLS-2_L_189	442	245	15	0.55	1276	0.235	9.3	0.0289	6.5	0.69	34.596	6.5	0.0591	6.6	569	144	215	18	184	12	68
KLS-2_L_190	66	28	4	0.43	152	0.389	9.5	0.0529	4.8	0.49	18.901	4.8	0.0534	8.3	345	187	334	27	332	16	4
KLS-2_L_191	165	82	9	0.50	1533	0.407	7.8	0.0512	3.4	0.42	19.549	3.4	0.0577	7.0	519	154	347	23	322	11	38
KLS-2_L_192	405	198	22	0.49	3678	0.330	8.2	0.0471	5.2	0.62	21.246	5.2	0.0508	6.4	231	147	289	21	296	15	-28
KLS-2_L_193	165	61	9	0.37	4818	0.359	6.9	0.0521	4.3	0.62	19.200	4.3	0.0500	5.4	194	125	311	19	327	14	-69
KLS-2_L_194	293	63	7	0.22	3826	0.163	8.3	0.0247	4.5	0.53	40.544	4.5	0.0479	6.9	94	164	153	12	157	7	-67
KLS-2_L_195	158	58	5	0.37	325	0.182	13.6	0.0269	5.9	0.43	37.203	5.9	0.0492	12.3	158	287	170	21	171	10	-8
KLS-2_L_196	224	115	11	0.51	460	0.304	6.7	0.0437	3.9	0.57	22.876	3.9	0.0504	5.4	214	126	269	16	276	11	-29
KLS-2_L_197	72	24	4	0.33	417	0.416	9.6	0.0577	4.7	0.48	17.337	4.7	0.0524	8.3	301	190	353	29	362	17	-20
KLS-2_L_198	107	50	3	0.47	388	0.172	14.7	0.0291	5.1	0.34	34.348	5.1	0.0428	13.8	-182	344	161	22	185	9	202
KLS-2_L_199	97	22	5	0.22	2528	0.323	9.6	0.0455	5.0	0.51	21.975	5.0	0.0515	8.2	263	189	284	24	287	14	-9
KLS-2_L_200	192	68	6	0.35	584	0.214	7.6	0.0310	5.2	0.68	32.292	5.2	0.0501	5.5	200	129	197	14	197	10	2
KLS-2_L_201	150	67	29	0.45	3494	1.632	5.6	0.1649	5.0	0.87	6.065	5.0	0.0718	2.6	980	53	983	35	984	46	0
KLS-2_L_202	98	53	5	0.53	168	0.375	8.0	0.0489	4.2	0.51	20.441	4.2	0.0556	6.8	435	152	323	22	308	13	29
KLS-2_L_203	87	22	5	0.26	1132	0.350	10.7	0.0514	5.7	0.53	19.452	5.7	0.0494	9.0	166	211	305	28	323	18	-94
KLS-2_L_204	144	52	4	0.36	164	0.202	12.6	0.0283	5.1	0.40	35.356	5.1	0.0517	11.5	272	264	186	21	180	9	34
KLS-2_L_205	102	41	3	0.40	175	0.203	9.3	0.0294	4.8	0.50	33.962	4.8	0.0499	8.0	192	187	187	16	187	9	2
KLS-2_L_206	660	287	18	0.44	1546	0.158	7.4	0.0242	4.5	0.60	41.371	4.5	0.0475	5.8	75	139	149	10	154	7	-106
KLS-2_L_207	170	96	8	0.56	890	0.303	8.0	0.0413	5.5	0.68	24.191	5.5	0.0532	5.8	339	131	269	19	261	14	23
KLS-2_L_208	62	21	3	0.35	410	0.377	9.6	0.0531	5.8	0.60	18.829	5.8	0.0515	7.6	262	175	325	27	334	19	-27
KLS-2_L_209	305	107	10	0.35	289	0.194	6.1	0.0292	3.7	0.59	34.257	3.7	0.0483	4.9	112	115	180	10	185	7	-66
KLS-2_L_210	299	95	8	0.32	706	0.151	8.9	0.0248	5.5	0.61	40.368	5.5	0.0443	7.0	-92	171	143	12	158	9	272
KLS-2_L_211	229	100	12	0.44	239	0.372	8.7	0.0460	5.0	0.57	21.758	5.0	0.0587	7.1	557	154	321	24	290	14	48

KLS-2_L_212	232	64	7	0.27	1491	0.188	7.2	0.0296	4.9	0.67	33.777	4.9	0.0462	5.3	6	126	175	12	188	9	-3287
KLS-2_L_213	515	259	14	0.50	3425	0.154	7.9	0.0234	3.5	0.43	42.736	3.5	0.0479	7.1	93	168	146	11	149	5	-60
KLS-2_L_214	239	112	7	0.47	2406	0.167	8.0	0.0270	3.1	0.37	37.062	3.1	0.0449	7.4	-59	180	157	12	172	5	390
KLS-2_L_215	251	68	7	0.27	543	0.182	6.8	0.0280	4.1	0.59	35.670	4.1	0.0470	5.4	49	130	170	11	178	7	-261
KLS-2_L_216	131	60	8	0.46	309	0.365	9.1	0.0518	4.6	0.49	19.299	4.6	0.0510	7.9	243	181	316	25	326	15	-34
KLS-2_L_217	757	857	42	1.13	2174	0.279	4.7	0.0376	3.3	0.69	26.609	3.3	0.0538	3.3	364	74	250	10	238	8	35
KLS-2_L_218	71	13	4	0.18	125	0.373	9.5	0.0500	4.2	0.43	19.998	4.2	0.0542	8.6	378	193	322	26	315	13	17
KLS-2_L_219	233	77	7	0.33	3366	0.216	8.1	0.0288	4.0	0.49	34.694	4.0	0.0543	7.0	384	158	198	15	183	7	52
KLS-2_L_220	107	86	5	0.80	321	0.295	11.2	0.0415	5.7	0.51	24.087	5.7	0.0516	9.6	267	220	263	26	262	15	2
KLS-2_L_221	454	175	12	0.39	1977	0.175	5.5	0.0250	3.7	0.65	39.989	3.7	0.0508	4.1	233	95	164	8	159	6	32
KLS-2_L_222	136	83	4	0.61	1379	0.186	9.5	0.0273	4.5	0.46	36.567	4.5	0.0492	8.4	158	197	173	15	174	8	-10
KLS-2_L_223	97	50	5	0.52	283	0.281	9.8	0.0431	5.2	0.52	23.205	5.2	0.0473	8.3	62	197	251	22	272	14	-337
KLS-2_L_224	367	93	12	0.25	2149	0.213	7.1	0.0308	4.9	0.68	32.507	4.9	0.0503	5.1	210	119	196	13	195	9	7
KLS-2_L_225	62	20	3	0.33	2498	0.346	10.7	0.0421	4.5	0.42	23.775	4.5	0.0597	9.7	592	209	302	28	266	12	55
KLS-2_L_226	132	70	4	0.53	292	0.196	8.3	0.0296	3.0	0.35	33.810	3.0	0.0480	7.7	98	182	181	14	188	5	-92
KLS-2_L_227	383	149	10	0.39	688	0.169	7.8	0.0247	4.9	0.62	40.497	4.9	0.0497	6.0	179	141	159	11	157	8	12
KLS-2_L_228	154	103	8	0.67	351	0.294	7.6	0.0415	4.7	0.61	24.078	4.7	0.0513	5.9	253	136	261	17	262	12	-4
KLS-2_L_229	143	89	7	0.62	209	0.294	9.0	0.0435	5.0	0.55	22.990	5.0	0.0491	7.4	151	175	262	21	274	13	-82
KLS-2_L_230	156	60	5	0.38	194	0.209	10.2	0.0310	4.4	0.42	32.215	4.4	0.0487	9.2	135	216	192	18	197	8	-46
KLS-2_L_231	324	119	11	0.37	608	0.208	5.7	0.0301	4.2	0.72	33.272	4.2	0.0503	3.8	208	89	192	10	191	8	8
KLS-2_L_232	166	69	9	0.42	200	0.363	8.0	0.0483	3.4	0.41	20.709	3.4	0.0545	7.2	390	162	314	21	304	10	22
KLS-2_S_234	689	120	17	0.17	2980	0.173	6.4	0.0242	3.8	0.57	41.278	3.8	0.0519	5.2	280	120	162	10	154	6	45
KLS-2_S_235	146	107	7	0.73	1065	0.287	9.3	0.0413	4.5	0.48	24.194	4.5	0.0503	8.1	211	187	256	21	261	12	-24
KLS-2_S_236	442	198	12	0.45	1325	0.168	6.2	0.0245	3.8	0.61	40.814	3.8	0.0498	4.8	184	112	158	9	156	6	15
KLS-2_S_237	189	83	6	0.44	419	0.209	9.6	0.0306	6.0	0.62	32.676	6.0	0.0495	7.4	174	174	193	17	194	12	-12
KLS-2_S_238	466	183	31	0.39	7241	0.448	6.3	0.0583	5.2	0.82	17.160	5.2	0.0558	3.5	444	77	376	20	365	18	18
KLS-2_S_239	789	361	21	0.46	827	0.157	6.9	0.0232	4.4	0.63	43.139	4.4	0.0492	5.3	156	124	148	10	148	6	5
KLS-2_S_240	191	60	10	0.31	1247	0.357	6.8	0.0502	5.0	0.72	19.924	5.0	0.0516	4.6	267	106	310	18	316	15	-18
KLS-2_S_241	246	101	8	0.41	1587	0.199	8.8	0.0280	4.1	0.45	35.752	4.1	0.0516	7.7	266	177	184	15	178	7	33
KLS-2_S_242	81	19	4	0.24	226	0.374	9.7	0.0503	5.0	0.50	19.887	5.0	0.0539	8.4	367	188	322	27	316	15	14
KLS-2_S_243	110	125	4	1.13	698	0.207	13.9	0.0281	7.0	0.50	35.649	7.0	0.0536	12.0	352	270	191	24	178	12	49
KLS-2_S_244	367	126	27	0.34	5141	0.615	14.0	0.0601	4.4	0.30	16.646	4.4	0.0743	13.3	1048	269	487	54	376	16	64
KLS-2_S_245	676	298	18	0.44	1299	0.154	8.5	0.0230	4.4	0.49	43.501	4.4	0.0487	7.3	132	173	146	12	146.5	6	-11
KLS-2_S_246	376	248	13	0.66	1313	0.211	8.4	0.0280	3.7	0.42	35.735	3.7	0.0547	7.5	399	169	194	15	178	7	55
KLS-2_S_247	195	59	64	0.30	6590	3.805	3.3	0.2597	2.7	0.71	3.851	2.7	0.1063	2.0	1736	37	1594	27	1488	35	14
KLS-2_S_248	275	168	16	0.61	786	0.393	5.7	0.0499	3.8	0.64	20.043	3.8	0.0571	4.2	497	93	337	16	314	12	37
KLS-2_S_249	227	47	7	0.21	549	0.197	8.9	0.0290	3.9	0.42	34.509	3.9	0.0494	8.0	165	186	183	15	184	7	-12

KLS-2_S_250	223	22	40	0.10	680	1.712	5.1	0.1594	3.6	0.66	6.272	3.6	0.0779	3.6	1144	72	1013	33	954	32	17
KLS-2_S_251	143	42	5	0.29	543	0.235	8.4	0.0319	3.2	0.36	31.312	3.2	0.0534	7.8	348	175	215	16	203	6	42
KLS-2_S_252	364	135	13	0.37	888	0.207	5.8	0.0311	4.0	0.65	32.179	4.0	0.0483	4.3	114	101	191	10	197	8	-72
KLS-2_S_253	167	80	6	0.48	511	0.200	12.1	0.0314	5.6	0.45	31.854	5.6	0.0462	10.8	10	259	185	21	199	11	-1874
KLS-2_S_255	125	56	37	0.45	927	3.031	5.6	0.2413	4.5	0.77	4.144	4.5	0.0911	3.3	1449	63	1416	43	1394	56	4
KLS-2_S_257	361	299	18	0.83	5580	0.278	7.6	0.0399	5.9	0.76	25.080	5.9	0.0506	4.8	221	111	249	17	252	15	-14
KLS-2_S_258	296	151	11	0.51	940	0.206	9.3	0.0311	4.7	0.49	32.195	4.7	0.0480	8.0	101	190	190	16	197	9	-94
KLS-2_S_260	1063	795	34	0.75	9000	0.183	8.7	0.0249	5.5	0.62	40.135	5.5	0.0533	6.7	343	152	171	14	159	9	54
KLS-2_S_261	197	116	12	0.59	646	0.398	7.5	0.0533	4.0	0.50	18.768	4.0	0.0542	6.4	379	143	340	22	335	13	12
KLS-2_S_262	172	81	6	0.47	297	0.217	8.4	0.0302	6.0	0.69	33.148	6.0	0.0522	6.0	295	136	200	15	192	11	35
KLS-2_S_263	331	119	10	0.36	325	0.194	7.2	0.0277	4.1	0.54	36.050	4.1	0.0506	5.9	223	137	180	12	176	7	21
KLS-2_S_264	206	76	7	0.37	1142	0.203	10.4	0.0293	6.4	0.60	34.156	6.4	0.0503	8.3	209	191	188	18	186	12	11
KLS-2_S_265	280	17	7	0.06	450	0.176	9.2	0.0268	5.1	0.54	37.321	5.1	0.0476	7.6	80	181	165	14	170	9	-114
KLS-2_S_267	387	43	10	0.11	255	0.166	9.0	0.0249	5.6	0.61	40.146	5.6	0.0482	7.1	111	167	156	13	159	9	-43
KLS-2_S_268	205	80	7	0.39	2838	0.188	10.5	0.0290	4.8	0.44	34.501	4.8	0.0471	9.4	56	223	175	17	184	9	-226
KLS-2_S_269	274	84	8	0.30	522	0.193	9.1	0.0273	3.9	0.40	36.604	3.9	0.0512	8.2	249	190	179	15	174	7	30
KLS-2_S_270	182	95	55	0.52	5179	2.928	5.7	0.2356	5.4	0.92	4.244	5.4	0.0901	1.9	1428	37	1389	44	1364	67	4
KLS-2_S_271	73	26	4	0.36	2557	0.370	11.6	0.0521	4.4	0.36	19.185	4.4	0.0514	10.7	261	246	319	32	328	14	-26
KLS-2_S_272	93	34	4	0.37	7224	0.303	9.4	0.0437	4.0	0.41	22.889	4.0	0.0503	8.5	209	197	269	22	276	11	-32
KLS-2_S_273	121	33	7	0.27	698	0.362	10.7	0.0524	5.0	0.45	19.080	5.0	0.0502	9.4	202	219	314	29	329	16	-63
KLS-2_S_274	175	120	9	0.69	671	0.329	10.3	0.0442	3.6	0.32	22.625	3.6	0.0540	9.7	370	218	289	26	279	10	25
KLS-2_S_275	300	79	10	0.26	719	0.229	6.7	0.0324	4.2	0.60	30.884	4.2	0.0513	5.2	254	119	209	13	205	9	19
KLS-2_S_276	230	256	9	1.11	3369	0.196	10.2	0.0297	5.4	0.51	33.626	5.4	0.0477	8.7	85	207	181	17	189	10	-122
KLS-2_S_277	254	198	8	0.78	360	0.185	11.7	0.0267	5.0	0.42	37.453	5.0	0.0502	10.5	205	244	172	18	170	8	17
KLS-2_S_278	79	28	5	0.36	205	0.380	10.6	0.0530	3.7	0.33	18.874	3.7	0.0520	9.9	285	227	327	30	333	12	-17
KLS-2_S_279	82	30	2	0.36	205	0.194	15.1	0.0268	7.4	0.49	37.268	7.4	0.0524	13.1	304	299	180	25	171	13	44
KLS-2_S_280	245	242	11	0.99	229	0.256	8.4	0.0358	4.6	0.53	27.939	4.6	0.0518	7.0	278	160	231	17	227	10	18
KLS-2_S_281	222	243	8	1.09	405	0.188	7.7	0.0271	4.3	0.53	36.902	4.3	0.0502	6.5	206	150	175	12	172	7	16
KLS-2_S_282	850	598	55	0.70	4579	0.368	11.0	0.0498	10.6	0.95	20.072	10.6	0.0536	3.1	356	70	318	30	313	32	12
KLS-2_S_283	164	65	6	0.40	200	0.223	8.4	0.0318	3.9	0.44	31.427	3.9	0.0509	7.5	238	172	205	16	202	8	15
KLS-2_S_284	123	58	7	0.48	4327	0.384	10.3	0.0525	4.9	0.46	19.064	4.9	0.0532	9.0	336	205	330	29	330	16	2
KLS-2_S_285	237	125	8	0.53	1559	0.214	8.3	0.0301	5.5	0.65	33.212	5.5	0.0516	6.2	266	142	197	15	191	10	28
KLS-2_S_286	65	54	3	0.83	152	0.261	11.3	0.0429	3.7	0.31	23.327	3.7	0.0442	10.7	-99	262	236	24	271	10	374
KLS-2_S_287	835	340	23	0.41	3663	0.170	6.7	0.0244	5.5	0.80	41.024	5.5	0.0506	3.9	220	89	159	10	155	8	30
KLS-2_S_288	1011	89	27	0.09	1137	0.176	6.2	0.0255	4.1	0.63	39.218	4.1	0.0500	4.6	195	107	164	9	162	7	17
KLS-2_S_290	113	52	6	0.46	657	0.391	7.4	0.0506	3.4	0.44	19.746	3.4	0.0560	6.5	452	144	335	21	318	11	30
KLS-2_S_291	101	51	6	0.50	626	0.390	10.4	0.0515	3.9	0.35	19.405	3.9	0.0549	9.7	408	217	334	30	324	12	21

KLS-2_S_292	214	94	8	0.44	1189	0.227	11.1	0.0328	5.3	0.46	30.473	5.3	0.0503	9.8	208	228	208	21	208	11	0
KLS-2_S_293	315	183	17	0.58	1919	0.355	5.5	0.0468	4.2	0.73	21.388	4.2	0.0551	3.5	418	79	309	15	295	12	29
KLS-2_S_294	432	186	23	0.43	5731	0.351	9.0	0.0455	6.3	0.69	21.986	6.3	0.0560	6.5	452	144	306	24	287	18	37
KLS-2_S_295	117	158	43	1.35	16222	3.404	4.8	0.2421	3.8	0.75	4.130	3.8	0.1020	2.9	1660	53	1505	37	1398	48	16
KLS-2_S_296	325	170	11	0.52	4463	0.208	6.4	0.0285	4.8	0.72	35.142	4.8	0.0529	4.3	325	98	192	11	181	9	44
KLS-2_S_297	377	209	26	0.56	11040	0.477	10.8	0.0584	9.1	0.83	17.121	9.1	0.0592	5.9	576	128	396	35	366	32	36
KLS-2_S_298	109	44	5	0.41	968	0.279	9.8	0.0415	5.9	0.59	24.073	5.9	0.0488	7.8	138	183	250	22	262	15	-90
KLS-2_S_299	248	73	7	0.30	953	0.182	9.4	0.0264	4.3	0.43	37.863	4.3	0.0499	8.4	192	195	170	15	168	7	12

Notes: Isotope ratios and ages are reported without initial common Pb correction; gas blank-corrected mass 204 signals were generally irresolvable from zero.

Isotope ratio and apparent age errors do NOT include systematic calibration errors of 0.25% for the $^{207}\text{Pb}/^{206}\text{Pb}$ ratio, and 0.56% for the $^{206}\text{Pb}/^{238}\text{U}$ ratio (1s).

Trace element concentrations in ppm, calculated using the mean count rate method, internal standardization to ^{29}Si , and calibration to NIST 610 and 612 glass standards.

Ablation using a 213 nm wavelength laser, spot size of 25 microns, repetition rate of 10 Hz, and fluence of ~5 J/cm².

APPENDIX B

**U-Pb Isotopic Data for Magmatic and Detrital Zircon Analyzed By LA-ICPMS and
CA-IDTIMS From Chapter 3**

Table B.1. U-Pb Isotopic Data for Magmatic Zircon from the Jackson Mountains for Chapter 3

Samp. (a)	Compositional Parameters					Radiogenic Isotope Ratios							Isotopic Ages						
	$\frac{^{206}\text{Pb}^*}{^{204}\text{Pb}}$ x10 ⁻¹³	mol %	$\frac{\text{Pb}^*}{\text{Pbc}}$	$\frac{\text{Pbc}}{\text{pg}}$	$\frac{^{206}\text{Pb}}{^{204}\text{Pb}}$	$\frac{^{208}\text{Pb}}{^{206}\text{Pb}}$	$\frac{^{207}\text{Pb}}{^{206}\text{Pb}}$	% err (e)	$\frac{^{207}\text{Pb}}{^{235}\text{U}}$	% err (e)	$\frac{^{206}\text{Pb}}{^{238}\text{U}}$	% err (e)	corr. coef.	$\frac{^{207}\text{Pb}}{^{206}\text{Pb}}$	± (f)	$\frac{^{207}\text{Pb}}{^{235}\text{U}}$	± (f)	$\frac{^{206}\text{Pb}}{^{238}\text{U}}$	± (e)
	(b)	(b)	(b)	(b)	(c)	(d)	(d)	(e)	(d)	(e)	(d)	(e)	(f)	(e)	(f)	(e)	(f)	(e)	(f)
HC-JM-1 (Happy Creek Igneous Complex)																			
z1a	2.0787	99.5%	55	0.90	3502	0.103	0.049928	0.099	0.206258	0.158	0.029961	0.070	0.909	191.66	2.30	190.41	0.27	190.31	0.13
z1b	0.3501	98.9%	27	0.31	1701	0.124	0.049922	0.264	0.206311	0.318	0.029973	0.084	0.725	191.38	6.13	190.45	0.55	190.38	0.16
z2	1.0567	99.7%	84	0.30	5325	0.109	0.049962	0.131	0.206331	0.187	0.029952	0.081	0.805	193.23	3.05	190.47	0.33	190.25	0.15
z4	0.8136	99.6%	80	0.26	4682	0.200	0.049974	0.172	0.206777	0.221	0.030009	0.075	0.754	193.79	3.99	190.84	0.38	190.61	0.14
z5	0.4329	99.2%	36	0.28	2331	0.096	0.049796	0.293	0.205662	0.341	0.029954	0.077	0.693	185.50	6.82	189.91	0.59	190.26	0.14
z6	0.2233	97.9%	14	0.40	856	0.169	0.049604	0.597	0.204887	0.651	0.029957	0.104	0.576	176.50	13.92	189.25	1.12	190.28	0.20
z7	0.1942	98.4%	19	0.26	1137	0.169	0.049692	0.503	0.205260	0.553	0.029958	0.110	0.531	180.60	11.72	189.57	0.96	190.29	0.21
HGP-1 (Harrison Grove pluton)																			
z1	0.3836	97.9%	15	0.70	847	0.281	0.049790	0.438	0.204546	0.492	0.029795	0.086	0.678	185.22	10.20	188.97	0.85	189.27	0.16
z2	0.1683	96.7%	9	0.47	554	0.197	0.049305	1.250	0.202515	1.345	0.029790	0.111	0.870	162.34	29.23	187.25	2.30	189.23	0.21
z3	0.2380	97.7%	13	0.47	781	0.196	0.049526	0.693	0.203403	0.757	0.029787	0.097	0.688	172.81	16.18	188.00	1.30	189.21	0.18
z4	0.6389	99.1%	37	0.47	2066	0.252	0.049840	0.335	0.204830	0.381	0.029807	0.077	0.671	187.54	7.79	189.21	0.66	189.34	0.14
z5	0.6973	99.4%	49	0.36	2880	0.189	0.049763	0.221	0.204617	0.269	0.029822	0.074	0.738	183.93	5.14	189.03	0.46	189.43	0.14
WCP-1 (Willow Creek pluton)																			
z1	0.2457	96.9%	10	0.65	582	0.227	0.049188	0.861	0.172434	0.925	0.025425	0.126	0.556	156.81	20.15	161.53	1.38	161.85	0.20
z2	0.3203	97.5%	12	0.69	714	0.216	0.049239	0.659	0.172609	0.724	0.025424	0.094	0.722	159.24	15.42	161.68	1.08	161.85	0.15
z3	0.4473	93.9%	5	2.39	302	0.166	0.049522	0.659	0.173604	0.717	0.025425	0.118	0.552	172.63	15.38	162.54	1.08	161.85	0.19
z4	0.3702	98.1%	18	0.58	977	0.277	0.049184	0.611	0.172328	0.669	0.025412	0.098	0.635	156.60	14.31	161.44	1.00	161.77	0.16
z5	0.5010	98.3%	18	0.72	1064	0.223	0.049248	0.415	0.172570	0.466	0.025414	0.082	0.679	159.66	9.70	161.65	0.70	161.78	0.13

(a) z1, z2, etc., are labels for fractions composed of single zircon or fragments; all zircon fractions were annealed and chemically abraded after Mattinson (2005)

(b) Pb* and Pbc represent radiogenic and common Pb, respectively; mol % 206Pb* with respect to radiogenic, blank and initial common Pb.

(c) Measured ratio corrected for spike and fractionation only. Fractionation estimated at 0.17 ± 0.03 (1-sigma) %/amu for Daly analyses, based on analysis of NBS-981 and NBS-982.

(d) Corrected for fractionation, spike, and common Pb; all common Pb was assumed to be procedural blank: 206Pb/204Pb = 18.042 ± 0.61%; 207Pb/204Pb = 15.537 ± 0.52%;

208Pb/204Pb = 37.686 ± 0.63% (all uncertainties 1-sigma).

(e) Errors are 2-sigma, propagated using the algorithms of Schmitz and Schoene (2007).

(f) Calculations are based on the decay constants of Jaffey et al. (1971). 206Pb/238U and 207Pb/206Pb ages corrected for initial disequilibrium in 230Th/238U using Th/U [magma] = 3.

Table B.2. U-Pb Isotopic Data for Detrital Zircon from the Jackson Mountains for Chapter 3

Samp.	Compositional Parameters					Radiogenic Isotope Ratios						Isotopic Ages											
	$^{206}\text{Pb}^*$ x10 ⁻¹³ mol	mol %	$\frac{\text{Pb}^*}{\text{Pbc}}$	$\frac{\text{Pbc}}{\text{Pb}^*}$	$\frac{^{206}\text{Pb}}{^{204}\text{Pb}}$	$\frac{^{208}\text{Pb}}{^{206}\text{Pb}}$	$\frac{^{207}\text{Pb}}{^{206}\text{Pb}}$	% err	$\frac{^{207}\text{Pb}}{^{235}\text{U}}$	% err	$\frac{^{206}\text{Pb}}{^{238}\text{U}}$	% err	corr.	$\frac{^{207}\text{Pb}}{^{206}\text{Pb}}$	\pm	$\frac{^{207}\text{Pb}}{^{235}\text{U}}$	\pm	$\frac{^{206}\text{Pb}}{^{238}\text{U}}$	\pm				
(a)	(b)	(b)	(b)	(c)	(d)	(d)	(e)	(d)	(e)	(d)	(e)	(d)	(e)	(f)	(e)	(f)	(e)	(f)	(e)	(f)	(e)	(f)	(e)
BCB-1 (Boulder Creek Beds – subunit 1)																							
z1	0.0870	95.6%	6	0.33	408	0.155	0.049698	1.961	0.233868	2.054	0.034130	0.163	0.600	180.88	45.69	213.39	3.95	216.34	0.35				
z2	0.0678	93.1%	4	0.42	260	0.111	0.046079	8.457	0.215547	8.897	0.033926	0.674	0.673	1.75	203.75	198.20	16.02	215.08	1.43				
z4	0.1827	96.6%	8	0.53	533	0.143	0.049708	1.661	0.232769	1.768	0.033962	0.171	0.655	181.36	38.70	212.48	3.39	215.30	0.36				
z5	1.0878	99.5%	61	0.41	3970	0.079	0.050451	0.151	0.236343	0.202	0.033976	0.072	0.805	215.82	3.49	215.42	0.39	215.39	0.15				
BCB-2 (Boulder Creek Beds – subunit 2)																							
z3	0.3859	98.9%	25	0.36	1605	0.107	0.049975	0.499	0.212577	0.551	0.030851	0.083	0.666	193.81	11.61	195.71	0.98	195.87	0.16				
z4	0.2358	98.0%	13	0.41	882	0.074	0.049484	0.849	0.209802	0.918	0.030750	0.109	0.674	170.82	19.82	193.39	1.62	195.24	0.21				
z5	0.5858	99.2%	35	0.40	2200	0.113	0.050030	0.262	0.212143	0.312	0.030754	0.079	0.708	196.40	6.09	195.35	0.56	195.26	0.15				
z6	0.2187	97.6%	12	0.44	764	0.109	0.049491	0.824	0.210352	0.907	0.030826	0.060	1.347	171.18	19.22	193.85	1.60	195.71	0.12				
BCB-3 (Boulder Creek Beds – subunit 3)																							
z1	0.0957	95.5%	6	0.38	398	0.100	0.049909	1.725	0.218292	1.831	0.031722	0.173	0.645	190.77	40.11	200.49	3.33	201.31	0.34				
z2	0.1139	95.8%	7	0.41	434	0.116	0.049761	1.129	0.217586	1.218	0.031713	0.129	0.718	183.85	26.29	199.90	2.21	201.26	0.26				
z3	0.0713	89.6%	2	0.69	174	0.082	0.048662	3.026	0.212634	3.191	0.031691	0.297	0.589	131.59	71.14	195.76	5.68	201.12	0.59				
z4	0.0488	90.0%	3	0.45	180	0.095	0.052326	9.135	0.229697	9.266	0.031837	0.352	0.389	299.69	208.31	209.95	17.57	202.04	0.70				
z6	0.6233	97.9%	13	1.09	877	0.075	0.050044	0.331	0.218886	0.381	0.031722	0.086	0.662	197.04	7.68	200.98	0.70	201.32	0.17				
z7	0.2277	95.4%	6	0.91	393	0.084	0.050790	1.059	0.221990	1.149	0.031700	0.093	0.973	231.30	24.44	203.56	2.12	201.18	0.18				
BCB-5 (Boulder Creek Beds – subunit 5)																							
z2	0.1313	93.9%	4	0.71	296	0.113	0.050641	1.215	0.227493	1.309	0.032581	0.139	0.708	224.52	28.08	208.13	2.46	206.68	0.28				
z3	0.0821	70.9%	1	2.79	63	0.122	0.052316	3.961	0.236581	4.073	0.032798	0.468	0.294	299.23	90.33	215.62	7.91	208.04	0.96				
z4	0.1076	96.9%	9	0.28	588	0.108	0.050444	1.046	0.227428	1.131	0.032699	0.129	0.694	215.49	24.22	208.07	2.13	207.42	0.26				
z5	0.4175	99.0%	28	0.36	1752	0.133	0.050023	0.296	0.222891	0.349	0.032316	0.077	0.739	196.06	6.89	204.31	0.65	205.03	0.16				
z6	0.1931	97.9%	14	0.34	868	0.128	0.049839	0.688	0.223532	0.754	0.032529	0.098	0.709	187.51	16.02	204.84	1.40	206.35	0.20				

(a) z1, z2, etc., are labels for fractions composed of single zircon or fragments; all zircon fractions were annealed and chemically abraded after Mattinson (2005)

(b) Pb* and Pbc represent radiogenic and common Pb, respectively; mol % 206Pb* with respect to radiogenic, blank and initial common Pb.

(c) Measured ratio corrected for spike and fractionation only. Fractionation estimated at 0.17 ± 0.03 (1-sigma) %/amu for Daly analyses, based on analysis of NBS-981 and NBS-982.

(d) Corrected for fractionation, spike, and common Pb; all common Pb was assumed to be procedural blank: $206\text{Pb}/204\text{Pb} = 18.042 \pm 0.61\%$; $207\text{Pb}/204\text{Pb} = 15.537 \pm 0.52\%$;

$^{208}\text{Pb}/^{204}\text{Pb} = 37.686 \pm 0.63\%$ (all uncertainties 1-sigma).

(e) Errors are 2-sigma, propagated using the algorithms of Schmitz and Schoene (2007).

(f) Calculations are based on the decay constants of Jaffey et al. (1971). $^{206}\text{Pb}/^{238}\text{U}$ and $^{207}\text{Pb}/^{206}\text{Pb}$ ages corrected for initial disequilibrium in $^{230}\text{Th}/^{238}\text{U}$ using Th/U [magma] = 3.

Table B.3. Magmatic Zircon LA-ICPMS U-Pb Geochronology for Chapter 3

Analysis	Composition						Corrected isotope ratios						Apparent ages (Ma)											
	U ppm	Th ppm	Pb ppm	Th/U	$\frac{^{206}\text{Pb}}{^{204}\text{Pb}}$	$\frac{^{207}\text{Pb}}{^{235}\text{U}}$	$\pm 2s$ (%)	$\frac{^{206}\text{Pb}}{^{238}\text{U}}$	$\pm 2s$ (%)	error corr.	$\frac{^{238}\text{U}}{^{206}\text{Pb}}$	$\pm 2s$ (%)	$\frac{^{207}\text{Pb}}{^{206}\text{Pb}}$	$\pm 2s$ (%)	$\frac{^{207}\text{Pb}}{^{206}\text{Pb}}$ (abs)	$\pm 2s$ (%)	$\frac{^{207}\text{Pb}}{^{235}\text{U}}$ (abs)	$\pm 2s$ (%)	$\frac{^{206}\text{Pb}}{^{238}\text{U}}$ (abs)	$\pm 2s$ (%)	% disc.			
HC-JM-1 (Happy Creek Igneous Complex)																								
HC-JM-1_L_28	187	83	7	0.44	356	0.229	7.8	0.0310	4.7	0.60	32.283	4.70	0.0536	6.2	355	141	209	15	197	9	45			
HC-JM-1_L_29	280	187	11	0.67	145	0.205	7.7	0.0310	4.3	0.55	32.305	4.29	0.0480	6.4	97	150	189	13	197	8	-102			
HC-JM-1_L_31	292	113	11	0.39	434	0.210	9.4	0.0311	3.9	0.41	32.200	3.87	0.0492	8.5	155	200	194	17	197	8	-27			
HC-JM-1_L_32	166	98	6	0.59	433	0.210	11.2	0.0303	4.3	0.38	33.024	4.32	0.0502	10.4	204	240	193	20	192	8	6			
HC-JM-1_L_33	243	109	9	0.45	724	0.218	7.5	0.0309	4.4	0.58	32.371	4.36	0.0513	6.1	254	141	201	14	196	8	23			
HC-JM-1_L_34	147	56	5	0.38	67	0.224	8.1	0.0303	3.8	0.46	32.960	3.81	0.0536	7.2	354	163	205	15	193	7	46			
HC-JM-1_L_35	260	213	10	0.82	343	0.184	8.7	0.0297	3.3	0.38	33.690	3.33	0.0448	8.0	-64	195	171	14	189	6	394			
HC-JM-1_L_36	237	210	10	0.89	863	0.217	8.1	0.0308	4.0	0.49	32.464	4.00	0.0510	7.1	243	164	199	15	196	8	20			
HC-JM-1_L_38	223	113	8	0.51	103	0.224	7.6	0.0310	3.7	0.49	32.223	3.74	0.0524	6.6	304	150	206	14	197	7	35			
HC-JM-1_S_204	146	91	5	0.63	857	0.229	8.9	0.0298	3.6	0.40	33.568	3.60	0.0557	8.1	439	180	209	17	189	7	57			
HC-JM-1_S_205	141	101	5	0.71	93	0.215	10.9	0.0303	4.2	0.38	32.977	4.19	0.0514	10.1	259	232	198	20	193	8	26			
HC-JM-1_S_207	192	169	8	0.88	344	0.212	7.2	0.0310	3.9	0.54	32.207	3.90	0.0496	6.0	178	140	196	13	197	8	-11			
HC-JM-1_S_208	131	68	5	0.52	117	0.221	9.6	0.0308	3.6	0.37	32.441	3.60	0.0519	8.9	283	203	203	18	196	7	31			
HC-JM-1_S_210	323	162	12	0.50	213	0.214	6.6	0.0297	2.7	0.40	33.626	2.68	0.0522	6.0	296	137	197	12	189	5	36			
HC-JM-1_S_214	698	491	27	0.70	5958	0.237	10.1	0.0297	3.7	0.36	33.663	3.73	0.0578	9.4	522	207	216	20	189	7	64			
HC-JM-1_S_223	273	203	11	0.75	801	0.248	8.9	0.0297	2.9	0.32	33.714	2.89	0.0607	8.4	629	182	225	18	188	5	70			
HC-JM-1_S_230	310	106	11	0.34	160	0.204	6.3	0.0297	2.3	0.34	33.710	2.25	0.0499	5.9	189	137	188	11	188	4	0			
Analysis	Composition						Corrected isotope ratios						Apparent ages (Ma)											
	U ppm	Th ppm	Pb ppm	Th/U	$\frac{^{206}\text{Pb}}{^{204}\text{Pb}}$	$\frac{^{207}\text{Pb}}{^{235}\text{U}}$	$\pm 2s$ (%)	$\frac{^{206}\text{Pb}}{^{238}\text{U}}$	$\pm 2s$ (%)	error corr.	$\frac{^{238}\text{U}}{^{206}\text{Pb}}$	$\pm 2s$ (%)	$\frac{^{207}\text{Pb}}{^{206}\text{Pb}}$	$\pm 2s$ (%)	$\frac{^{207}\text{Pb}}{^{206}\text{Pb}}$ (abs)	$\pm 2s$ (%)	$\frac{^{207}\text{Pb}}{^{235}\text{U}}$ (abs)	$\pm 2s$ (%)	$\frac{^{206}\text{Pb}}{^{238}\text{U}}$ (abs)	$\pm 2s$ (%)	% disc.			
HGP-1 (Harrison Grove pluton)																								
HGP_L_7	468	777	22	1.66	1328	0.195	5.9	0.0280	4.4	0.75	35.656	4.4	0.0504	3.9	211	90	181	10	178	8	16			
HGP_L_9	179	175	7	0.97	286	0.197	6.4	0.0287	4.4	0.69	34.833	4.4	0.0499	4.6	189	107	183	11	182	8	3			
HGP_L_10	165	157	7	0.95	251	0.201	7.0	0.0293	3.4	0.48	34.081	3.4	0.0497	6.2	179	144	186	12	186	6	-4			
HGP_L_19	473	834	22	1.76	731	0.192	5.9	0.0278	3.3	0.56	36.020	3.3	0.0502	4.8	206	112	179	10	177	6	14			
HGP_L_20	457	752	21	1.65	585	0.196	4.6	0.0285	3.2	0.69	35.129	3.2	0.0499	3.4	189	78	182	8	181	6	4			
HGP_L_25	199	256	9	1.29	174	0.226	8.6	0.0281	3.9	0.46	35.615	3.9	0.0585	7.7	548	167	207	16	179	7	67			
HGP_L_26	144	122	5	0.85	138	0.187	7.0	0.0283	3.8	0.55	35.358	3.8	0.0479	5.9	92	139	174	11	180	7	-95			
HGP_L_27	274	357	12	1.30	2082	0.198	7.1	0.0291	4.6	0.65	34.360	4.6	0.0494	5.3	166	125	184	12	185	8	-11			

HGP_L_28	440	604	19	1.37	757	0.199	6.4	0.0283	5.2	0.82	35.348	5.2	0.0509	3.7	238	85	184	11	180	9	24
HGP_L_29	442	617	19	1.40	5626	0.200	6.2	0.0286	5.1	0.83	34.984	5.1	0.0506	3.4	224	79	185	10	182	9	19
HGP_L_30	392	652	18	1.66	459	0.194	5.9	0.0287	4.2	0.70	34.785	4.2	0.0489	4.2	144	99	180	10	183	7	-27
HGP_L_31	241	223	10	0.92	229	0.202	6.4	0.0285	4.6	0.73	35.041	4.6	0.0512	4.4	252	101	187	11	181.4	8	28
HGP_L_32	275	261	11	0.95	401	0.193	7.0	0.0284	4.9	0.69	35.253	4.9	0.0493	5.1	160	119	179	12	180	9	-13
HGP_L_33	318	356	13	1.12	219	0.197	7.1	0.0285	4.6	0.65	35.073	4.6	0.0501	5.3	202	124	183	12	181	8	10
HGP_L_34	279	320	11	1.14	1005	0.200	5.9	0.0285	4.6	0.78	35.064	4.6	0.0508	3.7	232	87	185	10	181	8	22
HGP_L_35	499	318	18	0.64	1014	0.197	5.5	0.0284	4.6	0.84	35.172	4.6	0.0501	2.9	202	68	182	9	181	8	10
HGP_M_95	438	482	17	1.10	1079370	0.222	7.9	0.0302	5.8	0.74	33.074	5.8	0.0532	5.3	338	121	203	15	192	11	43
HGP_M_99	756	940	33	1.24	37101	0.249	14.8	0.0313	5.9	0.40	31.970	5.9	0.0577	13.5	519	297	226	30	199	11	62
HGP_M_108	710	765	28	1.08	331	0.206	6.7	0.0293	5.2	0.77	34.108	5.2	0.0509	4.2	237	98	190	12	186	9	21
HGP_M_112	532	453	20	0.85	568	0.204	8.4	0.0296	5.8	0.70	33.738	5.8	0.0498	6.0	188	140	188	14	188	11	0
HGP_M_113	1045	1004	39	0.96	405	0.200	6.4	0.0282	4.0	0.62	35.468	4.0	0.0513	5.0	256	115	185	11	179	7	30
HGP_M_135	526	499	21	0.95	3040	0.202	8.0	0.0297	5.4	0.68	33.662	5.4	0.0493	5.9	162	139	187	14	189	10	-17
HGP_M_136	382	154	13	0.40	534	0.205	7.2	0.0300	5.3	0.74	33.311	5.3	0.0496	4.8	175	113	190	12	191	10	-9
HGP_M_137	755	697	31	0.92	297	0.242	9.8	0.0302	6.5	0.66	33.119	6.5	0.0582	7.4	539	162	220	20	192	12	64
HGP_M_139	196	132	8	0.67	713	0.248	7.9	0.0295	4.8	0.61	33.895	4.8	0.0609	6.3	634	135	225	16	187	9	70
HGP_M_140	187	133	8	0.71	810	0.244	10.2	0.0303	4.8	0.47	33.026	4.8	0.0584	9.0	545	197	222	20	192	9	65
HGP_M_145	334	162	12	0.49	1016	0.189	6.8	0.0291	5.0	0.74	34.395	5.0	0.0471	4.6	53	109	176	11	185	9	-248
HGP_M_147	298	204	11	0.69	154	0.204	8.0	0.0294	5.5	0.69	34.070	5.5	0.0505	5.8	216	135	189	14	186	10	14
HGP_M_149	862	875	36	1.01	636	0.206	7.5	0.0293	6.0	0.80	34.150	6.0	0.0510	4.4	242	102	190	13	186	11	23
HGP_M_150	267	140	9	0.52	263	0.187	8.0	0.0289	5.1	0.64	34.639	5.1	0.0471	6.2	52	147	174	13	183	9	-253
HGP_M_153	522	460	21	0.88	1463	0.186	6.6	0.0288	4.8	0.72	34.742	4.8	0.0468	4.5	39	109	173	10	183	9	-365
HGP_M_154	504	517	21	1.02	355	0.214	7.2	0.0291	5.6	0.78	34.358	5.6	0.0534	4.6	344	103	197	13	185	10	46
HGP_M_161	460	514	18	1.12	1222	0.196	6.7	0.0293	4.7	0.69	34.163	4.7	0.0485	4.9	122	114	181	11	186	9	-53
HGP_M_166	504	537	20	1.07	922	0.195	7.5	0.0288	4.9	0.65	34.737	4.9	0.0490	5.6	148	132	180	12	183	9	-24
HGP_M_167	343	324	13	0.95	300	0.215	6.3	0.0290	4.6	0.73	34.519	4.6	0.0539	4.3	366	97	198	11	184	8	50
HGP_M_168	395	396	16	1.00	406	0.214	7.5	0.0299	6.6	0.87	33.452	6.6	0.0519	3.7	281	84	197	13	190	12	32
HGP_M_173	554	518	22	0.94	856	0.212	6.4	0.0297	5.3	0.84	33.687	5.3	0.0519	3.5	280	79	195	11	189	10	33
HGP_S_595	264	131	10	0.49	390	0.200	8.9	0.0303	6.3	0.71	32.976	6.3	0.0478	6.3	87	149	185	15	193	12	-122
HGP_S_597	391	211	14	0.54	359	0.201	7.5	0.0297	6.3	0.84	33.673	6.3	0.0491	4.0	151	95	186	13	189	12	-25
HGP_S_600	579	517	23	0.89	590	0.201	6.8	0.0295	5.5	0.80	33.904	5.5	0.0495	4.1	172	96	186	12	187	10	-9
HGP_S_601	279	188	10	0.67	423	0.199	8.8	0.0290	5.3	0.61	34.476	5.3	0.0497	6.9	182	162	184	15	184	10	-1
HGP_S_602	532	462	21	0.87	510	0.209	9.4	0.0288	6.6	0.70	34.721	6.6	0.0526	6.7	311	152	193	16	183	12	41
HGP_S_604	383	322	15	0.84	156	0.198	7.2	0.0288	6.0	0.83	34.679	6.0	0.0499	4.0	190	94	184	12	183	11	3
HGP_S_611	332	273	13	0.82	175	0.212	7.0	0.0301	4.2	0.60	33.231	4.2	0.0510	5.5	242	128	195	12	191	8	21
HGP_S_613	395	323	16	0.82	2782	0.202	8.0	0.0292	5.9	0.73	34.201	5.9	0.0501	5.5	199	127	187	14	186	11	6

	721	774	33	1.07	248	0.263	10.5	0.0302	4.1	0.39	33.107	4.1	0.0632	9.7	714	205	237	22	192	8	73
HGP_S_615	566	481	23	0.85	1007	0.210	6.8	0.0293	5.2	0.76	34.146	5.2	0.0520	4.4	286	100	194	12	186	10	35
HGP_S_616	385	275	16	0.71	175	0.222	6.1	0.0312	4.8	0.78	32.048	4.8	0.0516	3.8	266	88	203	11	198	9	26
HGP_S_617	252	182	10	0.72	169	0.205	7.9	0.0297	4.7	0.60	33.664	4.7	0.0501	6.4	199	148	190	14	189	9	5
HGP_S_620	494	302	19	0.61	1513	0.216	6.8	0.0307	4.5	0.65	32.538	4.5	0.0510	5.1	241	119	199	12	195	9	19
HGP_S_623	298	187	13	0.63	525	0.307	8.5	0.0315	4.7	0.56	31.763	4.7	0.0706	7.1	947	145	272	20	200	9	79
HGP_S_626	374	303	15	0.81	5759	0.201	8.1	0.0297	5.4	0.66	33.720	5.4	0.0491	6.1	155	142	186	14	188	10	-22
HGP_S_630	547	352	23	0.64	508	0.284	9.4	0.0316	7.0	0.74	31.649	7.0	0.0651	6.3	778	132	254	21	201	14	74
Composition			Corrected isotope ratios												Apparent ages (Ma)						
Analysis	U	Th	Pb	Th/U	$\frac{^{206}\text{Pb}}{^{204}\text{Pb}}$	$\frac{^{207}\text{Pb}}{^{235}\text{U}}$	$\pm 2\sigma$	$\frac{^{206}\text{Pb}}{^{238}\text{U}}$	$\pm 2\sigma$	error	$\frac{^{238}\text{U}}{^{206}\text{Pb}}$	$\pm 2\sigma$	$\frac{^{207}\text{Pb}}{^{206}\text{Pb}}$	$\pm 2\sigma$	$\frac{^{207}\text{Pb}}{^{206}\text{Pb}}$	$\pm 2\sigma$	$\frac{^{207}\text{Pb}}{^{235}\text{U}}$	$\pm 2\sigma$	$\frac{^{206}\text{Pb}}{^{238}\text{U}}$	$\pm 2\sigma$	%
	ppm	ppm	ppm		(%)			$\frac{^{238}\text{U}}{^{206}\text{Pb}}$	(%)	corr.	$\frac{^{206}\text{Pb}}{^{206}\text{Pb}}$	(%)	$\frac{^{207}\text{Pb}}{^{206}\text{Pb}}$	(%)	$\frac{^{207}\text{Pb}}{^{206}\text{Pb}}$	(abs)	$\frac{^{207}\text{Pb}}{^{235}\text{U}}$	(abs)	disc.		
WCP-1 (Willow Creek pluton)																					
WCP_L_59	413	547	16	1.32	326	0.171	5.1	0.0253	3.2	0.64	39.526	3.2	0.0490	3.9	147	92	160	8	161	5	-10
WCP_L_60	414	569	16	1.38	803	0.172	5.5	0.0244	3.7	0.67	40.916	3.7	0.0511	4.1	245	95	161	8	156	6	37
WCP_L_61	95	67	3	0.70	79	0.161	10.1	0.0252	4.6	0.46	39.728	4.6	0.0464	9.0	19	217	152	14	160	7	-766
WCP_L_64	160	153	5	0.96	67	0.164	11.5	0.0246	3.6	0.32	40.729	3.6	0.0486	10.9	126	257	155	16	156	6	-24
WCP_L_65	357	653	15	1.83	280	0.173	6.1	0.0251	4.3	0.70	39.778	4.3	0.0498	4.4	187	103	162	9	160	7	15
WCP_L_67	361	495	14	1.37	594	0.172	6.1	0.0247	4.0	0.65	40.473	4.0	0.0505	4.7	216	108	161	9	157	6	27
WCP_L_69	488	653	19	1.34	1011	0.169	6.4	0.0248	4.6	0.71	40.277	4.6	0.0495	4.5	171	105	159	9	158	7	8
WCP_L_70	183	171	6	0.94	71	0.167	7.6	0.0242	4.9	0.64	41.271	4.9	0.0499	5.8	190	135	157	11	154	7	19
WCP_L_71	274	331	10	1.21	992	0.175	6.9	0.0248	4.2	0.61	40.366	4.2	0.0513	5.5	252	126	164	10	158	7	38
WCP_L_74	235	254	8	1.08	652	0.174	7.8	0.0245	5.3	0.68	40.792	5.3	0.0515	5.7	264	132	163	12	156	8	41
WCP_L_78	288	497	12	1.73	388	0.168	6.9	0.0244	4.8	0.69	41.003	4.8	0.0501	5.0	198	116	158	10	155	7	22
WCP_L_80	243	357	10	1.47	319	0.172	7.0	0.0246	5.0	0.72	40.617	5.0	0.0507	4.9	227	113	161	10	157	8	31
WCP_M_177	277	211	9	0.76	966	0.179	8.2	0.0254	4.9	0.60	39.348	4.9	0.0510	6.6	241	151	167	13	162	8	33
WCP_M_178	411	476	16	1.16	410	0.192	10.6	0.0252	4.8	0.46	39.684	4.8	0.0553	9.4	423	211	178	17	160	8	62
WCP_M_180	395	319	13	0.81	936	0.192	7.8	0.0251	4.5	0.57	39.766	4.5	0.0553	6.4	426	143	178	13	160	7	62
WCP_M_181	216	120	7	0.56	69	0.167	9.7	0.0251	4.7	0.48	39.798	4.7	0.0482	8.5	110	202	157	14	160	7	-46
WCP_M_184	213	131	7	0.61	277	0.192	8.3	0.0254	4.4	0.53	39.296	4.4	0.0547	7.0	400	157	178	14	162	7	59
WCP_M_195	235	200	8	0.85	226	0.163	9.1	0.0250	6.9	0.75	39.979	6.9	0.0474	6.0	69	143	154	13	159	11	-132
WCP_M_202	173	88	6	0.51	598	0.178	11.3	0.0261	5.6	0.49	38.319	5.6	0.0495	9.8	170	230	166	17	166	9	2
WCP_M_203	345	293	12	0.85	282	0.188	7.8	0.0254	6.1	0.78	39.310	6.1	0.0536	4.8	356	109	175	13	162	10	54
WCP_M_204	303	237	10	0.78	983	0.173	6.3	0.0245	4.8	0.75	40.798	4.8	0.0512	4.1	249	95	162	9	156	7	37
WCP_M_207	236	152	8	0.64	113	0.173	8.8	0.0256	7.1	0.80	39.089	7.1	0.0490	5.3	147	124	162	13	163	11	-11
WCP_M_209	408	440	14	1.08	165	0.173	6.9	0.0244	5.6	0.81	40.926	5.6	0.0513	4.1	252	94	162	10	156	9	38
WCP_M_210	149	81	5	0.54	119	0.188	12.9	0.0269	6.7	0.52	37.173	6.7	0.0508	11.1	230	256	175	21	171	11	26

WCP_M_213	226	178	8	0.79	784	0.168	8.6	0.0248	4.1	0.47	40.326	4.1	0.0492	7.6	156	178	158	13	158	6	-1
WCP_M_215	277	244	10	0.88	881	0.190	12.8	0.0254	6.6	0.52	39.401	6.6	0.0543	10.9	383	245	177	21	162	11	58
WCP_M_218	142	92	4	0.65	222	0.187	9.0	0.0242	3.9	0.44	41.264	3.9	0.0559	8.1	447	179	174	14	154	6	65
WCP_M_220	200	106	6	0.53	232	0.186	8.8	0.0250	5.5	0.62	39.931	5.5	0.0540	6.9	371	156	174	14	159	9	57
WCP_M_222	234	151	8	0.64	121	0.164	8.1	0.0255	5.1	0.62	39.256	5.1	0.0467	6.4	36	153	154	12	162	8	-353
WCP_M_223	156	111	5	0.71	185	0.150	10.8	0.0238	5.0	0.47	42.049	5.0	0.0457	9.6	-20	232	142	14	152	8	844
WCP_M_225	128	78	4	0.60	86	0.176	9.0	0.0251	5.2	0.58	39.812	5.2	0.0507	7.3	227	169	164	14	160	8	30
WCP_M_229	201	100	6	0.50	1727	0.164	10.1	0.0254	6.0	0.59	39.316	6.0	0.0469	8.2	43	195	155	15	162	10	-279
WCP_M_230	333	332	11	1.00	402	0.162	8.4	0.0244	5.5	0.65	40.926	5.5	0.0480	6.4	98	151	152	12	156	8	-59
WCP_M_233	187	176	6	0.94	115	0.163	8.5	0.0251	4.5	0.52	39.906	4.5	0.0472	7.2	61	173	153	12	160	7	-162
WCP_M_236	138	83	4	0.60	99	0.186	10.9	0.0259	5.4	0.50	38.576	5.4	0.0519	9.4	283	216	173	17	165	9	42
WCP_M_238	288	230	10	0.80	362	0.256	14.3	0.0262	6.6	0.46	38.174	6.6	0.0708	12.7	952	259	231	30	167	11	82
WCP_M_239	308	350	11	1.14	164	0.209	14.3	0.0246	6.0	0.42	40.667	6.0	0.0615	13.0	658	279	192	25	157	9	76
WCP_M_240	239	161	8	0.67	128	0.210	15.0	0.0255	6.2	0.41	39.203	6.2	0.0597	13.6	593	296	194	26	162	10	73
WCP_M_243	430	606	16	1.41	249	0.166	7.1	0.0247	4.5	0.64	40.502	4.5	0.0487	5.5	133	128	156	10	157	7	-19
WCP_M_246	140	107	4	0.77	60	0.163	10.6	0.0252	5.9	0.56	39.740	5.9	0.0469	8.8	42	210	153	15	160	9	-279
WCP_M_247	190	99	6	0.52	150	0.158	10.5	0.0252	4.7	0.45	39.684	4.7	0.0455	9.4	-27	227	149	15	160	7	690
WCP_M_248	301	283	10	0.94	4033	0.166	7.8	0.0244	5.0	0.65	40.965	5.0	0.0494	5.9	167	139	156	11	155	8	7
WCP_M_249	280	229	9	0.82	281	0.160	9.9	0.0250	5.7	0.57	40.076	5.7	0.0464	8.1	18	194	150	14	159	9	-771
WCP_M_253	273	260	10	0.95	130	0.199	11.8	0.0262	7.1	0.60	38.219	7.1	0.0551	9.5	415	211	184	20	167	12	60
WCP_M_254	318	346	11	1.09	270	0.162	8.6	0.0244	6.0	0.69	40.947	6.0	0.0481	6.3	102	148	152	12	156	9	-53
WCP_M_255	705	594	24	0.84	387	0.171	8.4	0.0252	5.2	0.61	39.631	5.2	0.0493	6.7	162	156	161	13	161	8	1
WCP_M_256	333	268	11	0.81	181	0.170	7.1	0.0246	5.4	0.76	40.655	5.4	0.0501	4.6	201	106	159	10	157	8	22
WCP_M_259	192	132	6	0.69	388	0.162	9.8	0.0251	5.1	0.52	39.893	5.1	0.0468	8.4	41	200	152	14	160	8	-292
WCP_M_263	157	92	5	0.59	272	0.193	9.2	0.0258	5.4	0.59	38.721	5.4	0.0543	7.4	382	166	179	15	164	9	57
WCP_M_264	590	719	21	1.22	226	0.167	6.1	0.0246	4.4	0.72	40.660	4.4	0.0493	4.2	161	99	157	9	157	7	3
WCP_M_270	206	176	7	0.86	524	0.212	11.1	0.0251	4.7	0.43	39.847	4.7	0.0614	10.0	653	215	196	20	160	7	76
WCP_M_275	222	142	7	0.64	189	0.157	9.7	0.0241	4.7	0.49	41.476	4.7	0.0473	8.4	67	201	148	13	154	7	-131
WCP_M_276	267	195	9	0.73	537	0.176	7.0	0.0256	5.1	0.73	39.109	5.1	0.0500	4.8	196	113	165	11	163	8	17
WCP_M_277	638	549	22	0.86	830	0.172	6.1	0.0250	4.9	0.80	40.025	4.9	0.0500	3.7	196	86	161	9	159	8	19
WCP_M_278	401	383	14	0.96	205	0.168	7.7	0.0247	5.4	0.70	40.460	5.4	0.0494	5.5	169	128	158	11	157	8	7
WCP_M_283	288	187	9	0.65	114	0.179	9.0	0.0250	6.8	0.75	40.023	6.8	0.0520	6.0	285	137	167	14	159	11	44
WCP_M_286	256	189	9	0.74	395	0.200	8.7	0.0254	5.5	0.63	39.372	5.5	0.0570	6.7	492	149	185	15	162	9	67
WCP_M_288	298	181	10	0.61	215	0.203	9.2	0.0258	6.5	0.71	38.741	6.5	0.0570	6.5	491	144	188	16	164	11	67
WCP_M_289	331	335	12	1.01	309	0.193	14.3	0.0242	6.2	0.43	41.402	6.2	0.0581	12.9	534	282	180	24	154	9	71
WCP_M_290	163	103	5	0.63	280	0.167	8.7	0.0242	4.9	0.56	41.363	4.9	0.0502	7.2	205	167	157	13	154	7	25
WCP_M_293	213	132	7	0.62	137	0.159	9.5	0.0242	5.3	0.56	41.339	5.3	0.0476	7.9	82	188	150	13	154	8	-88

WCP_M_294	325	213	10	0.66	345	0.177	7.0	0.0247	4.9	0.70	40.493	4.9	0.0520	4.9	286	113	166	11	157	8	45
WCP_M_295	532	561	19	1.06	315	0.178	8.0	0.0248	5.9	0.74	40.306	5.9	0.0520	5.4	285	123	166	12	158	9	45
WCP_M_300	305	249	11	0.82	289	0.190	12.3	0.0256	7.2	0.59	39.001	7.2	0.0539	9.9	366	223	177	20	163	12	55
WCP_M_301	639	858	24	1.34	5869	0.161	6.8	0.0244	5.4	0.80	41.062	5.4	0.0479	4.0	94	96	151	10	155	8	-66
WCP_M_302	286	198	10	0.69	213	0.181	8.2	0.0259	5.8	0.71	38.577	5.8	0.0506	5.8	222	133	169	13	165	9	26
WCP_M_307	306	258	10	0.84	1307	0.159	9.0	0.0247	5.0	0.55	40.407	5.0	0.0467	7.5	33	180	150	13	158	8	-383
WCP_M_308	229	156	8	0.68	170	0.165	9.7	0.0255	4.7	0.48	39.281	4.7	0.0471	8.5	54	203	155	14	162	8	-201
WCP_M_311	461	469	17	1.02	984	0.177	7.9	0.0250	3.9	0.50	39.933	3.9	0.0513	6.9	252	158	165	12	159	6	37
WCP_M_336	290	265	10	0.91	749	0.195	10.9	0.0260	6.3	0.58	38.517	6.3	0.0544	8.9	388	199	181	18	165	10	57

Notes: Isotope ratios and ages are reported without initial common Pb correction; gas blank-corrected mass 204 signals were generally irresolvable from zero.

Isotope ratio and apparent age errors do NOT include systematic calibration errors of 0.25% for the $^{207}\text{Pb}/^{206}\text{Pb}$ ratio, and 0.56% for the $^{206}\text{Pb}/^{238}\text{U}$ ratio (1s).

Trace element concentrations in ppm, calculated using the mean count rate method, internal standardization to ^{29}Si , and calibration to NIST 610 and 612 glass standards.

Ablation using a 213 nm wavelength laser, spot size of 25 microns, repetition rate of 10 Hz, and fluence of ~5 J/cm².

Table B.4. Detrital Zircon LA-ICPMS U-Pb Geochronology for Chapter 3

Analysis	Composition						Corrected isotope ratios						Apparent ages (Ma)											
	U ppm	Th ppm	Pb ppm	Th/U	$\frac{^{206}\text{Pb}}{^{204}\text{Pb}}$	$\frac{^{207}\text{Pb}}{^{235}\text{U}}$	$\pm 2s$ (%)	$\frac{^{206}\text{Pb}}{^{238}\text{U}}$	$\pm 2s$ (%)	error corr.	$\frac{^{238}\text{U}}{^{206}\text{Pb}}$	$\pm 2s$ (%)	$\frac{^{207}\text{Pb}}{^{206}\text{Pb}}$	$\pm 2s$ (%)	$\frac{^{207}\text{Pb}}{^{206}\text{Pb}}$ (abs)	$\pm 2s$ (%)	$\frac{^{207}\text{Pb}}{^{235}\text{U}}$ (abs)	$\pm 2s$ (%)	$\frac{^{206}\text{Pb}}{^{238}\text{U}}$ (abs)	$\pm 2s$ (%)	% disc.			
BCB-1 (Boulder Creek Beds – subunit 1)																								
BCB-1_S_138	206	75	9	0.36	139	0.284	18.2	0.0358	9.5	0.52	27.954	9.5	0.0576	15.5	514	340	254	41	227	21	56			
BCB-1_S_139	275	114	11	0.41	164	0.254	10.0	0.0342	6.9	0.68	29.259	6.9	0.0538	7.3	365	165	230	21	217	15	41			
BCB-1_S_145	307	124	13	0.40	800	0.255	9.5	0.0357	5.4	0.57	28.009	5.4	0.0519	7.8	281	178	231	20	226	12	20			
BCB-1_S_148	269	128	14	0.48	117	0.650	11.2	0.0364	4.6	0.41	27.459	4.6	0.1295	10.2	2091	179	509	45	231	10	89			
BCB-1_S_151	383	182	16	0.47	13072	0.279	18.2	0.0345	7.2	0.40	29.002	7.2	0.0586	16.7	552	364	250	40	219	16	60			
BCB-1_S_154	275	178	117	0.65	2291	4.607	17.0	0.2953	13.9	0.82	3.386	13.9	0.1131	9.8	1851	178	1751	142	1668	205	10			
BCB-1_S_161	332	184	15	0.55	705	0.294	9.1	0.0355	4.7	0.52	28.130	4.7	0.0601	7.8	606	168	262	21	225	10	63			
BCB-1_S_162	258	94	10	0.36	388	0.229	9.5	0.0337	3.3	0.35	29.656	3.3	0.0492	8.9	160	209	209	18	214	7	-34			
BCB-1_S_176	440	139	18	0.31	358	0.314	10.2	0.0333	3.4	0.33	30.008	3.4	0.0684	9.6	880	199	277	25	211	7	76			
BCB-1_S_177	350	56	13	0.16	773	0.270	17.0	0.0340	6.7	0.39	29.393	6.7	0.0576	15.6	515	343	243	37	216	14	58			
BCB-1_S_179	304	188	15	0.62	3430	0.281	19.6	0.0371	6.6	0.34	26.973	6.6	0.0550	18.4	411	412	251	44	235	15	43			
BCB-1_S_190	340	239	14	0.70	834	0.253	8.0	0.0341	5.2	0.65	29.366	5.2	0.0539	6.1	369	138	229	17	216	11	41			
BCB-1_S_194	362	229	14	0.63	253	0.247	8.0	0.0330	3.2	0.40	30.259	3.2	0.0542	7.3	381	164	224	16	210	7	45			
BCB-1_S_195	298	178	11	0.60	855	0.236	9.6	0.0323	4.9	0.51	30.928	4.9	0.0529	8.3	323	188	215	19	205	10	37			
BCB-1_S_203	223	92	9	0.41	4745	0.278	14.8	0.0323	5.0	0.34	30.946	5.0	0.0625	13.9	690	297	249	33	205	10	70			
BCB-1_S_206	231	86	11	0.37	108	0.432	29.0	0.0363	12.5	0.43	27.514	12.5	0.0862	26.2	1343	505	365	89	230	28	83			
BCB-1_S_207	358	172	14	0.48	633	0.226	9.5	0.0328	6.5	0.69	30.464	6.5	0.0498	6.8	187	159	207	18	208	13	-11			
BCB-1_S_209	173	43	6	0.25	92	0.250	10.1	0.0326	5.2	0.51	30.668	5.2	0.0555	8.7	433	194	226	21	207	11	52			
BCB-1_S_210	245	72	9	0.29	1236	0.251	11.0	0.0336	5.8	0.53	29.718	5.8	0.0541	9.3	376	208	227	22	213	12	43			
BCB-1_S_214	378	181	15	0.48	1001	0.227	8.5	0.0326	4.3	0.50	30.651	4.3	0.0504	7.4	213	171	207	16	207	9	3			
BCB-1_S_219	289	142	11	0.49	330	0.228	8.9	0.0331	6.1	0.68	30.233	6.1	0.0501	6.5	198	151	209	17	210	13	-6			
BCB-1_S_222	435	219	26	0.50	159	0.488	32.3	0.0394	9.6	0.30	25.384	9.6	0.0899	30.8	1422	589	404	108	249	23	82			
BCB-1_S_225	297	183	26	0.62	80	1.225	16.1	0.0431	8.2	0.51	23.189	8.2	0.2060	13.9	2875	225	812	90	272	22	91			
BCB-1_S_227	277	120	12	0.43	1273	0.315	18.7	0.0354	7.1	0.38	28.258	7.1	0.0645	17.4	757	366	278	46	224	16	70			
BCB-1_S_228	204	78	9	0.38	192	0.312	18.7	0.0354	5.6	0.30	28.222	5.6	0.0638	17.8	735	377	275	45	224	12	69			
BCB-1_S_232	310	132	13	0.43	1963	0.245	10.7	0.0344	5.7	0.53	29.108	5.7	0.0518	9.0	276	207	223	21	218	12	21			
BCB-1_S_236	232	79	9	0.34	159	0.366	11.8	0.0342	4.2	0.35	29.261	4.2	0.0777	11.1	1140	220	317	32	217	9	81			
BCB-1_S_238	467	315	21	0.68	408	0.253	8.1	0.0351	4.4	0.55	28.477	4.4	0.0523	6.8	300	154	229	17	222	10	26			
BCB-1_S_239	283	109	11	0.38	2495	0.293	10.9	0.0343	4.5	0.41	29.132	4.5	0.0619	9.9	670	213	261	25	218	10	68			
BCB-1_S_240	792	645	34	0.81	442	0.227	7.1	0.0327	4.4	0.62	30.546	4.4	0.0503	5.6	207	130	208	13	208	9	0			

BCB-1_S_242	464	326	18	0.70	519	0.235	7.0	0.0318	4.1	0.59	31.439	4.1	0.0535	5.7	349	129	214	14	202	8	42
BCB-1_S_243	234	88	9	0.37	181	0.218	12.6	0.0335	4.5	0.36	29.882	4.5	0.0472	11.7	60	279	200	23	212	9	-252
BCB-1_S_248	284	139	11	0.49	5833	0.248	8.7	0.0338	3.8	0.44	29.602	3.8	0.0533	7.8	340	177	225	18	214	8	37
BCB-1_S_249	288	131	12	0.46	339	0.282	8.7	0.0348	5.1	0.59	28.716	5.1	0.0586	7.0	554	154	252	19	221	11	60
BCB-1_S_250	356	159	14	0.45	1003	0.240	8.9	0.0337	5.5	0.62	29.679	5.5	0.0517	7.0	272	160	219	17	214	11	21
BCB-1_S_252	409	246	19	0.60	190	0.336	28.3	0.0339	7.4	0.26	29.509	7.4	0.0720	27.3	985	555	294	72	215	16	78
BCB-1_S_256	265	137	11	0.52	170	0.250	10.0	0.0338	5.6	0.56	29.572	5.6	0.0536	8.3	356	187	227	20	214	12	40
BCB-1_S_258	232	85	10	0.36	412	0.387	9.4	0.0362	6.5	0.69	27.610	6.5	0.0774	6.8	1133	136	332	27	229	15	80
BCB-1_S_260	276	128	10	0.46	864	0.230	8.0	0.0335	4.3	0.54	29.851	4.3	0.0498	6.7	184	157	210	15	212	9	-15
BCB-1_S_261	256	123	11	0.48	258	0.340	17.0	0.0348	5.0	0.29	28.711	5.0	0.0707	16.2	949	332	297	44	221	11	77
BCB-1_S_264	276	137	11	0.50	3471	0.245	10.4	0.0341	5.1	0.49	29.300	5.1	0.0522	9.0	292	206	223	21	216	11	26
BCB-1_S_265	437	350	18	0.80	358	0.218	10.2	0.0323	4.0	0.39	30.942	4.0	0.0488	9.3	140	219	200	18	205	8	-47
BCB-1_S_266	342	95	13	0.28	308	0.301	17.2	0.0348	7.0	0.41	28.701	7.0	0.0627	15.7	698	334	267	40	221	15	68
BCB-1_S_270	163	68	6	0.42	187	0.241	10.4	0.0321	6.3	0.61	31.166	6.3	0.0544	8.2	389	185	219	20	204	13	48
BCB-1_S_272	291	141	11	0.48	115	0.225	9.1	0.0331	4.0	0.43	30.237	4.0	0.0494	8.2	167	192	206	17	210	8	-26
BCB-1_S_276	407	404	19	0.99	283	0.260	7.9	0.0358	4.7	0.60	27.913	4.7	0.0526	6.4	312	145	235	17	227	11	27
BCB-1_S_279	378	77	15	0.20	453	0.231	10.6	0.0351	5.7	0.54	28.491	5.7	0.0477	8.9	86	212	211	20	222	13	-159
BCB-1_S_280	153	63	10	0.41	60	0.711	30.9	0.0444	7.7	0.25	22.505	7.7	0.1161	29.9	1897	538	546	130	280	21	85
BCB-1_S_285	388	162	15	0.42	350	0.235	8.8	0.0333	7.1	0.81	30.043	7.1	0.0511	5.2	245	119	214	17	211	15	14
BCB-1_S_286	432	253	17	0.58	374	0.224	9.0	0.0327	6.8	0.75	30.547	6.8	0.0496	6.0	176	140	205	17	208	14	-18
BCB-1_S_287	333	164	13	0.49	221	0.226	14.6	0.0322	6.9	0.48	31.042	6.9	0.0508	12.8	231	296	206	27	204	14	11
BCB-1_S_289	388	215	18	0.55	458	0.309	20.2	0.0353	9.0	0.45	28.324	9.0	0.0634	18.1	721	383	273	48	224	20	69
BCB-1_S_296	230	77	9	0.34	127	0.243	12.0	0.0340	7.9	0.66	29.384	7.9	0.0517	9.0	272	207	221	24	216	17	21
BCB-1_S_298	301	140	12	0.46	248	0.241	7.4	0.0333	4.1	0.56	30.074	4.1	0.0525	6.1	308	140	219	15	211	9	32
BCB-1_S_299	335	108	13	0.32	197	0.254	8.2	0.0351	6.4	0.78	28.466	6.4	0.0524	5.1	305	117	230	17	223	14	27
BCB-1_S_301	392	220	27	0.56	90	1.056	6.3	0.0401	4.1	0.65	24.941	4.1	0.1910	4.8	2750	80	732	33	253	10	91
BCB-1_S_302	347	157	14	0.45	885	0.240	10.3	0.0337	5.8	0.56	29.635	5.8	0.0515	8.5	263	195	218	20	214	12	19
BCB-1_S_304	366	181	24	0.49	132	0.934	9.0	0.0408	6.4	0.71	24.531	6.4	0.1662	6.4	2520	107	670	44	258	16	90
BCB-1_S_305	223	78	9	0.35	437	0.263	15.3	0.0344	6.7	0.44	29.101	6.7	0.0555	13.8	431	307	237	32	218	14	49
BCB-1_S_306	236	99	9	0.42	982	0.244	9.3	0.0335	4.9	0.53	29.815	4.9	0.0529	7.9	323	180	222	19	213	10	34
BCB-1_S_307	226	89	10	0.39	189	0.309	17.2	0.0371	7.6	0.44	26.983	7.6	0.0604	15.4	618	333	273	41	235	18	62
BCB-1_S_317	512	392	21	0.77	477	0.219	6.8	0.0318	4.4	0.65	31.452	4.4	0.0500	5.2	193	120	201	12	202	9	-5
BCB-1_S_324	403	202	17	0.50	502	0.235	7.2	0.0348	4.9	0.68	28.759	4.9	0.0491	5.3	151	124	215	14	220	11	-46
BCB-1_S_326	324	140	13	0.43	334	0.232	7.5	0.0338	3.8	0.50	29.576	3.8	0.0497	6.4	182	150	212	14	214	8	-18
BCB-1_S_327	352	137	13	0.39	218	0.228	8.6	0.0326	4.3	0.50	30.634	4.3	0.0506	7.4	220	172	208	16	207	9	6
BCB-1_S_330	475	207	20	0.43	559	0.256	14.6	0.0350	5.4	0.37	28.589	5.4	0.0531	13.6	334	308	232	30	222	12	34
BCB-1_S_334	426	201	17	0.47	490	0.268	9.4	0.0335	5.7	0.61	29.837	5.7	0.0580	7.4	530	163	241	20	213	12	60

BCB-1_S_337	533	380	28	0.71	644	0.530	12.9	0.0359	5.7	0.44	27.838	5.7	0.1070	11.6	1749	212	432	45	228	13	87
BCB-1_S_349	425	249	17	0.59	1086	0.244	10.0	0.0324	3.6	0.36	30.829	3.6	0.0545	9.3	392	209	222	20	206	7	48
BCB-1_S_351	418	256	17	0.61	1445	0.292	8.7	0.0325	3.8	0.44	30.804	3.8	0.0652	7.8	782	164	260	20	206	8	74
BCB-1_S_356	275	113	10	0.41	979	0.260	15.0	0.0334	3.8	0.25	29.912	3.8	0.0564	14.5	467	321	235	31	212	8	55
BCB-1_S_369	329	112	12	0.34	967	0.227	10.6	0.0323	6.1	0.57	30.983	6.1	0.0510	8.7	242	200	208	20	205	12	15
BCB-1_S_375	516	284	21	0.55	356	0.243	13.1	0.0320	6.7	0.51	31.261	6.7	0.0551	11.3	417	252	221	26	203	13	51
BCB-1_S_377	197	72	8	0.37	72	0.273	16.7	0.0328	6.5	0.39	30.445	6.5	0.0603	15.4	613	333	245	36	208	13	66
BCB-1_S_382	437	237	18	0.54	329	0.259	19.4	0.0341	8.6	0.44	29.326	8.6	0.0551	17.4	417	390	234	41	216	18	48
BCB-1_S_383	288	130	12	0.45	209	0.246	17.4	0.0344	6.3	0.36	29.089	6.3	0.0518	16.2	278	371	223	35	218	13	22
BCB-1_M_506	342	180	13	0.53	458	0.231	6.6	0.0331	4.7	0.71	30.186	4.7	0.0505	4.7	217	108	211	13	210	10	3
BCB-1_M_507	305	171	13	0.56	214	0.266	10.1	0.0356	6.8	0.68	28.065	6.8	0.0542	7.4	380	166	240	21	226	15	41
BCB-1_M_509	412	105	15	0.25	758	0.247	7.7	0.0339	4.9	0.64	29.456	4.9	0.0527	5.9	314	133	224	15	215	10	32
BCB-1_M_512	353	167	14	0.47	593	0.244	6.4	0.0338	4.2	0.66	29.549	4.2	0.0523	4.8	297	109	222	13	215	9	28
BCB-1_M_519	532	191	20	0.36	1561	0.242	6.5	0.0335	4.1	0.63	29.847	4.1	0.0523	5.0	299	114	220	13	212	9	29
BCB-1_M_520	317	132	12	0.42	230	0.264	9.0	0.0345	5.0	0.56	29.020	5.0	0.0556	7.4	435	166	238	19	218	11	50
BCB-1_M_521	475	356	26	0.75	469	0.468	22.4	0.0362	6.4	0.29	27.658	6.4	0.0939	21.5	1505	406	390	73	229	14	85
BCB-1_M_523	223	106	9	0.48	4783	0.251	10.5	0.0336	4.9	0.47	29.781	4.9	0.0543	9.3	383	208	228	21	213	10	44
BCB-1_M_524	264	143	11	0.54	364	0.256	7.4	0.0348	4.2	0.57	28.715	4.2	0.0534	6.0	346	137	232	15	221	9	36
BCB-1_M_525	356	129	14	0.36	378	0.251	8.0	0.0352	4.9	0.60	28.400	4.9	0.0516	6.4	269	147	227	16	223	11	17
BCB-1_M_526	273	128	11	0.47	516	0.251	8.3	0.0352	5.1	0.61	28.443	5.1	0.0518	6.6	277	151	227	17	223	11	20
BCB-1_M_527	1145	764	50	0.67	40562	0.281	13.4	0.0338	4.7	0.35	29.601	4.7	0.0602	12.5	612	270	251	30	214	10	65
BCB-1_M_528	292	189	18	0.65	653	0.605	18.2	0.0417	7.4	0.41	23.960	7.4	0.1052	16.6	1718	306	481	70	264	19	85
BCB-1_M_530	330	151	13	0.46	448	0.290	10.4	0.0337	3.3	0.32	29.699	3.3	0.0624	9.8	689	209	258	24	213	7	69
BCB-1_M_531	226	117	9	0.52	100	0.256	10.6	0.0359	4.9	0.46	27.842	4.9	0.0517	9.4	273	215	232	22	227	11	17
BCB-1_M_532	273	150	18	0.55	97	0.874	15.0	0.0422	3.7	0.25	23.701	3.7	0.1502	14.6	2348	249	637	71	266	10	89
BCB-1_M_534	316	112	13	0.35	569	0.337	15.4	0.0350	3.7	0.24	28.567	3.7	0.0699	15.0	926	308	295	40	222	8	76
BCB-1_M_540	406	291	17	0.72	203	0.273	10.8	0.0346	3.7	0.34	28.881	3.7	0.0572	10.1	499	223	245	23	219	8	56
BCB-1_M_543	58	35	2	0.60	76	0.279	16.6	0.0360	5.4	0.32	27.742	5.4	0.0562	15.7	459	349	250	37	228	12	50
BCB-1_M_545	432	362	18	0.84	835	0.232	8.2	0.0347	5.6	0.68	28.793	5.6	0.0484	6.0	121	141	212	16	220	12	-83
BCB-1_M_546	239	88	9	0.37	129	0.243	9.5	0.0346	4.4	0.47	28.919	4.4	0.0509	8.4	238	194	221	19	219	10	8
BCB-1_M_547	226	84	11	0.37	737	0.418	18.6	0.0393	7.2	0.39	25.447	7.2	0.0772	17.2	1125	343	355	56	248	18	78
BCB-1_M_549	366	139	16	0.38	104	0.292	17.1	0.0358	5.1	0.30	27.947	5.1	0.0591	16.3	572	354	260	39	227	11	60
BCB-1_M_553	260	147	11	0.57	951	0.249	8.8	0.0352	5.2	0.60	28.431	5.2	0.0513	7.1	256	162	226	18	223	11	13
BCB-1_M_554	491	296	21	0.60	453	0.243	7.3	0.0361	5.8	0.79	27.685	5.8	0.0489	4.5	142	105	221	15	229	13	-61
BCB-1_M_558	279	138	12	0.49	2457	0.259	8.6	0.0351	6.2	0.72	28.521	6.2	0.0536	5.9	355	134	234	18	222	14	37
BCB-1_M_559	165	73	7	0.44	129	0.242	10.3	0.0350	4.3	0.42	28.562	4.3	0.0502	9.4	205	217	220	20	222	9	-8
BCB-1_M_560	485	151	18	0.31	374	0.238	6.1	0.0333	4.4	0.71	30.028	4.4	0.0519	4.3	283	98	217	12	211	9	25

BCB-1_M_561	490	215	18	0.44	402	0.223	6.0	0.0329	3.6	0.61	30.390	3.6	0.0491	4.7	150	111	204	11	209	7	-39
BCB-1_M_562	490	138	18	0.28	647	0.235	7.3	0.0334	4.6	0.62	29.950	4.6	0.0511	5.7	243	131	214	14	212	9	13
BCB-1_M_563	229	103	9	0.45	479	0.225	8.4	0.0336	4.8	0.57	29.726	4.8	0.0484	6.9	120	163	206	16	213	10	-78
BCB-1_M_565	198	58	8	0.29	441	0.226	9.3	0.0349	4.0	0.43	28.625	4.0	0.0470	8.4	49	200	207	17	221	9	-356
BCB-1_M_566	260	74	10	0.29	179	0.232	8.2	0.0343	4.1	0.50	29.120	4.1	0.0491	7.2	153	167	212	16	218	9	-43
BCB-1_M_567	309	131	13	0.42	418	0.256	7.0	0.0344	4.3	0.62	29.028	4.3	0.0538	5.6	363	125	231	15	218	9	40
BCB-1_M_568	239	98	10	0.41	299	0.241	8.9	0.0345	5.1	0.58	28.995	5.1	0.0507	7.2	225	168	219	17	219	11	3
BCB-1_M_569	414	154	16	0.37	351	0.239	6.7	0.0341	4.3	0.65	29.340	4.3	0.0508	5.1	232	119	217	13	216	9	7

Analysis	Composition						Corrected isotope ratios						Apparent ages (Ma)											
	U	Th	Pb		$\frac{^{206}\text{Pb}}{^{204}\text{Pb}}$	$\frac{^{207}\text{Pb}}{^{235}\text{U}}$	$\pm 2s$	$\frac{^{206}\text{Pb}}{^{238}\text{U}}$	$\pm 2s$	error	$\frac{^{238}\text{U}}{^{206}\text{Pb}}$	$\pm 2s$	$\frac{^{207}\text{Pb}}{^{206}\text{Pb}}$	$\pm 2s$	$\frac{^{207}\text{Pb}}{^{206}\text{Pb}}$	$\pm 2s$	$\frac{^{207}\text{Pb}}{^{235}\text{U}}$	$\pm 2s$	$\frac{^{206}\text{Pb}}{^{238}\text{U}}$	$\pm 2s$	%			
	ppm	ppm	ppm	Th/U		(%)		^{238}U	(%)	corr.	^{206}Pb	(%)		^{206}Pb	(%)	^{206}Pb	(abs)	^{207}Pb	(abs)	^{206}Pb	(abs)	disc.		
BCB-2 (Boulder Creek Beds – subunit 2)																								
BCB-2_L_39	66	38	2	0.58	5044	0.214	8.0	0.0297	4.3	0.53	33.667	4.3	0.0523	6.8	298	155	197	14	189	8	37			
BCB-2_L_40	65	43	2	0.66	661	0.193	12.5	0.0293	5.2	0.41	34.106	5.2	0.0478	11.4	89	269	179	21	186	9	-110			
BCB-2_L_41	47	24	2	0.50	114	0.223	12.3	0.0293	6.3	0.51	34.104	6.3	0.0551	10.5	417	236	204	23	186	12	55			
BCB-2_L_42	240	195	10	0.81	953	0.219	7.4	0.0300	5.3	0.72	33.281	5.3	0.0528	5.2	321	117	201	13	191	10	41			
BCB-2_L_43	61	29	2	0.47	286	0.219	12.7	0.0310	6.1	0.48	32.303	6.1	0.0514	11.1	258	255	201	23	197	12	24			
BCB-2_L_44	54	28	2	0.52	270	0.193	15.4	0.0292	5.6	0.36	34.238	5.6	0.0479	14.3	96	340	179	25	186	10	-94			
BCB-2_L_45	179	139	7	0.77	412	0.204	8.2	0.0296	4.2	0.51	33.763	4.2	0.0500	7.1	194	164	189	14	188	8	3			
BCB-2_L_46	53	28	2	0.52	111	0.190	13.6	0.0292	6.1	0.45	34.204	6.1	0.0472	12.2	62	290	177	22	186	11	-202			
BCB-2_L_47	74	36	3	0.49	161	0.203	9.4	0.0298	5.3	0.56	33.520	5.3	0.0494	7.8	166	182	188	16	190	10	-14			
BCB-2_L_48	65	29	3	0.45	61	0.490	16.2	0.0330	3.6	0.22	30.290	3.6	0.1076	15.8	1760	288	405	54	209	7	88			
BCB-2_L_49	72	36	3	0.49	64	0.185	10.4	0.0298	6.2	0.59	33.559	6.2	0.0450	8.4	-57	205	172	17	189	12	433			
BCB-2_L_50	88	35	3	0.40	839	0.206	8.5	0.0301	5.0	0.59	33.233	5.0	0.0497	6.8	183	159	191	15	191	10	-4			
BCB-2_L_51	53	25	2	0.47	88	0.242	19.7	0.0294	6.7	0.34	34.006	6.7	0.0596	18.5	589	402	220	39	187	12	68			
BCB-2_L_52	212	133	8	0.63	510	0.205	7.4	0.0296	5.9	0.79	33.775	5.9	0.0501	4.5	200	105	189	13	188	11	6			
BCB-2_L_53	306	356	14	1.16	398	0.216	8.2	0.0305	5.8	0.71	32.770	5.8	0.0514	5.7	258	132	199	15	194	11	25			
BCB-2_L_54	191	102	7	0.54	2068	0.202	7.8	0.0301	4.1	0.52	33.275	4.1	0.0488	6.7	137	157	187	13	191	8	-40			
BCB-2_L_55	73	29	2	0.40	48	0.219	9.7	0.0288	5.7	0.59	34.725	5.7	0.0552	7.8	419	175	201	18	183	10	56			
BCB-2_L_56	81	34	3	0.42	178	0.207	11.2	0.0298	4.1	0.37	33.545	4.1	0.0503	10.4	208	241	191	19	189	8	9			
BCB-2_L_57	57	25	2	0.45	53	0.197	9.7	0.0294	6.0	0.62	34.046	6.0	0.0486	7.6	127	178	182	16	187	11	-47			
BCB-2_L_58	92	39	3	0.43	374	0.192	9.7	0.0299	5.0	0.51	33.450	5.0	0.0465	8.3	22	200	178	16	190	9	-779			
BCB-2_S_294	322	152	12	0.47	266	0.242	14.1	0.0297	5.4	0.38	33.709	5.4	0.0593	13.0	576	283	220	28	188	10	67			
BCB-2_S_295	411	153	15	0.37	2482	0.286	15.4	0.0307	7.1	0.46	32.522	7.1	0.0674	13.6	851	283	255	35	195	14	77			
BCB-2_S_296	367	157	16	0.43	183	0.428	14.8	0.0315	4.3	0.29	31.717	4.3	0.0984	14.2	1594	264	362	45	200	9	87			

BCB-2_S_297	127	57	4	0.45	554	0.223	9.4	0.0304	5.4	0.57	32.853	5.4	0.0532	7.7	338	175	205	17	193	10	43
BCB-2_S_298	76	25	2	0.33	1157	0.179	11.8	0.0286	3.9	0.33	34.951	3.9	0.0454	11.1	-36	270	167	18	182	7	608
BCB-2_S_299	194	96	7	0.50	742	0.202	11.1	0.0298	5.0	0.45	33.573	5.0	0.0491	9.9	154	232	187	19	189	9	-23
BCB-2_S_300	168	66	6	0.39	685	0.208	7.4	0.0296	5.0	0.68	33.728	5.0	0.0509	5.4	235	125	192	13	188	9	20
BCB-2_S_301	67	28	2	0.41	57	0.237	11.6	0.0298	5.7	0.49	33.538	5.7	0.0577	10.2	520	223	216	23	189	11	64
BCB-2_S_303	378	172	14	0.46	268	0.208	7.3	0.0306	5.8	0.80	32.699	5.8	0.0494	4.4	167	102	192	13	194	11	-16
BCB-2_S_304	323	128	11	0.40	865	0.197	7.6	0.0287	4.6	0.60	34.844	4.6	0.0497	6.1	181	142	182	13	182	8	-1
BCB-2_S_306	427	183	15	0.43	435	0.219	13.0	0.0304	6.7	0.51	32.872	6.7	0.0522	11.2	293	255	201	24	193	13	34
BCB-2_S_307	427	148	15	0.35	40342	0.213	6.8	0.0307	5.2	0.77	32.589	5.2	0.0503	4.4	211	102	196	12	195	10	8
BCB-2_S_309	143	31	5	0.21	909	0.225	8.6	0.0305	3.7	0.44	32.832	3.7	0.0536	7.7	355	175	206	16	193	7	45
BCB-2_S_310	184	75	6	0.41	310	0.200	8.4	0.0298	4.9	0.59	33.574	4.9	0.0487	6.8	133	159	185	14	189	9	-42
BCB-2_S_311	479	173	20	0.36	581	0.264	18.1	0.0314	9.6	0.53	31.889	9.6	0.0611	15.3	643	330	238	38	199	19	69
BCB-2_S_312	145	56	5	0.39	153	0.207	10.3	0.0310	5.0	0.48	32.272	5.0	0.0484	9.0	118	213	191	18	197	10	-66
BCB-2_S_313	403	159	14	0.39	597	0.217	6.2	0.0298	4.7	0.76	33.583	4.7	0.0529	4.0	324	92	199	11	189	9	42
BCB-2_S_314	122	29	4	0.24	367	0.224	8.3	0.0306	4.9	0.59	32.703	4.9	0.0531	6.7	334	151	205	15	194	9	42
BCB-2_S_315	284	94	11	0.33	774	0.279	8.8	0.0322	5.7	0.66	31.052	5.7	0.0627	6.6	700	141	250	19	204	12	71
BCB-2_S_317	438	160	16	0.36	650	0.225	7.7	0.0313	5.3	0.69	31.936	5.3	0.0522	5.6	294	128	206	14	198.8	10	32
BCB-2_S_318	395	133	14	0.34	563	0.228	6.6	0.0313	4.7	0.71	31.927	4.7	0.0527	4.6	315	104	208	12	199	9	37
BCB-2_S_320	114	41	4	0.36	81	0.212	9.7	0.0307	3.7	0.38	32.610	3.7	0.0501	9.0	202	208	195	17	195	7	3
BCB-2_S_321	387	160	14	0.41	402	0.239	14.1	0.0308	6.3	0.45	32.511	6.3	0.0564	12.6	469	280	218	28	195	12	58
BCB-2_S_322	66	27	3	0.41	1231	0.399	15.1	0.0335	4.0	0.27	29.858	4.0	0.0864	14.6	1348	282	341	44	212	8	84
BCB-2_S_323	396	124	14	0.31	728	0.239	13.1	0.0310	5.1	0.39	32.271	5.1	0.0559	12.1	447	268	217	26	197	10	56
BCB-2_S_324	438	171	16	0.39	431	0.207	6.9	0.0311	5.0	0.72	32.200	5.0	0.0483	4.9	114	115	191	12	197	10	-72
BCB-2_S_327	282	116	10	0.41	30141	0.216	9.8	0.0308	5.3	0.54	32.446	5.3	0.0508	8.2	233	190	199	18	196	10	16
BCB-2_S_328	178	64	6	0.36	376	0.225	7.3	0.0304	4.5	0.61	32.843	4.5	0.0536	5.8	354	131	206	14	193	8	45
BCB-2_S_330	498	250	19	0.50	0	0.215	5.0	0.0312	3.9	0.79	32.068	3.9	0.0501	3.1	200	71	198	9	198	8	1
BCB-2_S_334	320	122	16	0.38	99	0.609	13.7	0.0338	3.8	0.28	29.577	3.8	0.1305	13.1	2105	230	483	52	214	8	90
BCB-2_S_335	967	753	52	0.78	159	0.513	14.6	0.0328	6.0	0.41	30.454	6.0	0.1133	13.3	1852	241	420	50	208	12	89
BCB-2_S_336	379	124	15	0.33	644	0.252	15.0	0.0330	8.8	0.59	30.279	8.8	0.0553	12.1	423	271	228	31	209	18	51
BCB-2_S_337	488	161	17	0.33	344	0.223	6.7	0.0300	4.5	0.67	33.358	4.5	0.0539	5.0	367	113	204	12	190	8	48
BCB-2_S_338	150	62	13	0.42	61	1.325	8.9	0.0418	6.7	0.75	23.946	6.7	0.2301	5.9	3053	94	857	52	264	17	91
BCB-2_S_339	539	137	40	0.26	122	1.152	13.6	0.0425	8.5	0.63	23.557	8.5	0.1968	10.6	2800	173	778	74	268	22	90
BCB-2_S_340	500	216	18	0.43	7059	0.220	6.0	0.0306	3.4	0.56	32.668	3.4	0.0522	5.0	296	114	202	11	194	6	34
BCB-2_S_342	62	22	2	0.36	50	0.234	15.6	0.0307	4.5	0.29	32.571	4.5	0.0553	14.9	423	333	213	30	195	9	54
BCB-2_S_343	63	24	2	0.38	47	0.242	12.5	0.0324	5.8	0.47	30.822	5.8	0.0540	11.1	373	250	220	25	206	12	45
BCB-2_S_344	121	44	4	0.36	68	0.226	9.6	0.0316	4.9	0.52	31.653	4.9	0.0519	8.2	280	187	207	18	201	10	28
BCB-2_S_346	258	88	10	0.34	235	0.248	6.4	0.0336	3.8	0.60	29.719	3.8	0.0535	5.1	350	116	225	13	213	8	39

BCB-2_S_347	355	183	14	0.52	632	0.217	8.7	0.0321	5.8	0.67	31.165	5.8	0.0489	6.4	145	151	199	16	204	12	-40
BCB-2_S_348	311	86	11	0.28	295	0.247	9.3	0.0319	5.0	0.54	31.326	5.0	0.0561	7.8	455	174	224	19	203	10	55
BCB-2_S_349	307	136	11	0.44	349	0.226	6.7	0.0319	2.4	0.35	31.339	2.4	0.0514	6.3	260	145	207	13	202	5	22
BCB-2_S_350	144	91	5	0.63	296	0.222	8.1	0.0319	3.0	0.38	31.315	3.0	0.0503	7.5	211	174	203	15	203	6	4
BCB-2_S_351	194	88	7	0.45	151	0.236	7.2	0.0319	3.9	0.54	31.336	3.9	0.0536	6.0	354	136	215	14	203	8	43
BCB-2_S_354	359	248	18	0.69	251	0.420	14.1	0.0353	3.3	0.23	28.296	3.3	0.0861	13.7	1340	264	356	42	224	7	83
BCB-2_S_356	121	51	4	0.42	221	0.218	9.8	0.0321	5.7	0.58	31.116	5.7	0.0493	8.0	162	187	201	18	204	11	-26
BCB-2_S_358	156	85	6	0.54	131	0.253	16.2	0.0327	7.3	0.45	30.558	7.3	0.0561	14.5	455	321	229	33	208	15	54
BCB-2_S_359	343	170	13	0.50	991	0.223	9.5	0.0313	4.8	0.50	31.944	4.8	0.0516	8.2	268	188	204	18	199	9	26
BCB-2_S_360	808	275	34	0.34	646	0.354	12.0	0.0329	3.7	0.31	30.424	3.7	0.0782	11.4	1151	227	308	32	208	8	82
BCB-2_S_361	125	64	5	0.51	38	0.248	11.1	0.0371	8.7	0.78	26.979	8.7	0.0486	6.9	127	163	225	22	235	20	-84
BCB-2_S_362	132	48	5	0.36	394	0.224	8.8	0.0321	4.6	0.52	31.191	4.6	0.0507	7.5	226	173	205	16	203	9	10
BCB-2_S_363	234	142	8	0.61	409	0.204	7.1	0.0299	5.1	0.72	33.497	5.1	0.0495	5.0	173	116	188	12	190	10	-9
BCB-2_S_364	130	66	5	0.51	603	0.227	10.0	0.0307	4.6	0.46	32.522	4.6	0.0536	8.9	356	202	208	19	195	9	45
BCB-2_S_366	506	213	19	0.42	1068	0.232	8.1	0.0322	7.1	0.87	31.029	7.1	0.0522	4.0	296	91	212	16	204	14	31
BCB-2_S_367	247	111	10	0.45	249	0.294	9.3	0.0319	4.7	0.51	31.343	4.7	0.0668	8.0	831	166	261	21	202	9	76
BCB-2_S_369	447	235	18	0.53	245	0.347	19.9	0.0311	5.3	0.26	32.200	5.3	0.0810	19.2	1221	377	302	52	197	10	84
BCB-2_S_370	437	213	17	0.49	6884	0.246	9.4	0.0325	6.0	0.64	30.748	6.0	0.0549	7.2	410	161	224	19	206	12	50
BCB-2_S_373	525	262	20	0.50	1950	0.208	6.6	0.0316	4.9	0.74	31.644	4.9	0.0478	4.5	87	106	192	12	201	10	-130
BCB-2_S_375	100	40	3	0.40	409	0.218	8.2	0.0307	4.8	0.59	32.530	4.8	0.0515	6.6	262	151	200	15	195	9	25
BCB-2_S_376	252	86	9	0.34	580	0.221	8.3	0.0332	5.6	0.67	30.149	5.6	0.0484	6.1	118	144	203	15	210	12	-79
BCB-2_S_377	430	182	16	0.42	1188	0.236	11.6	0.0309	6.4	0.55	32.321	6.4	0.0553	9.7	424	215	215	22	196	12	54
BCB-2_S_381	417	146	16	0.35	2082	0.256	15.2	0.0325	7.9	0.52	30.725	7.9	0.0570	12.9	491	285	231	31	206	16	58
BCB-2_S_382	178	63	6	0.35	280	0.222	8.4	0.0320	4.9	0.58	31.216	4.9	0.0502	6.8	206	158	204	15	203	10	2
BCB-2_S_383	501	232	18	0.46	1027	0.208	7.1	0.0304	5.7	0.80	32.926	5.7	0.0497	4.2	180	98	192	12	193	11	-7
BCB-2_S_384	198	72	7	0.36	252	0.228	9.2	0.0309	3.3	0.35	32.388	3.3	0.0535	8.7	352	195	209	17	196	6	44
BCB-2_S_385	236	103	9	0.44	178	0.259	7.9	0.0301	3.2	0.40	33.196	3.2	0.0624	7.3	687	155	234	17	191	6	72
BCB-2_S_386	55	15	2	0.28	56	0.189	16.2	0.0321	5.3	0.33	31.169	5.3	0.0428	15.3	-177	381	176	26	204	11	215
BCB-2_S_387	60	17	2	0.28	66	0.298	14.7	0.0330	4.6	0.31	30.321	4.6	0.0656	14.0	793	294	265	34	209	10	74
BCB-2_S_390	108	31	4	0.29	86	0.218	12.0	0.0331	6.9	0.57	30.169	6.9	0.0477	9.8	85	234	200	22	210	14	-147
BCB-2_S_391	170	59	6	0.35	1064	0.227	9.5	0.0331	4.5	0.48	30.222	4.5	0.0497	8.3	179	193	207	18	210	9	-17
BCB-2_S_392	376	127	14	0.34	657	0.216	7.0	0.0316	4.9	0.70	31.598	4.9	0.0495	5.0	173	117	199	13	201	10	-16
BCB-2_S_393	127	53	5	0.42	117	0.223	8.3	0.0330	4.2	0.50	30.337	4.2	0.0491	7.2	155	169	205	15	209	9	-35
BCB-2_S_394	255	80	10	0.31	3520	0.228	8.1	0.0333	5.6	0.69	30.070	5.6	0.0498	5.8	186	136	209	15	211	12	-13
BCB-2_S_399	523	232	19	0.44	280	0.254	8.3	0.0302	5.6	0.67	33.124	5.6	0.0611	6.2	644	132	230	17	192	11	70
BCB-2_S_402	142	52	5	0.37	356	0.184	9.8	0.0309	4.0	0.41	32.350	4.0	0.0433	8.9	-153	221	172	15	196	8	229
BCB-2_S_406	438	176	16	0.40	294	0.223	7.8	0.0306	6.0	0.77	32.703	6.0	0.0528	4.9	321	112	204	14	194	11	40

BCB-2_S_407	369	160	15	0.43	215	0.274	17.2	0.0320	6.9	0.40	31.203	6.9	0.0620	15.7	674	337	246	38	203	14	70
BCB-2_S_409	136	42	6	0.31	165	0.387	9.3	0.0326	3.3	0.36	30.704	3.3	0.0862	8.7	1344	168	332	26	207	7	85
BCB-2_S_410	350	121	12	0.35	1586	0.215	8.5	0.0306	5.4	0.64	32.665	5.4	0.0509	6.5	236	150	198	15	194	10	18
BCB-2_S_413	127	46	5	0.36	317	0.237	9.8	0.0319	5.6	0.57	31.348	5.6	0.0538	8.0	363	181	216	19	202	11	44
BCB-2_S_414	110	30	4	0.28	4280	0.245	20.6	0.0331	11.8	0.57	30.178	11.8	0.0536	16.8	356	380	223	41	210	24	41
BCB-2_S_415	407	146	15	0.36	559	0.223	6.8	0.0309	5.3	0.79	32.341	5.3	0.0524	4.2	304	96	205	13	196	10	35
BCB-2_S_418	368	124	13	0.34	472	0.208	5.9	0.0302	4.6	0.78	33.148	4.6	0.0501	3.7	200	86	192	10	192	9	4
BCB-2_S_420	220	77	8	0.35	112	0.232	9.7	0.0314	6.2	0.64	31.838	6.2	0.0537	7.5	357	168	212	19	199	12	44
BCB-2_S_421	81	21	3	0.26	698	0.203	15.2	0.0316	7.0	0.46	31.610	7.0	0.0465	13.5	26	323	188	26	201	14	-681
BCB-2_S_422	612	247	21	0.40	2491	0.205	6.1	0.0294	4.6	0.74	33.975	4.6	0.0506	4.1	222	95	190	11	187	8	16
BCB-2_S_423	75	20	3	0.27	62	0.194	13.1	0.0314	6.3	0.49	31.800	6.3	0.0447	11.4	-69	279	180	22	200	12	387
BCB-2_S_424	126	34	5	0.27	60	0.250	17.2	0.0321	7.6	0.44	31.164	7.6	0.0565	15.5	470	343	226	35	204	15	57
BCB-2_S_426	261	77	12	0.30	166	0.407	18.8	0.0347	7.8	0.42	28.840	7.8	0.0852	17.0	1321	330	347	55	219.7	17	83
BCB-2_S_427	102	32	4	0.31	95	0.238	15.6	0.0313	6.4	0.41	31.932	6.4	0.0551	14.2	418	317	217	30	199	13	52
BCB-2_S_428	99	42	5	0.42	66	0.380	24.2	0.0364	10.9	0.45	27.481	10.9	0.0757	21.6	1087	432	327	68	230	25	79
BCB-2_S_429	310	128	11	0.41	1769	0.227	8.2	0.0312	5.0	0.61	32.073	5.0	0.0529	6.5	325	147	208	15	198	10	39
BCB-2_S_434	93	32	3	0.35	95	0.264	13.7	0.0326	6.9	0.50	30.634	6.9	0.0587	11.9	554	259	238	29	207	14	63
BCB-2_S_436	97	35	4	0.36	164	0.246	15.3	0.0327	6.7	0.44	30.615	6.7	0.0547	13.8	400	308	224	31	207	14	48
BCB-2_S_437	418	210	15	0.50	548	0.228	10.8	0.0298	5.1	0.47	33.537	5.1	0.0555	9.5	433	212	209	20	189	9	56
BCB-2_S_438	59	26	2	0.44	123	0.139	19.3	0.0302	5.3	0.28	33.144	5.3	0.0335	18.5	-836	530	132	24	192	10	123
BCB-2_S_439	170	104	6	0.61	151	0.224	12.2	0.0305	5.9	0.48	32.813	5.9	0.0533	10.7	341	242	205	23	194	11	43
BCB-2_S_440	68	24	2	0.35	145	0.191	13.0	0.0314	5.8	0.44	31.881	5.8	0.0441	11.6	-105	286	177	21	199	11	290
BCB-2_S_442	165	66	6	0.40	194	0.250	12.1	0.0314	5.8	0.48	31.894	5.8	0.0579	10.6	526	232	227	25	199	11	62
BCB-2_S_446	385	260	14	0.68	240	0.244	8.1	0.0294	4.2	0.52	34.031	4.2	0.0603	6.9	614	149	222	16	187	8	70
BCB-2_S_447	170	112	6	0.66	193	0.229	9.4	0.0303	4.6	0.49	33.020	4.6	0.0549	8.2	407	183	209	18	192	9	53
BCB-2_S_449	324	139	12	0.43	145	0.215	8.6	0.0311	5.6	0.65	32.137	5.6	0.0502	6.6	205	152	198	16	198	11	4
BCB-2_S_450	226	80	8	0.35	234	0.257	11.0	0.0317	6.5	0.59	31.518	6.5	0.0586	8.9	554	195	232	23	201	13	64
BCB-2_S_451	62	23	2	0.38	27	0.199	12.2	0.0301	5.6	0.46	33.200	5.6	0.0480	10.9	99	257	185	21	191	10	-94
BCB-2_S_452	299	105	12	0.35	12565	0.279	11.7	0.0323	5.7	0.48	30.960	5.7	0.0626	10.2	696	217	250	26	205	11	71
BCB-2_S_454	703	220	24	0.31	447	0.230	6.3	0.0298	5.2	0.83	33.612	5.2	0.0560	3.5	454	79	210	12	189	10	58
BCB-2_S_455	360	119	13	0.33	531	0.260	5.1	0.0315	3.4	0.68	31.780	3.4	0.0598	3.7	598	80	234	11	200	7	67
BCB-2_S_456	177	50	6	0.28	316	0.213	8.0	0.0315	4.9	0.61	31.793	4.9	0.0492	6.3	156	148	196	14	200	10	-28
BCB-2_S_458	95	25	3	0.27	1352	0.227	9.4	0.0326	5.1	0.54	30.720	5.1	0.0506	7.9	225	183	208	18	206	10	8
BCB-2_S_459	91	38	3	0.42	88	0.202	11.2	0.0307	5.1	0.45	32.549	5.1	0.0478	10.0	87	238	187	19	195	10	-123
BCB-2_S_461	220	72	8	0.33	323	0.233	8.6	0.0319	5.2	0.61	31.310	5.2	0.0529	6.8	324	154	213	16	203	10	37
BCB-2_S_462	160	52	6	0.32	126	0.205	8.8	0.0311	5.3	0.61	32.112	5.3	0.0477	7.0	83	165	189	15	198	10	-139
BCB-2_S_467	430	282	24	0.66	139	0.564	18.0	0.0333	6.5	0.36	30.037	6.5	0.1229	16.8	1998	298	454	66	211	14	89

BCB-2_S_469	414	154	15	0.37	499	0.220	5.6	0.0305	4.0	0.71	32.818	4.0	0.0523	4.0	297	90	202	10	193	8	35
BCB-2_S_470	228	79	11	0.35	174	0.541	13.5	0.0342	8.1	0.60	29.279	8.1	0.1149	10.8	1879	194	439	48	216	17	88
BCB-2_S_471	521	250	21	0.48	2820	0.256	7.9	0.0333	5.6	0.71	30.010	5.6	0.0557	5.6	442	125	232	16	211	12	52
BCB-2_S_473	167	59	6	0.35	64	0.213	7.4	0.0309	4.4	0.59	32.346	4.4	0.0500	6.0	195	139	196	13	196	9	-1
BCB-2_S_474	329	112	14	0.34	215	0.329	14.5	0.0354	9.1	0.63	28.248	9.1	0.0673	11.3	848	234	289	36	224	20	74
BCB-2_S_476	181	69	8	0.38	210	0.272	17.4	0.0323	7.3	0.42	30.917	7.3	0.0610	15.8	638	341	244	38	205	15	68
BCB-2_S_479	89	31	3	0.35	1410	0.202	11.8	0.0301	5.0	0.42	33.253	5.0	0.0487	10.7	131	251	187	20	191	9	-45
BCB-2_S_481	657	253	24	0.38	527	0.218	7.1	0.0308	4.1	0.58	32.483	4.1	0.0513	5.8	256	132	200	13	195	8	24
BCB-2_S_482	89	34	3	0.38	167	0.244	14.0	0.0313	5.9	0.43	31.921	5.9	0.0565	12.6	471	279	222	28	199	12	58
BCB-2_S_483	302	91	12	0.30	224	0.304	10.3	0.0322	3.9	0.38	31.100	3.9	0.0685	9.6	884	197	269	24	204	8	77
BCB-2_S_484	420	173	16	0.41	248	0.240	9.3	0.0314	5.2	0.57	31.892	5.2	0.0554	7.6	428	170	218	18	199	10	54
BCB-2_S_485	137	73	7	0.53	735	0.490	16.4	0.0340	6.1	0.37	29.438	6.1	0.1045	15.2	1706	280	405	55	215	13	87
BCB-2_S_487	292	113	11	0.39	1062	0.213	7.8	0.0313	4.8	0.61	31.973	4.8	0.0494	6.2	168	146	196	14	199	9	-18
BCB-2_S_488	438	157	16	0.36	3213	0.231	9.2	0.0312	5.2	0.56	32.097	5.2	0.0537	7.6	359	173	211	18	198	10	45
BCB-2_S_489	143	44	5	0.31	61	0.243	9.2	0.0313	5.3	0.58	31.908	5.3	0.0562	7.5	459	166	221	18	199	10	57
BCB-2_S_490	88	32	4	0.37	58	0.315	19.5	0.0317	8.1	0.42	31.510	8.1	0.0719	17.8	983	362	278	47	201	16	80
BCB-2_S_491	146	52	5	0.36	1530	0.204	10.5	0.0301	5.5	0.53	33.219	5.5	0.0492	9.0	159	210	189	18	191	10	-20
BCB-2_S_492	551	262	20	0.48	501	0.205	7.1	0.0303	5.6	0.79	33.029	5.6	0.0491	4.3	150	102	189	12	192	11	-28
BCB-2_S_493	442	139	15	0.31	2739	0.202	6.5	0.0306	4.7	0.72	32.679	4.7	0.0480	4.5	97	107	187	11	194	9	-100
BCB-2_S_495	183	62	6	0.34	209	0.211	8.5	0.0300	5.2	0.61	33.355	5.2	0.0509	6.7	238	155	194	15	190	10	20
BCB-2_S_497	239	151	9	0.63	280	0.196	7.2	0.0300	4.3	0.60	33.383	4.3	0.0474	5.8	69	138	182	12	190	8	-176
BCB-2_S_499	121	35	4	0.29	126	0.209	9.7	0.0305	4.6	0.47	32.817	4.6	0.0496	8.6	178	200	192	17	194	9	-9
BCB-2_S_500	354	124	13	0.35	822	0.230	9.7	0.0316	5.8	0.60	31.618	5.8	0.0527	7.7	314	175	210	18	201	11	36
BCB-2_S_504	436	170	17	0.39	227	0.260	10.3	0.0315	5.0	0.48	31.705	5.0	0.0597	9.0	592	196	234	22	200	10	66
BCB-2_S_506	116	35	4	0.30	1751	0.201	9.9	0.0309	4.6	0.47	32.349	4.6	0.0471	8.8	55	210	186	17	196	9	-258
BCB-2_S_507	93	38	3	0.40	1882	0.206	13.8	0.0308	6.2	0.45	32.466	6.2	0.0485	12.4	125	292	190	24	196	12	-57
BCB-2_S_511	62	30	2	0.49	56	0.239	13.6	0.0313	6.2	0.46	31.965	6.2	0.0554	12.1	428	271	218	27	199	12	54
BCB-2_S_514	370	177	13	0.48	650	0.204	6.7	0.0299	4.1	0.62	33.390	4.1	0.0495	5.2	171	123	189	11	190	8	-11
BCB-2_S_515	81	34	3	0.42	125	0.213	12.1	0.0317	5.8	0.48	31.522	5.8	0.0486	10.6	128	249	196	21	201	12	-57
BCB-2_S_517	241	121	9	0.50	661	0.221	10.3	0.0308	5.8	0.57	32.471	5.8	0.0521	8.5	288	194	203	19	196	11	32
BCB-2_S_520	388	185	16	0.48	309	0.355	13.7	0.0314	5.8	0.42	31.892	5.8	0.0822	12.4	1250	242	309	36	199	11	84
BCB-2_S_521	148	55	7	0.37	456	0.484	18.2	0.0320	6.4	0.35	31.283	6.4	0.1098	17.0	1796	310	401	60	203	13	89
BCB-2_S_528	99	41	5	0.42	306	0.363	17.1	0.0451	7.0	0.41	22.194	7.0	0.0585	15.6	549	340	315	46	284	19	48
BCB-2_S_531	462	157	16	0.34	249	0.212	6.0	0.0297	3.9	0.66	33.630	3.9	0.0517	4.5	271	104	195	11	189	7	30
BCB-2_S_532	215	89	8	0.41	385	0.265	12.1	0.0321	8.1	0.67	31.119	8.1	0.0597	9.0	594	195	238	26	204	16	66
BCB-2_S_533	587	407	28	0.69	561	0.256	16.6	0.0330	10.1	0.61	30.336	10.1	0.0564	13.2	469	292	232	34	209	21	55
BCB-2_M_1	299	113	11	0.38	370	0.217	8.2	0.0318	4.8	0.58	31.420	4.8	0.0493	6.6	164	155	199	15	202	9	-23

BCB-2_M_2	77	27	3	0.35	241	0.229	11.3	0.0319	5.4	0.48	31.320	5.4	0.0520	9.9	287	226	209	21	203	11	29
BCB-2_M_3	103	48	4	0.46	99	0.206	7.3	0.0307	4.8	0.65	32.626	4.8	0.0487	5.5	132	129	190	13	195	9	-48
BCB-2_M_4	463	215	16	0.47	1182	0.204	7.0	0.0309	5.2	0.75	32.402	5.2	0.0479	4.6	92	109	188	12	196	10	-112
BCB-2_M_5	380	155	15	0.41	2760	0.312	9.3	0.0329	5.9	0.64	30.403	5.9	0.0688	7.2	892	148	276	22	209	12	77
BCB-2_M_6	77	26	3	0.34	180	0.190	10.0	0.0307	5.0	0.50	32.587	5.0	0.0450	8.7	-58	212	177	16	195	10	438
BCB-2_M_7	79	32	3	0.40	490	0.244	17.0	0.0295	6.6	0.39	33.950	6.6	0.0600	15.6	604	338	221	34	187	12	69
BCB-2_M_8	86	42	3	0.49	114	0.224	14.6	0.0303	4.4	0.30	32.966	4.4	0.0536	13.9	355	314	205	27	193	8	46
BCB-2_M_9	161	67	6	0.41	220	0.213	10.7	0.0328	6.1	0.58	30.492	6.1	0.0471	8.7	55	208	196	19	208	13	-281
BCB-2_M_10	164	30	5	0.18	1292	0.217	8.5	0.0313	5.0	0.59	31.910	5.0	0.0501	6.8	201	159	199	15	199	10	1
BCB-2_M_11	87	26	3	0.30	48	0.203	10.0	0.0304	5.2	0.52	32.938	5.2	0.0484	8.5	119	200	187	17	193	10	-62
BCB-2_M_12	104	31	3	0.29	365	0.210	11.7	0.0302	5.4	0.46	33.090	5.4	0.0505	10.4	217	240	194	21	192	10	12
BCB-2_M_14	310	105	10	0.34	322	0.195	6.3	0.0295	4.7	0.73	33.848	4.7	0.0479	4.3	96	102	181	11	188	9	-95
BCB-2_M_15	103	31	4	0.30	403	0.234	15.2	0.0307	6.5	0.43	32.619	6.5	0.0553	13.7	423	306	213	29	195	12	54
BCB-2_M_17	173	78	6	0.45	462	0.219	13.2	0.0297	5.6	0.42	33.644	5.6	0.0534	12.0	345	271	201	24	189	10	45
BCB-2_M_18	128	44	4	0.34	8588	0.203	9.2	0.0289	5.4	0.59	34.635	5.4	0.0509	7.4	237	171	187	16	183	10	23
BCB-2_M_19	385	184	13	0.48	186	0.217	8.6	0.0298	6.2	0.72	33.564	6.2	0.0528	6.0	319	136	199	16	189	12	41
BCB-2_M_20	252	78	8	0.31	515	0.203	8.4	0.0292	4.9	0.58	34.225	4.9	0.0505	6.9	216	160	188	14	186	9	14
BCB-2_M_21	584	604	24	1.03	4791	0.217	7.2	0.0307	6.2	0.86	32.582	6.2	0.0513	3.7	254	84	199	13	195	12	23
BCB-2_M_22	509	232	17	0.46	429	0.211	6.9	0.0298	6.0	0.88	33.538	6.0	0.0514	3.3	260	75	195	12	189	11	27
BCB-2_M_23	212	104	7	0.49	259	0.206	8.0	0.0300	5.1	0.63	33.351	5.1	0.0497	6.2	182	144	190	14	190	10	-5
BCB-2_M_24	174	63	6	0.36	819	0.215	7.2	0.0310	4.2	0.58	32.245	4.2	0.0503	5.8	208	135	198	13	197	8	5
BCB-2_M_25	117	43	4	0.37	49	0.202	9.0	0.0304	5.4	0.60	32.890	5.4	0.0482	7.2	108	170	187	15	193	10	-80
BCB-2_M_26	139	39	4	0.28	117	0.198	9.3	0.0291	5.3	0.57	34.313	5.3	0.0494	7.6	165	179	184	16	185	10	-13
BCB-2_M_27	187	78	6	0.42	280	0.223	7.8	0.0303	4.4	0.56	33.027	4.4	0.0533	6.5	344	147	204	14	192	8	44
BCB-2_M_28	401	207	14	0.52	1571	0.205	7.7	0.0298	5.9	0.76	33.551	5.9	0.0499	5.0	192	117	190	13	189	11	2
BCB-2_M_29	123	42	4	0.34	384	0.215	11.6	0.0312	5.6	0.48	32.035	5.6	0.0500	10.2	197	236	198	21	198	11	-1
BCB-2_M_30	425	149	14	0.35	347	0.208	6.7	0.0300	5.3	0.79	33.334	5.3	0.0502	4.1	203	95	191	12	191	10	6
BCB-2_M_31	212	52	7	0.25	612	0.206	7.1	0.0300	4.4	0.63	33.334	4.4	0.0498	5.5	187	129	190	12	191	8	-2
BCB-2_M_32	140	43	5	0.30	109	0.213	11.8	0.0310	5.8	0.49	32.287	5.8	0.0499	10.3	191	240	196	21	197	11	-3
BCB-2_M_33	313	141	11	0.45	707	0.202	6.7	0.0293	3.6	0.53	34.160	3.6	0.0502	5.7	202	132	187	11	186	7	8
BCB-2_M_34	97	26	3	0.27	109	0.198	10.5	0.0290	5.2	0.49	34.519	5.2	0.0495	9.1	173	213	183	18	184	9	-6
BCB-2_M_35	89	39	3	0.44	182	0.244	17.9	0.0305	6.0	0.34	32.833	6.0	0.0581	16.8	535	368	222	36	193	12	64
BCB-2_M_36	392	379	18	0.97	388	0.345	18.2	0.0309	2.4	0.13	32.368	2.4	0.0810	18.1	1222	355	301	47	196	5	84
BCB-2_M_37	1138	1125	44	0.99	9908	0.202	5.2	0.0288	4.7	0.91	34.728	4.7	0.0510	2.1	241	49	187	9	183	8	24
BCB-2_M_38	120	40	4	0.33	145	0.204	12.6	0.0304	4.5	0.36	32.912	4.5	0.0488	11.7	138	276	189	22	193	9	-40
BCB-2_M_39	87	34	6	0.39	30	0.926	18.3	0.0370	7.9	0.43	27.033	7.9	0.1815	16.5	2666	274	665	89	234	18	91
BCB-2_M_40	96	29	3	0.30	111	0.219	8.7	0.0301	4.8	0.55	33.202	4.8	0.0528	7.3	319	166	201	16	191	9	40

BCB-2_M_41	682	184	26	0.27	8401	0.373	15.6	0.0309	3.5	0.23	32.415	3.5	0.0877	15.2	1375	292	322	43	196	7	86
BCB-2_M_43	82	27	3	0.33	116	0.210	13.3	0.0290	6.0	0.45	34.463	6.0	0.0526	11.8	312	269	194	23	184	11	41
BCB-2_M_44	83	35	3	0.42	26	0.253	9.9	0.0306	5.9	0.59	32.632	5.9	0.0599	8.0	599	173	229	20	195	11	67
BCB-2_M_46	64	24	2	0.38	41	0.208	10.5	0.0302	4.4	0.42	33.074	4.4	0.0499	9.5	190	222	192	18	192	8	-1
BCB-2_M_47	211	85	7	0.40	1676	0.202	8.7	0.0291	3.7	0.42	34.323	3.7	0.0504	7.9	212	184	187	15	185	7	13
BCB-2_M_49	508	199	17	0.39	631	0.220	6.6	0.0294	4.4	0.67	33.960	4.4	0.0542	4.9	381	111	202	12	187	8	51
BCB-2_M_50	152	52	6	0.34	225	0.219	8.9	0.0323	5.0	0.56	30.916	5.0	0.0492	7.4	156	172	201	16	205	10	-32
BCB-2_M_51	100	31	3	0.31	46	0.197	18.5	0.0296	6.8	0.37	33.813	6.8	0.0482	17.2	111	405	182	31	188	13	-69
BCB-2_M_52	80	30	3	0.38	141	0.184	14.6	0.0299	5.2	0.36	33.457	5.2	0.0447	13.6	-69	332	172	23	190	10	374
BCB-2_M_53	251	79	8	0.32	131	0.218	7.5	0.0300	5.0	0.67	33.363	5.0	0.0526	5.5	313	126	200	14	190	9	39
BCB-2_M_54	385	154	14	0.40	255	0.224	9.3	0.0318	7.1	0.76	31.439	7.1	0.0511	6.1	245	140	205	17	202	14	18
BCB-2_M_55	100	32	3	0.31	131	0.167	12.9	0.0280	4.4	0.34	35.705	4.4	0.0431	12.1	-160	301	156	19	178	8	212
BCB-2_M_56	108	33	4	0.30	272	0.192	10.6	0.0302	5.5	0.52	33.142	5.5	0.0462	9.0	8	218	179	17	192	10	-2287
BCB-2_M_57	2336	1609	101	0.69	2018	0.294	8.1	0.0307	6.5	0.80	32.587	6.5	0.0696	4.8	916	99	262	19	195	12	79
BCB-2_M_58	548	203	29	0.37	225	0.553	20.7	0.0374	9.2	0.45	26.713	9.2	0.1071	18.5	1751	339	447	75	237	21	86
BCB-2_M_59	152	42	5	0.28	155	0.223	9.2	0.0307	6.0	0.65	32.605	6.0	0.0527	6.9	317	158	204	17	195	11	39
BCB-2_M_60	146	69	5	0.47	489	0.225	13.2	0.0300	5.0	0.38	33.291	5.0	0.0543	12.2	382	275	206	25	191	9	50
BCB-2_M_62	2482	719	123	0.29	196	0.644	4.7	0.0318	3.7	0.79	31.437	3.7	0.1469	2.9	2310	50	505	19	202	7	91
BCB-2_M_63	161	41	5	0.26	302	0.218	8.9	0.0298	5.3	0.59	33.513	5.3	0.0529	7.2	325	163	200	16	190	10	42
BCB-2_M_64	133	29	5	0.22	119	0.269	20.0	0.0328	8.6	0.43	30.505	8.6	0.0596	18.1	588	392	242	43	208	18	65
BCB-2_M_65	680	246	25	0.36	425	0.227	7.2	0.0315	5.5	0.77	31.699	5.5	0.0522	4.5	294	103	208	13	200	11	32
BCB-2_M_67	1463	1490	65	1.02	5730	0.312	6.1	0.0301	4.5	0.74	33.277	4.5	0.0752	4.1	1074	82	275	15	191	8	82
BCB-2_M_68	1466	1540	61	1.05	2031	0.205	4.5	0.0300	4.2	0.93	33.285	4.2	0.0495	1.7	174	39	190	8	191	8	-10
BCB-2_M_69	204	70	7	0.34	144	0.201	10.0	0.0298	5.7	0.57	33.520	5.7	0.0488	8.2	140	192	186	17	190	11	-36
BCB-2_M_74	207	90	7	0.43	101	0.210	9.0	0.0313	4.5	0.50	31.929	4.5	0.0486	7.8	127	183	193	16	199	9	-57
BCB-2_M_76	270	296	18	1.10	168	0.766	14.0	0.0388	5.0	0.35	25.778	5.0	0.1431	13.1	2266	226	577	62	245	12	89
BCB-2_M_79	158	56	6	0.35	2547	0.221	10.3	0.0320	5.5	0.53	31.247	5.5	0.0501	8.7	199	202	203	19	203	11	-2
BCB-2_M_81	406	216	15	0.53	276	0.224	8.0	0.0318	5.2	0.65	31.398	5.2	0.0510	6.1	243	140	205	15	202	10	17
BCB-2_M_82	194	79	7	0.40	122	0.220	9.1	0.0328	5.6	0.62	30.485	5.6	0.0486	7.2	128	170	202	17	208	12	-63
BCB-2_M_83	131	58	5	0.44	551	0.277	15.7	0.0313	4.1	0.26	31.971	4.1	0.0641	15.1	746	319	248	34	199	8	73
BCB-2_M_84	164	59	6	0.36	264	0.216	12.3	0.0318	5.5	0.45	31.431	5.5	0.0493	11.0	161	256	199	22	202	11	-26
BCB-2_M_85	132	69	5	0.52	80	0.272	18.2	0.0335	7.9	0.44	29.849	7.9	0.0589	16.3	564	356	244	39	212	17	62
BCB-2_M_86	489	175	17	0.36	2111	0.227	9.7	0.0315	6.3	0.66	31.696	6.3	0.0523	7.3	297	166	208	18	200	12	32
BCB-2_M_87	93	35	5	0.38	961	0.495	18.0	0.0346	3.5	0.19	28.924	3.5	0.1039	17.6	1694	325	408	60	219	7	87
BCB-2_M_90	177	85	6	0.48	149	0.216	7.8	0.0302	4.0	0.51	33.119	4.0	0.0518	6.7	277	153	198	14	192	8	31
BCB-2_M_91	144	49	5	0.34	311	0.237	10.5	0.0320	5.2	0.50	31.275	5.2	0.0538	9.1	362	205	216	20	203	10	44

Analysis	Composition						Corrected isotope ratios						Apparent ages (Ma)											
	U ppm	Th ppm	Pb ppm	Th/U	$\frac{^{206}\text{Pb}}{^{204}\text{Pb}}$	$\frac{^{207}\text{Pb}}{^{235}\text{U}}$	$\pm 2\sigma$ (%)	$\frac{^{206}\text{Pb}}{^{238}\text{U}}$	$\pm 2\sigma$ (%)	error corr.	$\frac{^{238}\text{U}}{^{206}\text{Pb}}$	$\pm 2\sigma$ (%)	$\frac{^{207}\text{Pb}}{^{206}\text{Pb}}$	$\pm 2\sigma$ (%)	$\frac{^{207}\text{Pb}}{^{206}\text{Pb}}$ (abs)	$\pm 2\sigma$ (%)	$\frac{^{207}\text{Pb}}{^{235}\text{U}}$ (abs)	$\pm 2\sigma$ (%)	$\frac{^{206}\text{Pb}}{^{238}\text{U}}$ (abs)	$\pm 2\sigma$ (%)	% disc.			
BCB-3 (Boulder Creek Beds – subunit 3)																								
BCB-3_B_677	86	32	9	0.37	76	0.376	54.2	0.0465	46.2	0.85	21.519	46.2	0.0587	28.4	556	620	324	150	293	132	47			
BCB-3_B_678	57	17	2	0.30	100	0.191	16.2	0.0302	3.1	0.19	33.087	3.1	0.0457	16.0	-17	386	177	26	192	6	1207			
BCB-3_B_679	117	31	4	0.26	340	0.190	10.3	0.0309	5.0	0.48	32.373	5.0	0.0446	9.0	-79	220	176	17	196	10	348			
BCB-3_B_680	222	62	8	0.28	133	0.216	7.5	0.0308	3.0	0.40	32.468	3.0	0.0508	6.9	230	159	198	14	196	6	15			
BCB-3_B_681	75	22	3	0.30	104	0.255	11.5	0.0359	7.3	0.64	27.846	7.3	0.0514	8.9	260	204	230	24	227	16	13			
BCB-3_B_682	122	39	5	0.32	173	0.230	11.3	0.0344	5.9	0.52	29.046	5.9	0.0485	9.6	122	226	210	21	218	13	-78			
BCB-3_B_683	261	120	11	0.46	1672	0.232	10.0	0.0352	7.5	0.74	28.387	7.5	0.0477	6.7	85	159	212	19	223	16	-163			
BCB-3_B_684	403	232	16	0.58	2395	0.208	8.0	0.0310	6.6	0.82	32.236	6.6	0.0486	4.6	129	108	192	14	197	13	-52			
BCB-3_B_686	48	18	2	0.37	38	0.240	12.0	0.0352	6.5	0.54	28.410	6.5	0.0495	10.1	172	235	219	24	223	14	-30			
BCB-3_B_687	108	30	4	0.27	122	0.204	12.0	0.0311	3.7	0.31	32.141	3.7	0.0475	11.5	76	272	188	21	198	7	-160			
BCB-3_B_688	73	23	3	0.32	185	0.187	15.3	0.0319	3.1	0.20	31.376	3.1	0.0427	15.0	-188	374	174	25	202	6	208			
BCB-3_B_690	148	45	5	0.31	123	0.217	10.0	0.0315	4.8	0.48	31.768	4.8	0.0500	8.8	195	205	199	18	200	9	-2			
BCB-3_B_691	261	100	9	0.38	197	0.215	6.4	0.0305	2.7	0.42	32.746	2.7	0.0511	5.8	243	133	198	11	194	5	20			
BCB-3_B_692	51	13	2	0.26	94	0.244	12.3	0.0332	5.0	0.40	30.078	5.0	0.0533	11.2	343	254	222	24	211	10	38			
BCB-3_B_693	88	25	3	0.29	240	0.224	11.5	0.0322	4.4	0.39	31.053	4.4	0.0504	10.6	215	245	205	21	204	9	5			
BCB-3_B_694	46	12	2	0.26	62	0.202	14.7	0.0342	7.5	0.51	29.205	7.5	0.0429	12.6	-175	314	187	25	217	16	224			
BCB-3_B_696	321	62	11	0.19	2509	0.225	12.8	0.0304	5.0	0.39	32.938	5.0	0.0537	11.8	357	266	206	24	193	10	46			
BCB-3_B_699	72	25	3	0.35	1514	0.195	14.0	0.0311	5.6	0.40	32.148	5.6	0.0455	12.9	-27	312	181	23	197	11	818			
BCB-3_B_702	117	46	4	0.39	5570	0.241	10.7	0.0325	4.8	0.44	30.785	4.8	0.0537	9.5	359	215	219	21	206	10	43			
BCB-3_B_703	115	42	4	0.36	213	0.207	13.0	0.0304	3.3	0.25	32.939	3.3	0.0495	12.6	172	294	191	23	193	6	-12			
BCB-3_B_704	67	24	2	0.36	73	0.220	11.7	0.0309	5.5	0.47	32.359	5.5	0.0517	10.3	271	236	202	21	196	11	27			
BCB-3_B_705	93	29	3	0.31	523	0.210	14.2	0.0325	3.3	0.23	30.743	3.3	0.0469	13.8	46	329	194	25	206	7	-351			
BCB-3_B_706	62	22	2	0.36	1884	0.213	14.4	0.0314	4.1	0.28	31.876	4.1	0.0492	13.8	159	323	196	26	199	8	-26			
BCB-3_S_329	137	34	5	0.25	64	0.215	7.7	0.0310	4.2	0.55	32.240	4.2	0.0503	6.4	211	148	198	14	197	8	7			
BCB-3_S_330	115	31	5	0.27	1337	0.361	21.7	0.0370	10.5	0.48	27.001	10.5	0.0706	19.0	946	389	313	58	234	24	75			
BCB-3_S_331	54	13	2	0.24	149	0.296	28.1	0.0340	7.7	0.27	29.443	7.7	0.0632	27.0	715	574	263	65	215	16	70			
BCB-3_S_335	91	25	4	0.27	7209	0.223	10.7	0.0343	5.4	0.50	29.116	5.4	0.0470	9.3	51	221	204	20	218	12	-328			
BCB-3_S_336	267	118	10	0.44	1682	0.209	5.9	0.0324	4.1	0.67	30.903	4.1	0.0469	4.3	42	104	193	10	205	8	-391			
BCB-3_S_340	137	59	6	0.43	288	0.229	9.0	0.0325	4.6	0.50	30.732	4.6	0.0511	7.7	247	178	210	17	206	9	16			
BCB-3_S_341	68	17	3	0.25	114	0.207	13.4	0.0332	4.3	0.32	30.140	4.3	0.0452	12.7	-47	308	191	23	210	9	549			
BCB-3_S_342	128	35	5	0.27	2484	0.232	11.2	0.0323	5.0	0.44	30.959	5.0	0.0521	10.0	290	228	212	21	205	10	29			
BCB-3_S_343	111	29	5	0.26	11639	0.302	22.8	0.0339	9.7	0.42	29.536	9.7	0.0647	20.6	765	434	268	54	215	20	72			

BCB-3_S_353	134	70	6	0.52	242	0.256	12.4	0.0350	8.1	0.65	28.608	8.1	0.0532	9.4	336	213	232	26	221	18	34
BCB-3_S_354	112	41	4	0.37	696	0.217	9.6	0.0322	3.3	0.34	31.063	3.3	0.0488	9.0	140	211	199	17	204	7	-46
BCB-3_S_356	190	85	8	0.45	325	0.318	18.7	0.0323	7.9	0.42	30.920	7.9	0.0713	17.0	967	347	280	46	205	16	79
BCB-3_S_357	76	21	3	0.28	309	0.223	15.3	0.0344	5.3	0.34	29.049	5.3	0.0471	14.4	53	343	205	28	218	11	-315
BCB-3_S_362	86	36	3	0.42	420	0.240	10.0	0.0326	1.9	0.18	30.714	1.9	0.0535	9.8	351	222	219	20	207	4	41
BCB-3_S_363	75	31	3	0.41	1169	0.279	24.7	0.0360	12.5	0.51	27.784	12.5	0.0562	21.2	462	471	250	55	228	28	51
BCB-3_S_366	158	45	6	0.28	248	0.258	11.4	0.0339	6.1	0.53	29.487	6.1	0.0551	9.7	418	216	233	24	215	13	49
BCB-3_S_367	112	28	5	0.25	479	0.315	22.3	0.0350	10.5	0.47	28.581	10.5	0.0654	19.6	787	412	278	54	222	23	72
BCB-3_S_379	81	34	4	0.42	185	0.379	26.3	0.0384	12.0	0.46	26.057	12.0	0.0717	23.4	976	476	326	73	243	29	75
BCB-3_S_383	91	33	3	0.36	197	0.205	10.9	0.0303	4.6	0.42	32.964	4.6	0.0489	9.9	143	232	189	19	193	9	-34
BCB-3_S_386	47	16	2	0.35	45	0.286	22.5	0.0328	8.1	0.36	30.491	8.1	0.0632	21.0	716	445	255	51	208	17	71
BCB-3_S_387	74	29	3	0.39	1777	0.238	12.0	0.0329	6.5	0.54	30.359	6.5	0.0524	10.1	301	230	217	23	209	13	31
BCB-3_S_388	72	20	3	0.28	40	0.237	12.8	0.0311	5.3	0.41	32.179	5.3	0.0552	11.6	421	259	216	25	197	10	53
BCB-3_S_389	63	17	2	0.27	327	0.215	23.0	0.0333	6.9	0.30	30.021	6.9	0.0468	21.9	38	524	198	41	211	14	-453
BCB-3_S_391	60	15	2	0.26	127	0.246	12.9	0.0331	5.1	0.39	30.250	5.1	0.0540	11.8	371	267	223	26	210	10	44
BCB-3_S_401	100	24	4	0.24	215	0.244	15.8	0.0373	6.4	0.40	26.846	6.4	0.0474	14.5	71	345	221	32	236	15	-230
BCB-3_S_402	128	44	6	0.34	4608	0.368	7.3	0.0351	3.7	0.51	28.453	3.7	0.0760	6.2	1095	125	318	20	223	8	80
BCB-3_S_407	376	194	17	0.52	2212	0.278	15.0	0.0363	11.2	0.75	27.535	11.2	0.0555	10.0	432	222	249	33	230	25	47
BCB-3_S_412	58	16	2	0.28	3709	0.246	13.2	0.0324	7.0	0.53	30.909	7.0	0.0551	11.1	415	249	223	26	205	14	50
BCB-3_S_416	44	17	2	0.39	44	0.300	11.1	0.0329	6.6	0.59	30.410	6.6	0.0662	8.9	814	187	267	26	209	14	74
BCB-3_S_417	53	15	2	0.27	729	0.195	15.6	0.0327	6.8	0.44	30.588	6.8	0.0433	14.0	-153	349	181	26	207	14	236
BCB-3_S_422	66	18	2	0.27	90	0.221	12.6	0.0324	5.1	0.40	30.909	5.1	0.0495	11.6	172	270	203	23	205	10	-19
BCB-3_S_424	77	28	3	0.36	126	0.273	15.4	0.0339	5.2	0.33	29.539	5.2	0.0586	14.5	551	316	245	34	215	11	61
BCB-3_S_425	116	38	5	0.33	3635	0.317	18.7	0.0333	6.5	0.35	30.053	6.5	0.0691	17.5	902	361	280	46	211	14	77
BCB-3_S_431	94	30	4	0.31	233	0.252	8.6	0.0319	4.9	0.57	31.303	4.9	0.0573	7.1	503	156	228	18	203	10	60
BCB-3_S_432	110	34	4	0.31	336	0.235	12.3	0.0316	4.9	0.39	31.642	4.9	0.0539	11.3	365	255	214	24	201	10	45
BCB-3_S_434	53	15	2	0.28	31	0.229	13.5	0.0315	5.2	0.38	31.734	5.2	0.0527	12.5	315	284	209	26	200	10	36
BCB-3_S_435	77	36	3	0.47	57	0.280	11.9	0.0300	4.8	0.40	33.325	4.8	0.0677	10.9	860	227	251	27	191	9	78
BCB-3_S_437	130	63	5	0.48	201	0.238	9.3	0.0335	5.3	0.56	29.818	5.3	0.0515	7.7	263	177	217	18	213	11	19
BCB-3_S_440	59	20	3	0.33	51	0.354	14.0	0.0354	5.2	0.37	28.224	5.2	0.0724	13.0	997	264	307	37	224	11	77
BCB-3_S_442	178	91	7	0.51	976	0.232	13.7	0.0327	4.3	0.31	30.547	4.3	0.0513	13.0	254	299	211	26	208	9	18
BCB-3_S_451	58	19	2	0.33	390	0.242	25.0	0.0322	9.5	0.38	31.059	9.5	0.0545	23.1	392	519	220	50	204	19	48
BCB-3_S_453	146	57	6	0.39	453	0.232	8.9	0.0327	6.4	0.72	30.563	6.4	0.0515	6.2	261	141	212	17	208	13	21
BCB-3_S_456	71	20	3	0.28	43	0.242	11.5	0.0321	6.0	0.52	31.196	6.0	0.0549	9.8	406	219	220	23	203	12	50
BCB-3_S_457	57	14	2	0.25	154	0.259	17.9	0.0333	7.4	0.41	30.074	7.4	0.0566	16.3	475	361	234	37	211	15	56
BCB-3_S_458	262	111	10	0.43	2134	0.204	6.2	0.0307	4.5	0.71	32.604	4.5	0.0482	4.3	111	102	189	11	195	9	-75
BCB-3_S_460	63	22	3	0.35	92	0.295	17.9	0.0360	9.0	0.50	27.779	9.0	0.0594	15.5	582	336	262	41	228	20	61

BCB-3_S_461	379	256	26	0.68	8870	0.385	5.1	0.0536	3.7	0.72	18.649	3.7	0.0521	3.5	291	80	331	14	337	12	-16
BCB-3_S_462	73	23	3	0.31	256	0.233	14.3	0.0312	4.7	0.33	32.031	4.7	0.0540	13.5	372	304	212	27	198	9	47
BCB-3_S_463	94	33	5	0.35	114	0.386	23.4	0.0372	11.3	0.48	26.850	11.3	0.0751	20.5	1071	413	331	66	236	26	78
BCB-3_S_464	62	20	3	0.32	86	0.484	28.6	0.0370	12.0	0.42	26.995	12.0	0.0948	25.9	1524	489	401	95	234	28	85
BCB-3_S_465	270	78	12	0.29	1419	0.275	7.0	0.0386	4.2	0.59	25.923	4.2	0.0517	5.7	271	130	247	15	244	10	10
BCB-3_S_466	146	57	6	0.39	1588	0.214	11.8	0.0331	5.0	0.43	30.231	5.0	0.0469	10.6	46	254	197	21	210	10	-355
BCB-3_S_467	153	48	5	0.31	1632	0.213	10.7	0.0311	3.6	0.34	32.184	3.6	0.0496	10.1	177	236	196	19	197	7	-11
BCB-3_S_470	129	40	5	0.31	63820	0.260	14.4	0.0358	8.4	0.58	27.914	8.4	0.0525	11.7	309	267	234	30	227	19	27
BCB-3_S_471	144	54	5	0.38	163	0.216	10.0	0.0322	5.1	0.51	31.104	5.1	0.0486	8.6	131	203	198	18	204	10	-56
BCB-3_S_472	52	15	2	0.30	38	0.251	13.3	0.0323	5.3	0.40	30.988	5.3	0.0565	12.2	472	271	228	27	205	11	57
BCB-3_S_473	80	30	3	0.38	254	0.232	10.4	0.0324	4.8	0.46	30.856	4.8	0.0518	9.2	278	211	211	20	206	10	26
BCB-3_S_475	172	61	6	0.35	943	0.219	7.9	0.0315	4.0	0.50	31.717	4.0	0.0504	6.8	214	158	201	14	200	8	7
BCB-3_S_478	54	13	2	0.24	58	0.182	22.1	0.0315	5.7	0.26	31.748	5.7	0.0419	21.3	-232	538	170	35	200	11	186
BCB-3_S_479	101	25	4	0.24	133	0.221	16.4	0.0329	4.7	0.28	30.405	4.7	0.0488	15.8	139	370	203	30	209	10	-50
BCB-3_S_480	171	69	7	0.40	131	0.233	9.6	0.0344	4.9	0.51	29.037	4.9	0.0491	8.2	152	192	213	18	218	11	-43
BCB-3_S_481	246	101	10	0.41	953	0.220	10.4	0.0336	5.6	0.53	29.771	5.6	0.0475	8.8	76	209	202	19	213	12	-181
BCB-3_S_482	132	37	5	0.28	258	0.273	11.1	0.0339	4.3	0.39	29.536	4.3	0.0586	10.2	551	223	245	24	215	9	61
BCB-3_S_484	64	22	3	0.34	70	0.248	8.9	0.0337	3.6	0.40	29.632	3.6	0.0533	8.1	340	184	225	18	214	8	37
BCB-3_S_486	209	61	8	0.29	181	0.212	8.8	0.0327	3.1	0.35	30.624	3.1	0.0470	8.3	49	197	195	16	207	6	-326
BCB-3_S_489	133	52	5	0.39	84	0.194	14.9	0.0310	4.1	0.27	32.296	4.1	0.0453	14.4	-37	349	180	25	197	8	625
BCB-3_S_490	59	18	2	0.30	77	0.228	18.1	0.0331	4.1	0.22	30.256	4.1	0.0500	17.6	193	409	208	34	210	8	-9
BCB-3_S_491	63	18	2	0.29	67	0.256	14.6	0.0329	6.3	0.43	30.403	6.3	0.0564	13.2	469	293	231	30	209	13	56
BCB-3_S_494	81	23	3	0.28	33	0.209	9.7	0.0314	4.1	0.41	31.862	4.1	0.0482	8.9	109	209	192	17	199	8	-82
BCB-3_S_495	132	42	5	0.32	41	0.219	12.4	0.0305	4.6	0.37	32.764	4.6	0.0520	11.5	284	263	201	23	194	9	32
BCB-3_S_496	521	275	22	0.53	1017	0.254	8.6	0.0339	4.6	0.53	29.492	4.6	0.0543	7.3	383	163	230	18	215	10	44
BCB-3_S_497	273	276	14	1.01	987	0.287	12.7	0.0357	5.0	0.40	27.973	5.0	0.0582	11.6	539	255	256	29	226	11	58
BCB-3_S_498	103	33	4	0.32	131	0.238	9.0	0.0330	4.4	0.48	30.289	4.4	0.0524	7.9	303	180	217	18	209	9	31
BCB-3_S_502	124	55	5	0.45	989	0.208	9.7	0.0320	3.1	0.32	31.210	3.1	0.0472	9.2	58	220	192	17	203	6	-252
BCB-3_S_503	74	35	4	0.48	253	0.413	19.7	0.0359	6.7	0.34	27.880	6.7	0.0834	18.6	1279	362	351	58	227	15	82
BCB-3_S_505	146	46	5	0.32	509	0.213	11.1	0.0311	3.6	0.33	32.171	3.6	0.0496	10.4	178	243	196	20	197	7	-11
BCB-3_S_510	121	34	5	0.28	366	0.241	11.5	0.0317	5.8	0.50	31.510	5.8	0.0551	9.9	418	222	220	23	201	12	52
BCB-3_S_511	85	25	3	0.30	125	0.194	10.8	0.0337	5.0	0.46	29.642	5.0	0.0418	9.6	-240	242	180	18	214	10	189
BCB-3_S_515	68	19	3	0.28	297	0.222	14.3	0.0346	6.2	0.43	28.880	6.2	0.0464	12.9	21	309	203	26	219	13	-953
BCB-3_S_516	97	47	6	0.48	198	0.584	22.6	0.0388	10.5	0.46	25.774	10.5	0.1091	20.0	1784	365	467	85	245	25	86
BCB-3_S_519	278	128	11	0.46	620	0.243	6.0	0.0329	3.7	0.61	30.403	3.7	0.0536	4.8	352	108	221	12	209	8	41
BCB-3_S_520	507	306	21	0.60	904	0.227	6.9	0.0323	4.0	0.57	30.971	4.0	0.0510	5.6	242	130	208	13	205	8	15
BCB-3_S_521	131	41	6	0.31	149	0.300	18.8	0.0352	9.2	0.49	28.389	9.2	0.0618	16.4	669	352	267	44	223	20	67

BCB-3_S_522	110	29	4	0.26	2266	0.232	10.1	0.0338	5.1	0.50	29.568	5.1	0.0497	8.7	179	203	211	19	214	11	-20
BCB-3_S_523	302	110	12	0.36	2337	0.225	7.1	0.0339	4.1	0.57	29.481	4.1	0.0482	5.8	108	136	206	13	215	9	-99
BCB-3_S_526	76	30	3	0.40	177	0.216	14.7	0.0315	6.1	0.42	31.753	6.1	0.0497	13.4	182	312	198	27	200	12	-10
BCB-3_S_527	100	34	4	0.34	79	0.212	12.1	0.0316	4.7	0.38	31.693	4.7	0.0488	11.2	138	263	195	22	200	9	-46
BCB-3_S_531	122	45	5	0.37	276	0.315	18.1	0.0341	6.6	0.37	29.336	6.6	0.0671	16.8	841	350	278	44	216	14	74
BCB-3_S_532	76	25	3	0.33	662	0.188	13.6	0.0337	5.4	0.40	29.717	5.4	0.0406	12.5	-315	320	175	22	213	11	168
BCB-3_S_535	227	72	8	0.32	116	0.212	7.6	0.0315	5.5	0.73	31.727	5.5	0.0488	5.2	140	121	195	13	200	11	-43
BCB-3_S_537	45	12	2	0.27	1529	0.211	18.8	0.0320	6.1	0.32	31.288	6.1	0.0480	17.8	97	420	195	33	203	12	-109
BCB-3_S_538	170	66	7	0.39	183	0.234	9.5	0.0333	5.7	0.59	30.043	5.7	0.0510	7.7	239	177	213	18	211	12	12
BCB-3_S_539	108	40	4	0.37	802	0.218	11.3	0.0302	4.8	0.42	33.162	4.8	0.0524	10.3	305	235	200	21	192	9	37
BCB-3_S_541	138	59	6	0.43	902	0.266	19.2	0.0344	8.6	0.45	29.090	8.6	0.0562	17.2	460	381	240	41	218	18	53
BCB-3_S_543	166	59	6	0.36	304	0.218	8.4	0.0311	5.0	0.59	32.187	5.0	0.0510	6.7	241	155	201	15	197	10	18
BCB-3_S_545	588	289	24	0.49	826	0.267	6.4	0.0325	4.0	0.63	30.804	4.0	0.0597	4.9	592	107	240	14	206	8	65
BCB-3_S_546	472	194	19	0.41	6259	0.226	8.8	0.0332	7.9	0.90	30.098	7.9	0.0494	3.8	168	89	207	16	211	16	-26
BCB-3_S_548	86	27	3	0.32	247	0.268	14.0	0.0331	6.3	0.45	30.182	6.3	0.0587	12.5	556	273	241	30	210	13	62
BCB-3_S_549	108	60	5	0.55	122	0.267	14.6	0.0359	8.1	0.56	27.872	8.1	0.0540	12.1	370	273	240	31	227	18	39
BCB-3_S_550	38	11	1	0.29	34	0.270	19.2	0.0329	6.1	0.32	30.369	6.1	0.0595	18.2	586	396	243	42	209	13	64
BCB-3_S_551	129	38	5	0.29	304	0.261	10.5	0.0334	5.4	0.51	29.925	5.4	0.0566	9.0	476	200	235	22	212	11	56
BCB-3_S_552	180	42	6	0.23	281	0.219	9.2	0.0308	3.1	0.33	32.429	3.1	0.0515	8.7	262	199	201	17	196	6	25
BCB-3_S_553	120	38	4	0.32	273	0.219	7.4	0.0319	4.2	0.57	31.327	4.2	0.0499	6.1	188	142	201	14	203	8	-8
BCB-3_S_554	77	23	3	0.30	355	0.204	10.9	0.0322	5.3	0.48	31.012	5.3	0.0459	9.6	-10	231	188	19	205	11	2224
BCB-3_S_556	77	29	3	0.37	347	0.217	10.7	0.0320	4.5	0.42	31.275	4.5	0.0493	9.7	161	228	200	19	203	9	-26
BCB-3_S_557	142	85	6	0.60	150	0.265	15.3	0.0342	7.0	0.46	29.236	7.0	0.0561	13.5	458	301	238	32	217	15	53
BCB-3_S_564	136	35	5	0.26	120	0.223	7.3	0.0335	4.5	0.61	29.856	4.5	0.0483	5.8	114	136	204	14	212	9	-86
BCB-3_S_565	126	34	5	0.27	743	0.223	13.8	0.0342	5.6	0.40	29.218	5.6	0.0473	12.6	64	299	205	25	217	12	-239
BCB-3_S_567	374	271	16	0.73	724	0.232	4.9	0.0325	2.6	0.53	30.790	2.6	0.0518	4.1	276	94	212	9	206	5	25
BCB-3_S_568	381	275	16	0.72	1417	0.220	5.5	0.0319	3.0	0.53	31.388	3.0	0.0500	4.7	195	109	202	10	202	6	-4
BCB-3_S_569	59	21	2	0.36	53	0.198	19.7	0.0333	5.5	0.28	30.003	5.5	0.0432	18.9	-159	469	184	33	211	11	233
BCB-3_S_570	107	54	4	0.50	277	0.222	8.3	0.0316	5.2	0.63	31.658	5.2	0.0510	6.4	239	148	204	15	200	10	16
BCB-3_S_575	134	76	7	0.57	131	0.319	6.4	0.0437	2.4	0.37	22.901	2.4	0.0529	5.9	326	134	281	16	276	6	15
BCB-3_S_576	140	51	8	0.36	326	0.387	17.3	0.0465	7.5	0.43	21.482	7.5	0.0603	15.6	614	337	332	49	293	21	52
BCB-3_S_582	139	62	5	0.44	235	0.226	10.5	0.0302	5.1	0.49	33.145	5.1	0.0544	9.2	388	206	207	20	192	10	51
BCB-3_S_583	113	55	4	0.49	89	0.215	11.4	0.0324	5.3	0.46	30.891	5.3	0.0481	10.1	102	240	197	21	205	11	-101
BCB-3_S_584	117	42	5	0.36	83	0.233	14.2	0.0341	7.6	0.53	29.366	7.6	0.0496	12.0	178	280	213	27	216	16	-21
BCB-3_S_585	93	31	3	0.33	444	0.212	11.9	0.0307	6.0	0.51	32.582	6.0	0.0500	10.2	195	237	195	21	195	12	0
BCB-3_S_586	72	25	3	0.35	83	0.200	16.1	0.0312	3.8	0.23	32.074	3.8	0.0465	15.7	23	376	185	27	198	7	-777
BCB-3_S_587	39	8	2	0.21	35	0.302	22.2	0.0334	7.5	0.34	29.937	7.5	0.0655	20.9	791	439	268	52	212	16	73

BCB-3_S_588	139	42	5	0.30	847	0.210	11.4	0.0333	4.9	0.42	30.010	4.9	0.0458	10.3	-12	250	194	20	211	10	1822
BCB-3_S_589	286	113	10	0.40	3977	0.210	7.6	0.0306	3.1	0.40	32.648	3.1	0.0498	7.0	187	162	194	13	194	6	-4
BCB-3_S_591	129	46	5	0.36	413	0.234	7.6	0.0324	4.4	0.57	30.876	4.4	0.0523	6.2	301	141	213	15	205	9	32
BCB-3_S_592	119	39	4	0.33	387	0.213	9.6	0.0321	4.8	0.50	31.150	4.8	0.0481	8.3	103	196	196	17	204	10	-98
BCB-3_S_594	116	42	5	0.36	228	0.228	17.9	0.0366	9.5	0.53	27.306	9.5	0.0452	15.2	-47	370	209	34	232	22	591
BCB-3_S_598	237	96	9	0.40	467	0.214	8.9	0.0316	6.0	0.67	31.611	6.0	0.0491	6.5	153	153	197	16	201	12	-31
BCB-3_S_608	148	54	6	0.36	4669	0.257	16.9	0.0323	6.5	0.38	30.927	6.5	0.0575	15.6	513	343	232	35	205	13	60
BCB-3_S_611	52	16	2	0.30	838	0.232	17.7	0.0344	6.8	0.38	29.044	6.8	0.0490	16.4	146	384	212	34	218	15	-49
BCB-3_S_612	47	13	2	0.27	993	0.234	15.9	0.0318	5.1	0.32	31.415	5.1	0.0532	15.1	338	341	213	31	202	10	40
BCB-3_S_613	120	43	5	0.36	301	0.217	9.1	0.0325	5.1	0.56	30.745	5.1	0.0484	7.5	117	177	199	16	206	10	-76
BCB-3_S_614	176	69	7	0.39	232	0.228	8.5	0.0323	4.0	0.46	30.977	4.0	0.0513	7.6	253	174	209	16	205	8	19
BCB-3_S_615	164	50	6	0.31	558	0.228	10.4	0.0324	5.3	0.51	30.887	5.3	0.0511	8.9	243	205	208	20	205	11	16
BCB-3_S_616	69	19	3	0.27	95	0.236	12.3	0.0324	6.1	0.49	30.873	6.1	0.0528	10.7	322	244	215	24	205	12	36
BCB-3_S_617	95	26	4	0.27	3344	0.305	15.2	0.0323	6.1	0.40	30.993	6.1	0.0686	13.9	888	286	271	36	205	12	77
BCB-3_S_618	208	88	9	0.42	925	0.303	20.2	0.0336	8.4	0.42	29.739	8.4	0.0653	18.4	784	386	269	48	213	18	73
BCB-3_S_619	49	14	2	0.29	135	0.224	21.4	0.0313	6.1	0.28	31.952	6.1	0.0518	20.5	278	469	205	40	199	12	29
BCB-3_S_620	117	34	4	0.29	454	0.226	9.6	0.0322	6.2	0.65	31.087	6.2	0.0509	7.3	235	168	207	18	204	13	13
BCB-3_S_623	61	19	2	0.30	57	0.213	14.4	0.0316	4.6	0.31	31.616	4.6	0.0489	13.7	144	322	196	26	201	9	-39
BCB-3_S_624	284	143	11	0.50	1959	0.219	7.1	0.0311	4.2	0.59	32.134	4.2	0.0511	5.7	246	131	201	13	198	8	20
BCB-3_S_626	129	45	5	0.35	539	0.255	14.6	0.0335	6.7	0.46	29.815	6.7	0.0551	13.0	415	291	230	30	213	14	49
BCB-3_S_628	209	88	8	0.42	1061	0.242	11.2	0.0314	3.6	0.32	31.844	3.6	0.0559	10.6	447	235	220	22	199	7	55
BCB-3_S_633	221	95	9	0.43	3034	0.230	7.4	0.0321	5.1	0.69	31.172	5.1	0.0521	5.4	288	123	210	14	204	10	29
BCB-3_S_635	209	88	7	0.42	178	0.210	8.0	0.0299	3.6	0.45	33.418	3.6	0.0509	7.2	235	165	193	14	190	7	19
BCB-3_S_636	141	51	5	0.36	180	0.244	12.4	0.0314	7.2	0.58	31.805	7.2	0.0562	10.1	462	225	222	25	200	14	57
BCB-3_S_639	107	45	37	0.42	668	3.793	4.0	0.2785	3.7	0.90	3.590	3.7	0.0988	1.7	1601	31	1591	32	1584	52	1
BCB-3_S_642	179	59	7	0.33	423	0.236	10.1	0.0324	5.0	0.49	30.888	5.0	0.0530	8.8	327	200	216	20	205	10	37
BCB-3_S_643	79	28	3	0.35	586	0.243	13.1	0.0322	5.6	0.42	31.061	5.6	0.0548	11.9	402	266	221	26	204	11	49
BCB-3_S_649	296	112	11	0.38	207	0.218	7.5	0.0317	4.9	0.65	31.577	4.9	0.0499	5.7	189	133	200	14	201	10	-7
Composition																					
Analysis		U	Th	Pb	$\frac{^{206}\text{Pb}}{^{204}\text{Pb}}$	$\frac{^{207}\text{Pb}}{^{235}\text{U}}$	$\pm 2\sigma$	$\frac{^{206}\text{Pb}}{^{238}\text{U}}$	$\pm 2\sigma$	error	$\frac{^{238}\text{U}}{^{206}\text{Pb}}$	$\pm 2\sigma$	$\frac{^{207}\text{Pb}}{^{206}\text{Pb}}$	$\pm 2\sigma$	$\frac{^{207}\text{Pb}}{^{206}\text{Pb}}$	$\pm 2\sigma$	$\frac{^{207}\text{Pb}}{^{235}\text{U}}$	$\pm 2\sigma$	$\frac{^{206}\text{Pb}}{^{238}\text{U}}$	$\pm 2\sigma$	%
Corrected isotope ratios																					
Apparent ages (Ma)																					

BCB-5 (Boulder Creek Beds – subunit 5)

BCB-5_S_1	938	839	39	0.89	1427	0.213	4.5	0.0313	3.5	0.76	31.953	3.5	0.0494	2.9	169	68	196	8	199	7	-18
BCB-5_S_2	545	360	23	0.66	614	0.223	6.1	0.0332	5.0	0.81	30.087	5.0	0.0487	3.6	133	84	204	11	211	10	-59
BCB-5_S_3	213	130	9	0.61	259	0.270	8.4	0.0330	4.4	0.53	30.317	4.4	0.0593	7.1	577	154	242	18	209	9	64
BCB-5_S_4	122	57	5	0.47	933	0.217	9.2	0.0306	3.9	0.42	32.672	3.9	0.0514	8.4	261	193	200	17	194	7	26

BCB-5_S_5	109	56	4	0.52	1429	0.228	8.9	0.0317	4.5	0.51	31.498	4.5	0.0522	7.7	292	175	209	17	201	9	31
BCB-5_S_6	112	54	5	0.48	137	0.318	17.5	0.0394	10.5	0.60	25.392	10.5	0.0585	14.0	550	306	280	43	249	26	55
BCB-5_S_7	87	33	3	0.38	123	0.233	7.4	0.0321	4.5	0.61	31.131	4.5	0.0526	5.9	309	134	212	14	204	9	34
BCB-5_S_8	108	40	4	0.37	79	0.221	9.4	0.0298	3.1	0.33	33.546	3.1	0.0537	8.8	359	200	203	17	189	6	47
BCB-5_S_10	126	64	5	0.51	3266	0.208	12.6	0.0328	4.2	0.33	30.485	4.2	0.0460	11.8	-1	286	192	22	208	9	186
BCB-5_S_13	106	44	4	0.42	102	0.216	10.9	0.0322	2.9	0.26	31.026	2.9	0.0485	10.5	124	248	198	20	204	6	-65
BCB-5_S_14	310	191	12	0.62	674	0.220	5.9	0.0314	4.0	0.67	31.858	4.0	0.0507	4.3	229	100	202	11	199	8	13
BCB-5_S_15	157	100	7	0.64	75	0.266	15.0	0.0332	5.9	0.39	30.146	5.9	0.0581	13.8	535	302	239	32	210	12	61
BCB-5_S_16	96	35	4	0.36	99	0.220	11.6	0.0331	5.2	0.45	30.236	5.2	0.0483	10.4	113	245	202	21	210	11	-85
BCB-5_S_18	460	254	21	0.55	488	0.267	11.1	0.0362	7.9	0.71	27.595	7.9	0.0535	7.9	348	178	240	24	229	18	34
BCB-5_S_19	183	83	7	0.46	472	0.213	6.1	0.0305	2.4	0.40	32.745	2.4	0.0506	5.6	223	129	196	11	194	5	13
BCB-5_S_21	564	817	30	1.45	673	0.262	9.2	0.0360	5.7	0.62	27.743	5.7	0.0527	7.2	315	163	236	19	228	13	28
BCB-5_S_22	661	588	31	0.89	2346	0.247	6.4	0.0356	5.5	0.86	28.114	5.5	0.0504	3.3	216	76	224	13	225	12	-4
BCB-5_S_23	147	78	6	0.53	216	0.311	14.8	0.0353	8.2	0.56	28.295	8.2	0.0638	12.2	735	259	275	36	224	18	70
BCB-5_S_27	111	50	4	0.45	4199	0.245	12.1	0.0330	5.1	0.42	30.273	5.1	0.0539	11.0	367	247	223	24	210	10	43
BCB-5_S_29	254	103	10	0.40	26	0.234	7.4	0.0316	3.5	0.46	31.656	3.5	0.0537	6.6	357	148	213	14	200	7	44
BCB-5_S_31	350	294	15	0.84	1053	0.240	9.0	0.0317	4.1	0.46	31.508	4.1	0.0548	8.0	403	180	218	18	201	8	50
BCB-5_S_33	72	31	3	0.43	109	0.282	16.5	0.0376	9.8	0.59	26.571	9.8	0.0544	13.3	388	298	252	37	238	23	39
BCB-5_S_37	177	95	8	0.54	141	0.287	13.7	0.0359	7.9	0.57	27.875	7.9	0.0581	11.2	533	246	256	31	227	18	57
BCB-5_S_42	419	177	17	0.42	162	0.350	38.0	0.0314	8.7	0.23	31.800	8.7	0.0807	37.0	1213	728	304	100	200	17	84
BCB-5_S_43	161	77	7	0.47	253	0.315	13.8	0.0351	8.0	0.58	28.481	8.0	0.0651	11.2	776	236	278	33	222	18	71
BCB-5_S_46	279	194	14	0.70	426	0.276	10.6	0.0375	5.1	0.48	26.661	5.1	0.0534	9.2	346	209	248	23	237	12	31
BCB-5_S_47	88	51	4	0.58	145	0.236	15.7	0.0363	5.1	0.32	27.511	5.1	0.0471	14.9	57	355	215	31	230	11	-306
BCB-5_S_50	94	48	4	0.51	42	0.299	14.2	0.0341	5.0	0.35	29.336	5.0	0.0637	13.3	730	283	266	33	216	11	70
BCB-5_S_52	116	63	5	0.54	92	0.375	19.1	0.0346	6.6	0.34	28.940	6.6	0.0786	17.9	1163	355	323	53	219	14	81
BCB-5_S_53	148	56	6	0.38	570	0.236	8.3	0.0323	3.7	0.44	30.924	3.7	0.0529	7.4	326	169	215	16	205	7	37
BCB-5_S_55	270	197	13	0.73	611	0.330	13.3	0.0363	5.2	0.39	27.582	5.2	0.0660	12.2	805	255	289	33	230	12	71
BCB-5_S_58	57	15	2	0.27	107	0.240	10.3	0.0338	5.4	0.52	29.624	5.4	0.0516	8.7	270	201	219	20	214	11	21
BCB-5_S_59	667	468	28	0.70	3177	0.230	7.2	0.0323	5.6	0.77	30.933	5.6	0.0515	4.5	263	104	210	14	205	11	22
BCB-5_S_60	230	90	9	0.39	251	0.224	7.3	0.0319	3.7	0.50	31.397	3.7	0.0510	6.3	239	144	205	13	202	7	15
BCB-5_S_61	169	65	7	0.38	227	0.274	17.6	0.0345	8.4	0.47	28.980	8.4	0.0576	15.5	515	341	246	39	219	18	58
BCB-5_S_63	216	106	9	0.49	210	0.212	6.6	0.0324	4.3	0.64	30.842	4.3	0.0474	5.0	67	120	195	12	206	9	-205
BCB-5_S_64	209	108	8	0.52	242	0.222	6.5	0.0322	4.6	0.71	31.051	4.6	0.0499	4.5	191	105	203	12	204	9	-7
BCB-5_S_65	376	161	15	0.43	520	0.211	8.0	0.0331	5.4	0.67	30.216	5.4	0.0462	5.9	6	143	194	14	210	11	-3400
BCB-5_S_68	144	56	5	0.39	265	0.223	8.1	0.0315	3.3	0.41	31.736	3.3	0.0514	7.4	259	169	205	15	200	7	23
BCB-5_S_79	160	44	6	0.28	219	0.247	8.4	0.0345	3.1	0.37	28.992	3.1	0.0519	7.8	281	178	224	17	219	7	22
BCB-5_S_81	63	17	3	0.27	110	0.247	12.0	0.0352	4.3	0.36	28.425	4.3	0.0509	11.2	238	258	224	24	223	9	6

BCB-5_S_84	98	45	4	0.47	124	0.254	15.1	0.0328	5.8	0.38	30.451	5.8	0.0560	13.9	452	309	229	31	208	12	54
BCB-5_S_85	1009	1132	45	1.12	527	0.207	4.1	0.0298	3.2	0.76	33.574	3.2	0.0505	2.6	219	61	191	7	189	6	14
BCB-5_S_87	104	35	4	0.34	135	0.225	13.7	0.0330	4.7	0.34	30.313	4.7	0.0496	12.8	175	300	206	26	209	10	-20
BCB-5_S_89	119	42	5	0.35	7180	0.254	10.1	0.0333	4.3	0.42	30.051	4.3	0.0554	9.1	429	204	230	21	211	9	51
BCB-5_S_90	195	85	8	0.43	16296	0.242	9.4	0.0332	5.0	0.53	30.101	5.0	0.0529	8.0	326	181	220	19	211	10	35
BCB-5_S_91	407	189	16	0.46	474	0.223	4.6	0.0321	3.7	0.80	31.173	3.7	0.0505	2.7	216	63	205	8	204	7	6
BCB-5_S_92	250	112	11	0.45	393	0.255	9.7	0.0363	7.7	0.79	27.581	7.7	0.0511	6.0	245	138	231	20	230	17	6
BCB-5_S_93	266	127	10	0.48	113	0.225	5.1	0.0309	2.5	0.49	32.399	2.5	0.0529	4.4	324	100	206	9	196	5	40
BCB-5_S_94	342	187	14	0.55	319	0.220	5.4	0.0319	2.8	0.50	31.383	2.8	0.0501	4.7	198	108	202	10	202	5	-2
BCB-5_S_95	387	167	15	0.43	606	0.227	6.5	0.0329	4.0	0.62	30.377	4.0	0.0500	5.1	193	119	208	12	209	8	-8
BCB-5_S_97	116	66	5	0.57	96	0.296	21.2	0.0337	8.0	0.38	29.703	8.0	0.0638	19.6	734	416	263	49	213	17	71
BCB-5_S_98	584	271	23	0.46	1426	0.216	5.7	0.0321	4.5	0.79	31.145	4.5	0.0488	3.5	137	82	199	10	204	9	-49
BCB-5_S_100	227	83	9	0.36	427	0.226	8.8	0.0325	6.7	0.76	30.802	6.7	0.0506	5.8	221	134	207	17	206	14	7
BCB-5_S_103	285	175	15	0.61	1590	0.348	16.7	0.0369	9.7	0.58	27.066	9.7	0.0682	13.6	875	281	303	44	234	22	73
BCB-5_S_104	145	41	7	0.28	149	0.330	18.8	0.0406	16.1	0.86	24.611	16.1	0.0588	9.7	561	212	289	47	257	40	54
BCB-5_S_105	518	239	19	0.46	294	0.216	6.4	0.0301	4.1	0.63	33.241	4.1	0.0520	4.9	287	113	198	12	191	8	33
BCB-5_S_107	633	283	24	0.45	382	0.222	4.9	0.0311	3.5	0.72	32.179	3.5	0.0518	3.4	277	78	204	9	197	7	29
BCB-5_S_108	208	76	9	0.37	300	0.289	15.4	0.0364	12.7	0.82	27.469	12.7	0.0575	8.7	511	192	258	35	231	29	55
BCB-5_S_111	115	49	5	0.42	107	0.241	13.9	0.0340	8.5	0.61	29.447	8.5	0.0514	11.0	261	252	219	27	215	18	17
BCB-5_S_112	159	60	6	0.38	237	0.229	12.4	0.0307	4.8	0.39	32.605	4.8	0.0541	11.4	376	257	209	23	195	9	48
BCB-5_S_114	352	125	14	0.35	489	0.249	10.4	0.0334	8.4	0.81	29.942	8.4	0.0540	6.0	370	135	225	21	212	18	43
BCB-5_S_115	748	308	30	0.41	1393	0.225	5.9	0.0324	4.6	0.78	30.822	4.6	0.0503	3.7	207	86	206	11	206	9	0
BCB-5_S_117	1024	802	47	0.78	20747	0.234	7.3	0.0329	5.3	0.72	30.405	5.3	0.0516	5.1	266	116	213	14	209	11	21
BCB-5_S_119	201	66	8	0.33	370	0.246	12.2	0.0348	8.2	0.67	28.718	8.2	0.0513	9.0	253	206	223	24	221	18	13
BCB-5_S_121	194	65	8	0.33	1608	0.237	15.0	0.0342	7.8	0.52	29.264	7.8	0.0503	12.7	208	295	216	29	217	17	-4
BCB-5_S_122	78	36	4	0.46	1520	0.412	19.3	0.0378	10.3	0.53	26.479	10.3	0.0791	16.4	1174	324	350	57	239	24	80
BCB-5_S_123	93	26	3	0.28	121	0.246	9.8	0.0326	6.0	0.61	30.659	6.0	0.0547	7.7	399	172	223	20	207	12	48
BCB-5_S_127	666	284	28	0.43	2229	0.248	10.8	0.0348	8.2	0.76	28.774	8.2	0.0518	6.9	277	159	225	22	220	18	20
BCB-5_S_130	282	108	11	0.39	695	0.230	7.0	0.0325	4.1	0.59	30.778	4.1	0.0514	5.6	258	130	210	13	206	8	20
BCB-5_S_131	292	145	13	0.50	184	0.278	11.4	0.0344	7.8	0.68	29.107	7.8	0.0587	8.3	556	182	249	25	218	17	61
BCB-5_S_132	177	69	9	0.39	357	0.391	20.3	0.0400	14.9	0.74	25.005	14.9	0.0710	13.7	957	280	335	58	253	37	74
BCB-5_S_135	349	179	16	0.51	381	0.328	16.2	0.0375	11.9	0.73	26.670	11.9	0.0635	11.0	726	234	288	41	237.3	28	67
BCB-5_S_139	199	159	9	0.80	218	0.310	13.0	0.0351	5.5	0.42	28.495	5.5	0.0640	11.8	743	249	274	31	222	12	70
BCB-5_S_140	264	134	10	0.51	218	0.214	8.4	0.0321	3.1	0.36	31.132	3.1	0.0484	7.8	120	185	197	15	204	6	-70
BCB-5_S_141	120	57	5	0.47	155	0.239	8.7	0.0338	4.6	0.52	29.567	4.6	0.0513	7.4	254	169	218	17	214	10	16
BCB-5_S_142	132	62	5	0.47	111	0.241	12.7	0.0314	4.3	0.34	31.841	4.3	0.0557	11.9	441	264	219	25	199	8	55
BCB-5_S_149	187	80	8	0.43	196	0.225	8.4	0.0331	5.3	0.63	30.198	5.3	0.0493	6.5	164	152	206	16	210	11	-28

BCB-5_S_151	223	134	12	0.60	111	0.542	18.7	0.0356	11.8	0.63	28.081	11.8	0.1104	14.5	1806	264	440	67	226	26	88
BCB-5_S_154	233	111	10	0.48	1371	0.267	15.3	0.0351	7.8	0.51	28.480	7.8	0.0552	13.1	420	293	240	33	222	17	47
BCB-5_S_156	292	156	12	0.53	2760	0.203	9.1	0.0316	7.0	0.77	31.600	7.0	0.0464	5.7	19	138	187	16	201	14	-945
BCB-5_S_157	107	45	5	0.42	424	0.375	22.5	0.0345	8.3	0.37	29.013	8.3	0.0790	20.9	1172	414	324	62	218	18	81
BCB-5_S_159	164	84	7	0.51	120	0.231	13.5	0.0314	8.0	0.59	31.874	8.0	0.0533	10.9	343	248	211	26	199	16	42
BCB-5_S_165	593	280	23	0.47	855	0.215	6.2	0.0303	5.3	0.86	33.019	5.3	0.0515	3.0	263	70	198	11	192	10	27
BCB-5_S_171	135	64	8	0.48	79	0.514	33.6	0.0368	14.7	0.44	27.181	14.7	0.1014	30.2	1649	560	421	116	233	34	86
BCB-5_S_173	116	39	4	0.34	172	0.210	14.1	0.0321	5.1	0.36	31.155	5.1	0.0475	13.2	72	313	194	25	204	10	-182
BCB-5_S_174	475	174	20	0.37	352	0.265	10.4	0.0362	6.3	0.60	27.616	6.3	0.0530	8.3	330	188	239	22	229	14	31
BCB-5_S_175	714	314	27	0.44	787	0.213	5.1	0.0303	3.8	0.75	32.967	3.8	0.0509	3.3	234	77	196	9	193	7	18
BCB-5_S_178	254	134	12	0.53	142	0.276	17.0	0.0347	10.7	0.63	28.821	10.7	0.0577	13.2	519	290	248	37	220	23	58
BCB-5_S_181	337	139	15	0.41	1607	0.268	13.6	0.0368	11.6	0.85	27.192	11.6	0.0528	7.0	320	160	241	29	233	27	27
BCB-5_B_61	93	34	4	0.36	243	0.213	10.3	0.0340	3.1	0.29	29.390	3.1	0.0454	9.8	-36	238	196	18	216	7	703
BCB-5_B_62	158	69	7	0.44	110	0.269	11.6	0.0365	7.3	0.62	27.417	7.3	0.0535	9.1	351	205	242	25	231	16	34
BCB-5_B_65	538	264	22	0.49	372	0.225	5.8	0.0337	3.0	0.51	29.664	3.0	0.0483	5.0	114	117	206	11	214	6	-87
BCB-5_B_66	820	554	34	0.68	3475	0.225	4.7	0.0326	3.3	0.69	30.713	3.3	0.0500	3.4	196	78	206	9	207	7	-6
BCB-5_B_67	507	252	20	0.50	1149	0.224	5.3	0.0331	2.9	0.54	30.190	2.9	0.0491	4.4	151	103	205	10	210	6	-39
BCB-5_B_68	349	162	14	0.46	2361	0.215	7.6	0.0329	2.7	0.35	30.386	2.7	0.0473	7.1	65	170	197	14	209	6	-223
BCB-5_B_69	122	45	5	0.37	3408	0.244	7.2	0.0336	2.5	0.34	29.741	2.5	0.0527	6.8	316	154	222	14	213	5	33
BCB-5_B_70	106	41	4	0.39	128	0.221	9.3	0.0347	3.8	0.40	28.849	3.8	0.0462	8.5	10	204	203	17	220	8	-2087
BCB-5_B_72	80	53	4	0.66	153	0.281	13.8	0.0346	8.9	0.64	28.903	8.9	0.0588	10.5	561	229	251	31	219	19	61
BCB-5_B_75	882	435	34	0.49	2188	0.224	5.8	0.0316	3.5	0.60	31.680	3.5	0.0514	4.6	258	105	205	11	200	7	22
BCB-5_B_77	87	36	3	0.42	75	0.258	12.4	0.0322	3.7	0.30	31.019	3.7	0.0580	11.9	528	260	233	26	205	7	61
BCB-5_B_78	156	74	6	0.47	341	0.228	9.3	0.0327	4.1	0.44	30.595	4.1	0.0506	8.4	221	193	208	18	207	8	6
BCB-5_B_79	153	67	6	0.44	168	0.237	7.9	0.0324	3.5	0.44	30.866	3.5	0.0531	7.1	334	160	216	15	206	7	39
BCB-5_B_80	140	68	5	0.49	118	0.208	9.9	0.0324	2.7	0.27	30.841	2.7	0.0464	9.5	20	229	192	17	206	5	-912
BCB-5_B_82	769	378	30	0.49	923	0.229	5.4	0.0327	3.9	0.71	30.574	3.9	0.0507	3.8	226	88	209	10	207	8	8
BCB-5_B_83	258	121	10	0.47	592	0.228	6.8	0.0321	3.1	0.45	31.193	3.1	0.0516	6.0	267	139	209	13	203	6	24
BCB-5_B_84	414	238	17	0.58	1309	0.227	5.7	0.0328	3.6	0.63	30.469	3.6	0.0502	4.4	204	102	208	11	208	7	-2
BCB-5_B_85	168	125	7	0.74	198	0.230	8.3	0.0334	4.0	0.49	29.901	4.0	0.0499	7.2	192	168	210	16	212	8	-10
BCB-5_B_86	83	49	4	0.58	216	0.314	20.1	0.0355	7.1	0.35	28.174	7.1	0.0641	18.8	745	397	277	49	225	16	70
BCB-5_B_87	205	91	8	0.44	321	0.241	8.2	0.0327	4.1	0.49	30.556	4.1	0.0535	7.1	351	161	220	16	208	8	41
BCB-5_B_88	232	103	9	0.44	270	0.237	6.4	0.0324	3.1	0.48	30.832	3.1	0.0530	5.6	328	126	216	12	206	6	37
BCB-5_B_89	344	216	134	0.63	3775	4.314	3.3	0.2897	2.7	0.80	3.452	2.7	0.1080	1.9	1766	35	1696	27	1640	39	7
BCB-5_B_90	307	247	125	0.80	10725	4.362	2.5	0.2936	2.2	0.84	3.406	2.2	0.1078	1.2	1762	23	1705	21	1659	32	6
BCB-5_B_91	111	51	4	0.46	74	0.281	8.8	0.0334	4.4	0.49	29.952	4.4	0.0611	7.7	642	165	252	20	212	9	67
BCB-5_B_92	173	90	7	0.52	266	0.245	9.4	0.0331	2.8	0.30	30.182	2.8	0.0536	8.9	353	202	222	19	210	6	40

BCB-5_B_93	904	835	39	0.92	419	0.225	4.9	0.0331	3.6	0.72	30.247	3.6	0.0494	3.4	168	79	206	9	210	7	-25
BCB-5_B_94	387	212	16	0.55	760	0.250	7.8	0.0359	5.4	0.70	27.873	5.4	0.0505	5.6	219	129	227	16	227	12	-4

Notes: Isotope ratios and ages are reported without initial common Pb correction; gas blank-corrected mass 204 signals were generally irresolvable from zero.

Isotope ratio and apparent age errors do NOT include systematic calibration errors of 0.25% for the $^{207}\text{Pb}/^{206}\text{Pb}$ ratio, and 0.56% for the $^{206}\text{Pb}/^{238}\text{U}$ ratio (1s).

Trace element concentrations in ppm, calculated using the mean count rate method, internal standardization to ^{29}Si , and calibration to NIST 610 and 612 glass standards.

Ablation using a 213 nm wavelength laser, spot size of 25 microns, repetition rate of 10 Hz, and fluence of $\sim 5 \text{ J/cm}^2$.

APPENDIX C

**U-Pb Isotopic Data for Magmatic and Detrital Zircon Analyzed By LA-ICPMS and
CA-IDTIMS From Chapter 4**

Table C.1. U-Pb Isotopic Data for Magmatic Zircon from the Jackson Mountains for Chapter 4

Samp. (a)	Compositional Parameters					Radiogenic Isotope Ratios						Isotopic Ages							
	$\frac{^{206}\text{Pb}^*}{^{238}\text{U}}$ $\times 10^{-13}$	mol %	$\frac{\text{Pb}^*}{\text{Pbc}}$	$\frac{\text{Pbc}}{\text{pg}}$	$\frac{^{206}\text{Pb}}{^{204}\text{Pb}}$	$\frac{^{208}\text{Pb}}{^{206}\text{Pb}}$	$\frac{^{207}\text{Pb}}{^{206}\text{Pb}}$	% err (e)	$\frac{^{207}\text{Pb}}{^{235}\text{U}}$	% err (d)	$\frac{^{206}\text{Pb}}{^{238}\text{U}}$	% err (d)	corr. coef.	$\frac{^{207}\text{Pb}}{^{206}\text{Pb}}$	\pm (f)	$\frac{^{207}\text{Pb}}{^{235}\text{U}}$	\pm (f)	$\frac{^{206}\text{Pb}}{^{238}\text{U}}$	\pm (e)
DCPP-1 (Deer Creek Peak pluton)																			
z1	1.3522	99.3%	42	0.77	2674	0.117	0.049905	0.160	0.209002	0.212	0.030374	0.073	0.799	190.56	3.73	192.71	0.37	192.89	0.14
z2	1.2301	99.1%	31	0.95	1967	0.120	0.049899	0.201	0.208934	0.250	0.030368	0.072	0.758	190.30	4.67	192.66	0.44	192.85	0.14
z3	0.3865	97.7%	12	0.75	796	0.101	0.050006	0.526	0.209813	0.583	0.030431	0.092	0.672	195.26	12.21	193.40	1.03	193.24	0.17
z4	0.7489	99.0%	30	0.61	1867	0.124	0.049854	0.391	0.208862	0.426	0.030385	0.098	0.453	188.18	9.10	192.60	0.75	192.96	0.19
z5	0.7436	98.8%	24	0.75	1509	0.131	0.049968	0.245	0.209282	0.295	0.030377	0.077	0.723	193.51	5.70	192.95	0.52	192.90	0.15
MSD-1 (Mary Sloan dikes)																			
z1	0.2150	98.1%	15	0.34	959	0.082	0.049588	0.604	0.203274	0.666	0.029730	0.096	0.690	175.74	14.08	187.89	1.14	188.86	0.18
z4	2.2475	99.7%	89	0.57	5909	0.045	0.049884	0.152	0.205024	0.204	0.029809	0.067	0.839	189.57	3.54	189.37	0.35	189.35	0.12
z5	0.4634	97.7%	13	0.91	786	0.141	0.049588	0.747	0.204473	0.808	0.029906	0.108	0.615	175.74	17.42	188.90	1.39	189.96	0.20
z6	0.3274	97.5%	10	0.70	720	0.033	0.049728	0.607	0.204871	0.675	0.029880	0.089	0.790	182.29	14.15	189.24	1.17	189.80	0.17
z7	2.1385	99.0%	29	1.80	1812	0.144	0.049913	0.123	0.205816	0.181	0.029907	0.071	0.884	190.92	2.86	190.04	0.31	189.96	0.13
z8	1.6403	99.7%	103	0.39	6256	0.155	0.049831	0.123	0.205401	0.176	0.029895	0.074	0.814	187.14	2.87	189.69	0.30	189.89	0.14
z9	0.5953	97.9%	12	1.07	856	0.039	0.050013	0.329	0.206370	0.381	0.029927	0.080	0.708	195.61	7.64	190.50	0.66	190.09	0.15
z10	0.2918	97.8%	12	0.54	824	0.039	0.049683	0.605	0.204805	0.666	0.029898	0.101	0.651	180.17	14.09	189.18	1.15	189.91	0.19
TCS-1 (Trout Creek stock)																			
z1	0.2713	96.6%	10	0.78	541	0.408	0.049224	1.044	0.172607	1.122	0.025432	0.125	0.654	158.49	24.43	161.68	1.68	161.90	0.20
z2	0.0757	89.9%	3	0.70	180	0.227	0.048627	3.238	0.170649	3.378	0.025452	0.225	0.644	129.91	76.14	159.98	5.00	162.02	0.36
z3	0.2296	93.6%	4	1.30	285	0.114	0.049710	0.966	0.209365	1.045	0.030546	0.128	0.658	181.46	22.50	193.02	1.84	193.97	0.24
z4	0.2017	96.0%	7	0.70	451	0.116	0.048746	0.837	0.204017	0.911	0.030355	0.105	0.737	135.64	19.67	188.52	1.57	192.77	0.20
z5	0.2050	93.6%	5	1.15	286	0.302	0.048736	0.976	0.170763	1.058	0.025412	0.125	0.691	135.17	22.93	160.08	1.57	161.77	0.20
z7	0.1394	95.1%	6	0.60	369	0.264	0.049213	1.138	0.172176	1.228	0.025374	0.121	0.770	157.98	26.62	161.31	1.83	161.53	0.19
z9	0.1314	93.6%	5	0.74	286	0.413	0.049346	1.366	0.173103	1.464	0.025442	0.142	0.717	164.32	31.92	162.11	2.19	161.96	0.23
DPP-1 (Delong Peak pluton)																			
z1	0.1006	91.5%	3	0.77	215	0.191	0.049363	2.529	0.172588	2.680	0.025357	0.218	0.714	165.13	59.09	161.66	4.01	161.43	0.35
z3	0.1067	95.4%	6	0.43	392	0.199	0.048996	1.819	0.171632	1.938	0.025406	0.176	0.699	147.63	42.64	160.83	2.88	161.73	0.28
z4	0.0779	93.2%	4	0.47	264	0.202	0.047805	2.632	0.167300	2.795	0.025382	0.337	0.531	89.64	62.36	157.07	4.07	161.58	0.54
z5	0.1764	96.7%	11	0.49	553	0.384	0.048215	1.981	0.168898	2.138	0.025406	0.480	0.426	109.85	46.78	158.46	3.14	161.73	0.77
z6	0.0792	93.2%	5	0.48	266	0.445	0.048521	2.115	0.170013	2.272	0.025413	0.326	0.535	124.74	49.80	159.43	3.35	161.77	0.52
z7	0.0376	89.7%	3	0.36	175	0.120	0.047793	4.241	0.199779	4.433	0.030317	0.425	0.490	89.04	100.51	184.94	7.50	192.53	0.81

- (a) z1, z2, etc., are labels for fractions composed of single zircon or fragments; all zircon fractions were annealed and chemically abraded after Mattinson (2005)
- (b) Pb* and Pbc represent radiogenic and common Pb, respectively; mol % $^{206}\text{Pb}^*$ with respect to radiogenic, blank and initial common Pb.
- (c) Measured ratio corrected for spike and fractionation only. Fractionation estimated at 0.17 ± 0.03 (1-sigma) %/amu for Daly analyses, based on analysis of NBS-981 and NBS-982.
- (d) Corrected for fractionation, spike, and common Pb; all common Pb was assumed to be procedural blank: $^{206}\text{Pb}/^{204}\text{Pb} = 18.042 \pm 0.61\%$; $^{207}\text{Pb}/^{204}\text{Pb} = 15.537 \pm 0.52\%$;
 $^{208}\text{Pb}/^{204}\text{Pb} = 37.686 \pm 0.63\%$ (all uncertainties 1-sigma).
- (e) Errors are 2-sigma, propagated using the algorithms of Schmitz and Schoene (2007).
- (f) Calculations are based on the decay constants of Jaffey et al. (1971). $^{206}\text{Pb}/^{238}\text{U}$ and $^{207}\text{Pb}/^{206}\text{Pb}$ ages corrected for initial disequilibrium in $^{230}\text{Th}/^{238}\text{U}$ using Th/U [magma] = 3.

Table C.2. Magmatic Zircon LA-ICPMS U-Pb Geochronology for Chapter 4

Analysis	Composition						Corrected isotope ratios						Apparent ages (Ma)											
	U ppm	Th ppm	Pb ppm	Th/U	$\frac{^{206}\text{Pb}}{^{204}\text{Pb}}$	$\frac{^{207}\text{Pb}}{^{235}\text{U}}$	$\pm 2s$ (%)	$\frac{^{206}\text{Pb}}{^{238}\text{U}}$	$\pm 2s$ (%)	error corr.	$\frac{^{238}\text{U}}{^{206}\text{Pb}}$	$\pm 2s$ (%)	$\frac{^{207}\text{Pb}}{^{206}\text{Pb}}$	$\pm 2s$ (%)	$\frac{^{207}\text{Pb}}{^{206}\text{Pb}}$ (abs)	$\pm 2s$ (%)	$\frac{^{207}\text{Pb}}{^{235}\text{U}}$ (abs)	$\pm 2s$ (%)	$\frac{^{206}\text{Pb}}{^{238}\text{U}}$ (abs)	$\pm 2s$ (%)	% disc.			
DCPP-1 (Deer Creek Peak pluton)																								
DCPP_L_83	139	77	5	0.55	393	0.216	6.5	0.0299	5.1	0.77	33.437	5.1	0.0523	4.1	297	95	198	12	190	9	36			
DCPP_L_86	102	89	4	0.88	331	0.197	11.9	0.0293	6.1	0.51	34.176	6.1	0.0487	10.2	135	240	182	20	186	11	-38			
DCPP_L_87	52	27	2	0.51	123	0.201	15.5	0.0298	5.1	0.33	33.613	5.1	0.0490	14.7	147	344	186	26	189	10	-29			
DCPP_L_88	67	47	2	0.70	26	0.191	12.6	0.0291	5.2	0.41	34.392	5.2	0.0477	11.5	83	272	178	20	185	9	-123			
DCPP_L_89	93	70	4	0.75	59	0.221	8.7	0.0307	4.2	0.48	32.589	4.2	0.0523	7.6	300	173	203	16	195	8	35			
DCPP_L_91	206	194	8	0.94	252	0.200	7.5	0.0291	4.2	0.56	34.382	4.2	0.0498	6.2	187	145	185	13	185	8	1			
DCPP_L_92	99	81	4	0.82	3976	0.199	9.8	0.0297	5.5	0.55	33.708	5.5	0.0485	8.2	126	193	184	17	188	10	-50			
DCPP_L_96	74	42	3	0.57	126	0.198	11.5	0.0295	4.9	0.42	33.929	4.9	0.0487	10.4	132	245	183	19	187	9	-42			
DCPP_L_97	86	56	3	0.66	62	0.194	10.2	0.0291	5.5	0.54	34.364	5.5	0.0483	8.5	114	201	180	17	185	10	-62			
DCPP_L_98	966	637	36	0.66	1136	0.196	6.4	0.0286	5.8	0.90	34.954	5.8	0.0498	2.8	184	65	182	11	182	10	1			
DCPP_L_99	593	342	22	0.58	2864	0.202	6.1	0.0295	4.8	0.79	33.950	4.8	0.0496	3.7	178	87	186	10	187	9	-5			
DCPP_M_132	185	171	7	0.93	143	0.213	7.8	0.0300	4.9	0.63	33.313	4.9	0.0514	6.1	257	140	196	14	191	9	26			
DCPP_M_136	100	102	4	1.01	432	0.195	11.6	0.0292	5.3	0.45	34.193	5.3	0.0484	10.4	117	244	181	19	186	10	-59			
DCPP_M_139	118	76	4	0.64	605	0.212	12.3	0.0301	3.7	0.30	33.276	3.7	0.0511	11.7	246	270	195	22	191	7	23			
DCPP_M_140	120	77	5	0.64	123	0.209	11.4	0.0320	4.6	0.40	31.217	4.6	0.0474	10.4	67	248	193	20	203	9	-202			
DCPP_M_145	126	84	5	0.66	1994	0.204	11.1	0.0300	4.0	0.36	33.320	4.0	0.0494	10.4	165	242	189	19	191	8	-16			
DCPP_M_146	309	189	11	0.61	245	0.214	6.5	0.0303	3.2	0.49	33.005	3.2	0.0513	5.6	253	130	197	12	192	6	24			
DCPP_M_148	104	47	4	0.45	97	0.210	10.2	0.0303	3.9	0.38	33.003	3.9	0.0503	9.4	210	219	194	18	192	7	8			
DCPP_M_149	692	285	25	0.41	500	0.217	5.2	0.0312	2.5	0.47	32.072	2.5	0.0505	4.5	217	105	199	9	198	5	9			
DCPP_M_150	256	114	9	0.44	1525	0.217	8.1	0.0296	3.0	0.36	33.780	3.0	0.0531	7.5	335	171	199	15	188	6	44			
DCPP_M_151	652	392	23	0.60	539	0.199	6.3	0.0293	2.9	0.46	34.177	2.9	0.0493	5.6	164	130	184	11	186	5	-13			
DCPP_M_154	114	69	4	0.61	206	0.200	12.2	0.0304	3.5	0.28	32.907	3.5	0.0478	11.7	91	277	185	21	193	7	-112			
DCPP_M_155	357	196	13	0.55	369	0.213	7.8	0.0312	3.6	0.46	32.048	3.6	0.0496	6.9	177	161	196	14	198	7	-12			
DCPP_M_156	143	76	5	0.53	116	0.246	7.4	0.0311	2.3	0.30	32.178	2.3	0.0573	7.0	503	154	223	15	197	5	61			
DCPP_M_157	212	171	8	0.81	613	0.203	10.2	0.0302	4.4	0.43	33.093	4.4	0.0488	9.1	139	215	188	17	192	8	-38			
DCPP_M_159	361	268	14	0.74	291	0.213	5.5	0.0306	2.7	0.48	32.630	2.7	0.0505	4.8	217	110	196	10	195	5	10			
DCPP_M_161	68	32	2	0.46	21	0.185	15.2	0.0313	6.3	0.42	31.945	6.3	0.0429	13.8	-175	343	172	24	199	12	213			
DCPP_M_162	48	20	2	0.41	39	0.225	27.3	0.0300	6.6	0.24	33.343	6.6	0.0545	26.5	391	595	206	51	190	12	51			
DCPP_M_165	458	244	17	0.53	1423	0.214	5.4	0.0310	4.1	0.74	32.240	4.1	0.0500	3.6	196	83	197	10	197	8	-1			
DCPP_M_170	113	76	4	0.67	52	0.208	11.0	0.0308	4.4	0.40	32.441	4.4	0.0491	10.1	150	236	192	19	196	9	-30			

DCPP_M_175	119	72	4	0.60	137	0.217	6.1	0.0310	3.6	0.58	32.285	3.6	0.0508	4.9	231	113	199	11	197	7	15
DCPP_M_177	142	91	5	0.64	291	0.208	10.0	0.0303	3.6	0.35	33.034	3.6	0.0497	9.4	183	218	192	17	192	7	-5
DCPP_M_179	198	135	7	0.68	650	0.212	7.6	0.0298	4.6	0.60	33.601	4.6	0.0518	6.0	274	138	196	14	189	9	31
DCPP_M_190	186	141	7	0.76	1286	0.215	6.7	0.0297	4.3	0.64	33.704	4.3	0.0526	5.1	311	116	198	12	188	8	39
DCPP_M_192	163	80	6	0.49	181	0.202	10.7	0.0295	4.8	0.44	33.889	4.8	0.0497	9.6	180	224	187	18	187	9	-4
DCPP_M_193	252	141	9	0.56	4033	0.194	7.3	0.0306	4.1	0.56	32.657	4.1	0.0458	6.0	-11	145	180	12	194	8	1949
DCPP_M_194	121	65	4	0.54	81	0.195	13.5	0.0299	4.8	0.35	33.446	4.8	0.0474	12.6	68	300	181	22	190	9	-180
DCPP_M_197	107	64	4	0.60	362	0.187	15.2	0.0301	6.8	0.45	33.199	6.8	0.0449	13.6	-60	331	174	24	191	13	418
DCPP_M_199	120	78	4	0.65	209	0.198	14.1	0.0317	4.4	0.31	31.570	4.4	0.0452	13.4	-43	325	183	24	201	9	572
DCPP_M_200	375	214	14	0.57	305	0.208	4.7	0.0312	2.8	0.58	32.009	2.8	0.0484	3.8	117	90	192	8	198	5	-69
DCPP_M_205	152	93	6	0.61	74	0.217	8.0	0.0310	3.4	0.42	32.242	3.4	0.0507	7.2	227	166	199	14	197	7	13
DCPP_M_206	130	79	5	0.61	1354	0.225	6.6	0.0319	4.4	0.67	31.301	4.4	0.0511	4.8	247	111	206	12	203	9	18
DCPP_M_208	233	190	9	0.81	128	0.302	10.3	0.0297	3.0	0.29	33.659	3.0	0.0738	9.9	1035	200	268	24	189	6	82
DCPP_M_210	101	59	4	0.59	158	0.198	9.9	0.0304	4.2	0.42	32.847	4.2	0.0472	8.9	58	212	183	17	193	8	-234
DCPP_M_211	131	91	5	0.69	312	0.197	7.1	0.0297	4.5	0.62	33.647	4.5	0.0482	5.5	109	130	183	12	189	8	-74
DCPP_M_212	152	85	6	0.56	129	0.199	11.8	0.0306	4.4	0.37	32.692	4.4	0.0471	11.0	53	262	184	20	194	8	-269
DCPP_M_220	150	83	5	0.56	84	0.193	7.7	0.0295	3.9	0.50	33.866	3.9	0.0475	6.6	74	158	179	13	188	7	-154
DCPP_M_222	221	141	8	0.64	175	0.211	9.6	0.0305	4.8	0.49	32.806	4.8	0.0502	8.3	204	193	194	17	194	9	5
DCPP_M_224	115	64	4	0.55	234	0.214	10.6	0.0306	5.7	0.54	32.653	5.7	0.0508	8.9	230	205	197	19	194	11	16
DCPP_M_225	121	61	4	0.51	250	0.198	13.3	0.0299	4.5	0.33	33.493	4.5	0.0482	12.5	110	296	184	22	190	8	-73
DCPP_M_226	117	58	4	0.49	383	0.205	16.8	0.0299	4.7	0.28	33.411	4.7	0.0497	16.1	183	375	190	29	190	9	-4
DCPP_M_227	109	66	4	0.61	135	0.201	10.5	0.0309	3.3	0.31	32.401	3.3	0.0473	10.0	63	239	186	18	196	6	-211
DCPP_M_231	161	84	6	0.52	79	0.217	8.4	0.0305	4.4	0.51	32.738	4.4	0.0516	7.2	269	165	200	15	194	8	28
DCPP_M_232	180	131	7	0.73	129	0.212	8.0	0.0302	4.4	0.54	33.150	4.4	0.0511	6.7	244	155	196	14	192	8	21
DCPP_M_233	125	57	4	0.46	153	0.194	9.3	0.0308	4.7	0.50	32.495	4.7	0.0458	8.1	-11	195	180	15	195	9	1881
DCPP_M_234	135	67	5	0.50	849	0.221	6.7	0.0297	5.0	0.75	33.695	5.0	0.0540	4.4	370	98	203	12	189	9	49
DCPP_M_237	240	111	9	0.46	123	0.219	6.6	0.0307	3.2	0.48	32.579	3.2	0.0517	5.7	273	131	201	12	195	6	29
DCPP_M_238	119	56	4	0.47	60	0.214	11.8	0.0310	6.8	0.58	32.207	6.8	0.0499	9.6	190	223	197	21	197	13	-3
DCPP_M_239	98	59	4	0.60	73	0.204	12.5	0.0314	4.3	0.34	31.886	4.3	0.0471	11.7	56	280	188	21	199	8	-255
DCPP_M_240	90	52	3	0.58	87	0.211	12.7	0.0318	4.3	0.33	31.420	4.3	0.0480	11.9	101	282	194	22	202	8	-100
DCPP_M_241	99	64	5	0.64	172	0.350	19.0	0.0333	3.8	0.20	30.043	3.8	0.0763	18.6	1104	372	305	50	211	8	81
DCPP_M_243	115	69	4	0.60	50	0.212	12.4	0.0291	3.6	0.29	34.420	3.6	0.0528	11.9	322	269	195	22	185	7	43
DCPP_M_246	122	65	5	0.53	78	0.240	12.8	0.0314	3.7	0.29	31.884	3.7	0.0556	12.3	436	273	219	25	199	7	54
DCPP_M_252	206	122	8	0.59	151	0.212	7.1	0.0306	3.8	0.53	32.656	3.8	0.0503	6.0	208	138	195	13	194	7	7
DCPP_M_253	112	65	4	0.58	173	0.239	7.5	0.0305	3.0	0.39	32.792	3.0	0.0569	6.9	489	152	218	15	194	6	60
DCPP_M_255	117	59	4	0.51	941	0.197	8.3	0.0305	4.1	0.49	32.827	4.1	0.0470	7.2	48	173	183	14	193	8	-302
DCPP_M_256	264	151	9	0.57	606	0.214	6.1	0.0294	3.0	0.47	34.001	3.0	0.0528	5.3	321	121	197	11	187	5	42

DCPP_M_257	118	56	4	0.48	12595	0.212	11.6	0.0306	6.4	0.55	32.650	6.4	0.0502	9.7	204	225	195	21	194	12	5
DCPP_M_258	124	61	5	0.49	761	0.222	6.9	0.0310	5.4	0.78	32.260	5.4	0.0520	4.3	287	99	204	13	197	11	31
DCPP_M_261	180	91	6	0.51	384	0.217	7.3	0.0292	3.5	0.47	34.223	3.5	0.0539	6.4	367	144	200	13	186	6	49
DCPP_M_262	151	74	5	0.49	326	0.201	11.6	0.0296	3.4	0.28	33.730	3.4	0.0493	11.1	162	260	186	20	188	6	-16
DCPP_M_263	210	145	8	0.69	403	0.212	7.6	0.0299	3.8	0.50	33.474	3.8	0.0515	6.6	265	151	195	14	190	7	28
DCPP_M_264	129	71	5	0.55	177	0.209	10.6	0.0298	3.8	0.35	33.526	3.8	0.0509	9.9	238	229	193	19	189	7	20
DCPP_M_265	358	166	13	0.46	811	0.213	7.3	0.0295	4.7	0.64	33.897	4.7	0.0523	5.6	297	127	196	13	187	9	37
DCPP_M_268	141	73	5	0.52	385	0.204	9.5	0.0322	3.8	0.39	31.048	3.8	0.0460	8.7	-1	211	189	16	204	8	15515
DCPP_M_269	138	63	5	0.45	690	0.198	7.2	0.0317	3.4	0.47	31.593	3.4	0.0453	6.3	-38	153	183	12	201	7	632
DCPP_M_271	107	59	4	0.55	72	0.191	15.3	0.0301	4.3	0.28	33.273	4.3	0.0460	14.6	0	353	177	25	191	8	30605
Composition			Corrected isotope ratios												Apparent ages (Ma)						
Analysis	U	Th	Pb	$\frac{^{206}\text{Pb}}{^{204}\text{Pb}}$	$\frac{^{207}\text{Pb}}{^{235}\text{U}}$	$\pm 2s$	$\frac{^{206}\text{Pb}}{^{238}\text{U}}$	$\pm 2s$	error	$\frac{^{238}\text{U}}{^{206}\text{Pb}}$	$\pm 2s$	$\frac{^{207}\text{Pb}}{^{206}\text{Pb}}$	$\pm 2s$	$\frac{^{207}\text{Pb}}{^{206}\text{Pb}}$	$\pm 2s$	$\frac{^{207}\text{Pb}}{^{235}\text{U}}$	$\pm 2s$	$\frac{^{206}\text{Pb}}{^{238}\text{U}}$	$\pm 2s$	%	
	ppm	ppm	ppm	Th/U	$\frac{^{204}\text{Pb}}{^{235}\text{U}}$	(%)	$\frac{^{238}\text{U}}{^{206}\text{Pb}}$	(%)	corr.	$\frac{^{206}\text{Pb}}{^{206}\text{Pb}}$	(%)	$\frac{^{206}\text{Pb}}{^{206}\text{Pb}}$	(abs)	$\frac{^{207}\text{Pb}}{^{206}\text{Pb}}$	(abs)	$\frac{^{207}\text{Pb}}{^{235}\text{U}}$	(abs)	$\frac{^{206}\text{Pb}}{^{238}\text{U}}$	(abs)	disc.	
MSD-1 (Mary Sloan dikes)																					
MSD_L_118	131	122	5	0.93	203	0.221	9.0	0.0287	4.8	0.54	34.852	4.8	0.0560	7.6	451	169	203	17	182	9	60
MSD_L_120	283	284	11	1.01	557	0.203	5.4	0.0280	3.8	0.71	35.748	3.8	0.0526	3.8	311	86	188	9	178	7	43
MSD_L_121	280	265	11	0.95	281	0.193	6.7	0.0289	4.5	0.67	34.641	4.5	0.0485	4.9	121	117	179	11	183	8	-51
MSD_L_122	200	207	8	1.04	202	0.221	7.8	0.0294	4.4	0.57	34.071	4.4	0.0545	6.4	393	144	203	14	186	8	53
MSD_L_123	314	226	13	0.72	286	0.231	8.4	0.0304	4.1	0.49	32.888	4.1	0.0551	7.3	418	163	211	16	193	8	54
MSD_L_124	1535	1532	64	1.00	2563	0.194	4.9	0.0286	4.4	0.89	34.909	4.4	0.0491	2.2	154	51	180	8	182	8	-18
MSD_L_125	75	47	3	0.63	242	0.207	10.3	0.0295	6.1	0.60	33.949	6.1	0.0511	8.3	245	191	191	18	187	11	23
MSD_L_126	160	119	6	0.75	190	0.200	9.9	0.0292	5.4	0.55	34.299	5.4	0.0497	8.3	182	193	185	17	185	10	-2
MSD_L_127	2840	2223	113	0.78	4876	0.197	5.0	0.0279	4.6	0.92	35.882	4.6	0.0512	1.9	252	44	183	8	177	8	30
MSD_M_467	3228	1418	130	0.44	1495	0.275	9.0	0.0304	6.3	0.70	32.845	6.3	0.0656	6.4	792	134	247	20	193	12	76
MSD_M_484	2577	1611	105	0.63	3414	0.264	7.4	0.0313	6.6	0.88	31.952	6.6	0.0613	3.5	649	75	238	16	199	13	69
MSD_M_506	2277	388	91	0.17	2130	0.280	9.7	0.0322	8.3	0.86	31.052	8.3	0.0631	5.0	710	107	251	22	204	17	71
MSD_S_530	319	169	13	0.53	191	0.235	15.0	0.0312	10.3	0.68	32.023	10.3	0.0545	11.0	392	246	214	29	198	20	49
MSD_S_540	2628	853	108	0.32	858	0.292	5.9	0.0310	4.1	0.70	32.310	4.1	0.0683	4.2	879	86	260	13	196	8	78
MSD_S_546	1675	407	61	0.24	1107	0.227	4.4	0.0315	3.7	0.85	31.752	3.7	0.0522	2.3	295	53	208	8	200	7	32
MSD_S_547	1557	377	55	0.24	2158	0.245	5.6	0.0300	4.2	0.76	33.385	4.2	0.0593	3.7	578	80	222	11	190	8	67
MSD_S_552	1894	253	71	0.13	1205	0.278	6.2	0.0306	4.3	0.70	32.646	4.3	0.0657	4.4	797	92	249	14	195	8	76
MSD_S_554	2418	1114	99	0.46	626	0.297	8.0	0.0292	6.2	0.78	34.237	6.2	0.0738	5.0	1037	101	264	19	186	11	82
MSD_S_573	2754	1492	153	0.54	280	0.397	19.2	0.0322	10.4	0.54	31.030	10.4	0.0893	16.1	1411	308	339	55	204	21	86
MSD_S_574	1538	826	61	0.54	3939	0.251	8.1	0.0311	6.6	0.82	32.163	6.6	0.0586	4.6	552	101	228	17	197	13	64

Notes: Isotope ratios and ages are reported without initial common Pb correction; gas blank-corrected mass 204 signals were generally irresolvable from zero.

Isotope ratio and apparent age errors do NOT include systematic calibration errors of 0.25% for the $^{207}\text{Pb}/^{206}\text{Pb}$ ratio, and 0.56% for the $^{206}\text{Pb}/^{238}\text{U}$ ratio (1s).

Trace element concentrations in ppm, calculated using the mean count rate method, internal standardization to ^{29}Si , and calibration to NIST 610 and 612 glass standards.

Ablation using a 213 nm wavelength laser, spot size of 25 microns, repetition rate of 10 Hz, and fluence of ~5 J/cm².

APPENDIX D

Pb, Sr, and Nd Isotopic Data for Intrusive Rocks of the Jackson Mountains

Table D.1. Pb Isotopic Data for Intrusive Rocks of the Jackson Mountains

Sample	$\frac{^{208}\text{Pb}}{^{204}\text{Pb}}$	$\pm 1\text{s}$ [abs]	$\frac{^{207}\text{Pb}}{^{204}\text{Pb}}$	$\pm 1\text{s}$ [abs]	$\frac{^{206}\text{Pb}}{^{204}\text{Pb}}$	$\pm 1\text{s}$ [abs]	$\frac{^{208}\text{Pb}}{^{206}\text{Pb}}$	$\pm 1\text{s}$ [abs]	$\frac{^{207}\text{Pb}}{^{206}\text{Pb}}$	$\pm 1\text{s}$ [abs]	$\frac{^{238}\text{U}}{^{204}\text{Pb}}$	$\frac{^{232}\text{Th}}{^{238}\text{U}}$	$\frac{\text{U}}{\text{Pb}}$	$\frac{\text{Th}}{\text{U}}$	<u>ICPMS</u>
<u>Early Jurassic Suite</u>															
DCPP #4	38.3616	0.0020	15.6190	0.0008	18.6501	0.0009	2.0569	0.0000	0.8375	0.0000	0.6740	1.5933	0.0106	1.5418	
DCPP #5	38.3051	0.0025	15.6136	0.0010	18.6604	0.0012	2.0527	0.0000	0.8367	0.0000	1.6877	2.7650	0.0265	2.6756	
PPP #4	38.3570	0.0008	15.6132	0.0003	18.6542	0.0003	2.0562	0.0000	0.8370	0.0000	2.9457	1.0453	0.0462	1.0115	
PPP #5	38.3098	0.0008	15.6012	0.0002	18.6361	0.0002	2.0557	0.0000	0.8372	0.0000	2.4113	1.1911	0.0379	1.1526	
HGP #4	38.3557	0.0004	15.6072	0.0002	18.6593	0.0002	2.0556	0.0000	0.8364	0.0000	1.2933	1.3990	0.0203	1.3537	
HGP #5	38.3129	0.0005	15.5986	0.0002	18.6365	0.0002	2.0558	0.0000	0.8370	0.0000	0.8833	1.5922	0.0139	1.5407	
MSD #4	38.4012	0.0069	15.5950	0.0028	18.6140	0.0034	2.0630	0.0000	0.8378	0.0000	12.9923	0.1744	0.2032	0.1687	
MSD #5	38.3837	0.0064	15.6075	0.0025	18.5393	0.0030	2.0704	0.0000	0.8419	0.0000	10.8579	0.1095	0.1701	0.1059	
<u>Late Jurassic Suite</u>															
TCS #4	38.5598	0.0040	15.6221	0.0016	18.7871	0.0020	2.0525	0.0000	0.8315	0.0000	10.3164	1.0150	0.1606	0.9822	
TCS #5	38.5804	0.0069	15.6071	0.0028	18.6948	0.0034	2.0637	0.0000	0.8348	0.0000	19.1029	0.6490	0.2968	0.6280	
WCP #4	39.0917	0.0241	15.6341	0.0098	18.9598	0.0121	2.0618	0.0001	0.8246	0.0001	28.6341	0.9063	0.4380	0.8770	
WCP #5	39.2482	0.0057	15.6450	0.0022	18.9912	0.0027	2.0666	0.0000	0.8238	0.0000	28.8966	0.7376	0.4410	0.7138	
DPP #4	38.5224	0.0009	15.6077	0.0004	18.7790	0.0005	2.0514	0.0000	0.8311	0.0000	4.3680	1.2290	0.0682	1.1893	
DPP #5	38.5345	0.0009	15.6104	0.0003	18.7815	0.0004	2.0517	0.0000	0.8312	0.0000	3.9759	0.8382	0.0621	0.8111	

Tabulated isotope ratios include an external fractionation correction of $0.10 \pm 0.02\%$ (1-sigma) per a.m.u., based upon NBS981 measurements on similar sized ion beams at the same run temperatures. The listed uncertainties are in-run relative 1-sigma standard errors; fractionation uncertainty imposes the following minimum absolute uncertainties (1-sigma): $^{208}\text{Pb}/^{204}\text{Pb}$, 0.019; $^{207}\text{Pb}/^{204}\text{Pb}$, 0.007; $^{206}\text{Pb}/^{204}\text{Pb}$, 0.008; $^{208}\text{Pb}/^{206}\text{Pb}$, 0.0009; $^{207}\text{Pb}/^{206}\text{Pb}$, 0.0004.

Uncertainties for ICPMS ratios range between 1-5%. Bold analyses are interpreted as the better measure of initial Pb and are used in plots.

Table D.2. Rb-Sr Isotopic Data for Intrusive Rocks of the Jackson Mountains

Sample	Age (Ma)	Rb (ppm)	Sr (ppm)	<u>Rb</u> <u>Sr</u>	$\frac{^{87}\text{Rb}}{^{87}\text{Sr}}$	$\pm 2\sigma$ [abs]	$^{87}\text{Sr}/^{86}\text{Sr}$ (Measured)	$\pm 2\sigma$ [abs]	$^{87}\text{Sr}/^{86}\text{Sr}$ (Initial)
Early Jurassic Suite									
DCPP	192.89 ± 0.07	61.80	257.97	0.2396	0.6932	0.0014	0.706509	0.000015	0.704636
PPP	190.28 ± 0.07	44.06	531.71	0.0829	0.2397	0.0005	0.704507	0.000014	0.703860
HGP	189.32 ± 0.07	15.29	817.73	0.0187	0.0541	0.0001	0.704039	0.000011	0.703916
MSD	189.94 ± 0.06	161.67	235.35	0.6869	1.9877	0.0040	0.708736	0.000013	0.703366
Late Jurassic Suite									
TCS	161.88 ± 0.11	10.13	809.56	0.0125	0.0362	0.0001	0.704073	0.000013	0.703991
WCP	161.88 ± 0.07	29.58	299.87	0.0986	0.2854	0.0006	0.704993	0.000014	0.704344
DPP	161.63 ± 0.18	27.88	1121.49	0.0249	0.0719	0.0001	0.704108	0.000011	0.703945

Notes: 100 mg of powder were dissolved with 3 mL 29M HF + 1 mL 15M HNO₃ in Savillex PFA beakers at 150°C for 60 hours, dried and redissolved in 5 mL 6M HCl at 150°C for 16 hours. A 10% aliquot of the solution was spiked with ⁸⁷Rb and ⁸⁴Sr tracers, fluxed overnight, dried and redissolved in 5 mL 1M HCl + 0.1M HF at 150°C overnight. Rb and Sr were separated by standard cation exchange chemistry (by elution in 2.5M HCl on 6mm i.d. x 20cm columns of AG-50W-X8 resin, H⁺ form, 200-400 mesh). The Rb fraction was further purified by either; a) ion exchange in 0.6M HCl on 6mm i.d. x 10cm columns of AG-50W-X8 resin (H⁺ form, 200-400 mesh), or b) treatment with 29M HF to precipitate residual alkaline earths and extraction in ultrapure water for mass spectrometry. Rb and Sr were loaded in 0.1N H₃PO₄ along with a tantalum oxide emitter solution (R. Creaser, pers. comm.) on single degassed Re filaments, and their isotope ratios measured on the Isoprobe-T in the Boise State University Isotope Geology Laboratory. The ⁸⁷Rb/⁸⁵Rb ratio was measured in static Faraday mode; a mass bias correction was estimated by external analysis of natural Rb standards. Sr isotope ratios were analyzed in dynamic mode, fractionation corrected with an exponential law relative to ⁸⁶Sr/⁸⁸Sr = 0.1194, and are reported as spike-stripped and bias corrected relative to the accepted value of the NBS-987 standard (0.710248). The quoted uncertainty for each analysis is the internal standard error; the external reproducibility of the NBS-987 standard over the course of the study was 0.710251 ± 3 (1s); uncertainty in [Rb], [Sr] and ⁸⁷Rb/⁸⁶Sr are estimated at ≤ 0.2% (1s). Initial ⁸⁷Sr/⁸⁶Sr is calculated assuming an ⁸⁷Rb decay constant of 1.42x10⁻¹¹ y⁻¹.

Table D.3. Sm-Nd Isotopic Data for Intrusive Rocks of the Jackson Mountains

Sample	Age (Ma)	Sm (ppm)	Nd (ppm)	$\frac{^{147}\text{Sm}}{^{144}\text{Nd}}$	$\pm 2\text{s}$ [abs]	$^{143}\text{Nd}/^{144}\text{Nd}$ (Measured)	$\pm 2\text{s}$ [abs]	$^{143}\text{Nd}/^{144}\text{Nd}$ (Initial)	εNd (Initial)
Early Jurassic Suite									
DCPP	192.89 ± 0.07	3.94	16.89	0.1409	0.0003	0.512743	0.000008	0.512812	3.40
PPP	190.28 ± 0.07	3.45	13.97	0.1491	0.0003	0.512805	0.000008	0.512864	4.41
HGP	189.32 ± 0.07	4.35	21.37	0.1231	0.0002	0.512759	0.000006	0.512837	3.87
MSD	189.94 ± 0.06	2.57	15.95	0.0973	0.0002	0.512750	0.000004	0.512874	4.60
Late Jurassic Suite									
TCS	161.88 ± 0.11	3.03	14.21	0.1287	0.0003	0.512817	0.000003	0.512889	4.89
WCP	161.88 ± 0.07	4.05	20.56	0.1190	0.0002	0.512760	0.000008	0.512841	3.96
DPP	161.63 ± 0.18	4.74	20.25	0.1416	0.0003	0.512803	0.000004	0.512860	4.34

Notes: 50 mg of sample powder were spiked with a mixed 149Sm-150Nd tracer, dissolved with 5 mL 29M HF + 15M HNO₃ (3:1) in Parr pressure vessels at 200°C for 72 hours, dried and redissolved in 5 mL 6M HCl at 120°C for 24 hours. Total dissolutions were dried and redissolved in 5 mL 1M HCl + 0.1M HF at 120°C overnight. Bulk rare earth elements were separated by standard dilute HCl and HNO₃ based cation exchange chemistry on 6mm i.d. x 20cm columns of AG-50W-X8 resin, H⁺ form, 200-400 mesh); Sm and Nd were separated by reverse phase HDEHP chromatography on 4mm i.d. x 10cm columns of Eichrom Ln-spec resin, 50-100 mesh. Sm and Nd isotopes were measured on a IsotopX Isoprobe-T in static and dynamic Faraday modes, respectively. Instrumental mass fractionation of Sm and Nd isotopes was corrected with an exponential law relative to 146Nd/144Nd = 0.7219 and 152Sm/147Sm = 1.783. 143Nd/144Nd ratio is reported as spike-stripped and bias-corrected relative to the accepted value of JNd_i-1 standard (0.512110). The quoted uncertainty for each analysis is the internal standard error; the external reproducibility of the JNd_i-1 standard over the course of the study was 0.512103 ± 3 (2s); uncertainty in [Sm], [Nd] and 147Sm/144Nd are estimated at $\leq 0.2\%$ (2s). Present-day $\varepsilon\text{Nd}(0)$ calculated with $(143\text{Nd}/144\text{Nd})\text{CHUR} = 0.512638$; $\varepsilon\text{Nd}(2.6)$ calculated at age of crystallization.

APPENDIX E

**Compilation of Pb, Sr, and Nd Isotopic Data for Jurassic Plutons from the Western
United States**

Table E.1. Compilation of Pb, Sr, and Nd Isotopic Data for Jurassic Plutons (165-150 Ma) Located Between 38°-42°N and 113°-121°W

Location (State)	Age (Ma)	Latitude (°N)	Longitude (°W)	$\frac{^{206}\text{Pb}}{^{204}\text{Pb}_i}$	$\frac{^{207}\text{Pb}}{^{204}\text{Pb}_i}$	$\frac{^{208}\text{Pb}}{^{204}\text{Pb}_i}$	$\frac{^{87}\text{Sr}}{^{86}\text{Sr}_i}$	ϵNd_i	Reference(s)
Grouse Ridge pluton (CA)	163	39.39	120.61	18.772	15.562	38.445	0.705		Wooden et al., 1999
Downey Lake pluton (CA)	163	39.40	120.59	18.815	15.651	38.683	0.705		Wooden et al., 1999
Omo Ranch pluton (CA)	152	38.58	120.55	18.969	15.621	38.671	0.705		Wooden et al., 1999
French Lake pluton (CA)	163	39.42	120.54	18.930	15.657	38.779	0.706		Wooden et al., 1999
Desert Creek Porphyry (CA)	155	38.54	119.43	19.665	15.672	39.189	0.706		Wooden et al., 1999
main Desert Creek pluton (CA)	155	38.58	119.42	19.047	15.643	38.783	0.705		Wooden et al., 1999
Desert Creek Diorite (CA)	155	38.59	119.42	18.844	15.614	38.612	0.704		Wooden et al., 1999
Log Cabin Creek pluton (CA)	161	38.22	119.32	18.923	15.636	38.624	0.704		Wooden et al., 1999
Santa Rita Flat Pluton (CA)	164	38.90	118.19	18.718	15.656	38.896	0.707		Wooden et al., 1999
Santa Rita Flat Pluton (CA)	164	38.90	118.19	18.666	15.641	38.811	0.707		Wooden et al., 1999
Santa Rita Flat Pluton (CA)	164	38.90	118.19	18.690	15.639	38.803	0.707		Wooden et al., 1999
Lee Peak pluton, East Range (NV)	153	40.57	117.85	19.402	15.708	39.118	0.709		Elison et al., 1990
Lee Peak pluton, East Range (NV)	153	40.57	117.85	19.484	15.740	39.184	0.708		Elison et al., 1990
Goldbank B pluton, East Range (NV)	150	40.54	117.77	19.424	15.710	39.017	0.706		Elison et al., 1990
Goldbank A pluton, East Range (NV)	150	40.57	117.76	19.495	15.720	39.191	0.707		Elison et al., 1990
Lee Peak pluton, East Range (NV)	153	40.57	117.75	19.430	15.724	39.180	0.709		Elison et al., 1990
Lee Peak pluton, East Range (NV)	153	40.57	117.75	19.439	15.697	39.099	0.709		Elison et al., 1990
Lee Peak pluton, East Range (NV)	153	40.57	117.75	19.395	15.745	39.295	0.709		Elison et al., 1990
S. Tobin Range (NV)	150	40.21	117.61	19.370	15.688	39.103	0.706		Elison et al., 1990
Buffalo Mountain syenite (NV)	159	40.70	117.45	19.322	15.678	38.917	0.706		Wooden et al., 1999
Buffalo Mountain syenite (NV)	159	40.70	117.45	19.430	15.693	39.035	0.706	-4.3	Wright and Wooden, 1991; Farmer and DePaolo, 1983
Buffalo Mountain syenite (NV)	159	40.71	117.45	19.318	15.678	38.913	0.706		Wooden et al., 1999

Cain Creek stock, Shoshone Mtns. (NV)	159	40.01	117.27	19.489	15.718	39.058	0.710	Wooden et al., 1999	
McCoy stock, Fish Creek Mtn. (NV)	153	40.30	117.24	19.527	15.713	39.090	0.707	Wooden et al., 1999	
Northumberland, Toquima Range (NV)	155	38.96	116.87	19.215	15.673	38.817	0.706	Wooden et al., 1999	
granodiorite, N. Toquima Range (NV)	157	38.96	116.87	19.215	15.673	38.817		Wooden et al., 1999	
Northumberland, Toquima Range (NV)	155	39.95	116.83	19.056	15.639	38.584	0.706	Kistler and Lee, 1989	
SW Cortez Mountains (NV)	154	40.20	116.60	19.445	15.715	39.031	0.710	Wooden et al., 1999	
granodiorite, Cortez Mtns. (NV)	155	40.27	116.45	19.636	15.694	39.299	0.706	Wooden et al., 1999	
granodiorite, Cortez Mtns. (NV)	155	40.27	116.45	19.832	15.711	39.330	0.706	Wooden et al., 1999	
granodiorite, Cortez Mtns. (NV)	155	40.27	116.45	19.675	15.726	39.291	0.706	Wooden et al., 1999	
Cortez Mountains (NV)	155	40.33	116.40	18.929	15.669	38.777	0.706	Kistler and Lee, 1989	
Duff Creek Pluton, Cortez Mtns. (NV)	155	40.34	116.35	21.354	15.835	40.769	0.706	Wooden et al., 1999	
Cortez Mountains (NV)	155	40.37	116.35	19.523	15.713	38.952	0.707	Kistler and Lee, 1989	
Cortez Mountains, monzodiorite (NV)	154	40.28	116.33	19.572	15.698	39.170		Wooden et al., 1999	
White Rock pluton (NV)	155	41.72	116.17	19.678	15.780	39.402	0.705	Kistler and Lee, 1989	
White Rock pluton (NV)	155	41.70	116.15	19.844	15.792	39.217	0.705	Kistler and Lee, 1989	
Whistler Mtn aplite (NV)	155	39.66	116.09	19.419	15.692	39.001	0.709	Wooden et al., 1999	
Columbia Stock (NV)	154	41.68	116.08	19.221	15.661	38.955	0.705	Kistler and Lee, 1989	
Columbia Stock (NV)	154	41.68	116.07	19.104	15.644	38.830	0.705	Kistler and Lee, 1989	
Jurassic granite, Ruby Range (NV)	160	40.37	115.50	19.263	15.788	39.988	0.714	Kistler et al., 1981	
Jurassic granite, Ruby Range (NV)	160	40.37	115.50	19.867	15.787	39.418	0.714	Kistler et al., 1981	
Jurassic granite, Ruby Range (NV)	160	40.37	115.50	19.785	15.746	39.303	0.714	Kistler et al., 1981	
Jurassic granite, Ruby Range (NV)	160	40.33	115.50	19.940	15.768	39.634	0.714	Kistler et al., 1981	
Ruby Range (NV)	150	40.37	115.40	19.792	15.773	39.373	0.711	Wright and Wooden, 1991	
Granite Range (NV)	155	41.73	114.78	19.779	15.746	39.709	0.705	-3.1	Wright and Wooden, 1991

Dolly Varden Mountains (NV)	158	40.27	114.78	19.802	15.804	40.404	0.707	-5.4	Wright and Wooden, 1991; Miller and Hoisch, 1995
Contact Pluton (NV)	155	41.75	114.77	19.799	15.741	39.458	0.705		Kistler and Lee, 1989
Dolly Varden pluton (NV)	150	40.35	114.55	19.615	15.777	39.979	0.707		Wright and Wooden, 1991
biotite Granodiorite, Silver Zone Pass (NV)	162	40.90	114.30	19.953	15.781	40.003	0.705	-2.5	Wright and Wooden, 1991
Silver Zone Pass (NV)	162	40.90	114.30	19.960	15.763	39.962	0.705		Wright and Wooden, 1991
White Horse Granite (NV)	158	40.23	114.27				0.707	-5.5	Miller and Hoisch, 1995
Snake Creek pluton, Snake Range (NV)	155	38.93	114.25	19.241	15.712	39.292	0.707		Wright and Wooden, 1991
Snake Range (NV)	160	39.25	114.17	19.231	15.752	39.665	0.708		Wright and Wooden, 1991
Snake Range (NV)	160	39.15	114.17	19.574	15.766	39.563	0.707		Wright and Wooden, 1991
Miners Spring (UT)	160	41.00	114.00	19.712	15.814	39.865	0.710		Wright and Wooden, 1991
Gold Hill (UT)	152	40.16	113.83	19.537	15.812	40.170	0.709		Stacey and Zartman, 1978
Gold Hill (UT)	152	40.08	113.83	19.566	15.841	40.230	0.709		Stacey and Zartman, 1978
Gold Hill (UT)	152	40.16	113.83	19.645	15.832	40.173	0.709		Stacey and Zartman, 1978
Gold Hill (UT)	152	40.18	113.82	19.976	15.862	40.682	0.709		Stacey and Zartman, 1978
Gold Hill (UT)	152	40.11	113.82	19.611	15.838	40.302	0.709		Stacey and Zartman, 1978
Gold Hill (UT)	152	40.16	113.81	19.733	15.860	40.366	0.709		Stacey and Zartman, 1978
Gold Hill (UT)	152	40.13	113.79	19.568	15.812	40.139	0.708		Stacey and Zartman, 1978
Silver Island Range (UT)	152	41.02	113.78				0.706	-4.9	Miller and Hoisch, 1995
Gold Hills southern stock (UT)	152	40.09	113.77				0.710	-8.6	Farmer and DePaolo, 1983
Gold Hill (UT)	155	40.15	113.75	19.277	15.816	40.550	0.710		Kistler and Lee, 1989
Silver Island Mountains (UT)	160	41.30	113.75	19.603	15.773	40.119	0.706		Wright and Wooden, 1991
Silver Island Mountains (UT)	160	41.30	113.75	19.636	15.793	40.165	0.706		Wright and Wooden, 1991
Newfoundland Mountain (UT)	160	41.23	113.38	19.602	15.761	40.116	0.705		Wright and Wooden, 1991